Université Pierre et Marie Curie

Ecole doctorale Chimie Physique et Chimie Analytique de Paris - ED388

Institut de Recherche Chimie Paris, CNRS - Chimie ParisTech

Laboratoire Interface Electrochimie Energie

Mécanismes de corrosion de l'acier revêtu d'alliage à base de ZnMgAl en tests accélérés et en environnement naturel

Par Marcele SALGUEIRO AZEVEDO

Thèse de doctorat en Chimie Physique et Chimie Analytique

Dirigée par Kevin OGLE

Présentée et soutenue publiquement le 29 avril 2014

Devant un jury composé de :

M. K. OGLE	Professeur (Chimie ParisTech)	Directeur de thèse
Mme. P. VOLOVITCH	Maître de conférence (Chimie ParisTech)	Encadrante de thèse
M. D. THIERRY	Directeur de l'Institut de la Corrosion	Rapporteur
M. M. ZHELUDKEVICH	Directeur de Recherche (Kiel University)	Rapporteur
M. C. ALLELY	Ingénieur de recherche (ArcelorMittal)	Examinateur
M. B. TRIBOLLET	Professeur (LISE – UPMC)	Examinateur

Except where otherwise noted, this work is licensed under
http://creativecommons.org/licenses/by-nc-nd/3.0/

Corrosion mechanisms of ZnMgAl coated steel in accelerated tests and natural environment

“La raison est la seule chose qui nous rend hommes”

Descartes

Acknowledgment

This thesis is the result of a research work carried out in the frame of a collaboration between the Laboratoire de Physico-Chimie de Surface of the Ecole Nationale Supérieure de Chimie de Paris and the Surfaces and Coatings department of the Automotive Centre of ArcelorMittal Maizières Research and would not have been possible without the great help and support of many people.

First and foremost, praises and thanks to God for His blessing throughout my research work.

To my thesis director, Kevin Ogle, and to my supervisor, Polina Volovitch, I would like to express my most sincere gratitude for their numerous advices and scientific contributions and also for the warmth that they have always shown towards me.

Special thanks to my company supervisor, Christian Allély, who has continuously supported me in this work and has always been present. I would like to thank him for his guidance, for all his answers and explanations, for the useful suggestions and for his extreme kindness. I owe him a lot.

My thanks are also addressed to Michel Babbit, head of the Automotive Centre of ArcelorMittal Maizières Research, and Jacques Petitjean, head of the Surface and Coatings department of this centre, for having me in the team and trusting me, after my internship, for the realization of this work.

To Maxime Monnoyer, who supervised me during my internship and recommended me to this work, and Tiago Machado, who not only supported me before my PhD but also during all these years of study, my warmest thanks.

I also thank Dominique Thierry and Mikhail Zheludkevich for having evaluated this work as reporters and Bernard Tribollet for agreeing to participate in my thesis committee.

I would also like to gratefully acknowledge Astrid Coffigny, Charifa Riani and Aymériс Corbel not only for sharing with me the laboratory of electrochemistry, but also for their patience in helping me with other techniques as the scanning electron microscope, the sample preparation, the accelerated corrosion tests, etc. They were always joyous and ready to assist me.

I would like to express my gratitude to Yves Basselin and Arnaud Pirson for receiving me in their laboratory in the Mining Centre and for the valuable assistance with characterizations in the X-ray diffraction and in the scanning electron microscope; to

Françoise Broquedis and Alexey Koltsov for their Raman analysis; to Laurence Daheron for her help with XRD analysis. They all have strongly contributed to this work.

I also wish to thank Maria Serdechnova and Viacheslav Shkirskiy who helped me a lot during staying in the school and who patiently answered all my questions about the AESEC. Besides them, I also thank Sophie Lebouil and Lily Jiang, who helped me with the ICP and with the titration experiments. To Dr. François Brisset, thanks for the great MEB-FEG analysis.

Thanks also to Laurence Dosdat and Stéphane Morel for the samples from field exposure; to Catherine Marani and Claude Arnoux for their help and good humor with the accelerated corrosion test chambers.

Thanks also to all my colleagues from both Laboratoire de Physico-Chimie de Surfaces and Surface and Coatings department not yet cited, Matthieu Siebentritt, Audrey Lhermeroult, David Zapico and the others, for the good spirits they make prevail at work and for all assistance they gave me in the different laboratories. I also want to thank others friends-colleagues from ArcelorMittal Maizières Research, Christophe Ramassamy, Francisco Lobato, Kevin Tihay and Adriana Carvallo, for their help with administrative and personal needs.

Besides all people who helped me during my doctorate, I also would like to thank my professors, supervisors and friends in Brazil, specially Dr. Julio Medrano, Dr. Flavio Ferreira and Dr. Tadeu de Medeiros, who encouraged me to begin my PhD.

Finally, I would like to unconditionally thank my family and my friends for the support received. More especially, I want to accentuate my gratefulness to my mother, Ester, my sisters, Thaisa and Lilian, my grandmother Maria Auxiliadora and my boyfriend, Leandro Dijon, for their affection and for encouraging me before and during my doctorate.

Marcele Salgueiro Azevedo

April 2014, Maizières-lès-Metz

Corrosion mechanisms of ZnMgAl coated steel in accelerated tests and natural environment

Abstract

The aim of this work was to understand the role of the environment on the corrosion mechanisms of ZnMgAl (ZM) coatings on steel.

In order to establish the critical elements in the environment, the corrosion rates and the nature of the corrosion products formed on ZM, Galfan (ZA) and hot dip galvanized (GI) coatings were determined for field exposures and for accelerated tests using different electrolytes. On the basis of these tests, a new test electrolyte is selected, containing NH_4^+ and HCO_3^-, which shows an improved correlation with field exposure in particular respecting the relative corrosion rates of different compositions and the absence or at least the delay in the formation of layered double hydroxides (LDH).

We have separated the effect of different ions on different steps of corrosion mechanism considering dissolution-precipitation model.

The role of NH_4^+ and HCO_3^- on the intrinsic reactivity of ZM coating and the leaching of Zn, Al and Mg ions in aqueous solutions containing Cl^- was investigated using atomic emission spectroelectrochemistry. NH_4^+ increased the anodic reactivity of Zn, suppressed the accumulation of zinc corrosion products and inhibited Al dissolution at open circuit (OC). HCO_3^- increased the accumulation of insoluble zinc corrosion products as well as the anodic reactivity. The anodic reactivity of ZM was higher than the anodic reactivity of GI. A preliminary anodic polarization did not affect the cathodic current on ZM in NaCl but increased it in mixed electrolyte (containing both NH_4^+ and HCO_3^-). The cathodic dissolution of Al, in contrast, was strongly delayed or even suppressed by a preliminary anodic polarization of ZM in mixed electrolyte. The effect was significantly less pronounced on ZA coating. The kinetic effect was explained by the presence on the surface of anodically formed magnesium carbonates, blocking mass transport and consuming electrochemically generated hydroxide.

The effect of corrosion products on the oxygen reduction was demonstrated using cathodic polarization of different coatings, on which the corrosion products were preliminary formed by open circuit exposure. A strong stable inhibiting effect of corrosion products was observed under long applied cathodic potential on ZM but the cathodic current increased significantly with time on GI coating. The XRD demonstrated that, on

GI, the initially formed basic zinc salts (simonkolleite, hydrozincite, zinc hydroxysulphate...) were transformed into zinc oxide under cathodic polarization. Layered double hydroxide or zinc salts formed on ZM were stable under cathodic polarization. In different tests, the selective dissolution of Mg-rich phase resulted in a formation of a metallic Al "skeleton" that would increase the compactness of the corrosion products.

The formation and stability of corrosion products was studied using acid-base titrations of Zn^{2+} in different solutions (Na_2SO_4, NaCl, $NaHCO_3$, NH_4Cl) with and without addition of Mg^{2+} and Al^{3+} ions. It demonstrated the important role of added ions on the precipitation kinetics. Addition of Mg^{2+} delayed about 48 h the transformation of basic zinc salts into zinc oxide or hydroxide. In presence of Al^{3+}, Zn-Al layered double hydroxides were immediately formed, except in SO_4^{2-} solution, in which an intermediate formation of BZS was observed.

Different compositions of ZnMgAl coated steel were also compared in accelerated corrosion tests and in electrochemical tests, using different electrolytes. Coatings with similar microstructure, even with very different composition, demonstrated similar tendencies in reaction rates and corrosion products evidencing the importance of a homogenous microstructure.

To conclude, the presence of bicarbonate, sulfate and ammonium ions can significantly influence the kinetics of different elemental steps of corrosion mechanisms of ZM coatings.

Content

List of Tables..... xv
List of Figures..... xix
List of acronyms and abbreviations..... xxvii
Introduction 1
Chapter I – State of the art 5
1 The development of ZnMgAl coated steels in the last decades..... 7
2 ZnMgAl microstructure as function of Al and Mg contents..... 8
3 Corrosion resistance in accelerated corrosion tests..... 9
4 Corrosion resistance in field exposure tests..... 13
5 Corrosion mechanisms..... 16
6 Corrosion products properties..... 22
7 Conclusion of the state of the art..... 27
References..... 28
Chapter II – Experimental..... 31
1 Materials..... 33
2 Accelerated corrosion tests..... 34
3 Natural environments corrosion tests..... 35
4 Corrosion products removal and determination of the corrosion rate..... 36
5 Corrosion products characterization..... 37
6 Titration..... 37
7 Atomic emission spectroelectrochemistry (AESEC)..... 38
8 Electrochemical experiments..... 38
References..... 39
Chapter III – The role of electrolyte composition on the nature of corrosion products and relative corrosion rate 41
Abstract..... 43
1 Introduction..... 44
2 Experimental..... 45
2.1 *Materials*..... 45
2.2 *Corrosion tests*..... 46
2.3 *Corrosion damage characterization*..... 47

2.4 *Corrosion product characterization*……..... 48
2.5 *Titration experiments*……..... 49
3 Results……..... 49
3.1 *Buffer capacity of rain water*……..... 49
3.2 *Corrosion rates from different corrosion tests*…… 50
3.3 *Corrosion products*…….. 52
3.4 *Corrosion product distribution*…… 52
3.4 *Mass balance during salt spray test (SST)*……... 57
4 Discussion……. 59
4.1Corrosion rates and corrosion products in accelerated tests with RW electrolyte compared to the field exposure and accelerated tests using NaCl electrolyte……... 59
4.2 *The formation of corrosion products in different electrolytes*……. 60
5 Conclusion…… 62
References……... 65
Chapter IV – The effect of HCO_3^- and NH_{IV}^+ ions on the intrinsic reactivity of the Zn(Mg,Al) coating …… 69
Abstract……. …….. 71
Graphical abstract…….……... 72
1 Introduction…….…….. 73
1.1 *Context*…….…… 73
1.2 *Intrinsic reactivity measurement by AESEC*…….……... 74
2 Experimental…….…… 78
2.1 *Materials*…….……. 78
2.2 *Experimental parameters*…….…… 78
2.3 *Corrosion product characterization*…….……... 79
3 Results…….…….. 80
3.1 *Coatings reactivity measured by AESEC at open circuit and under applied anodic potential*…… 80
3.2 *Anodic reactivity of ZM under anodic-cathodic polarization cycles*……... 84
3.3 *Cathodic reactivity of ZM under anodic-cathodic polarization cycles*…… 86
3.4 *Reactivity of ZA compared to ZM under anodic-cathodic polarization cycles*……..… 88

4 Discussion……. 89
4.1 *Cathodic and anodic reactivity and the formation of corrosion products*... 89
4.2 *Role of hydrogen-carbonate and ammonium ions on the formation of a barrier layer*……... 93
5 Conclusion…… 94
References…… 96
Chapter V - The effect of Mg and Al on the formation and properties of corrosion products……... 99
Abstract…… 101
Graphical abstract…… 102
1 Introduction……... 103
2 Experimental……. 104
2.1 *Materials*…….. 104
2.2 *Electrochemical experiments*……... 105
2.3 *Titration experiments*……... 105
2.4 *Corrosion products and corrosion profile characterization*…… 107
3 Results……... 108
3.1 *Effect of precipitated corrosion products on oxygen reduction rate*……... 108
3.2 *Morphology of corroded samples after different exposures*…… 110
3.3 *Formation and stability of the precipitated artificial corrosion products*... 113
4 Discussion……. 118
4.1 *Influence of Mg and Al on the stability of Zn-containing corrosion products*…….. 118
4.2 *Effect of precipitated corrosion products on oxygen reduction rate*……... 120
5 Conclusion…… 121
References…… 122
Chapter VI – Comparative study of ZnMgAl coatings with different compositions……. 125
Abstract…… 127
1 Introduction…….…….. 128
2 Experimental……. 129
2.1 *Materials*…….. 129
2.2 *Corrosion tests*……. 130

2.3 *Corrosion damage characterization*……..……. 131
2.4 *Corrosion products characterization*……... 131
2.5 *Electrochemical experiments*……... 132
3 Results……... 132
3.1 *Corrosion rates from different accelerated corrosion tests*……. 132
3.2 *Corrosion products*…….. 133
3.3 *Corrosion products distribution*……..…… 135
3.4 *Electrochemical behavior – effect of corrosion products on oxygen reduction rate*…… 138
4 Discussion……. 140
4.1 *Corrosion rate and corrosion products of ZM coatings in accelerated corrosion tests*…… 140
4.2 *Effect of corrosion products on the corrosion rate of ZM coating*…….. 142
5 Conclusion…… 143
References…… 144
Chapter VII – Conclusion and perspectives...…….…….. 147
Appendix……... 157
Résumé ……. 163
1 Introduction……... 163
2 Objectifs…… 168
3 Structure de la thèse et principaux résultats…….. 168

List of Tables

Chapter I

Table 1. List of the latest ZnMgAl coatings with their respective composition. [1-3,6-8]……... 8

Table 2. Comparison of the different ZnMgAl composition and their corresponding microstructures. "+" represents minor presence of the phase and "++", major presence…….. 9

Table 3. Exposure sites and their environmental conditions of [23-24] studies…… 15

Table 4. Corrosion products found on ZnMg coating on steel comparing to GI. ZHC is simonkolleite…….. 21

Table 5. Corrosion products found on ZnMgAl comparing to GI in different tests. ZHS means simonkolleite; LDH are the layered double hydroxides; HZ is hydrozincite; ZHS are zinc hydroxysulfates……... 21

Table 6. Properties of corrosion products. [33]…….. 25

Chapter II

Table 1. Classification of field exposure environments. As an example, a field categorized as C2 for Zn is less corrosive than another field C5, but at the same time, both fields can be C3 for steel. [10]……... 35

Table 2. Outdoor concentration of some of the most important pollutants in different types of environments. [10]…….. 36

Table 3. Classification of the exposure sites used in this work based on the standard ISO 9223 [10]……... 36

Chapter III

Table 1. Thickness and chemical composition of the coatings…….. 46

Table 2. Composition and concentration of the Rain Water (RW) electrolyte used on the corrosion tests. Average content of real rain water calculated from various references [30-41]……... 47

Table 3. Description of the performed corrosion tests: electrolyte, concentration and duration……. 48

Table 4. Tested solution in titration experiments……... 49

Table 5. Consumed thickness of GI, ZA and ZM after various corrosion tests……. 51

Table 6. Equivalence between the name of corrosion products, its composition and the chosen abbreviation. ……. 52

Table 7. Summary of corrosion products observed by XRD and/or Raman spectroscopy on different samples. …… 56

Table 8. The distribution of Zn, Al and Mg between water soluble and insoluble corrosion products and the mass balance measured after 100 h of a) SST NaCl 1% and b) SST RW 1%. Each value represents an average of 3 measurements (3 different samples with corroded surface of about 160 cm^2 each). Column I represents the total masses of oxidized elements in soluble form, calculated from the concentrations of ions found in the electrolyte collected under the sample during the test and in rinsing water; values in column II show the masses of elements present in insoluble product which are obtained from the analysis of the glycine solution used for corrosion product removal; column IV gives the measured weight loss and the masses of each element in corrosion product expected from the bulk composition in hypothesis of homogenous dissolution (marked by *)…… 58

Chapter IV

Table 1. Thickness and chemical composition of the coatings…….. 78

Table 2. Analytical parameters of sensitivity ($C_{2\sigma}$) for ICP experiment, which are twice the standard deviation of the intensity of the electrolyte not contacted with the sample. ……. 79

Table 3. Anodic reactivity of ZM coating in different electrolytes at the end of anodic polarization (quasi steady-state). Initial pH was adjusted to 8.5 if not indicated. The fractions of soluble Zn and Mg currents in the total current (%) are calculated from the ICP data. All values which are calculated using the methodology presented in section 1.2. are marked by *. The total insoluble current j^{ins} is calculated from the balance equation (3). The fractions of the insoluble currents of elements j_{Zn}^{ins}, j_{Mg}^{ins}, j_{Al}^{ins} are calculated in the hypothesis of homogenous oxidation of the coating (fractions of oxidation currents of Zn, Mg and Al expected as 81%, 7% and 12% respectively). Results from electrolyte number 4) 0.1 M NaCl + 0.1 NaHCO3 are not shown in the Fig……... 81

Table 4. Water insoluble crystalline products detected by XRD on ZM and on ZA after the cyclic polarization tests shown in Fig. 3 - 6.. …….. 89

Chapter V

Table 1. Thickness and chemical composition of the coatings…….. 105

Table 2. Composition and concentration of the Rain Water (RW) electrolyte…….. 106

Table 3. Experimental conditions of the titration experiments, with label used on the figures and number of the figures where they are shown……. 106

Table 4. Equivalence between the name of corrosion products, its composition and the chosen abbreviation……... 107

Table 5. Corrosion products identified on GI and ZM from the polarization experiment. The circled numbers 1 and 2 represent the sampling time (Fig. 2)……. 110

Table 6. Summary of synthesized corrosion products in each titration condition described at Table 3. …….. 116

Chapter VI

Table 1. Thickness and chemical composition of the coatings…….. 129

Table 2. Description of the performed corrosion tests. ……. 131

Table 3. Composition and concentration of (a) Rain Water (RW) electrolyte and (b) modified-RW electrolyte used on the corrosion test described in Table 2……... 131

Table 4. Consumed thickness of GI, ZM1, ZM2 and ZM3 coatings after corrosion tests. …… 133

Table 5. Equivalence between the name of corrosion products, its composition and the chosen abbreviation. ……. 133

Table 6. Summary of corrosion products observed by XRD and/or Raman spectroscopy on different samples…….. 135

Table 7. Corrosion products identified on GI and ZM from the polarization experiment. The circled numbers 1 and 2 represent the sampling time (Fig. 7)……. 140

Appendix

Table A.1. Equivalence between the name of corrosion products, its composition, the chosen abbreviation and label used on the XRD figures. …… 159

List of Figures

Chapter I

Fig. 1. Timeline of Zn-Al and ZnMgAl coating [1-3,6-8]…… 8

Fig. 2. Schema of cross-sections of ZnMgAl alloys produced by hot-dip galvanizing. Binary phase is composed by Zn lamellas (bright color) and Zn_2Mg lamellas (dark colour); and ternary phases by these two together with an Al mesh distributed among them……... 9

Fig. 3. Cross section of ZnMgAl coatings: a) ZM Ecoprotect (ThyssenKrupp), Zn-Mg1-Al1 [6], b) MagiZinc® (Tata Steel), Zn-Mg1.5-Al1.5 [7], c) Corrender (voestalpine), Zn-Mg2-Al2 [10], d) Magnelis (ArcelorMittal), e) Zn-Mg3-Al6 and f) Zn-Mg3-Al11 [Courtesy of ArcelorMittal R&D]. ……... 10

Fig. 4. Improvement of Zn-(1-3 wt.%)Mg-(1-3 wt.%)Al coated steel pre-contaminated samples compared to GI as function of chloride load after 4 weeks exposure in static and cyclic tests. [5] ……... 13

Fig. 5. Environment characteristics in terms of accumulated sulfate and chloride during 30 days of sheltered exposure [20]…… 14

Fig. 6. Simonkolleite structure [36], in which the dark layer is the hydroxyl and the light-color pyramids are the tetrahedrally and octahedrally coordinated Zn…… 23

Fig. 7. Hydrozincite structure [36], in which the dark connected spheres represents the carbonates groups and the pyramids are the tetrahedrally and octahedrally coordinated zinc atoms. ……... 23

Fig. 8. Zinc hydroxysulfate structure [36] in which the dark triangles represent the sulfate groups, and the pyramids are the tetrahedrally and octahedrally coordinated zinc atoms. ……... 24

Fig. 9. LDH structure [37]…… 25

Fig. 10. Packing models of corrosion products with different morphology [41]……. 26

Chapter II

Fig. 1. SEM backscattered electron (BSE) image of uncorroded ZnMgAl coating in with annotated phases. ……. 34

Chapter III

Fig. 1. SEM backscattered electron (BSE) images of uncorroded coatings in cross section with their respective phases: (a) GI, (b) ZM and (c) ZA coating…… 46

Fig. 2. Titration curves of different electrolytes with 1.0 M NaOH at 50 µl/min. The initial volume of the solutions was 50 ml. (a) 0.171 M NaCl, (b) 0.153 M RW, (c) 0.008 M $NaHCO_3$, (d) 0.028 $(NH_4)_2SO_4$, (e) 0.008 M $NaHCO_3$ + 0.028 M $(NH_4)_2SO_4$, (f) 0.117 M RW w/o (NH_4^+ + HCO_3^-)……..... 50

Fig. 3. X-ray diffraction patterns of (a) GI and (b) ZM coatings after a two years natural exposure in three different sites. The detected products are shown by numbers (see Table 6 for identification). Intermediary peaks not labeled in Fig. 4 b correspond to the intermetallic phase Zn_2Mg (number 8)…….... 53

Fig. 4. Raman spectra of the ZM coating after two years of atmospheric exposure. No peak at 3620 cm^{-1}, confirming the absence of $Mg(OH)_2$. No peak at 3480 cm^{-1}, confirming the absence of simonkolleite (ZHC). Peaks at 447, 563 and 580 cm^{-1} correspond to Zn-O bond; 952 and 980 cm^{-1} to sulfates; 1061 cm^{-1} to carbonates; 1355 and 1593 cm^{-1} to amorphous carbon; 3550 cm^{-1} to hydroxides……..... 54

Fig. 5. X-ray diffraction patterns of (a) GI, (b) ZM and (c) ZA coatings after accelerated corrosion tests (lines 2, 8, 9 and 10 respectively from Table 3). The numbers from 1 to 10 on the figures correspond to the detected corrosion products (see Table 6). ……. 55

Fig. 6. SEM images of corroded (a) GI, (b) ZA and (c) ZM cross section after SST WR 1%; (d) is the SEM image of ZM cross section after SST-WR 1% and the detected elements by EDS analysis – Mg is not indentified and only a small amount of Cl is found.. 57

Fig. 7. Schematic illustration of the mechanism of formation of ZnO and LDH in NaCl and RW electrolytes on GI and ZM coatings. The reactions which are possible only on ZM are shown with grey background. Steps shown by numbers: I. Electrochemical reactions at neutral pH; II. Precipitation at medium pH; III. Dissolution at high pH (cathodic Al dissolution, dissolution of basic zinc salts); IV. Formation of ZnO and LDH (drying or concentration increase). In RW electrolyte, the buffering effect of NH_4^+ and HCO_3^- ions can delay step III which can be considered as positive for GI (stabilization of zinc corrosion products) but controversial for ZM (stabilization of zinc corrosion products but delayed formation of LDH). …… 63

Chapter IV

Fig. 1. Evolution of the elemental leaching rate of Zn (j_{Zn}) and of the total current (j_e) for GI coating in various electrolytes during spontaneous dissolution rates before and after applying potential and under applied anodic potential -0.95 V vs. SCE (middle peaks with $j_e > 0$). (a) 0.1 M NaCl at pH 8.5, (b) 0.1 M NaCl + 0.01 M $NaHCO_3$ at pH 8.5, (c) 0.1 M NH_4Cl + 0.1 M $NaHCO_3$ at pH 8.5, (d) 0.1 M NH_4Cl at pH 7..……... 80

Fig. 2. Evolution of the elemental leaching rates of Zn, Al and Mg (j_{Zn}, j_{Al} and j_{Mg}) and of the total current (j_e) from ZM coating in various electrolytes during spontaneous dissolution rates before and after applying potential and under applied anodic potential -0.95 V vs. SCE (middle peaks with $j_e > 0$). (a) 0.1 M NaCl at pH 8.5, (b) 0.1 M NaCl + 0.01 M $NaHCO_3$ at pH 8.5, (c) 0.1 M NH_4Cl + 0.1 M $NaHCO_3$ at pH 8.5, (d) 0.1 M NH_4Cl at pH 7. …….. 81

Fig. 3. Evolution of the elemental leaching rates (j_{Zn} and j_{Mg}) and of the total current (j_e) from ZM coating in 0.1 M NaCl under applied cycles of anodic (A) and cathodic (C) potentials. Only anodic current and dissolution of elements detectable in anodic domain are shown. OC domains represent the spontaneous dissolution rates before and after cycling. Applied potential sequence is C: -1.25 V vs. SCE, A: -0.95 V vs. SCE. …….. 85

Fig. 4. Evolution of the elemental leaching rates (j_{Zn} and j_{Mg}) and of the total current (j_e) from ZM coating in 0.1 M NH_4Cl + 0.1 M $NaCO_3$ under applied cycles of anodic (A) and cathodic (C) potentials. Only anodic currents and Zn and Mg leaching are shown. OC domains represent the spontaneous dissolution rates before and after cycling. Applied potential sequence: C: -1.25 V vs. SCE, A: -0.95 V vs. SCE. ……. 86

Fig. 5. Evolution of the elemental leaching rates of Al (j_{Al}) and of the total current (j_e) from ZM coating in (a) 0.1 M NaCl and (b) 0.1 M NH_4Cl + 0.1 M $NaHCO_3$ under applied cycles of anodic (A) and cathodic (C) potentials. Only cathodic currents are shown. OC domains represent the spontaneous dissolution rates before and after cycling. Applied potential sequence is C: -1.25 V vs. SCE, A: -0.95 V vs. SCE. ……... 87

Fig. 6. Evolution of the sum of elemental leaching rates ($j_\Sigma = j_{Zn} + j_{Al}$), the Al leaching rate (j_{Al}) and the total current (j_e) for ZA coating in (a) 0.1 M NaCl and (b) 0.1 M NH_4Cl + 0.1 M $NaHCO_3$. Applied potential sequence is C: -1.25 V vs. SCE, A: -0.95 V vs. SCE. …….. 88

Fig. 7. Predominant equilibrium species predicted for 2mM Zn^{2+} + 1mM Mg^{2+} + 1mM Al^{3+} + CO_3^{2-} using the Hydra-Medusa software [41] and associated database of equilibrium constants at 25C°. The complexes used in the simulation include (a) for Mg species alone: $Mg_4(OH)_4^{4+}$, $MgOH^+$, $Mg(OH)_2$ (c), with CO_3^{2-}: $MgCO_3$, $MgCO_3$ (c), $MgHCO_3^+$, $MgCO_3.3H_2O$ (c), $Mg_5(CO_3)_4(OH)_2.4H_2O$ (c), $MgCO_3$:$Mg(OH)_2.3H_2O$ (c), MgO (cr); Zn species alone: $Zn(OH)_2$, $Zn(OH)_3^-$, $Zn(OH)_4^{2-}$, $Zn_2(OH)_6^{2-}$, Zn_2OH^{3+}, $Zn_4(OH)_4^{4+}$, $ZnOH^+$, ZnO (cr), with CO_3^{2-}: $Zn(CO_3)_2^{2-}$, $ZnCO_3$, $ZnCO_3$ (c), $ZnCO_3.H_2O$ (c), $ZnHCO_3^+$, $Zn_5(OH)_6(CO_3)_2$ (c); Al species alone: $Al(OH)_2^+$, $Al(OH)_3$, $Al(OH)_4^-$, $Al_2(OH)_2^{4+}$, $Al_3(OH)_4^{5+}$, $AlOH^{2+}$, $Al(OH)_3$ (am), $Al(OH)_3$ (cr), AlOOH (cr); mixed species: $MgAl_2O_4$ (c); (b) including layered double hydroxides (LDH): $Mg_2Al(OH)_6(CO_3)_{0.5}$, $Zn_2Al(OH)_6(CO_3)_{0.5}$ [40]..……... 90

Fig. 8. Intrinsic reactivity of ZnMgAl coating in NaCl and NH_4Cl + $NaHCO_3$ electrolytes for cyclic polarization experiment……... 92

Chapter V

Fig. 1. SEM backscattered electron (BSE) images of uncorroded coatings in cross section with their respective phases……..... 105

Fig. 2. Polarization experiment performed in (a) NaCl and (b) Rain water (RW) [15] electrolyte. Cathodic currents before and after open circuit (OC) exposure on GI and ZM coatings. Numbers 1 and 2 show points at which the experiment was stopped for corrosion product characterization…… 109

Fig. 3. SEM images and EDS analysis of ZM after 100h of SST performed in Rain water (RW) electrolyte. (a) ZM partially corroded: i. corroded ternary phase; ii. preferentially corroded ternary phase (Zn lamellas still metallic); iii. zoomed zone for Fig. (b) . (b) lamellas of the corroded ternary phase of ZM in which the numbered points shows the position of EDS punctual analysis of Fig. (c). (c) EDS punctual analysis: Al is mainly present at the dark lamellas (labeled by even numbers)…….. 111

Fig. 4. (a) Optical micrograph of ZM after five weeks of cyclic VDA corrosion test [26] with NaCl 10 g l^{-1} electrolyte: (i) external layer of precipitated corrosion products; (ii) corroded coating; (iii) metallic coating. **(b)** Raman spectra 'A' obtained at (i) and spectra 'B' and 'C' obtained at (ii). 'A' is identified as LDH; 'B' shows presence of ZHC and HZ; 'C' is identified as HZ…….. 111

Fig. 5. Typical residual microstructure of ZM coating showing residual metallic Al after anodic dissolution at applied potential -0.95 V vs SCE in different electrolytes and following removal of zinc patinas in glycine solution. **(a)** Top view of the remaining coating (Al fiber) after dissolution in 0.171 M Na_2SO_4 . **(b)** Cut edge view of the same sample with EDS analysis showing at (1) the Al fiber forming a mesh or "skeleton" due to the dissolution of Zn and Zn_2Mg lamellas and (2) the filled with resin cavity from Zn dendrites dissolution. **(c)** Top view of the remaining coating (Al fiber) after dissolution in 0.171 M NaCl……... 112

Fig. 6. Titration curves of different electrolytes with 1.0 M NaOH at 50 µl/min. The numbers (i), (ii) and (iii) show the sampling for characterization of the precipitate. **(a)** 0.171 M NaCl, **(b)** 0.171M Na_2SO_4, **(c)** 0.008 M $NaHCO_3$ and **(d)** 0.171 M NH_4Cl solvent in presence of (1) 0.04M Zn^{2+}, (2) 0.04 M Zn^{2+} + 0.02 M Mg^{2+}, (3) 0.04 M Zn^{2+} + 0.02 M Al^{3+}, (4) 0.04 M Zn^{2+} + 0.02 M Mg^{2+} + 0.02 M Al^{3+}……... 114

Fig. 7. SEM images and EDS analysis of recovered precipitated at some steps of the titration experiment: (a) Zn^{2+} + Al^{3+} in 0.171 M NaCl solvent after the second plateau (Fig. 6a, curve 3 i); (b) Zn^{2+}+ Mg^{2+} + Al^{3+} in 0.171 M NaCl solvent after the third plateau (Fig. 6a, curve 4 ii); and (c) Zn^{2+} + Al^{3+} in 0.171 M Na_2SO_4 solvent after the second plateau (Fig. 6b, curve 3 i)……..... 117

Fig. 8. XRD analysis of the precipitated products of Zn^{2+} + Mg^{2+} in 0.171 M NaCl (a.2 iii) at (a) the end of titration experiment and (b) after 48h of stirring. The corrosion products abbreviations are identified in Table 4…….. 118

Fig. 9. Schematic illustration of the formation and transformation of different corrosion products……..... 119

Chapter VI

Fig. 1. Backscattered electron (BSE) images of uncorroded (a) GI, (b) ZM1, (c) ZM2 and (d) ZM3 coatings in cross section with their respective phases…… 130

Fig. 2. X-ray diffraction patterns of (a) GI, (b) ZM1, (c) ZM2 and (d) ZM3 coatings after accelerated corrosion tests described in Table 2. The numbers in the figures correspond to the detected products (see Table 5 for identification)……... 134

Fig. 3. SEM BSE images of GI coating after (a) SST-NaCl, (b) SST-RW and (c) SST modified-RW……... 135

Fig. 4. SEM BSE images of ZM1 coating after (a) SST-NaCl, (b) SST-RW and (c) SST modified-RW……... 136

Fig. 5. SEM BSE images of ZM2 coating after (a) SST-NaCl, (b) SST-RW and (c) SST modified-RW. ……. 137

Fig. 6. SEM BSE images of ZM2 coating after (a) SST-NaCl, (b) SST-RW and (c) SST modified-RW..……. 137

Fig. 7. Evolution of cathodic current $|j|$ during polarization cycles of different coatings as indicated in (a) NaCl and (b) Rain water (RW) [11] electrolyte. The applied cathodic potential (Ec = -1.15 V vs SCE) is alternated with free corrosion at open circuit (OC) potential in order to accumulate corrosion products. Numbers 1 and 2 show the sampling for corrosion products analysis…….……... 139

Chapter VII

Fig. 1. Schematic illustration of the mechanism of formation of ZnO and LDH in NaCl and RW electrolytes on GI and ZM coatings. The reactions which are possible only on ZnMgAl are shown with grey background. Steps of corrosion mechanisms shown by numbers: I. Electrochemical reactions at neutral pH; II. Precipitation at medium pH; III. Dissolution at high pH (cathodic Al dissolution, dissolution of basic zinc salts); IV. Formation of ZnO and LDH. In RW electrolyte, the buffering effect of NH_4^+ and HCO_3^- ions can delay step III which can be considered as positive for GI (stabilization of zinc corrosion products) but controversial for ZM (stabilization of zinc corrosion products but delayed formation of LDH)……... ……... 150

Fig. 2. Schematic illustration of the effect of Mg^{2+} and of the mechanism of formation of LDH in different electrolytes (containing Cl^- and/or NH_4^+ and HCO_3^-)..... 151

Fig. 3. Schematic illustration of the different steps of corrosion products precipitation…. 152

Appendix

Fig. A.1. Climatic chamber used for accelerated corrosion tests. [Courtesy of ArcelorMittal R&D] …… 157

Fig. A.2. Temperature and humidity variation during a one week single cycle of the accelerated corrosion test VDA 233-102 [1]…….... 157

Fig. A.3. Sample desk in natural exposure site in Maizières, France. [Courtesy of ArcelorMittal R&D] ……..... 158

Fig. A.4. Schematic illustration of the flow cell used for the measurement with the AESEC technique. The represented schema shows an anodic polarization, in which i_{total} is the total current measured by the potentiostat; i_{Me} is the elemental dissolution rate of a metal Me, expressed as current and calculated from downstream electrolyte concentration measured with the ICP-OES; and $Q_{insoluble}$ is the quantity of insoluble products (precipitated oxides). ……..... 158

Fig. A.5. XRD patterns of the precipitated artificial corrosion products (Chapter V – section 3.1) by means of titration with 1.0 M NaOH at 50 µl / s in 0.171 M NaCl in presence of Zn^{2+} and/or Mg^{2+} and/or Al^{3+}. The numbers correspond to the corrosion products identified in Table A.1. The numbers (i, ii, iii, iv) represent the sampling time from the titration curves showed in Fig.2 of section 3.1 (Chapter V)……..... 159

Fig. A.6. XRD patterns of the precipitated artificial corrosion products (Chapter V – section 3.1) by means of titration with 1.0 M NaOH at 50 µl / s in 0.171 M Na_2SO_4 in presence of Zn^{2+} and/or Mg^{2+} and/or Al^{3+}. The numbers correspond to the corrosion products identified in Table A.1. The numbers (i, ii, iii, iv) represent the sampling time from the titration curves showed in Fig.2 of section 3.1 (Chapter V)……. 160

Fig. A.7. XRD patterns of the precipitated artificial corrosion products (Chapter V – section 3.1) by means of titration with 1.0 M NaOH at 50 µl / s in 0.008 M $NaHCO_3$ in presence of Zn^{2+} and/or Mg^{2+} and/or Al^{3+}. The numbers correspond to the corrosion products identified in Table A.1. The numbers (i, ii, iii, iv) represent the sampling time from the titration curves showed in Fig.2 of section 3.1 (Chapter V)……. 160

Fig. A.8. XRD patterns of the precipitated artificial corrosion products (Chapter V – section 3.1) by means of titration with 1.0 M NaOH at 50 µl / s in 0.171 M NH_4Cl in presence of Zn^{2+} and/or Mg^{2+} and/or Al^{3+}. The numbers correspond to the corrosion products identified in Table A.1. The numbers (I, ii, iii, iv) represent the sampling time from the titration curves showed in Fig.2 of section 3.1 (Chapter V)……..... 161

List of acronyms and abbreviations

The following table describes the significance of various abbreviations and acronyms used throughout the thesis. The page on which each one is first used and/or defined is also given.

Abbreviation	Meaning	Page
GI	Galvanized steel	7
SST	Salt Spray Test (accelerated corrosion test)	11
AZ	AlZn coated steel, Galvalume® – Al(55 wt. %)-Zn(43.5 wt. %)-Si(1.5 wt. %)	15
PVD	Physical vapor deposition	16
ZHC	Simonkolleite (corrosion product)	16, 23
LDH	Layered Double Hydroxides (corrosion product)	18, 24
ZHS	Zinc hydroxysulphate (corrosion product)	19, 24
ZSC	Gordaite (corrosion product)	19
HZ	Hydrozincite (corrosion product)	23
BZS	Basic Zinc Salts (corrosion products like ZHC, ZHS, HZ)	25
VDA	Verband der Automobiliindustrie – "Association of Automobile Industry", used in this work to represent the accelerated cyclic corrosion test VDA 233-102	35
XRD	X-ray diffraction	37
SEM	Scanning electron microscopy	37
EDS	Energy dispersive spectroscopy	37
AESEC	Atomic Emission Spectroelectrochemistry	38
ICP-OES	Inductively coupled Plasma – optical emission spectroscopy	38
ZM	ZnMgAl coated steel, different compositions are possible	44
ZA	ZnAl coated steel, Galfan® – Zn-Al(5 wt. %)	45
RW	Synthetic concentrated "rain water" electrolyte	47

Introduction

The development of ZnMgAl coatings for steel over the past 30 years mainly aimed to improve the corrosion resistance of Zn-based coatings and reduce the coating thickness. This can be achieved by addition of alloying elements like Al and Mg.

Various ZnMgAl coatings compositions were developed during the last decades. For their evaluation, the accelerated tests are traditionally used in order to compare coatings quicker than natural exposure or in service tests. The last two are more realistic and give more reliable results in terms of corrosion rate, but take much longer time.

Nowadays, practically all available corrosion resistance data for ZnMgAl coatings come from accelerated corrosion tests with high chloride loads. Recent data from natural exposures shows that NaCl-accelerated corrosion tests do not well reproduce the atmospheric corrosion mechanisms. In addition, the literature indicates that ZnMgAl corrosion resistance strongly depends on the corrosive environment. Hence, the first important question is: “What are the most important species in the environment which are crucial for the corrosion mechanisms of ZnMgAl coatings, in order to reproduce specific features of the atmospheric corrosion mechanisms in model tests?” Secondly, the role of these species on the intrinsic reactivity of the coating should be understood.

Another important issue concerns the role of Mg and Al alloying on the mechanisms of corrosion protection in different environments. The literature, discussed in Chapter I, proposed the formation of protective corrosion products containing Mg and Al, as well as the pH buffering effects due to precipitation of Mg and Al hydroxides. These hypotheses were mainly based on the results of accelerated tests in NaCl or Na_2SO_4 environments. Hence, it seems interesting to verify the hypotheses of pH buffering and modification of corrosion products in presence of Al and Mg, to propose, if necessary, complementary or alternative mechanisms for more complex electrolytes in order to understand the formation and the stability of formed products and their role on the modification of coating reactivity.

The last question deals with the role of Mg and Al content for corrosion mechanisms. Although, over the past decade, European steelmakers have developed ZnMgAl coatings of different compositions, the literature describes few studies on the influence of Mg and Al content on corrosion mechanisms. In addition, the microstructure aspect is not discussed. The few articles on the subject are very empirical, with corrosion

results limited to the observation that compositions containing more Mg and Al are more efficient. However, there is no justification presented.

In this context, this PhD aims at a better understanding of ZnMgAl corrosion mechanisms in natural environments through the selection of three specific topics which have been identified as important:

- The role of the different species present in the electrolyte on the elemental steps of the ZnMgAl's corrosion mechanisms (anodic dissolution, oxygen reduction and precipitation);
- The role of Mg and Al on the formation and stability of different corrosion products in more representative electrolyte;
- The common features in corrosion mechanisms of ZnMgAl coatings with different Mg and Al content.

Structure of this PhD

This PhD is organized into 3 parts and seven chapters.

The first part contains this introduction, the first chapter which reviews the state of the art and the second chapter, about the experimental methodology. The first chapter details the state of the art concerning the corrosion mechanisms of the Zn(Mg,Al) coatings in different environments. The most important works are listed and the proposed mechanisms are analyzed in details. The second chapter, "Experimental", describes succinctly the methodology used in this work. The physico-chemical methods used to synthesize and characterize corrosion products and to test the reactivity are briefly reviewed. The principles of accelerated corrosion tests and natural exposure are briefly explained. Finer description of the experimental parameters is given at the beginning of each technical chapter.

The second part, and most important, of the dissertation consists of four technical chapters presented in form of four publications. These chapters aim to answer the specific question asked in introduction.

The third part of the dissertation comprises the last and final chapter, which presents the general conclusions brought by this thesis.

The third chapter, "The role of electrolyte composition on the nature of corrosion products and relative corrosion rates", is essentially focused on the measure of corrosion rate and on the identification of corrosion products after accelerated corrosion tests using

different electrolytes and in different sites of atmospheric exposure. It explains the logic that led us to propose a new electrolyte for accelerated tests, containing ammonium and bicarbonate. This electrolyte simulates the corrosion mechanisms during accelerated tests for which the rate determining features seem to be closer to atmospheric corrosion than in standard tests using NaCl electrolyte. The titration experiments are used to confirm the importance of these two ions for buffering effect of the electrolyte.

The forth chapter "The effect of HCO_3^- and NH_4^+ ions on the intrinsic reactivity of the coating", studies the role of these two specific ions, ammonium and bicarbonate, on the intrinsic reactivity and on the selective phase dissolution of the coating. The anodic and cathodic currents are measured in different electrolytes, comparing the behavior of Zn(Mg,Al) coatings.

The fifth chapter "The role of Mg and Al on the formation and stability of corrosion products and their barrier effect for the oxygen reduction" concerns the role of Mg and Al on the precipitation step in corrosion mechanisms of the ZnMgAl alloy and on the barrier properties of formed corrosion products. The barrier effect of the corrosion products formed on GI and on ZnMgAl, during OC exposure, on oxygen reduction was compared under cathodic polarization. In order to understand the effect of Mg^{3+} and Al^{2+} on the formation and stability of corrosion products containing Zn^{2+}, titration experiments with following XRD characterization were used. The important kinetic effects of alloying elements on the precipitation kinetics were observed in some environments. The distribution of corrosion products on the surface at early stages of corrosion was also studied.

The sixth chapter, "The importance of the microstructure for the selective dissolution and stability of corrosion products", compares ZnMgAl with three different compositions in terms of corrosion rates and formed corrosion products after accelerated corrosion tests as well as the electrochemical behavior in different electrolytes.

The seventh and last chapter gives the general conclusions of this PhD and proposes a corrosion mechanism for the ZnMgAl coatings.

Chapter I

State of the Art

Chapter I – State of the art

This chapter is constructed based on a literature review, considering papers from well-known journals in the area of corrosion, materials and electrochemistry and from international conferences. It is non-exhaustive and additional literature review is made in the introduction of each result chapter.

1 The development of ZnMgAl coated steels in the last decades

In the last decades, large number of researches has been carried out to improve the corrosion resistance of hot-dip galvanized steel sheets (GI) by alloying. This work has led to the development of ZnAl coatings with higher aluminium contents than the alloy used in the conventional galvanizing process, with less than 0.2 wt% Al. Some of the notable Zn-Al commercial alloys are Galvalume® (1972) and Galfan® (1980) containing respectively 55 wt.% and 5 wt.% of Al. [1-3]

Nevertheless, the steel industry was concerned about the relatively low level of sacrificial protection afforded by the Zn-Al alloy coatings which otherwise were excellent protective coatings. Then, it was observed that even a limited amount of magnesium, up to 0.1 wt.%, significantly enhances the corrosion resistance of Zn-4.5 wt.% Al alloy coating (Super Zinc) compared to one without Mg (Galfan, Zn-5.0 wt.% Al) in both atmospheric and aqueous environments [4]. This led to the development of several ZnMgAl coatings during the last 30 years. [1-3,5]

The first breakthrough came in 1998 when Nisshin Steel introduced the ZnMgAl alloy coating known as ZAM®. ZAM, with 6 wt.% Al and 3.0 wt.% Mg, not only retained the excellent barrier corrosion resistance of Zn-Al alloy but also showed considerably improved cathodic protection due to the presence of magnesium in the alloy. Since then, Nippon Steel Corporation developed SuperDyma, with 11 wt.% Al and 3.0 wt.% Mg. Fig. 1 shows the timeline of ZnAl(Mg) coating development from 1970 to 2010.

At present, several European steel companies are developing new ZnMgAl alloys with different alloying element contents. The chemical composition of the main coating systems containing zinc, aluminium and magnesium is listed in Table 1. The label Zn-Mg*x*-Al*y* (*x* = weight fraction of Mg, *y* = weight fraction of Al) will be used from now, to simplify the notations, as showed in Table 1 by “label”.

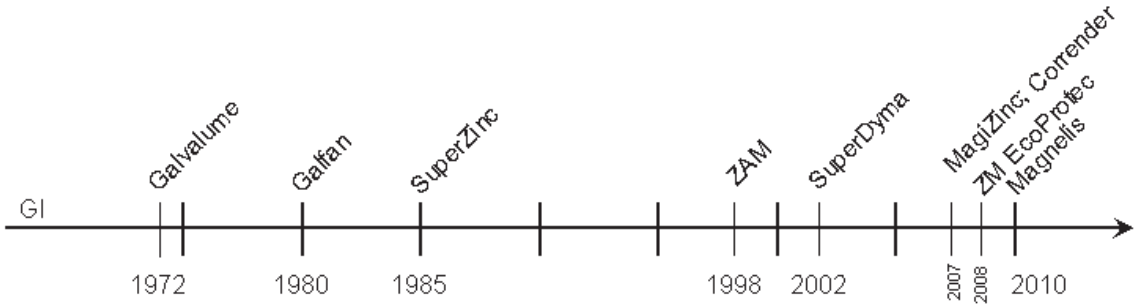


Fig. 1. Timeline of Zn-Al and ZnMgAl coating [1-3,6-8].

Table 1. List of the latest ZnMgAl coatings with their respective composition. [1-3,6-8]

Company	Trade name	Label	Zn (wt.%)	Mg (wt.%)	Al (wt.%)
TyssenKrupp	ZM Ecoprotec	Zn-Mg1-Al1	98.0	1.0	1.0
NipponSteel Corp	SuperZinc	Zn-Mg0.1-Al4.5	95.4	0.1	4.5
Tata Steel	Magizinc	Zn-Mg1.5-Al1.5	97.0	1.5	1.5
Voestalpine	Corrender	Zn-Mg2-Al2	96.0	2.0	2.0
ArcelorMittal	Magnelis	Zn-Mg3-Al3.7	93.3	3.0	3.7
Nisshin	ZAM	Zn-Mg3-Al6	91.0	3.0	6.0
NipponSteel Corp.	SuperDyma	Zn-Mg3-Al11	86.0	3.0	11

2 ZnMgAl microstructure as function of Al and Mg contents

When the hot-dip galvanizing process is applied for a ZnMgAl coated steel sheet, mainly four different solid phases form in the metallic coating: a Zn-rich phase, an Al-rich phase and the two intermetallic phases Zn_2Mg and Mg_2Zn_{11}. They can exist in the form of the binary eutectic Zn_2Mg-Zn, the binary eutectic Zn-Al and/or the ternary eutectic Zn-Al-Zn_2Mg depending upon the composition of the coating (Fig. 2). However, the intermetallic Mg_2Zn_{11} is rarely detected. [1-3]

According to Commenda et al. [9] the rapid solidification of the ZnMgAl coating results in a deviation in the chemical composition of the phases compared to the equilibrium values. Furthermore, the high cooling rates result in a very fine and complex microstructure.

The different ZnMgAl coatings listed in Table 1 have different microstructure – some of them are shown in Fig. 3, with the annotated phases.

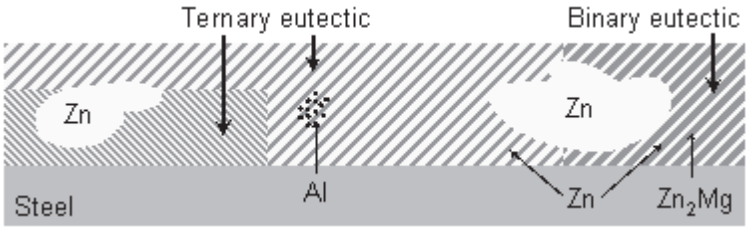


Fig. 2. Schema of cross-sections of ZnMgAl alloys produced by hot-dip galvanizing. Binary phase is composed by Zn lamellas (bright color) and Zn_2Mg lamellas (dark colour); and ternary phases by these two together with an Al mesh distributed among them.

From analysis of Fig. 3, it was possible to construct Table 2 that shows the phase distribution as function of Al and Mg contents in ZnMgAl coatings [Courtesy of ArcelorMittal R&D].

Elvins et al. [11] studied the effect of Mg in ZnMgAl coating containing 4.5 wt.% Al and Mg content between 0.0 and 0.05 wt.%. They observed that the primary zinc dendrites are concentrated close to the steel coating interface, which results from their nucleation on the steel surface. They also noticed that the volume fraction of the primary phase and the number of primary dendrites increase with the magnesium content.

Table 2. Comparison of the different ZnMgAl composition and their corresponding microstructures. "+" represents minor presence of the phase and "++", major presence.

Label	Primary Zn-rich phase	Binary eutectic Zn-Zn_2Mg	Ternary eutectic Zn-Al-Zn_2Mg	Primary Al-rich phase
Zn-Mg1-Al1	++		+	
Zn-Mg1.5-Al1.5	++	+	+	
Zn-Mg2-Al2	++	+	+	
Zn-Mg3-Al3.7	+		++	
Zn-Mg3-Al6			++	+
Zn-Mg3-Al11				++

3 Corrosion resistance in accelerated corrosion tests

3.1 ZnMgAl corrosion resistance at unpainted state

For the evaluation of the corrosion resistance, many accelerated corrosion tests are available [12-16]. The samples are compared in terms of time to red rust appearance (iron

corrosion products, indicating the perforation of the metallic coating and lost of cathodic protection) or in terms of consumed thickness (measured as a difference between the initial mass of the sample and final mass after the corrosion test – higher the consumed thickness, higher the corrosion rate). A review of corrosion tests is described on Chapter II – Experimental.

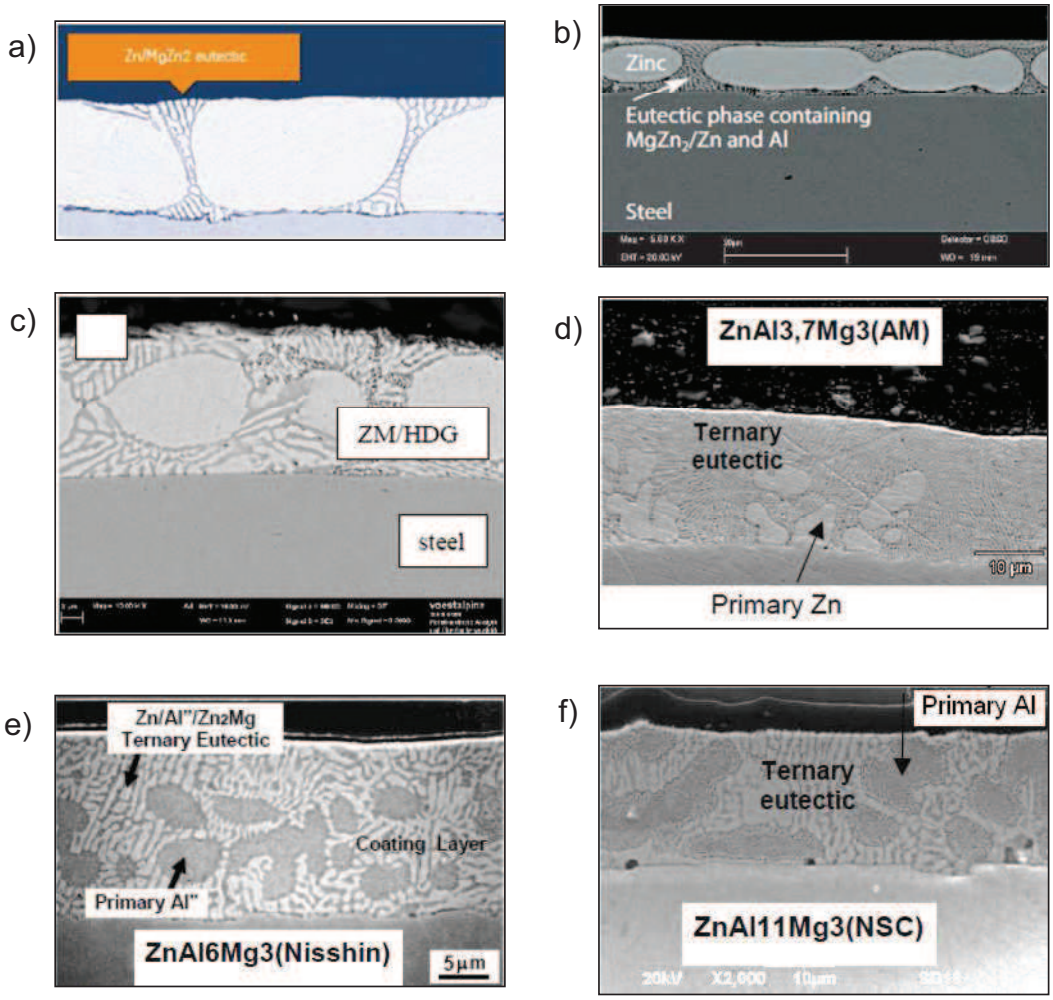


Fig. 3. Cross section of ZnMgAl coatings: a) ZM Ecoprotect (ThyssenKrupp), Zn-Mg1-Al1 [6], b) MagiZinc® (Tata Steel), Zn-Mg1.5-Al1.5 [7], c) Corrender (voestalpine), Zn-Mg2-Al2 [10], d) Magnelis (ArcelorMittal), e) Zn-Mg3-Al6 and f) Zn-Mg3-Al11 [Courtesy of ArcelorMittal R&D].

In this section, some results from the literature are listed, for comparison of the corrosion resistance in different accelerated tests, and then a short conclusion of what we retain is made.

3.1.1 Performance in corrosion tests with high Cl^- loads

S. Schuerz et al. [1] studied the corrosion resistance of Zn-Mg2-Al2 coated steel compared to GI steel in the continuous salt spray test (SST, [12]). They showed that the Zn-Mg2-Al2 corrosion resistance is much higher than that of GI:

- for GI, red rust starts to form after 100h of exposure to the salt solution; after 600h, the samples are completely covered with red rust;

- for Zn-Mg2-Al2, traces of white rust are visible on the surface after 100h exposure; no red rust is observed even after 600h corrosion testing.

These results were confirmed by G. Luckeneder et al. [10], who observed that Zn-Mg2-Al2 enhances the corrosion resistance in the salt spray test by a factor 10 in comparison to a GI coated steel with same thickness.

T. Prosek et al. [17], tested non-painted shaped samples of Zn-Mg1.5-Al1.5 coating, Galfan and GI steel in a cyclic corrosion test (Volvo ACT – with NaCl solution 1 wt.%). The samples were deep drawn in the form of cups, and the test evaluation was done mainly by the time to red rust appearance. They showed that ZnMgAl outperformed both GI and Galfan, with a time to red rust appearance delayed by a factor 3 to 4 compared with the GI product.

According to P. Schouller-Guinet et al. [18], after standard salt spray test (SST), Zn-Mg3-Al3.5 corrosion rate is found 30 times lower than that of GI. In a cyclic corrosion test, the ZnMgAl corrodes 8 times slower than that of GI.

M. Uranaka et al. [19], conducted an evaluation of the corrosion resistance of ZAM coated samples (Zn-Mg3-Al6) comparing to GI samples in an accelerated cyclic corrosion test (JIS H 8502: two hours of salt spray at 35°C with 5% of NaCl, four hours of drying at 60°C and 30% R.H., and two hours of humid at 50°C and 95% R.H.) and also in natural environment conditions in Canada (see section 4 of this chapter). The results of the accelerated cyclic corrosion tests with flat samples showed that, after 180 cycles, GI was completely covered with red rust, and ZAM, in contrast, had only white rust. This result still confirms the outstanding corrosion resistance properties of ZnMgAl compared to GI.

3.1.2 Corrosion test in Cl^- free environments

Scarce information is available in the literature regarding ZnMgAl coating's corrosion resistance in accelerated corrosion test without chloride ions:

G. Luckeneder et al. [10] compared a Zn-Mg2-Al2 coated steel sheet with conventional GI in a chloride-free test (exposure to condensation – determination of resistance to humidity). The results are always in favor of ZnMgAl but no quantitative data are given.

The corrosion resistance in alkaline environment was studied by P. Schouller-Guinet et al. [18]. A corrosion test in ammonia atmosphere with high pH confirms the better corrosion resistance of Zn-Mg3-Al3.5 compared with GI.

3.1.3 Influence of Cl^- content on ZnMgAl corrosion resistance

D. Thierry et al. [5] studied the corrosion behavior of ZnMgAl coatings (Al and Mg between 1 wt.% and 3 wt.% each) in different conditions. Fig. 4 shows the results obtained on samples pre-contaminated with different concentrations of chloride [5]. It appears that the relative performance of ZnMgAl coating compared to GI is dependent on both chloride load and also on the exposure conditions as the interval of salt fog and relative humidity. In general, ZnMgAl shows higher relative corrosion performance in an environment involving a high time of wetness and high chloride load (as neutral salt spray test and cyclic corrosions tests for the automotive industry) compared to conventional zinc coatings (GI). Although ZnMgAl corrosion performance is generally superior to that of GI (independently of the exposure conditions), the lowest improvements was found under natural weathering conditions (marine and rural atmospheres).

3.2 Conclusion on ZnMgAl's corrosion resistance in accelerated tests

All corrosion results involving accelerated tests with high chloride loads (SST or cyclic test) confirm the excellent corrosion resistance of ZnMgAl coatings in such rich chloride atmospheres. Nevertheless, almost no data are available on corrosion tests with free or low chloride content or on different environments than NaCl.

An important result is the one presented by D. Thierry et al. [5] on the influence of chloride content on ZnMgAl resistance, with performance similar to a pure zinc coating for low Cl^- containing atmospheres. However, these data were obtained for the Zn-Mg1.5-Al1.5 coated steel and may be different for other ZnMgAl compositions.

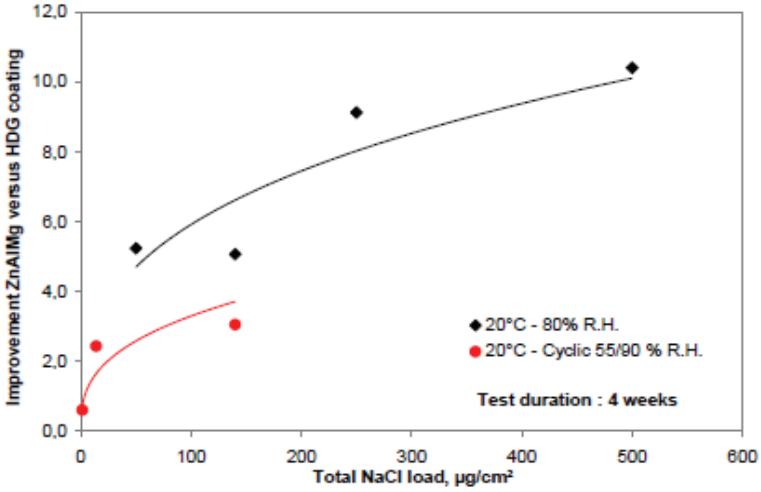


Fig. 4. Improvement of Zn-(1-3 wt.%)Mg-(1-3 wt.%)Al coated steel pre-contaminated samples compared to GI as function of chloride load after 4 weeks exposure in static and cyclic tests. [5]

Corrosion results from accelerated tests in chloride free or with low chloride containing atmospheres are limited and reveal the general lack of knowledge on the real behavior of ZnMgAl coatings in various corrosive environments. It is a target of this PhD to get such knowledge.

4 Corrosion resistance in natural environments

In order to verify the real improvement of corrosion resistance of ZnMgAl coated steels, steel making companies habitually expose their coated sheets in different natural environments, using the standard hot dip galvanizing steel sheet (GI) as a reference material. Useful complementary information may be obtained from on-vehicle tests. The environments are classified as 4 main types: marine (coastal), industrial, urban and rural (country). Fig. 5 shows the classification of the sites according to the accumulated concentrations in SO_4^{2-} and Cl^- ions [20]. Marine sites are in general more aggressive than the others because of high corrosivity of chloride anions. A review of the field exposure tests is presented in Chapter II – Experimental.

The effect of atmospheric pollutants, like sulfur, nitrogen dioxide and ozone, also needs to be considered, even if these pollutants are in general not inserted in most of standard accelerated laboratory corrosion tests. It is known that sulfur dioxide really exceeds the effect of the other air pollutants in the corrosion of zinc, resulting in the formation of zinc sulfates. Ozone plays a significant role in the corrosion of aluminium, while the effect of sulfur and nitrogen dioxide is considered smaller. [21]

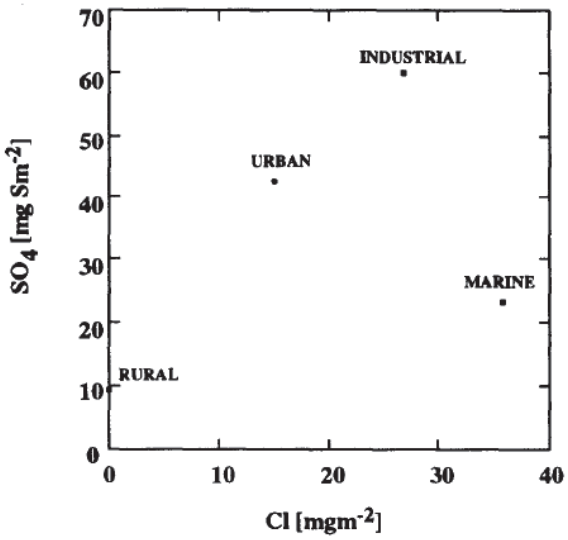


Fig. 5. Environment characteristics in terms of accumulated sulfate and chloride during 30 days of sheltered exposure [20].

The presence of these pollutants can participate in the corrosion mechanisms of the coatings, modifying the formed corrosion products and their barrier properties.

4.1 Data from marine atmosphere

P. Schouller-Guinet et al. [18] quantified the corrosion behavior of full panels and perforated sheets coated with Zn-Mg3.0-Al3.7 after two years of outdoor exposure in Brest marine environment (C5-M site [22] – see Chapter II – Experimental for exposure sites classification). It was shown that the ZnMgAl coated steel sheet has a durability expected to be of three to four times longer than GI. After 1-year exposure, the mean corrosion depth for GI is indeed 1.2 μm against 0.4 μm for the ZnMgAl coating. While analyzing the cut edges of perforated samples, they showed a self healing effect of the Zn-3Mg-3.7Al coated steel sheet, as the samples present 70% of red rust after 3 months of exposure, but this decreased and reached a steady state of 10% after 16-months exposure.

Shimizu et al. [23], investigated the corrosion of ZAM, Zn-Mg3-Al6, after a 5-year exposure in severe marine and rural sites (Table 3), comparing this coating's performance with GI and SuperZinc, Zn-Mg0.1-Al4.5. The corrosion resistance of ZAM is found superior to that of SuperZinc and GI in the coastal exposure sites.

In another study, Shimizu et al. [24] verified different Zn-based coatings on steel (Galfan, ZAM, Galvalume and GI) after 5 years of exposure in coastal and rural environment. There were shaped and flat samples, so the bent and flat portions of the

specimens were analyzed. The natural exposure fields are the same of [23] (Table 3). The authors verified that ZAM generated the smallest amount of white rust, and GI, the highest. The Galvalume samples formed a little red rust in the bent part, caused by cracks in its surface. At the coastal location, all bent portions of the samples showed less corrosion resistance than the flat portions.

Table 3. Exposure sites and their environmental conditions of [23-24] studies.

Atmospheric exposure test location	Environment	Air salinity (mg NaCl/m^2·day)	The yearly mean		Annual rainfall (mm)
			Temperature (℃)	Relative humidity (%)	
Okinawa	Coastal	51	22.7	75	2037
Gunma	Rural	3	14.2	65	1163

4.2 Results in rural/urban atmospheres

N. Shimoda et al. [25] and K. Ueda et al. [26] have investigated the corrosion resistance of SuperDyma, Zn-Mg3-Al11, in natural environments. Comparative corrosion results on bare GI, SuperDyma and Galvalume (AZ) after 5 years in outdoor marine exposure were discussed. The mass loss between SuperDyma and AZ are similar and found 3.8 times lower than on GI.

In a rural exposure site, Shimizu et al. [23] investigated the atmospheric corrosion of ZAM, Zn-Mg3-Al6, after 5 years of exposure, comparing with GI and SuperZinc, Zn-Mg0.1-Al4.5. It is found that ZAM has a better corrosion resistance comparing to the two others coatings, as well as in the marine site described in section 4.1. However, in the same rural location, the authors observed that, on the contrary to the marine location, no difference of corrosion resistance was observed between bent and flat portions for each studied samples [23].

4.3 Results on vehicles

M. Uranaka et al [19] presented the corrosion results of automotive parts made of ZAM, Zn-Mg3-Al6, from vehicles driven during 5 years in Canada. They compared the corrosion resistance of a radiator fan motor cover made of GI and a rear bumper bracket made of ZAM. After 5 year exposure on vehicle, the ZAM part only showed a 4 μm

corrosion depth in the coating layer whereas the GI part was completely corroded, even having a coating layer thicker than the ZAM layer. Furthermore, the GI part was exposed in a region of the vehicle with less severe corrosion environment than the location of ZAM part. The authors also observed an excellent corrosion resistance of ZnMgAl parts in portions where cracks formed in the coating. This favorable behavior is attributed to the formation of dense corrosion products that decrease the corrosion rate.

4.4 Conclusion on corrosion resistance in natural environments

All the results in natural environments (field and on vehicle exposure) confirm the enhanced corrosion resistance of ZnMgAl coatings in comparison with conventional GI coating. Nevertheless, quantitative data are scarce and it is difficult to evaluate the real benefit of ZnMgAl versus GI and or the effect of Al and Mg content on the corrosion resistance improvement. Shimizu et al. [23] was one of few to compare different ZnMgAl compositions in the same corrosion tests – the result shows that more alloyed the coating, better the corrosion resistance. However, only two compositions were tested and there it would be significantly dangerous to extrapolate their results to other compositions.

5 Corrosion mechanisms

The reason for the enhanced corrosion resistance of ZnMg(Al) coated steel is not yet completely explained [1,5,10-11,17]. Many results of corrosion test are published and different interpretations are suggested. However, it is important to notice that only a small number of authors propose real corrosion mechanisms, explaining the different steps of corrosion and different reactions during corrosion.

The majority of works use the protection provided by corrosion products as explanation for the enhanced corrosion resistance of ZnMgAl coatings. The next section of this chapter describes some properties of selected corrosion products.

5.1 ZnMg corrosion mechanism

Kawafuku et al. [27] gave two reasons for the enhanced corrosion performance of ZnMg coatings produced by Physical Vapor Deposition (PVD) in chloride containing environment: the formation of a dense layer of corrosion product simonkolleite (ZHC),

plus the long lasting cathodic protection of the novel coating during corrosion. ZHC is believed to improve corrosion resistance properties and was detected on electrogalvanized samples together with zinc oxide (ZnO), whereas on ZnMg coated samples, only ZHC with no additional corrosion product was detected.

Hosking et al. [28] tested a ZnMg coating produced via PVD technique in a standard automotive laboratory corrosion test comprising salt spraying, drying and humidity cycles. They explain the enhanced corrosion resistance of the coating with the formation of ZHC layer on the surface which acts as a barrier for further corrosive attacks. In addition, the oxygen reduction at cathodes is suppressed by the formation of magnesium hydroxide, $Mg(OH)_2$, which is transformed into a carbonate-containing hydroxide in a next step.

Morishita et al. [29] carried out X-ray diffraction measurements on corroded ZnMg coated steel after corrosion test consisting in dipping the samples in 5 wt.% NaCl solution. They found magnesium oxide (MgO) beside zinc oxide (ZnO), zinc hydroxide ($Zn(OH)_2$) and ZHC on the surface. Comparative samples of pure magnesium, exposed to the same conditions as the Zn-Mg coated specimen, showed magnesium hydroxide ($Mg(OH)_2$) as the only corrosion product. Due to the fact that magnesium hydroxide is very porous and non-adherent, this corrosion product is considered to not provide sufficient corrosion protection and has no influence on the enhanced corrosion performance. The authors supposed that magnesium oxide played an important role in the corrosion mechanism, mostly because of morphological rather than chemical aspects.

P. Volovitch et al. [30] explained the clear beneficial anticorrosion effect of ZnMg alloys on steel as compared to conventional GI by the enhanced stability of ZHC in the ZnMg coating. On GI, ZHC was only observed during the early stages. To explain the protective influence of Mg^{2+} ions formed by the anodic dissolution of the ZnMg coating, the authors propose two mechanisms: buffering of the pH around 10 due to the precipitation of $Mg(OH)_2$ and/or the preferential reaction of Mg^{2+} with carbonate to form $MgCO_3$, thereby removing carbonate ions from the system and stabilizing ZHC and other Zn-based corrosion products.

Prosek et al. [31] tested model ZnMg alloys containing 1-32 wt.% magnesium in comparison to pure zinc and pure magnesium. The samples were contaminated with sodium chloride and exposed to humid air for 28 days. The improved corrosion resistance of Zn-Mg alloys is supposed to be connected with the formation of a magnesium-based

film on the metal surface, which ensures stable passivity in chloride environment and limits the rate of oxygen reduction.

5.2 ZnMgAl corrosion mechanism

Tsujimura et al. [32] analyzed the behavior of ZnMgAl coatings exposed to a cyclic corrosion test including alternating periods of salt spraying, drying and humidity. The ZAM coating, Zn-Mg3-Al6, showed the best corrosion performance of all samples and ZHC was detected as the only corrosion product. The SuperZinc, Zn-Mg0.1-Al4.5, also formed ZnO and $Zn(OH)_2$ besides ZHC. The authors assumed that the main reason for the enhanced corrosion performance was the formation of a Mg-containing ZHC corrosion product. However, the role of Al was not explained.

Uranaka et al. [19] explained that the reason of the excellent ZAM corrosion resistance at cut edges is the formation of dense Zn-based corrosion products, suppressing oxygen reduction. As Tsujimura et al. [32], they observe that ZnO is the main corrosion product on GI steel, and that ZHC is dominant at ZAM surface. Concerning the automotive parts exposed to natural environments, the ZAM part showed dense zinc corrosion products containing Mg and Al.

Schuerz et al. [1] concluded that even after short exposure times to a salt spray test (SST) the entire metallic ZnMgAl coating is transformed into a stable aluminium-rich oxide layer, which adheres on the steel substrate and protects it against corrosive attack. This protecting layer was considered extremely long lasting and the main reason for the enhanced corrosion resistance of the ZnMgAl coating in comparison to GI in NaCl-containing environment. According to them, the transformation of the metallic ZnMgAl coating into the Al-rich oxide layer is the key reaction in the corrosion process and necessary for the enhancement of the corrosion resistance of this coating system. However, no explanations were given to the role of Mg.

G. Luckeneder et al. [10] investigated the corrosion mechanism of a Zn-Mg2-Al2 coated steel and they attributed the improvement of the corrosion resistance to a stable Al-rich layer formed during the first stages of corrosion, the layered double hydroxides (ZnAl-LDH) – that is compact and well adherent. Once more, the role of Mg was not explained.

Shimoda et al. [25] studied the SuperDyma, Zn-Mg3-Al11, in natural exposure for five years at country environment: they also showed ZnAl-LDH as the main corrosion

product, instead of ZnO and zinc hydroxycarbonates or zinc hydroxysulfate found on GI. The role of Mg was not clarified.

Ueda et al. [26] studied the SuperDyma pre-painted samples in natural environment (semitropical coast district) and the analysis of corrosion products after removing the paint film showed ZHC and Gordaite (ZSC), $NaZn_4(SO_4)Cl(OH)_6.6H_2O$. Near cut edges, the analysis shows ZnAl-LDH as well. $Mg(OH)_2$ and $Zn(OH)_2$ were also identified on the exposed cut edge, so the authors explain that the dual corrosion product layer under the paint film and the Mg-rich product on the exposed steel cut edge are the primary factors to enhance the cut edge corrosion resistance of the pre-painted SuperDyma.

P. Volovitch et al. [25], studied the corrosion mechanism of Zn-(16 wt.%)Mg (produced by PVD) and Zn-Mg3-Al3.7 (produced by hot dip galvanization) coatings in Cl^- and Cl^--free atmospheres. Their results demonstrated a clear beneficial anti-corrosion effect of ZnMgAl alloys as compared to GI for both types of environments. This improvement is attributed to the synergistic effect of the two alloying elements: Mg and Al. The mechanism of their action is complex and seems to be different at different stages of corrosion. Qualitative analysis of the corrosion products indicate that ZHC and zinc hydroxyl-sulfate (ZHS) are stabilized on the ZnMg and ZnMgAl coatings throughout the cyclic corrosion test exposure in different atmospheres, and also ZnAl-LDH on ZnMgAl, while they are not observed on GI coating at advanced stages of corrosion.

On the basis of thermodynamic equilibrium calculations, P. Volovitch [25] proposed that ZHC and ZHS compounds are stabilized in the presence of Mg^{2+} by the reaction of this ion with anions that could form soluble or low protective complexes with Zn (CO_3^{2-} and excess SO_4^{2-}). The role of Al is also explained: in the early stages of corrosion Al remains on the coating in an insoluble form; when the surface pH increases sufficiently for Al dissolution to occur, the presence of Al^{3+} in the solution inhibits corrosion by two different mechanisms: (1) by buffering the pH of the electrolyte due to the precipitation of $Al(OH)_3$, thereby preventing the dissolution of Zn-based corrosion products into soluble hydroxide complexes and promoting the formation of ZHC in place of ZnO; and (2) by promoting the formation of LDH, in accordance with the works described above ([1,10,25-26]), which seem to have interesting properties for corrosion protection. The authors explain that the barrier properties of LDH seem to be of the same nature of ZHC: plate-like morphology, low electron density and layered structure with difficult ion-transfer through the layer.

Sohn et al. [4] tested the corrosion behavior of Zn-Zn_2Mg eutectic structure in a ZnMgAl coating, and they observed that, in a SST with NaCl, Zn_2Mg phase dissolves first in the binary eutectic structure. This phenomenon could be a source of corrosion products containing magnesium and it is possible that it improves the corrosion resistance of the coatings.

D. Thierry et al. [5] studied the behavior of ZnMgAl coatings on steel sheets in natural exposure, and proposed that the role of Mg is probably linked to a decrease of alkalinity of the cathodes and the formation of magnesium hydroxycarbonates and possibly of magnesium hydroxychloride at the anodes. It is also explained that magnesium is preferentially dissolved independently on the exposure conditions resulting in a lower surface pH, what results in a very high relative performance of ZnMgAl coating compared to GI. They also affirm that in presence of Al, different types of LDH may be formed and due to their high ion exchange properties and compactness may result in lower corrosion rates.

5.3 Conclusion on corrosion mechanisms

The common point of the majority of papers is that the corrosion resistance of ZnMgAl coatings is essentially due to the formation of protective corrosion products which main effect is to lower oxygen access to the metallic surface.

Tables 4 and 5 are a summary of the main corrosion products that form on ZnMg and ZnMgAl, respectively, in accelerated corrosion tests and in natural atmosphere conditions. This comparison shows similarities and discrepancies in the corrosion mechanism analysis.

- In accelerated corrosion tests with high Cl^- loads, the main shared viewpoint is that ZnMgAl contributes to the formation of protective corrosion products as ZHC and ZnAl-LDH, and in the same time, suppress the formation of poorly protective ZnO. Nevertheless, some other researchers have a completely different analysis and attribute the protective effect to the formation of Mg-containing corrosion products.
- In field atmosphere, similarities are observed between the corrosion products formed in marine environment and Cl^- based accelerated test. In rural or urban environments, ZHC is rarely observed and the benefit of ZnMgAl is mainly attributed to ZnAl-LDH and the absence of ZnO.

Table 4. Corrosion products found on ZnMg coating on steel comparing to GI. ZHC is simonkolleite.

ZnMg	Main corrosion products on ZnMg	Main corrosion products on GI
Kawafuku [18]	ZHC	ZHC + ZnO
Hosking [19]	ZHC + $Mg(OH)_2$	
Morishita [20]	MgO + ZnO + $Zn(OH)_2$, ZHC	
Volovitch [21]	ZHC + $MgCO_3$	
Prosek [22]	Passive Mg-based film	

Table 5. Corrosion products found on ZnMgAl comparing to GI in different tests. ZHS means simonkolleite; LDH are the layered double hydroxides; HZ is hydrozincite; ZHS are zinc hydroxysulfates.

Company	Accelerated test (high Cl^-)		Natural or field exposure			
			Marine site		Urban/rural sites	
	ZnMgAl	GI	ZnMgAl	GI	ZnMgAl	GI
Nippon Steel Co. [16,17]			ZHC + ZnAl LDH (underpaint)	Red rust (after 9 years)	ZHC + ZHS + HZ + LDH (no ZnO)	ZHC + ZHS + HZ + ZnO
Nisshin [11,15]	ZHC + Mg-containing ZHC	ZnO	ZHC + LDH + HZ (no ZnO)	ZHC + HZ + ZnO	ZnAl-LDH (no ZnO, no ZHC)	HZ + ZnO
ArcelorMittal [21]	ZHC + LDH (no ZnO)	ZHC + HZ + ZnO				
Voest [1,8]	LDH	Not analyzed				
French Corrosion Institut [4]	Mg-hydroxy-carbonate + LDH + stable ZHC + HZ	ZHC + HZ + ZnO				

If the literature is quite large concerning the identification of efficient corrosion products, almost no information is given on the role of Mg and Al in the formation of corrosion products. This points out the lack of chemical-physical analysis in most of articles. Furthermore, no information is available to really understand the effect of Mg and Al contents in the coating on the corrosion resistance and on the nature of corrosion products that form in the different corrosive environments.

6 Corrosion products properties

As described above, the corrosion products are considered to play an important role for the enhancement of the corrosion resistance of the coatings. Compact corrosion products are able to prevent the oxygen access to the metallic surface and thus to reduce the oxygen reduction rate, which is the main reaction controlling the corrosion rate of the coating in neutral environments.

The corrosion rate of a metal is limited by the transport of oxygen in the electrolyte film and by the formation of corrosion products that retains the access of oxygen on the metallic surface [34]. In order to understand how the transport of oxygen can be influenced by the layer of corrosion products, it is possible to use a variation of Fick's Law (Eq. 1):

$$N_{O_2} = k_{mf} c_{O_2,b} \quad (1)$$

in which N_{O_2} is the flux of oxygen at the surface, c_{O2} is the oxygen solubility and K_{mf} is a coefficient characterizing both transport of oxygen via convection in the electrolyte film (K_m) and inside the corrosion products layer (K_f), considering the diffusion coefficient of oxygen (D_{O_2}), the electrolyte film/solid layer thickness (δ) and the porosity (θ_p) of the solid layer:

$$\frac{1}{k_{mf}} = \frac{1}{k_m} + \frac{1}{k_f} \text{ with } k_m = \frac{D_{O_2}}{\delta} \text{ and } k_f = \frac{D_{O_2}\theta_p}{\delta_f} \quad (2)$$

Therefore, one can notice that the porosity of the corrosion products layer is a determinant factor on the flux of oxygen that will have access to the metallic surface and therefore, govern its corrosion rate.

Another important parameter that is considered to influence the corrosion rate is the permeability of the corrosion product layer, which depends on the possibility of ion-transfer. The structure of the crystals and the bond nature between the layers that form the corrosion products (in case of crystalline ones) is determinant for the permeability. The most common corrosion products detected on Zn(Mg,Al) coatings, zincite (ZnO), simonkolleite (ZHC), hydrozincite (HZ), zinc hydroxysulfate (ZHS) and layered double hydroxides (LDH) are described above:

- Zinc oxides and hydroxides: zinc oxide, called zincite, ZnO, is a product that may be formed instantaneously on metallic zinc in dry air and room temperature. Zincite has a hexagonal cell structure. Zinc hydroxides are possibly formed in humid air. There are several forms of zinc hydroxides, the most common detectable corrosion product of zinc is

ε-$Zn(OH)_2$, Wulfingite. The cell structure is orthorhombic and is built up from tetrahedrally coordinated zinc atoms forming a three-dimensional network with hydroxyl ions. [35-36]

- Simonkolleite (ZHC), $Zn_5(OH)_8Cl_2.H_2O$: the structure, shown in Fig. 6, consists in electrically neutral sheets of both octahedrally and tetrahedrally coordinated zinc atoms, held together by weak O-H ··· Cl bonds. Chlorine atoms are located in each top corner of the zinc tetrahedron.

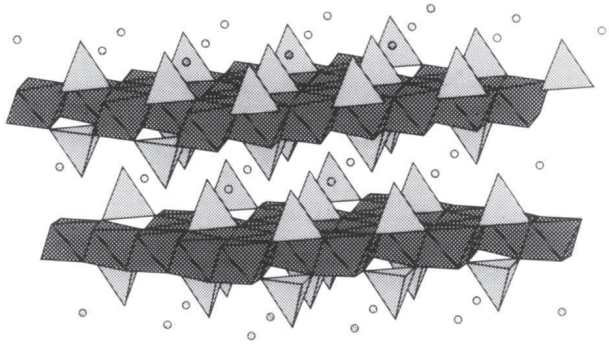


Fig. 6. Simonkolleite structure [36], in which the dark layer is the hydroxyl and the light-color pyramids are the tetrahedrally and octahedrally coordinated Zn.

- Hydrozincite (HZ), $Zn_5(CO_3)_2(OH)_6$: shown in Fig. 7, is very similar to simonkolleite, with a sheet structure consisting of both octahedrally and tetrahedrally coordinated zinc atoms, but they are held together by carbonate ions. Carbonate ions can easily be replaced by hydroxyl ions and also by chloride ions, which results in changes in the lattice such as disordering. [36]

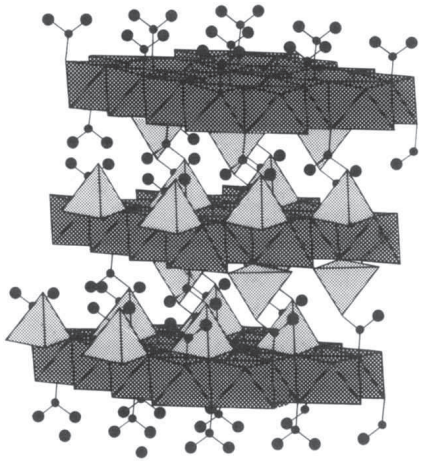


Fig. 7. Hydrozincite structure [36], in which the dark connected spheres represents the carbonates groups and the pyramids are the tetrahedrally and octahedrally coordinated zinc atoms.

- Zinc (hydroxy-)sulfate: zinc sulfates are water soluble but also common as corrosion products in natural environments very loaded in SO_2. They have monoclinic structure and are found to have four or six water molecules. Zinc hydroxyl-sulfates are also found with different water molecules, having a triclinic cell structure, as shown in [35]. As ZHC and HZ, they have layered structures with octahedrally and tetrahedrally coordinated zinc atoms (Fig. 8). Sulfate groups are connected on the neutral sheets that are held together by strong hydrogen bonding. [36]

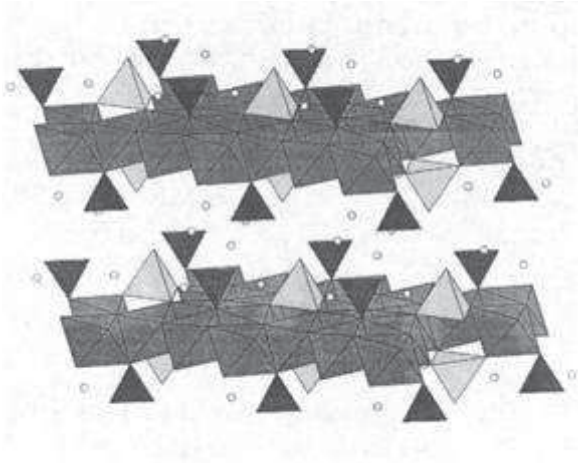


Fig. 8. Zinc hydroxysulfate structure [36] in which the dark triangles represent the sulfate groups, and the pyramids are the tetrahedrally and octahedrally coordinated zinc atoms.

- Layered double hydroxides (LDH): this type of corrosion product differs from the others described above (ZHC, HZ, ZHS) by its double layered structure, the others being basic layered hydroxides. The LDH layered structure may have wide chemical compositions (due to variable isomorphous substitution of metallic cations), variable layer charge density, ion-exchange properties and reactive interlayer space. They also demonstrate anion-exchange properties. As hydrotalcite, $Mg_6Al_2(OH)_{16}CO3.4H_2O$, is one of the most representative mineral of the group, LDH are also called 'hydrotalcite-like compounds' (HTlc). The structure of hydrotalcite is related to that of brucite, $Mg(OH)_2$, in which some of the Mg^{2+} cations in the layer structure were replaced by Al^{3+}. Carbonate anions are intercalated between the layers to maintain electroneutrality. The general formulae for other members of the family, based on a combination of divalent and trivalent metal cations, can be written as $[M^{II}_{1-x}M^{III}_x(OH)_2]^{x+}$ $[X_{x/q}.nH_2O]^{x-}$, where $[M^{II}_{1-x}M^{III}_x(OH)_2]$ represents the layer, and $[X_{x/q}\ nH_2O]$ the interlayer composition. Fig. 9 shows the structure of LDH compounds. [37]

In the context of ZnMgAl coatings, LDH may have M^{II} being Zn^{2+} and/or Mg^{2+} and M^{III} as Al^{3+}. The interlayer anion may be CO_3^{2-}, Cl^-, SO_4^{2-}, etc. The variations of these ions may changes the properties of the LDH. Regarding the interlayer anions, the aqueous solubilities of LDH are affected by them; for comparison, carbonate decreases solubility, while sulfate increases it. [38]

Tedim et al. [40] investigated the influence of the Zn^{2+} concentration in solution for the formation of LDH and its corrosion barrier properties: the results showed that thinner layer of LDH demonstrated better corrosion resistance than ticker and more compact layer containing 2 orders of magnitude more Zn.

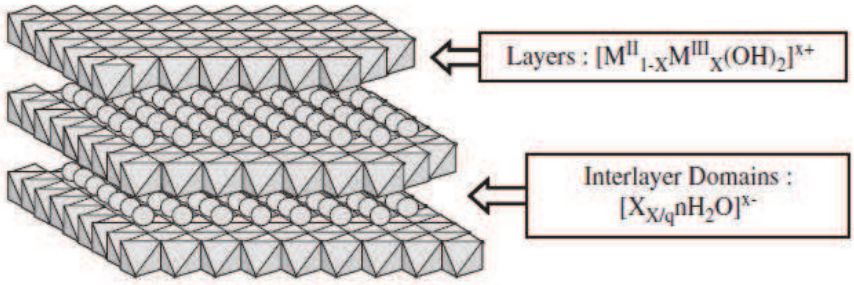


Fig. 9. LDH structure [37].

These different corrosion products, ZHC, HZ, ZHS that together form a group called basic zinc salts (BZS), ZnO and LDH, were investigated by Volovitch et al. [33], who observed their formation on the surface of Zn(Mg,Al) coatings. They summarized different properties, observed in their work or taken from the literature – showed in Table 6.

Table 6. Properties of corrosion products. [33]

Property	ZnO	ZHC	HZ	ZHS	LDH
Density (g/cm^3)	5.56	3.2	3.5	2.0	2.06 (MgAl)
Hardness (Mohs)	4-5	1.5	2-2.5	2-2.7	2 (MgAl)
Crystallinity	Crystalline	Crystalline	Amorphous	Crystalline	Crystalline
Aspect	Granular or eagles	Platelets	Platelets, fibers or aggregates	Platelets	Platelets
pH range for solubility	Acid or base	Acid or strong base	Acid or strong base		Strong acid
pKs	~17	~13.7	~14.6	~16.6	~25.4 (MgAl) ~20.8 (ZnAl)
Permeability for air (10^3 torr/s)	93	About 10	About 10		0.3-30

6.1 Influence of Mg and Al on the properties of corrosion products

In a study of the influence of small additions of Al and Mg (as well as other metals) in the formation of artificial Zn-corrosion products, Ishikawa et al. [39] showed that Al is more efficient in the formation of ZHC than Mg. They also observed that these additions changed the morphology of the Zn-product, increasing its compactness. In another study [41], the artificially produced LDH was showed less air permeable than the large porous agglomerates of ZnO (Fig. 10 shows the different morphologies), and it was suggested that the addition of Mg reduces the size of products' particles, which could contribute to their compactness.

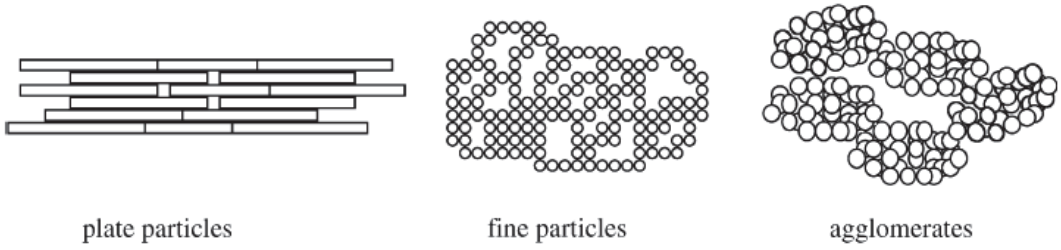


Fig. 10. Packing models of corrosion products with different morphology. [41]

Comparing ZnAl-LDH with MgAl-LDH, the stability of the first one, evaluated in terms of its solubility in water, is higher than the second one. This is in accordance with the solubility constant pK_{sp} values of the corresponding metal hydroxides, because the pK_{sp} of $Mg(OH)_2$ is smaller than that of $Zn(OH)_2$, Mg-based LDH are more soluble [42].

6.2 Conclusion on the corrosion products properties

Corrosion products have different structures and physico-chemical properties. The group of basic zinc salts (BZS) is structured in single layer containing Zn, anionic species and hydroxides. LDH is another group, with two layers and at least two metal anions, as showed in Fig. 9. In the case of ZnMgAl coatings, LDH are called Al-containing corrosion product, as for its formation, Al is imperative at the place of M^{III}.

As described above, the BZS have very similar structures, enabling the anion exchange and ease transformation into other products. ZnO have simpler structures than the others discussed products and is showed to form a porous and air permeable layer. LDH, in contrast, are known to form plate and less permeable particles.

These different properties enables the classification of the corrosion products into more or less protective for the Zn(Mg,Al) coatings – ZnO being the least protective, followed by BZS and then by LDH.

7 Conclusion of the state of the art

The corrosion behavior of ZnMgAl coatings in accelerated corrosion tests appears very dependant on the test conditions. Moreover, some discrepancies exist between the results in accelerated corrosion tests and the results in field exposure, indicating that the corrosion mechanism could be tightly dependent on the nature of the corrosive environment. The development of a new accelerated corrosion test more representative of field exposure seems a good way to improve our knowledge of the corrosion mechanism. In particular, a new test would allow us to quantify the effect of test parameters such as the electrolyte composition.

Some mechanisms have been proposed to explain the role of Mg and Al on the corrosion mechanism of ZnMgAl coatings. They essentially consider the effect of these elements on the precipitation of corrosion products. Further investigations are required to improve our understanding of the corrosion mechanisms and in particular to better explain the role of Mg^{2+} ions on the protection mechanism.

The last topic is related to the influence of Mg and Al content on the corrosion mechanisms. It is recognized that in most corrosive conditions, ZnMgAl coated steels are more corrosion resistant than GI. However the real benefit of high Mg and/or Al content remains unclear and insufficiently explained. Deeper investigations are also necessary on this topic to define the optimal composition of ZnMgAl products.

References

[1] S. Schuerz, M. Fleischanderl, G.H. Luckeneder, K. Preis, T. Haunschmied, G. Mori, A.C. Kneissl "Corrosion behaviour of Zn-Al-Mg coated steel sheet in sodium chloride-containing environment" Corros. Sci. 51 (2009) 2355-2363

[2] M. Dutta, A. K. Halder, S. B. Singh "Morphology and properties of hot dip Zn-Mg and Zn-Mg-Al alloy coatings on steel sheet" Surf. & Coat. Technol. 205 (2010) 2578-2584

[3] R.P. Edavan, R. Kopinski, Corrosion Resistance of Painted Zinc Alloy Coated Steels, Corros. Sci. 51 (2009) 2429-2442

[4] H.-K. Sohn, J-W. Lee, Y. Yoo, J. Min, K.Y. Kim "Corrosion behaviour of Zn-$MgZn_2$ eutectic structure in Zn-Al-Mg coatings" Galvatech '11, Genova, Italy

[5] D. Thierry, T. Prosek, N. Le Bozec, E. Diller "Corrosion protection and corrosion mechanisms of continuous galvanized steel sheet with focus on new coating alloys" Galvatech '11, Genova, Italy

[6] "ZM EcoProtect® - The innovative Coating", brochure of ThyssenKrupp Steel Europe AG (2010), available at www.thyssenkrupp-steel-europe.com

[7] "MagiZinc® - The innovative metallic coating for pre-finished steel", brochure of Tata Steel (2012), available at www.colocoat-online.com

[8] "Development and properties of zinc-aluminum alloy coated steel sheet with high corrosion resistance (Super Zinc)" Nippon Steel Corporation, Transport. Res. Board 25 (1985) pp.29-37

[9] C. Commenda, J. Pühringer "Microstructural characterization and quantification of Zn-Al-Mg surface coatings" Materials Characterization 61(2010) 943-951

[10] G. Luckeneder, M. Fleischanderl, T. Steck, K-H. Stellnberger, J. Faderl "Corrosion mechanisms and cosmetic corrosion aspects of zinc-aluminium-magnesium and zinc-chromium alloy coated steel strip" Galvatech '11, Genova, Italy

[11] J. Elvins et al., The effect of Magnesium additions on the microstructure and cut edge corrosion resistance of zinc aluminium alloy galvanised steel, Corros. Sci. 50 (2008) 1650-1658

[12] ISO 9227:2006 "Corrosion tests in artificial atmospheres – Salt spray tests" July 2006

[13] ISO 14993-2001 "Corrosion of metals and alloys – Accelerated testing involving cyclic exposure to salt mist, 'dry' and 'wet' conditions", September 2011

[14] ISO 16701 "Corrosion of metals and alloys – Corrosion in artificial atmosphere – Accelerated corrosion test involving exposure under controlled conditions of humidity cycling and intermittent spraying of a salt solution", December 2003

[15 Test Method D17 2018 / - - C, "Corrosion test by automatic change of phases of salt spray, dryig and humidity (ECC1)" Standardization of Renault Automobiles – DMI / Service 65810, revision of October 2007

[16] VDA 233-102 "Cyclic corrosion testing of materials and components in automotive construction" June 2013

[17] T. Prosek, N. Larché, M. Vlot, F. Goodwin and D. Thierry" Corrosion performance of Zn–Al–Mg coatings in open and confined zones in conditions simulating automotive applications" Materials and Corrosion 61 (2010) 412-420

[18] P. Schouller-Guinet, C. Allély, P. Volovitch "ZnAlMg: an innovative metallic coating that offers protection in the harshest environments" in: Proceedings of Galvatech '11, Genova, Italy, 2011

[19] M. Uranaka, T. Shimizu "Corrosion resistance of hot-dip Zn-6%Al-3%Mg alloy coated steel sheet used in automotive parts" Galvatech '11, Genova, Italy

[20] I. Odnevall, C. Leygraf "Formation of Zn4Cl2(OH)4SO4.5H2O in an urban and an industrial atmosphere" Corros. Sci., 36 (1994) 1551-1567

[21] S. Oesch and M. Faller "Environmental effect on material: the effect of the air pollutants SO_2, NO_2, NO and O_3 on the corrosion of copper, zinc and aluminium. A short literature survey and results of laboratory exposures" Corr. Sci. 39 (1997) 1505-1530

[22] European standard – French standard, NF EN ISO 9223 "Corrosion of metals and alloys – Corrosivity of atmospheres – Classification, determination and estimation" March 2012

[23] T. Shimizu, F. Yoshizaki, Y. Miyoshi, A. An-doh "Corrosion products of hot-dip Zn-6%Al-3%Mg coated steel subjected to atmospheric exposure" The Iron and Steel Institute of Japan (ISIJ), Tetsu-to-Hagané, Vol. 89 (2003), No. 1

[24] T. Shimizu, F. Yoshizaki "Atmospheric corrosion behaviour of hot-dip zinc alloy coated steel sheet subjected to forming" Galvatech '11, Genova, Italy

[25] N. Shimoda, M. Nakazawa, H. Nomura, Y. Morimoto "Atmospheric corrosion resistance of Zn-11%Al-3%Mg-0.2%Si coated steel" Galvatech '11, Genova, Italy

[26] K. Ueda, A. Takahashi, Y. Kubo, Investigation of corrosion resistance of pre-painted Zn-11%Al-3%Mg-0,2%Si alloy coated steel sheet through outdoor exposure test in Okinawa, Galvatech '11, Genova, Italy

[27] J. Kawafuku, J. Katoh, M. Toyama, K. Ilkeda, H. Nishimoto, H. Sato "Properties of zinc alloy coated steel sheets obtained by continuous vapour deposition pilotline" in: Proceedings of the 5th Automotive Corr. & Prevention Conference, Michigan, United States, October 21–23, 1991

[28] N.C. Hosking, M.A. Strom, P.H. Shipway, C.D. Rudd, Corrosion resistance of zinc–magnesium coated steel, Corros. Sci. 49 (2007) 3669–3695

[29] M. Morishita, K. Koyama, M. Murase, Y. Mori, Improvement in the corrosion resistance of zinc-plated steel by electrodeposition of magnesium from a molten salt, ISIJ Int. 36 (6) (1996) 714–719

[30] P. Volovitch, C. Allély, K. Ogle "Understanding corrosion via corrosion product characterization: I. Case study of the role of Mg alloying in Zn-Mg coating on steel" Corros. Sci. 51 (2009) 1251-1262

[31] T. Prosek, A. Nazarov, U. Bexell, D. Thierry, J. Serak, Corrosion mechanism of model zinc-magnesium alloys in atmospheric conditions, Corros. Sci. 50 (2008) 2216-2231

[32] T. Tsujimura, A. Komatsu, A. Andoh, Influence of Mg content in coating layer and coating structure on corrosion resistance of hot-dip Zn–Al–Mg–Si alloy coated steel sheet, in: Proceedings of the Galvatech '01, Brussels, Belgium

[33] P. Volovitch, T.N. Vu, C. Allély, A. Abdel Aal, K. Ogle "Understanding corrosion via corrosion products characterization: II. Role of alloying elements in improving the corrosion resistance of Zn-Al-Mg coatings on steel" Corros. Sci. 53 (2011) 2437–2445

[34] D. Landolt "Corrosion and Surface Chemistry of Metals" EPFL Press, 2007, first English edition. Originally published in French as Corrosion et Chimie de Surfaces des Métaux, Copyright 1993, 1997, 2003 Presses Polytechinques et Universitaires Romandes. Translated and updated from the revised second French version

[35] I. Odnevall, C. Leygraf "Formation of $NaZn_4Cl(OH)_6SO_4.6H_2O$ in a marine atmosphere" Corros. Sci., Vol. 34, No. 8, pp. 1213-1229 (1993)

[36] I. Odnevall, C. Leygraf "Reaction sequences on atmospheric corrosion of zinc" Atmospheric Corrosion, ASTM STP 1239, W. W. Kirk and Hebert H. Lawson, Eds., American Society for Testing and Materias, Philadelphia, 1995

[37] C. Forano, T. Hibino, F. Leroux, C. Taviot-Guého "Layred Double Hydroxides" in Handbook of Clay Science (2006), Chapter 13.1, pp. 1021, Developm. Clay Sci., Vol. 1

[38] R. K. Allda, A. Navrotsky, H. T. Berbeco, W. H. "Thermochemistry and aqueous solubilities of hydrotalcite-like solids" Science 296 (2002) 721–723

[39] T. Ishikawa, K. Matsumoto, A. Yasukawa, K. Kandori, T. Nakayama, T. Tsubota "Influence of metal ions on the formation of artificial zinc rusts" Corros. Sci. 46 (2004) 329-342

[40] J. Tedim, M. L. Zheludkevich, A. C. Bastos, A. N. Salak, A. D. Lesenkov, M. G. S. Ferreira "Influence of preparation conditions of Layered Double Hydroxide conversion filmeon corrosion protection" Electhochim. Acta 117 (2014) 164-171

[41] T. Ishikawa, M. Ueda, K. Kandori, T. Nakayama "Air permeability of the artificially synthesized Zn-Al-Mg alloy rusts" Corros. Sci. 49 (2007) 2547-2556

[42] C. A. Johnson, F. P. Glasser "Hydrotacilte-like minerals (M2Al(OH)6(CO3)0.5.xH2O, where M = Mg, Zn, Co, Ni) in the environment: synthesis, characterization and thermodynamic stability" Clays Clay Miner., Vol. 51, No. 1, 1-8, 2003

Chapter II

Experimental

Chapter II – Experimental

Based on the literature review presented on Chapter I – State of the art, different techniques were chose for the investigation of the corrosion mechanisms of the coated steel. Accelerated and natural exposure corrosion tests were performed followed by stripping of corrosion products for evaluation of the corrosion rate of the coatings. Post-mortem corrosion products characterization was also realized. Atomic emission spectroelectrochemistry (AESEC) were used for the investigation of phase selective dissolution and intrinsic reactivity of the coatings in presence of different ions. Titration experiments allowed us to verify the buffer effect of the different electrolytes used in the corrosion tests and to synthesize artificial corrosion products. Electrochemical experiments, as cathodic and/or anodic polarizations, helped to evaluate the barrier protection of the corrosion products and to evidence the structure formed by the ZnMgAl coating during the first steps of corrosion.

This chapter consists in giving an overview of the materials and techniques used in this work. Their choice and limitations will be explained, but the details and parameters used in each specific investigation are given in the beginning of the respective result chapter.

1 Materials

The samples used in this work were ZnMgAl coated steel, with various compositions, and galvanized steel (GI) and ZnAl coated steel (ZA) as reference materials. GI and ZA are Zn-based coatings with less than 0.2 wt. % and 5.0 wt. % Al, respectively.

GI and ZA are the standard coatings for steel in the automotive and construction industry. ZnMgAl, as reviewed in the first chapter, is the new alloy intended to replace these standard coatings as they are considered more corrosion resistant. [1-3]

Many compositions of ZnMgAl coatings exist. In this work, we chose three of them in order to be representative of the different types of alloying: one less alloyed (1.5 wt. % Mg and 1.5 wt. % Al), an intermediary one (3.0 wt. % Mg and 3.7 wt. % Al) and a high alloyed coating (3.0 wt. % Mg and 11.0 wt. % Al) are used. The first three result chapters of this manuscript use only the intermediary one for comparison with GI and ZA. The forth and last result chapter make a comparison between them.

Fig. 1 shows a SEM top view image of a ZnMgAl coating with 3.0 wt. % Mg and 3.7 wt. % Al. The main phases formed in this type of coating may be seen: primary Zn (Zn dendrites), binary eutectic Zn-Zn_2Mg, binary eutectic Zn-Al and ternary eutectic Zn-Al-Zn_2Mg.

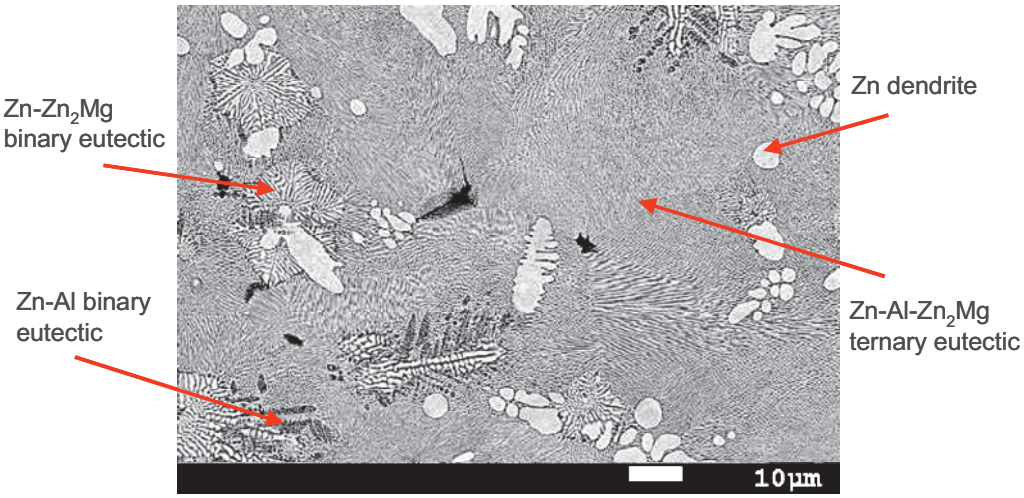


Fig. 1. SEM backscattered electron (BSE) image of uncorroded ZnMgAl coating in with annotated phases.

SEM cross sections images of various ZnMgAl coatings were shown on Chapter I - State of the art, and more details of the samples from this work are showed in the Experimental section of the chapters in which they are considered.

2 Accelerated corrosion tests

Various accelerated laboratory corrosion tests are available to evaluate metallic coatings [4-9]. They consist, in general, to expose the samples to a fog of salt solution inside a climatic chamber (see Appendix, Fig. A.1), controlling the temperature and relative humidity, over a period of time that may vary between some days to some weeks. During the exposure, all parameters are possible to be varied: the fog can be intermittent, the temperature and relative humidity may change, etc. These variations generate cyclic tests [6-9].

An interesting characteristic of the accelerated laboratory corrosion test is that any condition can be tailored to achieve desired levels of corrosion damage. The concentration and/or pH of the salt solution, the duration of the test, etc. can be modified.

The most common salt solution of accelerated corrosion tests for the automotive industry is NaCl in concentrations of 1 or 5 wt.%, in order to represent the most aggressive in service conditions – roads with de-icing salts during winter and coastal regions near the sea. [8-9]

The simplest and faster corrosion tests is the Salt Spray Test (SST), composed by a continuous fog of electrolyte (5 wt.% NaCl solution), at 35°C [5-6]. More complex tests are also available in order to better represent the atmospheric or in service corrosion. In the present work, SST and a cyclic corrosion test, VDA 233-102 [9], were performed. For more details of the cyclic VDA test, see Appendix, Fig. A.2.

The majority accelerated tests performed in this work was the SST, because of their ease of reproduction and faster duration to obtain significant corrosion damage. Few cyclic VDA was also performed in comparison with SST because it is considered to be more representative of the atmospheric corrosion.

3 Natural environments corrosion tests

Natural environment corrosion tests, also called field exposures, are used for the real evaluation of corrosion performance of coated steel. The different environments are classified in terms of corrosivity of zinc and steel and are characterized as being “marine”, “rural”, “industrial” and “urban” sites in function of their content in pollutants like Cl^- and SO_2. Table 1 shows the characterization of the categories, between C1 and CX in terms of corrosivity. The sites are categorized separately for different metals – the same category is used for zinc, steel or aluminium. For example, a site can be C2 for zinc and C4 for steel. Table 2 shows the classification in terms of pollutants.

Table 1. Classification of field exposure environments. As an example, a field categorized as C2 for Zn is less corrosive than another field C5, but at the same time, both fields can be C3 for steel. [10]

Category	Corrosivity
C1	Very low
C2	Low
C3	Medium
C4	High
C5	Very high
CX	Extreme

Three different exposure sites were used in the present work – Table 3 shows their classification and categories. These sites are normalized by standard ISO 9223 [10]. They are managed by ArcelorMittal R&D or by contractors. Fig. A.3 in the Appendix shows a sample desk for natural environment corrosion test.

Details as durations of the tests, preparation of the samples and exposure conditions are given in the Experimental section of the respective result chapter.

Table 2. Outdoor concentration of some of the most important pollutants in different types of environments. [10]

Pollutant	Concentration/deposition (yearly average value)	Source
SO_2	Rural: 2 – 15 (µg/m^3) Urban: 5 – 100 (µg/m^3) Industrial: 50 – 400 (µg/m^3)	The main sources for SO2 are the use of coal and oil and emission from industrial plants.
Cl^-	0,1 – 200 (µg/m^3) depending on geographic situation – in marine atmospheres 300 – 1500 (µg/m^3)	The main sources are the ocean and de-icing of roads.
NH_3	Normally low concentrations: < 20 (µg/m^3) close to source: up to 3000 (µg/m^3)	Fertilization in the agricultural area source and emission from industry and food production can give the highest average values.

Table 3. Classification of the exposure sites used in this work based on the standard ISO 9223 [10].

Exposure site	Classification	Corrosivity category for Zn	SO_2 concentration (µg m^{-2} day^{-1})	Cl^- concentration (mg m^{-2} day^{-1})
Brest, France	Marine-Urban	C3-C4	5 – 10	800 – 1800
Maizières, France	Rural	C2-C3	< 5	< 0.1
Chicago, USA	Urban	C2-C3	5 - 10	< 0.1

4 Corrosion products removal and determination of the corrosion rate

After corrosion test, the corrosion rate of coated steel is determined by Eq. (1) [11]:

$$v_{corr} = \frac{\Delta m}{A \cdot \rho \cdot t} \quad (1)$$

where v_{corr} is the corrosion rate (µm/unit of time), Δm is the mass loss (g) during the corrosion test, A is the exposed surface area (m^2), ρ is the density of the metallic coating (g/cm^3) and t is the exposure time (units of time). This calculation may be used for accelerated and also natural environments corrosion test – the difference will be the unit of time (per cycle or per week for accelerated test and per year for natural environments).

For obtainment of the mass loss during the corrosion test, the samples have to be weighed before exposure and at the end of the test. However, as corrosion products are precipitated on the surface of the samples, their stripping is necessary. The corrosion products removal is standardized by ISO 8407 [12]. For zinc and zinc alloys, a solution of 250 g/L of glycine (NH_2CH_2COOH) in distilled water is used, during 1 to 10 min, depending on the corrosion damage of the sample, at room temperature (20 – 25°C). [11-12]

5 Corrosion products characterization

A combination of techniques is necessary to the completely characterization of the corrosion products: X-ray diffraction (XRD), Raman spectroscopy and Scanning electron microscope (SEM) were used in this work.

XRD is used for crystalline corrosion products general identification. The samples may be the powder of corrosion products collected from the corroded coating or the corroded metallic coating itself. In the last case, attention should be taken to disregard the peaks from the metallic coating. [13-14]

Raman spectroscopy is used as complementary to XRD, in order to identify amorphous products. An interest of this technique is the possibility of microscopic analysis with the use of Raman microscopy – a corroded cross section of a coating is possible to be mapped. [15]

SEM enables the microscopic observation of the corrosion products and of the coating's corrosion profile, through cross section, by secondary electrons (SE) for topographic morphology and by backscattered electrons (BSE) for chemical contrast. Energy-dispersive X-ray spectroscopy (EDS) provides qualitative and semi-quantitative elemental composition of the corrosion products. The EDS analysis is important for the corrosion products identification as XRD characterization presupposes that the present elements are known. [16-17]

6 Titration

Titration technique [18] is used to determine the unknown concentration of an identified analyte or the stoichiometry of the reaction if the concentrations are known. In the present work, two types of titration were used: acid-base and precipitation.

Acid-base titration was used for verification of the pH buffer capacity of the electrolytes from accelerated tests.

Precipitation titration was performed for the synthesis of artificial corrosion products.

7 Atomic emission spectroelectrochemistry (AESEC)

AESEC technique [19-22] consists of an electrochemical flow cell coupled with an Inductively Coupled Plasma Optical Emission Spectroscopy (ICP-OES). The ICP-OES analyses the ionic elements from a solution and gives its concentration. The flow cell is a tool in which we place the metallic sample in order to enable its contact with an electrolyte flow. The reaction between the sample and the aggressive electrolyte occurs, leading to the production of dissolved ions. The electrolyte is transported to the ICP-OES, where its composition is continuously analyzed.

Fig. A.4 in Appendix illustrates the reactions between the sample and the electrolyte as well as the pathway to the ICP-OES.

AESEC is used for the measurement of the elemental dissolution rates of the metallic coatings. In this way we can investigate the phase selective dissolution and the intrinsic reactivity of the coating in different electrolytes.

Detailed explanation of the considerations and parameters used on the AESEC measurements is given in the section Experimental of Chapter IV - The effect of HCO_3^- and NH_4^+ ions on the intrinsic reactivity of the coating.

8 Electrochemical experiments

Classical electrochemical experiments were also performed using a three electrodes cell – saturated calomel electrode as reference electrode, platinum as counter electrode and the sample as work electrode.

The description of the experiments is detailed on the experimental section of the respective result chapter.

References

[1] D. Thierry, T. Prosek, N. Le Bozec, E. Diller "Corrosion protection and corrosion mechanisms of continuous galvanized steel sheet with focus on new coating alloys" Galvatech '11, Genova, Italy

[2] G. Luckeneder, M. Fleischanderl, T. Steck, K-H. Stellnberger, J. Faderl "Corrosion mechanisms and cosmetic corrosion aspects of zinc-aluminium-magnesium and zinc-chromium alloy coated steel strip" Galvatech '11, Genova, Italy

[3] P. Schouller-Guinet, C. Allely, P. Volovitch "ZnAlMg: an innovative metallic coating that offers protection in the harshest environments" in: Proceedings of Galvatech '11, Genova, Italy, 2011

[4] ASTM International B 117 – 09 "Standard practices for operating salt spray (fog) apparatus" (2009)

[5] ISO 9227:2006 "Corrosion tests in artificial atmospheres – Salt spray tests" July 2006

[6] ISO 14993-2001 "Corrosion of metals and alloys – Accelerated testing involving cyclic exposure to salt mist, 'dry' and 'wet' conditions", September 2011

[7] ISO 16701 "Corrosion of metals and alloys – Corrosion in artificial atmosphere – Accelerated corrosion test involving exposure under controlled conditions of humidity cycling and intermittent spraying of a salt solution", December 2003

[8] Test Method D17 2018 / - - C, "Corrosion test by automatic change of phases of salt spray, dryig and humidity (ECC1)" Standardization of Renault Automobiles – DMI / Service 65810, revision of October 2007

[9] VDA 233-102 "Cyclic corrosion testing of materials and components in automotive construction" June 2013

[10] European standard – French standard, NF EN ISO 9223 "Corrosion of metals and alloys – Corrosivity of atmospheres – Classification, determination and estimation" March 2012

[11] European standard – French standard, NF EN ISO 9226 "Corrosion of metals and alloys – Corrosivity of atmospheres – Determination of corrosion rate of standard specimens for the evaluation of corrosivity" March 2012

[12] ISO 8407:2009 "Corrosion of metals and alloys – Removal of corrosion products from corrosion test specimens" November 2009

[13] D. M. Moore, R. C. Reynolds Jr. "X-ray diffraction and the identification and analysis of clay minerals" Second Edition, Oxford University Press, 1997

[14] H. P. Klug, L. E. Alexander "X-ray diffraction procedures: for polycrystalline and amorphous materials" Second Edition, ISBN 0-471-49369-4, Wiley-VCH, 1974

[15] J. Ferraro, K. Nakamoto "Introductory Raman Spectroscopy" Academic Press Inc., New York, 1994

[16] A. E. Vladar, M. T. Postek "The Scanning Electron Microscope" in Handbook of Charged Particle Optics, Second Edition, CRC Press, 2008

[17] P. Echlin, J. Goldstein, L. Sawyer, D. E. Newbury, C. E. Lyman, D. C. Joy E. Lifshin, J. R. Michael “Scanning Electron Microscopy and X-ray Microanalysis” Third Edition, Springer, 2003

[18] S. M. Khopkar, “Chapter 5. Volumetric analysis – Acid-base titrations” and “Chapter 7. Precipitation titrations” in Basic concepts of analytical chemistry, Second Edition, New Age International, 2004, p. 30, p. 54

[19] K. Ogle, J. Baeyens, J. Swiatowska, P. Volovitch “Atomic emission spectro-electrochemistry applied to dealloying phenomena: I. The formation and dissolution of residual copper films on stainless steel” Electrochim. Acta 54 (2009) 5163-5170

[20] M. Mokaddem, P. Volovitch, F. Rechou, R. Oltra, K. Ogle “The anodic and cathodic dissolution of Al and Al-Cu-Mg alloy”, Electrochim. Acta 55 (2010) 3779-3786

[21] J. Swiatowska, P. Volovitch, K. Ogle “The anodic dissolution of Mg in NaCl and Na_2SO_4 electrolytes by atomic emission spectroelectrochemistry” Corros. Sci. 52 (2010) 2372-2378

[22] K. Ogle, M. Mokaddem, P. Volovitch, "Atomic emission spectroelectrochemistry applied to dealloying phenomena II. Selective dissolution of iron and chromium during active - passive cycles of an austenitic stainless steel" Electrochimica Acta 55 (2010) 913-921

Chapter III

The role of electrolyte composition on the nature of corrosion products and relative corrosion rate

M. Salgueiro Azevedo, C. Allély, K. Ogle, P. Volovitch

Corrosion Science (submitted in February 2014)

Corrosion mechanisms of Zn(Mg,Al) coated steel in accelerated tests and natural exposure: The role of electrolyte composition on the nature of corrosion products and relative corrosion rate

Abstract

The corrosion rates and the nature of the corrosion products on Zn, ZnAl and ZnMgAl coatings on steel are determined for field exposures and for accelerated tests using different electrolytes. A new test electrolyte is proposed, containing NH_4^+ and HCO_3^-, which shows an improved correlation with field exposure in particular respecting the relative corrosion rates and the absence or at least delayed formation of layered double hydroxides. The role of buffer effect on the difference in corrosion mechanisms of ZnMgAl coating in accelerated tests using a "standard" NaCl and in the new electrolytes is discussed.

Keywords: Electrogalvanized steel (A); ZnMgAl (A); X-ray diffraction (B); Corrosion product (C); Atmospheric corrosion (C); Corrosion mechanisms (C)

1 Introduction

ZnMgAl (ZM) coatings have undergone extensive development over the past decade. Compared to conventional hot dip galvanized (GI) steel, ZM coated steel has demonstrated a significantly higher corrosion resistance in accelerated corrosion tests with high chloride content [1-14]. Nevertheless, it has also been observed that under conditions of natural exposure, the ratio of corrosion rates of GI and ZM was not as high as that obtained in the "standard" high chloride accelerated tests [10-15] indicating an altered corrosion mechanism. This difference needs to be understood and among different factors which can control the rate determining step, the chemical composition of the electrolyte should play one of the leading roles.

The corrosion of Zn based coatings is usually described by dissolution-precipitation mechanisms [16]. The Zn^{2+} ions, dissolved at anodic areas, form protective corrosion products by being combined with the hydroxide-ions, formed by cathodic reactions, and the anions present in the electrolyte. The inhibiting effect of several patinas, either synthetic or formed during field exposure, on the electrochemical reactivity of the Zn-based coatings has been demonstrated by many authors [1-5,7,10-15]. The precipitation process of different patinas can also buffer the surface pH at slightly alkaline pH which corresponds to the minimal zinc dissolution rate [17]. The effect of various ions present in the environment on the corrosion of Zn-based coating is complex, because both coating's intrinsic reactivity and precipitated corrosion products vary [18-23]. In the presence of Al and/or Mg, oxide layers and complex corrosion products are formed that are not observed on GI [1-7,10-15,24]. Often, the improved corrosion resistance of ZnMgAl and ZnAl coatings is attributed to the presence of these new products, in particular aluminum oxides and layered double zinc-aluminum hydroxides (ZnAl-LDH) with general formula $Zn_xAl_y(A)_m(OH)_n.zH_2O$ (where A is an anion, in studies of atmospheric corrosion often it is carbonate) [1-4,15]. A stabilizing effect of Mg on some zinc corrosion products considered as protective versus their transformation into less protective products was also proposed [1,4,25] by binding the excess anions (carbonates, sulfates, hydroxides…) which are able to form soluble complexes with Zn.

In order to approach the factors controlling corrosion mechanisms of ZnMgAl in natural environments we have undertaken a series of studies in which the corrosion rates, mass balance, intrinsic reactivity, selective dissolution and corrosion products in different environments and exposure conditions are studied. This publication presents the first part

of this work and its first objective is to understand the role of selected ions which are typical in field exposures on the nature of the corrosion products. The second objective is to select key species for a model electrolyte for which the corrosion mechanisms during accelerated tests may be closer to atmospheric corrosion than the mechanisms observed in conventional NaCl tests. To achieve these goals, conventional accelerated corrosion tests were performed in which only the electrolyte was modified. The average consumed thickness (calculated from the weight loss in hypothesis of homogenous dissolution) and the oxide layers formed in different tests were compared for different zinc based coatings. Corroded coatings from field exposures were analyzed in the same manner. On the basis of these results, a new test electrolyte is proposed in which a good correlation is achieved probably indicating similar corrosion mechanisms. The composition of the electrolyte is based upon a statistical study of natural rainwater composition respecting the ratio of the various species while maintaining a total dissolved salt content equivalent to standard corrosion testing electrolytes. The role of different ions on the corrosion mechanism is studied by titration. Some hypotheses about the formation mechanisms of different corrosion products and the variation of the relative ratio of corrosion rates of Zn and ZnMgAl coatings in different environments are proposed.

2 Experimental

2.1 Materials

The coated steel samples were supplied by ArcelorMittal. The reference samples were the conventional hot dip galvanized steel (GI), with coating thickness of 20 µm, and composition Zn-Al(0.2 wt. %), and Galfan® (ZA), with coating thickness of 20 µm and composition Zn-Al(5 wt. %). The ZnMgAl coated steel (ZM) was also prepared by hot dip process with thickness of 20 µm and composition Zn-Mg(3.0 wt. %)-Al(3.7 wt. %). The mean coating composition and thickness are summarized in Table 1. Typical microstructure of the three studied coatings is shown in Fig. 1: GI coating (Fig. 1a) contains homogenous Zn layer; ZM coating (Fig. 1b) is composed by Zn dendrites and a ternary eutectic containing Zn, Al and intermetallic Zn_2Mg; ZA coating (Fig. 1c) contains Zn dendrites in a binary Zn/Al matrix.

For corrosion testing, the exposed surface was 100 mm x 100 mm; prior to exposure, the samples were degreased in an ether solution at room temperature during 20 min and the cut edges were protected with adhesive tape.

Table 1. Thickness and chemical composition of the coatings.

Label	Coating	Thickness	Zn %wt	Al %wt	Mg %wt
GI	Conventional hot-dip galvanized	20µm	99.8	0.2	-
ZM	ZnMgAl	20µm	93.3	3.7	3.0
ZA	Galfan ®	20µm	95.0	5.0	-

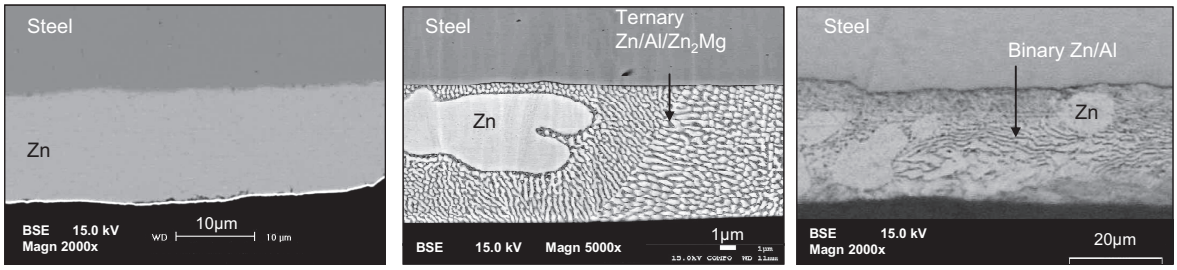


Fig. 1. SEM backscattered electron (BSE) images of uncorroded coatings in cross section with their respective phases: (a) GI, (b) ZM and (c) ZA coating.

2.2 Corrosion tests

For atmospheric corrosion, the samples were exposed in three outdoor stationary sites: marine site of Brest (France), urban site of Chicago (USA) and rural site of Maizières-lès-Metz (France), at an angle of 45°. All sites are normalized by the International Organization for Standardization [26-27].

Continuous salt spray test (SST) [28] and VDA 233-102 cyclic corrosion test (called new-VDA) [29] were performed with samples at an angle of 20° to the vertical. Both kinds of tests were performed with the standard procedure keeping the same temperature, relative humidity, pH and flow rate but with modified electrolyte's composition. The one week cycle of the VDA 233-102 consists of alternating salt spray, wetting, freezing and ambient (or drying) phases, in which the salt solution has pH between 6.5 and 7.2. Continuous salt spray tests (SST) were performed in a SUGA chamber during variable periods of time. The original VDA 233-102 test was performed in

a 15 m^3 chamber supplied by Airtemp; a modified VDA test was performed using an Ascott chamber. Each material was represented by four samples in every test.

Different electrolytes were used in the accelerated tests: NaCl, Na_2SO_4 and synthetic "rain water" (RW), a new electrolyte proposed in this work, with the mean composition (given in Table 2) calculated from the relative fractions of different ions in rain water found in the literature [30-41], but more concentrated than a real rain water. The salt concentration for all tested electrolytes was varied between 0.1 wt. % and 5 wt. %. Table 3 summarizes the accelerated corrosion tests performed in this work.

Table 2. Composition and concentration of the Rain Water (RW) electrolyte used on the corrosion tests. Average content of real rain water calculated from various references [30-41].

	Real rain water				Rain water based electrolyte for corrosion tests		
Ions	Average content (g/l)	Minimum content (mg/l)	Maximum content (mg/l)	% wt	Average content (g/l)	Salts for preparation	Average content (g/l)
Cl^-	0.0042 ± 0.0041	0.0005	0.0138	26.5	2.5	$CaCl_2$	3.91
SO_4^{2-}	0.0036 ± 0.0024	0.0007	0.0092	22.5	2.5	$(NH_4)_2SO_4$	1.82
NO_3^-	0.0021 ± 0.0010	0.0010	0.0045	13.4	1.3	Na_2SO_4	1.77
HCO_3^-	0.0007 ± 0.0022	0.0000	0.0093	4.6	0.5	$NaNO_3$	1.81
Na^+	0.0025 ± 0.0025	0.0003	0.0104	15.6	1.3	$NaHCO_3$	0.69
Ca^{2+}	0.0021 ± 0.0018	0.0002	0.0065	13.3	1.4	Total:	10.00
NH_4^+	0.0006 ± 0.0004	0.0000	0.0016	4.1	0.5		
Total:	0.0158 g/l			100%	10.0 g/l		

An additional measurement of the runoff metals from the ZM samples was made in some tests. The electrolyte was collected via a vessel positioned just below the samples inside the corrosion chamber, during the rinsing of the samples with deionized water before the corrosion product removal and during the stripping of the corrosion products with glycine. The recovered solutions were analyzed by inductively coupled plasma optical emission spectrometer (ICP-OES).

2.3 Corrosion damage characterization

The samples were compared on the basis of their average consumed thickness, calculated from the weight loss, measured as a difference between the initial weight of the uncorroded sample and the final weight of the corroded sample after removing the corrosion products. The stripping of corrosion products was done by dipping the sample in an ultrasonic bath with glycine according to standard ISO 8407 [42]. The weight loss

measurement was made for three samples of each material in each test and the average value was calculated.

Table 3. Description of the performed corrosion tests: electrolyte, concentration and duration.

	Corrosion test	Electrolyte	Concentration	Duration
1	SST-NaCl 0.1%	NaCl	0.1%	100h
2	SST-NaCl 1%	NaCl	1%	100h
3	SST-NaCl 5%	NaCl	5%	100h
4	SST-NaCl 0.4%	NaCl	0.4%	400h
5	VDA-NaCl 1%	NaCl	1%	5 cycles
6	SST-Na_2SO_4	Na_2SO_4	1%	100h
7	SST-RW 0.1%	RW*	0.1%	100h
8	SST-RW 1%	RW*	1%	200h
9	VDA-RW 0.1%	RW*	0.1%	10 cycles
10	SST modified-RW	modified-RW **	1%	200h

(*) See Table 2 for Rain Water (RW) electrolyte's composition.

(**) RW without NH_4^+ and HCO_3^- ions.

2.4 Corrosion product characterization

The corrosion products were characterized by X-ray diffraction (XRD) using the Cu(Ka1) radiation in a PANalytical X'Pert diffractometer, directly on the corroded surface of the samples. The analyzed area was approximately 20 mm x 20 mm. The XRD were collected with angular resolution of 0.02° over the angular range 5–80° (2θ) with 0.3 s acquisition time. The evaluation of the data was done using the HighScore Plus software package, containing the JCPDS (ICDD) database files (version 2013).

Raman spectrometry was performed directly on the corroded samples using a LabRAM Aramis spectrometer, from Horiba Jobin Yvon, with green laser 532 nm. The results were compared with reference spectra taken from the literature [3,43-45] and from the RRUFF™ spectral database for minerals [46].

The samples were also observed by scanning electron microscopy (SEM), using a Gemini 1530 microscope with FEG-source (Scottky-type) and energy dispersive spectroscopy (EDS) for elemental analysis with Si(Li) detector and QUANTAX evaluation software (Bruker AXS). The cross section observations were done on samples mounted in resin, cut and polished mechanically. Before observation, a layer of 10 nm of carbon was sputtered on the cross section in order to ensure the charge evacuation from the surface that could contain non-conducting corrosion products.

2.5 Titration experiments

Titration experiments were done with a Mettler Toledo One Click® Titration G20, using a 1.0 M NaOH solution and the pH was continuously monitored with a combined KCl 3 mol/L glass electrode (Mettler Toledo), calibrated with disposable standard buffer solutions (Merck). The complete pH vs. volume of NaOH was recorded using a Mettler Toledo LabX® light titration software. The tested solutions, listed in Table 4, were prepared with analytical reagent grade (>99.5%) and aerated before beginning of the experiment. The concentration of NaCl and Rain Water (RW) solutions was the corresponding to the concentration used in the accelerated corrosion test from this work (equivalent to 10 g/l). The others solutions were based on the RW concentration. Table 4 summarizes the tested solution and their concentrations. The initial volume of the solutions was 50 ml and the added volume of NaOH was 50 µl every 60 s. The temperature of the solutions during experiment was stable (25 ± 2 °C).

Table 4. Tested solution in titration experiments.

Solution for titration	Concentration
NaCl	171 mmol/L
Rain Water (RW)	153 mmol/L (*)
$NaHCO_3$	8 mmol/L
$(NH_4)_2SO_4$	28 mmol/L
$NaHCO_3$ + $(NH_4)_2SO_4$	36 mmol/L (*)
RW w/o HCO_3^- + NH_4^+	117 mmol/L (*)

(*) Synthetic concentrated rain water electrolyte. For intermediary concentration, see Table 2.

3 Results

3.1 Buffer capacity of rain water

New “rain water” electrolyte (RW) was chosen as a representative synthetic concentrated rain water electrolyte on the basis of a bibliographical study of various references of rain water around the world [30-41]. From the acid-base titration curves of different tested compositions (Fig. 2), it is clear that the behavior of RW electrolyte can be very different from other tested electrolytes due to its buffering capacity, because of the

presence of both NH_4^+ and HCO_3^-. In absence of both of these ions, the acid-base behavior of RW seems to be similar to the behavior of NaCl electrolyte. In order to verify the importance of the pH buffering effect and the dominant role of NH_4^+ and HCO_3^-, we decided to continue the corrosion testing not only with RW electrolyte, but also with an electrolyte without those ions, called, in this work, modified-RW electrolyte.

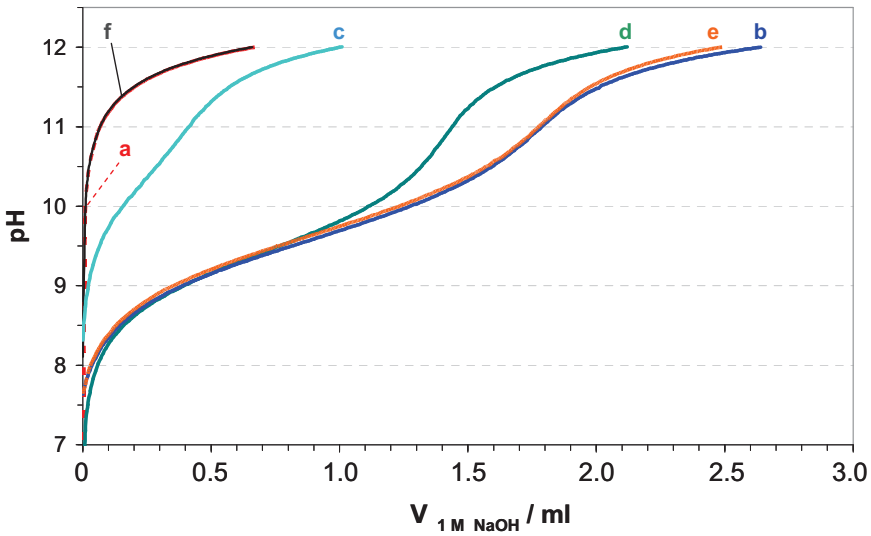


Fig. 2. Titration curves of different electrolytes with 1.0 M NaOH at 50 µl/min. The initial volume of the solutions was 50 ml. (a) 0.171 M NaCl, (b) 0.153 M RW, (c) 0.008 M $NaHCO_3$, (d) 0.028 $(NH_4)_2SO_4$, (e) 0.008 M $NaHCO_3$ + 0.028 M $(NH_4)_2SO_4$, (f) 0.117 M RW w/o (NH_4^+ + HCO_3^-).

3.2 Corrosion rates from different corrosion tests

Table 5 summarizes the consumed thickness calculated from the weight loss result, assuming uniform corrosion, after different accelerated corrosion tests and after two years of atmospheric exposure in different sites – marine Brest (high Cl^-: 700mg/m^2 day), rural Maizières (Cl^-: 0.01mg/m^2 day) and urban Chicago (Cl^-: 0.09 mg/m^2 day). The ratio of corrosion rates (last column in Table 5) between GI and ZM after two years of atmospheric exposure is approximately 3, which is in agreement with previous studies [10-12,14-15]. In contrast, for both accelerated tests, SST and cyclic new-VDA, with NaCl or Na_2SO_4, the ratio between GI and ZM corrosion rates is always higher than 6 (lines 1 to 6), often even higher than 10. The over estimation of ZM coating performance in accelerated tests using NaCl electrolyte is also in agreement with the literature [10-15].

Another important observation is that if the chloride content is increased from 0.1 wt. % (line 1) to 5.0 wt. % (line 3), the increase of the consumed thickness for GI coating

(the difference of more than 5 µm) is much higher than for ZM coating (0.4 µm). This can be interpreted as a higher sensitivity of GI to the chloride content in the electrolyte as compared to ZM. In addition, after two years of the atmospheric exposure, while GI is much less corroded than after 100 h of the accelerated NaCl tests, ZM has almost the same consumed thickness (or is even more corroded) than after 100h of the accelerated NaCl test. All these results demonstrate that the corrosion mechanisms in NaCl and Na_2SO_4 electrolytes can be very different from the field exposure.

Table 5. Consumed thickness of GI, ZA and ZM after various corrosion tests.

	Corrosion test	GI	ZA	ZM	Ratio of consumed thickness	
		consumed thickness (µm)	consumed thickness (µm)	consumed thickness (µm)	GI/ZA	GI/ZM
	Natural exposure - Brest	2.9±0.9	*	1.2± 0.2	-	2.4
	Natural exposure - Chicago	1.4± 0.2	*	0.5± 0.1	-	2.8
	Natural exposure - Maizières	1.0± 0.04	*	0.3± 0.02	-	3.3
1	SST-NaCl 0.1%	5.4± 0.4	0.6± 0.02	0.5± 0.1	9.0	10
2	SST-NaCl 1%	6.9± 0.01	0.5± 0.03	0.3± 0.04	14	20
3	SST-NaCl 5%	11. 2± 0.1	*	0.9± 0.1	-	13
4	SST-NaCl 0.4%	14.0± 1.0	4.0± 0.2	2.3± 0.1	3.5	6.1
5	VDA-NaCl 1%	5.8± 0.7	2.0± 0.2	0.6± 0.1	2.9	9.1
6	SST-Na_2SO_4	3.2± 0.1	*	0.3± 0.01	-	11
7	SST-RW 0.1%	3.6± 0.1	*	1.2± 0.1	-	3.0
8	SST-RW 1%	8.5± 0.6	4. 5± 0.4	3.1± 0.2	1.9	2.7
9	VDA-RW 0.1%	7.4± 0.01	3.4± 0.2	1.9± 0.04	2.1	3.8
10	SST modified-WR	4.7± 1.2	*	0.7± 0.2	-	6.7

(*) Sample not tested in this corrosion test.

In all accelerated tests with RW electrolyte, compared to natural exposure, the corrosion of both GI and ZM was more severe in accelerated tests and the ratios between the consumed thickness of GI and ZM were about 3, which is close to the ratio observed after atmospheric exposure. Interestingly, the ratio for the modified-RW (line 10 from Table 5), which does not contain NH_4^+ and HCO_3^-, is more than two times larger than for the full RW electrolyte. These results confirmed the importance of the buffering effect of HCO_3^- and NH_4^+ ions for corrosion mechanisms.

After 100 h of SST in NaCl (both, 0.1 wt. % and 1 wt. %), the corrosion resistance of ZA coating is close to the corrosion resistance of ZM, but in longer tests (line 4 and 5 in Table 3, 400 h and 5 weeks respectively), ZA loses its resistance compared to ZM. It is

observed that the ratio between GI and ZA from the NaCl-accelerated tests is higher than in RW-tests (about 2). From the literature, ZA compared to GI is on average twice more resistant in atmospheric corrosion exposure [14,24]. The good correlation of the relative corrosion rates suggests that the corrosion mechanisms during accelerated tests in RW electrolyte are closer to the natural exposure than the mechanisms in accelerated tests using NaCl for both, ZA and ZM coatings.

3.3 Corrosion products

3.3.1 X-ray diffraction (XRD) and Raman spectroscopy

XRD and Raman spectroscopy were used in order to identify the corrosion products formed on GI, ZA and ZM samples after the accelerated corrosion tests and also after 2 years of atmospheric exposure (for GI and ZM). Table 6 designates the corrosion products named in this work and shows the equivalence between the corrosion product, its abbreviation and label used on the figures.

Table 6. Equivalence between the name of corrosion products, its composition and the chosen abbreviation.

Label	Name	Abbreviation	Chemical formula
1	Layered double hydroxide	LDH	$M(II)_xM(III)_y(A^-)_m(OH)_n.zH_2O$ $M(II) = Zn^{2+}, Mg^{2+}$, $M(III) = Al^{3+}$ $A^- = CO_3^{2-}, Cl^-, SO_4^{2-}$
2	Simonkolleite	ZHC	$Zn_5(OH)_8Cl_2.H_2O$
3	Zinc hydroxysulphate	ZHS	$Zn_4(OH)_6SO_4.nH_2O$, n=3-5
4	Hydrozincite	HZ	$Zn_5(OH)_6(CO_3)_2.H_2O$
5	Gordaite	ZSC	$NaZn_4(SO_4)Cl(OH)_6.6H_2O$
6	Zincite	ZnO	ZnO
7	Metallic zinc		Zn
8	Intermetallic zinc-magnesium		Zn_2Mg
9	Metallic alumimium		Al
10	Metallic iron		Fe

Fig. 3 shows the X-ray diffraction patterns of GI and ZM from different atmospheric exposure sites – Brest, Chicago and Maizières-lès-Metz – after the two years exposure, while Fig. 4 shows representative Raman spectra for the ZM coating after two years of atmospheric corrosion in the three sites. The corrosion products identified by XRD on the samples from the accelerated tests are shown in Fig. 5. The corrosion products identified after different field exposures and accelerated tests are summarized in Table 7.

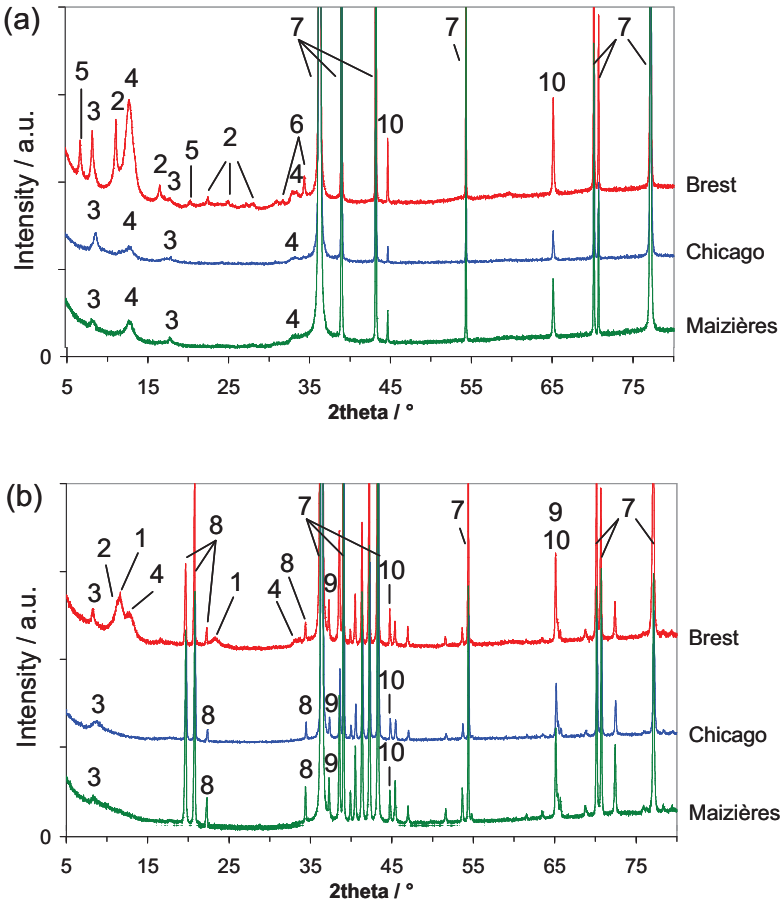


Fig. 3. X-ray diffraction patterns of (a) GI and (b) ZM coatings after a two years natural exposure in three different sites. The detected products are shown by numbers (see Table 6 for identification). Intermediary peaks not labeled in Fig. 4 b correspond to the intermetallic phase Zn_2Mg (number 8).

It may be noted that zinc hydroxysulfate (ZHS) is always present on all samples when the corrosion test contained sulfate ions, while simonkolleite (ZHC, zinc hydroxychloride) is only present on samples from tests containing mostly chloride ions: Brest field exposure and SST-NaCl. In the tests with electrolytes containing multiple anions, the preferential precipitation of ZHS is observed. Gordaite (ZSC, sodium-zinc hydroxysulphate-chloride) is also indentified in some environments: Brest site and SST-

modified-RW. On GI, hydrozincite (HZ) is formed in all tests. Interestingly, no pure Al or Mg oxide/hydroxide species, like brucite, MgO, etc, was detected on ZM coating.

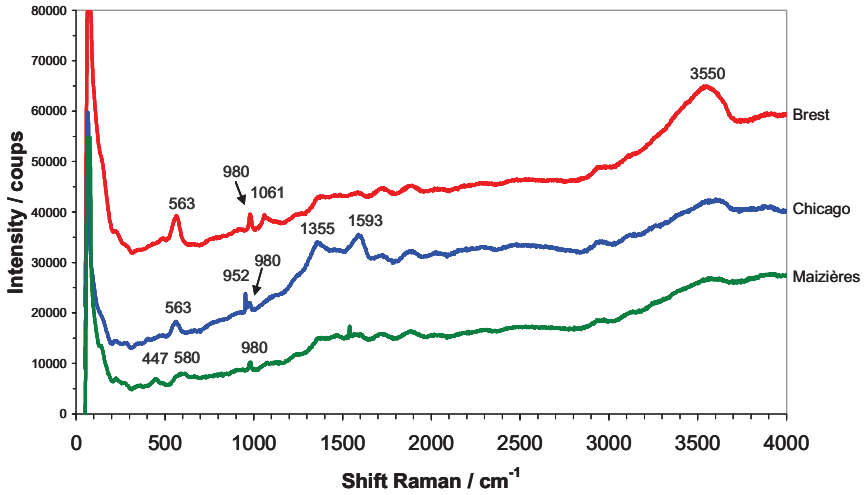


Fig. 4. Raman spectra of the ZM coating after two years of atmospheric exposure. No peak at 3620 cm^{-1}, confirming the absence of $Mg(OH)_2$. No peak at 3480 cm^{-1}, confirming the absence of simonkolleite (ZHC). Peaks at 447, 563 and 580 cm^{-1} correspond to Zn-O bond; 952 and 980 cm^{-1} to sulfates; 1061 cm^{-1} to carbonates; 1355 and 1593 cm^{-1} to amorphous carbon; 3550 cm^{-1} to hydroxides.

Some specific features are observed for ZnO and layered double hydroxides (LDH) which will be discussed below.

3.3.1.1 Detection of Zincite (ZnO)

On GI, zincite (ZnO) is present in all performed tests except on the samples from field exposures in Chicago and Maizières-lès-Metz that can be considered the least aggressive corrosion tests performed in this work. In all conditions of accelerated tests in this work, ZnO was systematically found on ZA coating but not on ZM in the same tests.

3.3.1.2 Detection of Layered Double Hydroxides (LDH)

In ZA and ZM coatings the Zn-Al or Mg-Al layered double hydroxides (LDH) are identified after all accelerated tests except SST-RW 0.1% and 1% (lines 7 and 8 in Table 7). The absence of LDH in SST-RW is not related to the aggressiveness of the corrosion test, because LDH was observed after other SST tests in which the consumed thickness was smaller and in VDA-RW. The variation of the electrolyte composition by itself is also

insufficient to predict the formation or not of LDH because both SST-RW 0.1% and VDA-RW 0.1% were performed with 0.1 wt. % RW electrolyte. The presence of the dry phase and the difference in the test duration – 100h (approximately four days) for SST-RW 0.1% and five cycles (five weeks) for VDA-RW 0.1% – can be considered as important factors. In atmospheric corrosion, LDH is only identified on ZM from Brest (marine site).

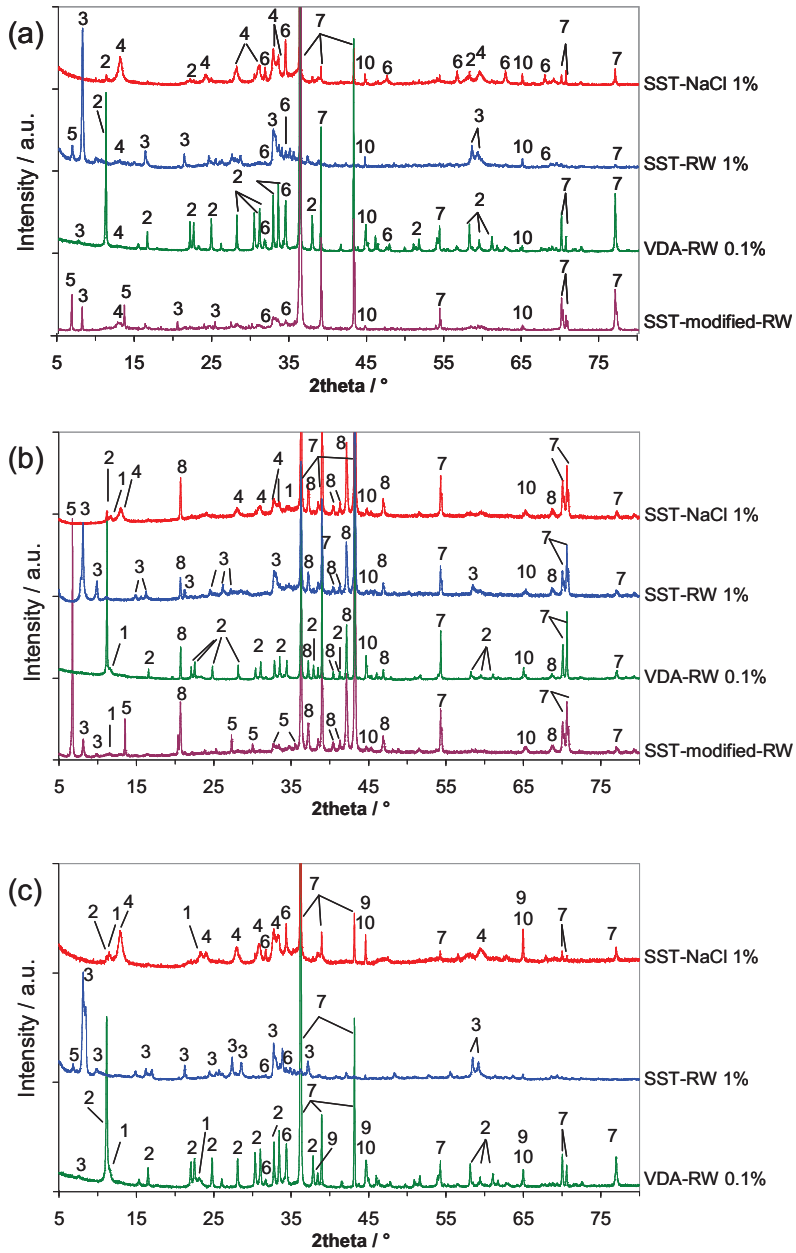


Fig. 5. X-ray diffraction patterns of (a) GI, (b) ZM and (c) ZA coatings after accelerated corrosion tests (lines 2, 8, 9 and 10 respectively from Table 3). The numbers from 1 to 10 on the figures correspond to the detected corrosion products (see Table 6).

Table 7. Summary of corrosion products observed by XRD and/or Raman spectroscopy on different samples.

Corrosion test			Detected corrosion products on the coatings after corrosion tests		
			GI	ZA	ZM
Natural exposure		Brest	ZHC, ZHS, ZSC, HZ, ZnO	-	LDH, ZHC, ZHS, HZ
		Chicago	ZHS, HZ	-	ZHS
		Maizières	ZHS, HZ	-	ZHS
Accelerated tests	1	SST-NaCl 0.1%	ZHC, HZ, ZnO	LDH, ZHC, HZ, ZnO	LDH, ZHC, HZ
	2	SST-NaCl 1%	ZHC, HZ, ZnO	LDH, ZHC, HZ, ZnO	LDH, ZHC, HZ
	3	SST-NaCl 5%	ZHC, HZ, ZnO	-	LDH, ZHC, HZ
	4	SST-NaCl 0.4%	ZHC, HZ, ZnO	LDH, ZHC, HZ, ZnO	LDH, ZHC, HZ
	5	VDA-NaCl 1%	ZHC, HZ, ZnO	LDH, ZHC, HZ, ZnO	LDH, ZHC, HZ
	6	SST-Na_2SO_4	ZHS, HZ, ZnO	-	LDH, ZHS, HZ
	7	SST-RW 0.1%	ZHS, HZ, ZSC, ZnO	-	ZHS
	8	SST-RW 1%	ZHS, HZ, ZSC, ZnO	ZHS, ZnO	ZHS
	9	VDA-RW 0.1%	ZHC, ZHS, HZ, ZnO	LDH, ZHC, ZHS, ZnO	LDH, ZHC, ZHS
	10	SST modified-WR	ZHC, HZ, ZSC, ZnO	-	LDH, ZHS, ZSC

3.3.2 Corrosion product distribution

Fig. 6 shows the corrosion profiles after corrosion test SST-RW 1% of the three coatings: (a) GI, (b) ZA and (c) ZM. The corrosion profiles are very heterogeneous in all samples. The images are representative for both kinds of tests, SST and VDA, and for all tested electrolytes. On ZM the ternary phase Zn/Al/Zn_2Mg is preferentially corroded while Zn dendrites stay intact, which is in accordance with results from ZnMgAl in NaCl accelerated tests, for similar [1] or slightly different [2-3,13] Al and Mg contents**.**

Fig. 6(d) shows the EDS analysis of corrosion products formed on ZM after the SST-RW 1% that did not reveal Mg, which is in accordance with the identified corrosion products described on the section below that did not show Mg-containing corrosion products. Chlorine is only present in a small amount, also in accordance with the identified corrosion products. Al was found on the internal corroded zone, not on the precipitated layer of corrosion products. It is important to note that no Al-corrosion product was found by XRD and Raman on ZM after SST-RW 1% test.

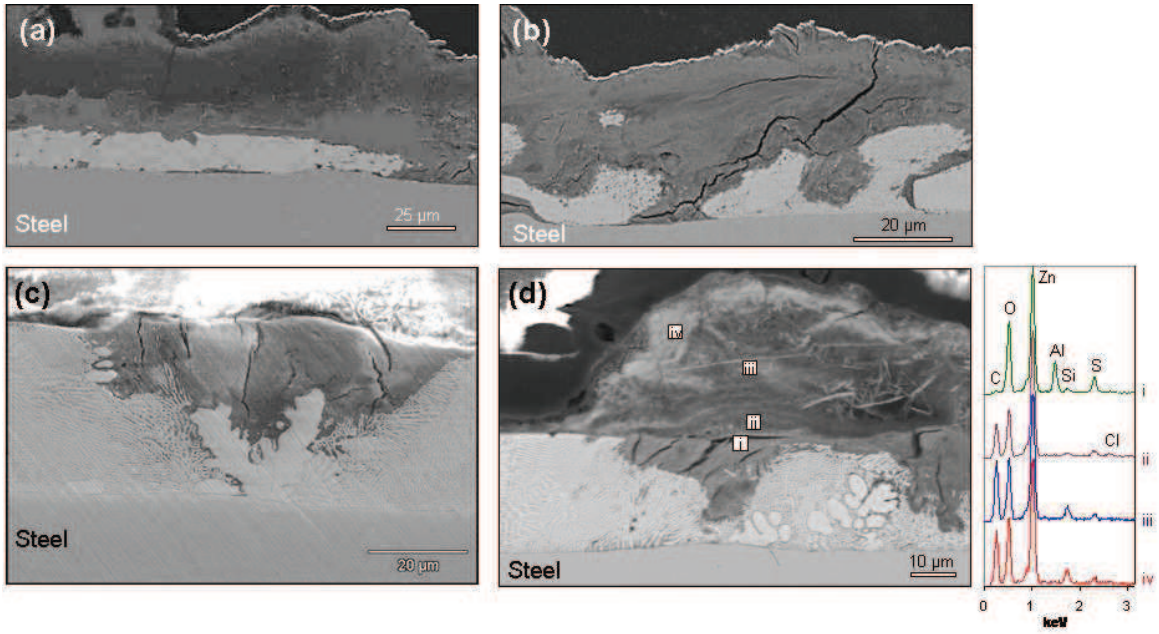


Fig. 6. SEM images of corroded (a) GI, (b) ZA and (c) ZM cross section after SST WR 1%; (d) is the SEM image of ZM cross section after SST-WR 1% and the detected elements by EDS analysis – Mg is not indentified and only a small amount of Cl is found.

3.4 Mass balance during salt spray test (SST)

Table 8 shows the results of the material balance performed for ZM sample during the salt spray tests (a) SST-NaCl 1% and (b) SST-RW 1% (lines 2 and 8 of Table 3). Column "I. Runoff and rinsing water" represents the total masses of oxidized elements in soluble form, calculated from the concentrations of ions found by ICP-OES in the electrolyte collected under the sample during the corrosion test and in rinsing water. Values in column "II. Water insoluble corrosion products" show the masses of elements present in insoluble product which are obtained from the ICP-OES analysis of the glycine solution used for corrosion product removal. The sum of columns I. and II. gives the total quantity of elements detected in corrosion products (column "III. Total leached". Column "IV. Sample weight loss" represents the measured weight loss and the calculated masses of Zn, Al, and Mg which can be expected in corrosion product from the mass loss in hypothesis of the homogenous dissolution. The total mass lost during the corrosion test, which is the difference between the initial mass of the sample before test and the final mass after corrosion products striping, was measured as described in section 2.3. Each value represents an average of 3 measurements (3 different samples with corroded surface of about 80 cm^2 each). The error between the average mass lost calculated from the analysis

of corrosion products and from the average measured weight loss is less than 8 % for both tests.

Table 8. The distribution of Zn, Al and Mg between water soluble and insoluble corrosion products and the mass balance measured after 100 h of a) SST NaCl 1% and b) SST RW 1%. Each value represents an average of 3 measurements (3 different samples with corroded surface of about 160 cm^2 each). Column I represents the total masses of oxidized elements in soluble form, calculated from the concentrations of ions found in the electrolyte collected under the sample during the test and in rinsing water; values in column II show the masses of elements present in insoluble product which are obtained from the analysis of the glycine solution used for corrosion product removal; column IV gives the measured weight loss and the masses of each element in corrosion product expected from the bulk composition in hypothesis of homogenous dissolution (marked by *).

a) SST NaCl	I. Run off and rinsing water	II. Water insoluble corrosion products	III. Total leached: (I +II)	IV. Sample weight loss	Comment
$\mathbf{m_{Zn}}$, mg	2.6	34.5	37.1	42.1*	**Zn**: mainly insoluble
$\mathbf{m_{Al}}$, mg	0.0	0.4	0.4	1.7*	**Al**: only insoluble, 3 times less than expected
$\mathbf{m_{Mg}}$, mg	3.7	0.9	4.6	1.4*	**Mg**: 80 % soluble, 3 times more than expected
Total, mg	6.3	35.8	42.1	45.1	**Total mass balance**: error about 7%

b) SST RW	I. Run off and rinsing water	II. Water insoluble corrosion products	III. Total leached: (I +II)	IV. Sample weight loss	Comment
$\mathbf{m_{Zn}}$, mg	7.9	471.3	479.2	447.4*	**Zn**: mainly insoluble
$\mathbf{m_{Al}}$, mg	0.0	2.3	2.3	17.7*	**Al**: only insoluble, 8 times less than expected
$\mathbf{m_{Mg}}$, mg	32.6	2.2	34.8	14.4*	**Mg**: 93 % soluble, 2 times more than expected
Total, mg	40.5	475.8	516.3	479.5	**Total mass balance**: error about 8%

The only visible difference between RW and NaCl tests is the fraction of Al found in corrosion products: in RW electrolyte, it is 8 times less than could be expected from homogenous dissolution and, in NaCl electrolyte, only 3 times less. The fraction of Mg in corrosion products (about 10 wt. %) is much closer to the value expected from the dissolution of Zn_2Mg phase (16 wt. % of Mg) than from the bulk composition (3 wt. %) which correlates well with the SEM observations of corroded samples and confirms that the hypothesis of homogenous dissolution of ZM coating is wrong for both tests.

All oxidized Al is found in the water insoluble corrosion products. On the contrary, most of Mg is found in the solution recovered inside the corrosion chamber during the salt spray test, which indicates that Mg is selectively leached and only a small amount contributes to corrosion product formation.

4 Discussion

4.1 Corrosion rates and corrosion products in accelerated tests with RW electrolyte compared to the field exposure and accelerated tests using NaCl electrolyte

The absence of LDH after accelerated corrosion SST of ZM coating is observed for the new electrolyte proposed in this work, the RW – Table 7. This is an important issue because LDH compounds were not detected on the ZM surfaces after relatively short field exposures (2 years) in low-Cl^- sites (Chicago, Maizières-lès-Metz). In these accelerated tests, the SST with RW electrolyte, the ratio of the consumed thickness (calculated from the weight loss measurement) of GI and ZM is close to the ratios observed in field exposures (about 3). On the basis of these results, one can expect that the use of RW electrolyte may lead to a better understanding of the corrosion mechanisms of ZM in atmospheric conditions.

From the results of accelerated corrosion tests (Table 5), it seems that, compared to GI, the corrosion of ZM is not significantly accelerated with increasing chloride content, but it is increased by a factor of 4 in the presence of bicarbonate and ammonium ions (compare SST modified-RW with SST-RW 1% – in Table 5, lines 10 and 8).

This accelerating effect at high carbonate concentrations on ZM corrosion contradicts the previously communicated [47] accelerating effect of carbon dioxide free environments on the corrosion rate of another ZnMgAl coating. We suppose that this contradiction is related to the exposure conditions which result in different corrosion advancement and corrosion mechanism.

In the previous study [47], ZnMgAl coated steel initially contaminated with NaCl was characterized after 14 days (336 h) of exposure in humid atmosphere with varied carbon dioxide concentration and the red rust appears after 15 days of the exposure. This indicates that at 14 days the corrosion can be already very advanced compared to 4-9 days in our tests.

The corrosion test of the present work SST-NaCl 0.1% has a chloride concentration intermediary to the ones of the two SST-RW tests, indicating that the absence of LDH is not related to the change of chloride concentration. At the same time, the LDH in our work was formed in the cyclic VDA-RW 0.1% test, which is much longer than both SST-RW. This demonstrates that the formation of LDH is probably delayed in the rain water electrolyte (RW), and that the mechanism can change with time, modifying the relation

between the LDH formation and the presence of bicarbonate in the electrolyte during the wet cycle. This also demonstrates the importance of the dry phase for the understanding of the LDH formation.

4.2 The formation of corrosion products in different electrolytes

From the results of titration experiments and from the comparison of the corrosion rates ratios between the coatings, we concluded that the NH_4^+ and HCO_3^- ions are responsible for the different behavior of GI, ZA and ZM coatings in RW compared to standard NaCl tests. The absence of the LDH in RW electrolyte could be explained by a buffering effect of the electrolyte which results in the impossibility to dissolve Al. However, this hypothesis still needs an experimental verification.

It is known for ZnMgAl alloys that, during corrosion, Zn_2Mg phase is the most active and consequently Mg^{2+} and Zn^{2+} ions are formed due to anodic reactions (1)-(2), while Al-rich phase is expected to be responsible for the cathodic reaction (3).

$$Zn \rightarrow Zn^{2+} + 2e^- \quad (1)$$

$$Mg \rightarrow Mg^{2+} + 2e^- \quad (2)$$

$$O_2 + 2H_2O + 4e^- \rightarrow 4OH^- \quad (3)$$

Due to pH increase by the reaction (3) corrosion products can be formed as represented by reactions (4) to (8):

$$Zn^{2+} + 2OH^- \rightarrow Zn(OH)_2 \qquad (\text{or } ZnO + H_2O) \quad (4)$$

$$5Zn^{2+} + 8OH^- + 2Cl^- \rightarrow Zn_5(OH)_8Cl_2 \quad (5)$$

$$5Zn^{2+} + 6OH^- + 2CO_3^{2-} \rightarrow Zn_5(OH)_6(CO_3)_2 \quad (6)$$

$$Zn_5(OH)_8Cl_2 + 2HCO_3^- \rightarrow Zn_5(OH)_6(CO_3)_2 + 2H_2O + 2Cl^- \quad (7)$$

$$Mg^{2+} + 2OH^- \rightarrow Mg(OH)_2 \quad (8)$$

As supposed in a previous work [19], the precipitation of $Mg(OH)_2$ that happens at pH around 10 would avoid the transformation of the products formed by reactions (5) and (6) into ZnO. In parallel, the dissolution of Al becomes possible as shown in reaction (9) because of the passive oxide instability at alkaline pH (reaction (10))

$$Al + 4OH^- \rightarrow Al(OH)_4^- + 3e^- \quad (9)$$

$$Al_2O_3 + 3H_2O + 2OH^- \rightarrow 2Al(OH)_4^- \quad (10)$$

Which can lead the formation of LDH:

$$2Al(OH)_4^- + 6Zn^{2+} + 8OH^- + CO_3^{2-} \rightarrow Zn_6Al_2(OH)_{16}CO_3 \quad (11)$$

$$2Al(OH)_4^- + 6Mg^{2+} + 8OH^- + CO_3^{2-} \rightarrow Mg_6Al_2(OH)_{16}CO_3 \quad (12)$$

Considering that LDH was detected after the accelerated corrosion test in NaCl on the ZM surface, while ZnO was absent, we can propose that the LDH can be formed by a direct precipitation, while a direct precipitation of ZnO (and/or $Zn(OH)_2$) is not expected because, in alkaline solutions containing Al ions, the formation of LDH or ZHC is favoured compared to ZnO [48]. As consequence, the formation of ZnO may be considered as being a transformation of the precipitated zinc salts (ZHC, HZ, etc…) with advance of corrosion:

$$Zn_5(OH)_8Cl_2 + 2OH^- \rightarrow 5ZnO + 5H_2O + 2Cl^- \quad (13)$$

$$Zn_5(OH)_6(CO_3)_2 + 2OH^- \rightarrow 5ZnO + 2HCO_3^- + 3H_2O \quad (14)$$

or a transformation from the soluble zincate complexes during drying:

$$Zn_5(OH)_8Cl_2 + 12OH^- \rightarrow 5Zn(OH)_4^{2-} + 2Cl^- \quad (15)$$

$$Zn(OH)_4^{2-} \rightarrow ZnO + H_2O + 2OH^- \quad (16)$$

However, on ZA alloy, despite the LDH detected, ZnO was also formed in accelerated tests using NaCl. Therefore, we suggest that the absence of ZnO on ZM coating is related to the presence of Mg^{2+} that contributes to the prevention of these mechanisms as previously suggested for ZnMg coatings [19].

According to the mass balance performed during both SST-NaCl and SST-RW, Mg is found to be lixiviated from the surface, which is in agreement with the absence of Mg-containing corrosion products. This could reinforce the idea of Mg being available to buffer the pH via formation of $Mg(OH)_2$. The role of Mg ions on the corrosion mechanisms will be addressed in a forthcoming publication.

Comparing corrosion products and corrosion resistance of ZM, the formation of LDH is detected in NaCl tests, in which the coating shows better behavior than in RW tests. Regarding the accelerated tests with RW, LDH was not detected after SST-RW, but was present after longer VDA-RW test which also includes dry periods. This could suggest either that Al forms very small quantity of the amorphous oxides or hydroxides which are below the detection limits of Raman spectroscopy or that Al is not oxidized and remains in a metallic form.

From the mass balance of the accelerated corrosion tests, it seems that the quantity of the oxidized Al is smaller than expected from homogenous dissolution and that oxidized Al stays on the surface in insoluble form. Further study on the role of Al on the corrosion mechanisms of ZnMgAl coating is in progress.

Comparing an improved corrosion resistance with the higher fraction of corroded Al and the presence of LDH, one can suppose that LDH plays an important role for the

corrosion behavior and an overestimated anticorrosion performance of ZM versus GI, in standard accelerated tests, can be related to the fact that the formation of LDH is favored in these tests due to the rapid pH increase. In RW, the cathodic Al dissolution can be delayed, probably because of the buffer capacity of the electrolyte which is improved through the continuous renewal of the electrolyte in the continuous salt spray test. This would justify why no Al-corrosion products were detected after the SST-RW 0.1% and 1% at the surface of ZM coating, and were detected after the VDA-RW 1.0%.

The mechanisms of the formation of ZnO and LDH on ZM coating is schematically presented in Fig. 7. This schema can explain the difference in the role of buffering effect of the electrolyte on the corrosion resistance. Considering zinc patinas and LDH as a barrier layer for oxygen diffusion [49], the buffering effect of the electrolyte is expected to prevent the dissolution of zinc patinas (step III in Fig. 7) and hence to benefit the corrosion resistance on GI. The effect is much more complex for ZM coatings, because zinc patinas are stabilized but the formation of LDH is delayed at the same time. Moreover, assuming that, on ZM, the pH can be limited through the precipitation of magnesium hydroxide, the buffering effect of RW electrolyte is less important for ZM than for GI. Interestingly, the weight loss of both, GI and ZM, in RW was higher than in modified-RW, indicating that the reality is more complex and other possible effects of NH_4^+ and HCO_3^- such as a modification of the intrinsic anodic reactivity should be also considered.

5 Conclusion

1. On the basis of our results, we confirm that the corrosion mechanisms in accelerated tests differ significantly in function of the electrolyte composition. Taking into account i) the comparison of the corrosion products detected after accelerated corrosion tests using different electrolytes and after field exposure tests and ii) the relative corrosion rates of different zinc based alloys, it seems that the tests using artificial “rain water” (RW) electrolyte represented some characteristic features of the corrosion mechanisms which are closer to the rate-determining features in natural exposure.

2. After all accelerated tested conditions as well as after 2 years of field exposure in 3 different sites, ZM coating shows a better corrosion resistance than GI (in terms of consumed thickness calculated from the weight loss).

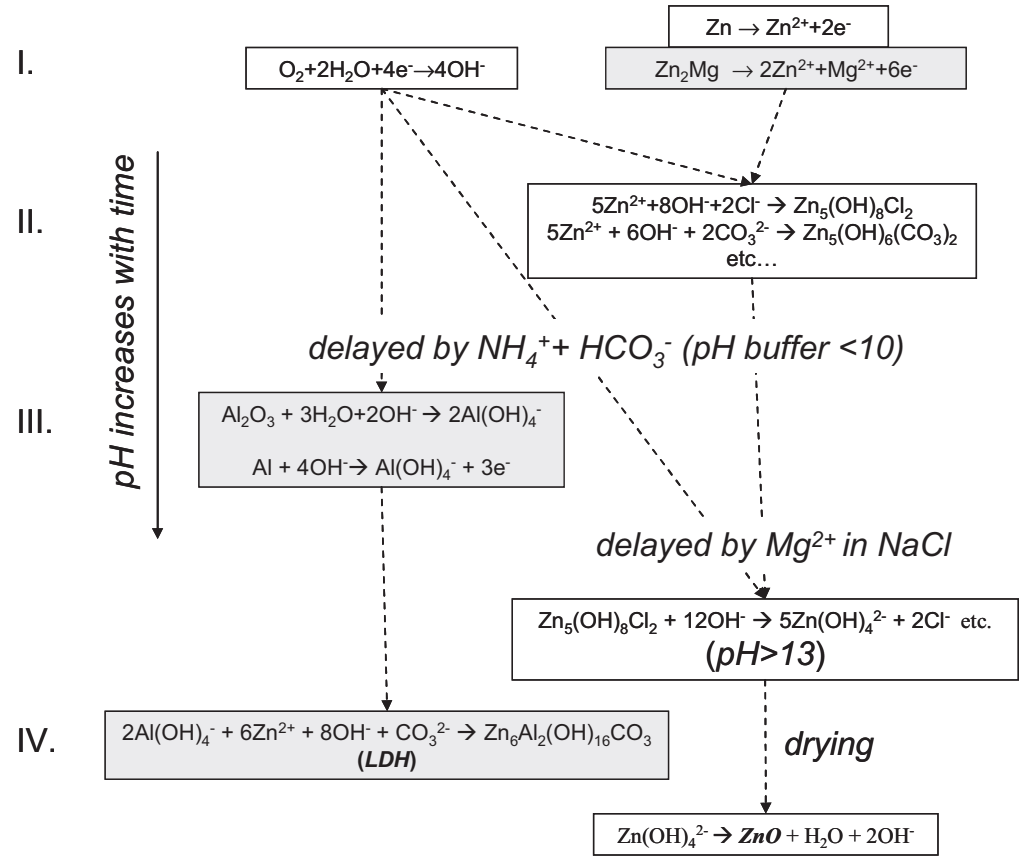


Fig. 7. Schematic illustration of the mechanism of formation of ZnO and LDH in NaCl and RW electrolytes on GI and ZM coatings. The reactions which are possible only on ZM are shown with grey background. Steps shown by numbers: I. Electrochemical reactions at neutral pH; II. Precipitation at medium pH; III. Dissolution at high pH (cathodic Al dissolution, dissolution of basic zinc salts); IV. Formation of ZnO and LDH (drying or concentration increase). In RW electrolyte, the buffering effect of NH_4^+ and HCO_3^- ions can delay step III which can be considered as positive for GI (stabilization of zinc corrosion products) but controversial for ZM (stabilization of zinc corrosion products but delayed formation of LDH).

3. The corrosion products detected on GI, ZA and ZM coatings are different in the same corrosion test. In particular, ZnO was not detected on ZM when it was detected on ZA and on GI. The corrosion products vary also with the electrolyte composition. The importance of Mg ions on the formation of different corrosion products is evident but seems to be very complex and worthy of investigation as a separate subject.

4. By comparison of RW and modified-RW effects on the corrosion rates and on the nature of corrosion products, we propose that the action of RW electrolyte is in particular determined by HCO_3^- and NH_4^+ ions. On the basis of the titration experiments, we attribute the effect of these ions to the buffering at slightly alkaline surface pH (between 8 and 10), which prevents the Al dissolution and further formation of protective LDH.

Acknowledgements

The results of this work were presented during the 3rd International Symposium "Coil coated steel: Durability and testing of advanced materials", on 28/11/2012 in Paris (France) and during European Conference EUROCORR 2013 in Estoril (Portugal). Authors are grateful for all colleagues participating in discussions of this work during these conferences.

References

[1] P. Volovitch, T.N. Vu, C. Allély, A. Abdel Aal, K. Ogle "Understanding corrosion via corrosion products characterization: II. Role of alloying elements in improving the corrosion resistance of Zn-Al-Mg coatings on steel" Corros. Sci. 53 (2011) 2437–2445

[2] S. Schuerz, M. Fleischanderl, G.H. Luckeneder, K. Preis, T. Haunschmied, G. Mori, A.C. Kneissl "Corrosion behaviour of Zn-Al-Mg coated steel sheet in sodium chloride-containing environment" Corros. Sci. 51 (2009) 2355–2363

[3] S. Schürz, G.H. Luckeneder, M. Fleischanderl, P. Mack, H. Gsaller, A.C. Kneissl, G. Mori "Chemistry of corrosion products on Zn–Al–Mg alloy coated steel" Corros. Sci. 52 (2010) 3271–3279

[4] D. Persson, D. Thierry, N. LeBozec, T. Prosek "In situ infrared reflection spectroscopy studies of the initial atmospheric corrosion of Zn-Al-Mg coated steel" Corros. Sci. 72 (2013) 54-63

[5] P. Schouller-Guinet, C. Allély, P. Volovitch "ZnAlMg: an innovative metallic coating that offers protection in the harshest environments" in: Proceedings of Galvatech '11, Genova, Italy, 2011

[6] T. Prosek, D. Thierry, D. Persson, J. Stoulil "Corrosion products formed on ZnMg and ZnAlMg coatings in model atmospheric conditions" in: Proceedings of Galvatech '11, Genova, Italy, 2011

[7] T. A. Keppert, G. Luckeneder, K-H Stellnberger, G. Mori "Influence of the pH value on the corrosion of Zn-Al-Mg hot-dip galvanized steel sheets in chloride containing environments" in: Proceedings of NACE International – Corrosion Conference & Expo 2012, C2012-0001493

[8] G. Luckeneder, M. Fleichanderl, T. Steck, K-H Stellnberger, J. Faderrl, S. Schuerz, G. Mori "Corrosion mechanisms and cosmetic corrosion aspects of zinc-aluminium-magnesium and zinc-chromium alloy coated steel strip" in: Proceedings of Galvatech '11, Genova, Italy, 2011

[9] M. Dutta, A. K. Halder, S. B. Singh "Morphology and properties of hot dip Zn-Mg and Zn-Mg-Al alloy coatings on steel sheet" Surf. & Coat. Technol. 205 (2010) 2578-2584

[10] K. Ueda, A. Takahashi, Y. Kubo, "Investigation of corrosion resistance of pre-painted Zn-11%Al-3%Mg-0.2%Si alloy coated steel sheet through outdoor exposure test in Okinawa" La Metallurgia Italiana – Corrosione, n. 2/2012, 13-19

[11] T. Prosek, N. Larché, M. Vlot, F. Goodwin, D. Thierry "Corrosion stability of Zn-Al-Mg coatings in open and confined zones in conditions simulating automotive applications" in: Proceedings of Galvatech '11, Genova, Italy, 2011

[12] D. Thierry, T. Prosek, N. Le Bozec, E. Diller "Corrosion protection and corrosion mechanisms of continuous galvanised steel sheet with focus on new coatings alloys" in: Proceedings of Galvatech ''11, Genova, Italy, 2011

[13] M. Uranaka, T. Shimizu "Corrosion resistance of hot dip Zn-6%Al-3%Mg alloy coated steel sheet used in automotive parts" in: Proceedings of Galvatech '11, Genova, Italy, 2011

[14] N. LeBozec, D. Thierry, A. Peltola, L. Luxem, G. Luckeneder,G. Marchiaro, M. Rohwerder "Corrosion performance of Zn–Mg–Al coated steel in accelerated corrosion tests used in the automotive industry and field exposures" Mater. Corros. 64 (2013) No. 9999, pp. 1-10

[15] N. Shimoda, M. Nakazawa, H. Nomura, Y. Marimoto "Atmospheric corrosion resistance of Zn-11%Al-3%Mg-0.2%Si coated steel" in: Proceedings of Galvatech '11, Genova, Italy, 2011

[16] X. G. Zhang "Corrosion and Electrochemistry of Zinc" Plenum Press, New York, 1996.

[17] T-N. Vu, P. Volovitch, K. Ogle "The effect of pH on the selective dissolution of Zn and Al from Zn–Al coatings" Corros. Sci. 67 (2013) 42–49

[18] X. Zhang, C. Leygraf, I. O. Wallinder "Atmospheric corrosion of Galfan coating on steel in chloride-rich environment" Corros. Sci. 73 (2013) 62–71

[19] P. Volovitch, C. Allély, K. Ogle "Understanding corrosion via corrosion products characterisation: I. Case study of the role of Mg alloying in Zn-Mg coating on steel" Corros. Sci. 51 (2009) 1251-1262

[20] Z.Y. Chen, D. Persson, C. Leygraf "Initial NaCl-particle induced atmospheric corrosion of zinc – Effect of CO_2 and SO_2" Corros. Sci. 20 (2008) 11-123

[21] L. Jiang, P. Volovitch, M. Wolpers, K. Ogle "Activation and inhibition of Zn-Al and Zn-Al-Mg coatings on steel by nitrate in phosphoric acid solution" Corros. Sci. 60 (2012) 256–264

[22] T. Prosek, D. Thierry, C. Taxe, J. Maixner "Effect of cations on corrosion of zinc and carbon steel covered with chloride deposits under atmospheric conditions" Corros. Sci. 49 (2007) 2676–2693

[23] S. Oesch, M. Faller "Environmental effects on materials: the effect of the air pollutants SO_2, NO_2, NO and O_3 on the corrosion of copper, zinc and aluminium. A short literature survey and results of laboratory exposures" Corros. Sci. 39 (1997) 1505-1530

[24] K. Ogle, S. Morel, D. Jacquet "Observation of self-healing functions on the cut edge of galvanized steel using SVET and pH microscopy" J. Electrochem. Soc. 153 (2006) B1-B5

[25] I. Odnevall, C. Laygraf "Reaction sequences in atmospheric corrosion of zinc" Atmospheric Corrosion, ASTM STP 1239, W. W. Kirk, H. H. Lawson, Eds., American Society for Testing and Materials, Philadelphia, 1995

[26] FN EN ISO 9223:2012 "Corrosion of metals and alloys – Corrosivity of atmospheres"

[27] FN EN ISO 9226:2012 "Corrosion of metals and alloys – Corrosivity of atmospheres: determination of corrosion rate of standard specimens for the evaluation of corrosivity"

[28] ISO 9227:2006 "Corrosion tests in artificial atmospheres"

[29] F. Beier, K-H. Dtellnberger, S. Geisler "A new accelerated cyclic corrosion test for automotive substrates" in: Proceeding of the Eurocorr, Nice, France, September 2009

[30] I. Lekouch, M. Mileta, M. Muselli, I. Milimouk-Melnytchouk, V. Šojat, B. Kabbachi, D. Beysens "Comparative chemical analysis of dew and rain water" Atmos. Research 95 (2010) 224-234

[31] G. S. Satsangi, A. Lakhani, P. Khare, S. P. Singh, K. M. Kumari, S. S. Srivastava "Composition of rain water at semi-arid rural site in India" Atmos. Environ. 32 (1998) 3783-3793

[32] D. Beysensa, C. Ohayon, M. Muselli, O. Clus "Chemical and biological characteristics of dew and rain water in an urban coastal area (Bordeaux, France)" Atmos. Environ. 40 (2006) 3710-3723

[33] P. S. Prakasa Rao, G. A. Momin, P. D. Safai, A. G. Pillai, L. T. Khemani "Rain water and throughfall chemistry in the Silent Valley Forest in south India" Atomos. Environ. 29 (1995) 2025-2029

[34] M. R. Williams, T. R. Fisher "Chemical composition and deposition of rain in the central Amazon, Brazil" Atmos. Environ. 31 (1996) 207-217

[35] G. S. Zhang, J. Zhang, S. M. Liu "Chemical composition of atmospheric wet depositions from the Yellow Sea and East China Sea" Atmos. Res. 85 (2007) 84-97

[36] S. Tsakovski, M. Tobiszewski, V. Simeonov, Z. Polkowska, J. Namiesnik " Chemical composition of water from roofs in Gdank, Poland" Environ. Pollut. 158 (2010) 84-91

[37] Ch. Anatolaki, R. Tsitouridou "Relationship between acidity and ionic composition of wet precipitation. A two years study at an urban site, Thessaloniki, Greece" Atmos. Res. 92 (2009) 100-113

[38] P. Panettiere, G. Cortecci, E. Dinelli, A. Bencini, M. Guidi "Chemistry and sulphur isotopic composition of precipitation at Bologna, Italy" Appl. Geochem. 15 (2000) 1455-1467

[39] A. H. M. Jawad Al Obaidy, H. Joshi " Chemical composition in tropical urban area of northern India" Atmos. Environ. 40 (2006) 6886-6891

[40] M. Vasjari, A. Merkoçi, S. Alegret "Potentiometric characterisation of acid rains using corrected linear plots" Anal. Chim. Acta 405 (2000) 173-178

[41] E. Bernardi, C. Chiavari, B. Lenza, C. Martini, L. Morselli, F. Ospitali, L. Robbiola "The atmospheric corrosion of quaternary bronzes: The leaching action of acid rain" Corros. Sci. 51 (2009) 159-170

[42] ISO 8407:2009 "Corrosion of metals and alloys – Removal of corrosion products from corrosion test specimens"

[43] C. Merlin "Approches analytique et électrochimique de la dégradation des tôles d'acier revêtues cataphorésées en atmosphères corrosive contenant des ions sulfates" Thèse de doctorat de l'université Henri Poincaré, Nancy I, 1999

[44] M.C. Bernard, A. Hugot-Le Goff, D. Massinon, N. Phillips "Underpaint corrosion of zinc-coated steel sheet studied by in situ Raman spectroscopy" Corros. Sci. 35 (1993) 1339–1349

[45] R. Autengruber, G. Luckeneder, A. W. Hassel "Corrosion of press-hardened galvized steel" Corros. Sci. 63 (2012) 12-19

[46] RRUFF database, available at http://rruff.info

[47] N. LeBozec, D. Thierry, M. Rohwerder, D. Persson, G. Luckeneder, L. Luxem "Effect of carbon dioxide on the atmospheric corrosion of Zn-Mg-Al coated steel" Corros. Sci. 74 (2013) 379-386

[48] T. Ishikawa, K. Matsumoto, A. Yasukawa, K. Kandori, T. Nakayama, T. Tsubota "Influence of metal ions on the formation of artificial zinc rusts" Corros. Sci. 46 (2004) 329-324

Chapter IV

The effect of HCO_3^- and NH_4^+ ions on the intrinsic reactivity of the coating

M. Salgueiro Azevedo, C. Allély, K. Ogle, P. Volovitch

Electrochimica Acta (submitted in April 2014)

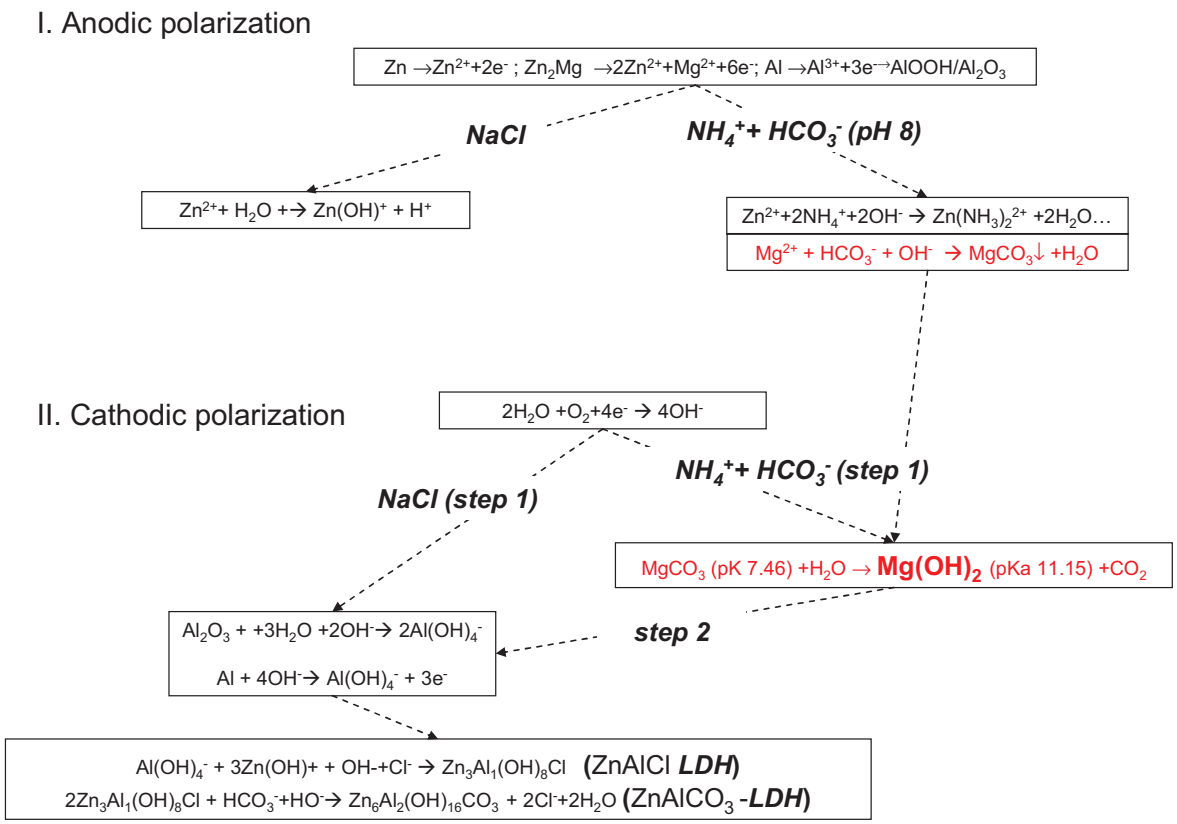
Corrosion mechanisms of Zn(Mg,Al) coated steel: The effect of HCO_3^- and NH_4^+ ions on the intrinsic reactivity of the coating

Abstract

The role of NH_4^+ and HCO_3^- additions in aqueous solutions containing Cl^- ion on the intrinsic reactivity of Zn(Mg,Al) coatings on steel was studied by direct measurement of the elemental dissolution rates of Zn, Mg and Al by atomic emission spectroelectrochemistry (AESEC). The intrinsic anodic reactivity of ZM was higher compared to GI in all electrolytes and Mg rich phases were selectively dissolved. NH_4^+ increased the anodic reactivity of Zn, suppressed the accumulation of zinc corrosion products and inhibited Al dissolution at open circuit (OC). HCO_3^- increased the accumulation of insoluble zinc corrosion products as well as the anodic reactivity. The cathodic current on the fresh surface of ZnMgAl in 0.1 M NaCl and in the mixture of 0.1 M NH_4Cl and 0.1 M $NaHCO_3$ was the same but cathodic dissolution of Al was higher in the mixed electrolyte. A preliminary anodic polarization did not affect the cathodic current on ZnMgAl in NaCl but increased it in mixed electrolyte. It also significantly delayed the cathodic Al dissolution on ZnMgAl alloy. Less pronounced delay of Al dissolution are observed for ZnAl coating. The observed kinetic effects were explained by a possible formation of Mg carbonates during anodic polarization. Layered double hydroxides were not detected on Zn(Mg,Al) coatings after short experiments in mixed electrolyte. In contrast, $Mg(OH)_2$, which is thermodynamically less stable at slightly alkaline pH, was detected. This indicates the importance of kinetic factors for the formation of corrosion products during the first stages of corrosion.

Keywords: cathodic dissolution of Al; anodic dissolution; selective dissolution; atomic emission spectroelectrochemistry; ZnMgAl.

Graphical abstract



1 Introduction

1.1. Context

The presence of pollutants in the electrolyte during atmospheric corrosion of Zn-based coatings is considered as one of the most important factors affecting corrosion resistance [3-7]. The role of different ions is usually discussed in relation to the nature of corrosion products formed on the coating and sometimes in relation to the soluble complexes which result in the absence of protective corrosion product layer. The ions present in the electrolyte affect not only the rate of accumulation and the nature of corrosion products but also modify the intrinsic reactivity of the alloy by itself [1,2]. For alloyed materials, which are multiphase systems, the effect can be different on the reactivity of different constituents of the alloy. Moreover, it can also differ from the effect which can be expected on the basis of the behavior of pure metal in the presence of the same ions [1,8].

ZnAl (ZA) and ZnMgAl (ZM) coatings, which have been developed during the past decades [9-11], are composed by elements that have very different reactivity in aqueous electrolytes, leading to an incongruent dissolution. Further, the non uniform phase distribution (presence of lamellar eutectic and dendrites [9,12]) may lead to a heterogeneous reactivity between the same element present in different forms: Zn in intermetallic Zn_2Mg or in ternary Zn_2Mg/Zn/Al eutectic or in Zn-rich dendrites.

The preferential corrosion of binary and ternary eutectic phases in some conditions was observed by local electrochemistry and post-mortem microstructure observations [2,12-14]. However the mechanisms during these tests were complex and included multiple steps. The role of the individual solution components on the kinetic of dissolution of each coating component has never been clarified.

Several previous works demonstrated that the behavior of ZM coating in corrosion tests and the corrosion products formed during the test strongly depend on the presence of carbon dioxide [15-16], HCO_3^- [17] and NH_4^+ [17-18] ions. We have recently shown that the use of the electrolyte containing HCO_3^- and NH_4^+ simulates corrosion mechanisms that seem to be more representative of natural exposure than the conventional NaCl electrolyte [17]. This was attributed to the buffering effect of these ions which could delay the dissolution of Al and the formation of Al-containing corrosion products.

The objective of this work is to understand how HCO_3^- and NH_4^+ ions modify the intrinsic reactivity of ZnMgAl coating on steel and the initial formation of corrosion products by a direct measurement of elemental dissolution rates in different electrolytes using Atomic Emission Spectroelectrochemistry (AESEC).

1.2 Intrinsic reactivity measurement by Atomic emission spectroelectrochemistry (AESEC)

1.2.1. Principle of measurement of anodic reactivity and residual film

AESEC was used in order to quantify elementary dissolution phenomena [19]. The principle of the AESEC measurement has been described in detail previously [19-22]. Briefly, it consists of an electrochemical flow cell coupled with an ICP-OES. In the flow cell, the reaction between the sample and the aggressive electrolyte occurs, leading to the production of dissolved ions. The electrolyte is transported to the ICP-OES where its composition is continuously analyzed. The instantaneous dissolution rate of an element M in the cell, v_M, is directly related to the instantaneous downstream concentration (in nmol s^{-1} cm^{-2}) as:

$$v_M = C_M f / A \quad (1)$$

where C_M is the concentration of element M (M = Zn, Al or Mg, in the case of ZnMgAl alloys), f is the flow rate of the electrolyte, and A is the surface area of the exposed sample's surface. The concentrations of Zn, Al and Mg in the solution, measured by ICP during the spontaneous reactivity or under applied potential, can be recalculated as leaching rates of Zn, Al and Mg ions and expressed as elementary dissolution currents j_{Zn}, j_{Al} and j_{Mg} using Faraday's law with the number of electrons transferred per atom, n = 2 for Zn and Mg and n = 3 for Al – all calculations in this work are made in assumption of Zn(II), Mg(II) and Al(III):

$$j_M = \mathrm{n\ F}\ v_M \quad (2)$$

This approach has been demonstrated previously for a number of chemical elements, including Zn [8,23], Al [24-26] and Mg [25].

The elemental dissolution rate detected by ICP for each element M, j_M (M = Zn, Al or Mg in this work), are composed by two terms: (i) dissolution rate of ions leached from the metallic surface due to electrochemical oxidation (j_M^{ech}) and (ii) pure chemical dissolution of surface oxides (j_M^{chem})

$$j_{Zn} = j_{Zn}^{ech} + j_{Zn}^{chem} \quad (3a)$$

$$j_{Al} = j_{Al}^{ech} + j_{Al}^{chem} \quad (3b)$$

$$j_{Mg} = j_{Mg}^{ech} + j_{Mg}^{chem.} \quad (3c)$$

The total leaching rate of all elements, j_Σ, for ZnMgAl alloy should be presented as:

$$j_\Sigma = j_M^{ech} + j_M^{chem} = (j_{Zn}^{ech} + j_{Al}^{ech} + j_{Mg}^{ech}) + (j_{Zn}^{chem} + j_{Al}^{chem} + j_{Mg}^{chem}) \quad (4)$$

The total electrochemical current, j_e measured with the potentiostat can be decomposed into the cathodic and anodic components (j_c and j_a, respectively)

$$j_e = j_c + j_a \quad (5)$$

The oxidation current j_a is used for formation of soluble species (j_M^s) and insoluble species (j_M^{ins}), with $j_M^s = j_M^{ech}$, analyzed by ICP:

$$j_a = \Sigma j_M^s + \Sigma j_M^{ins} = (j_{Zn}^{ech} + j_{Al}^{ech} + j_{Mg}^{ech}) + (j_{Zn}^{ins} + j_{Al}^{ins} + j_{Mg}^{ins}) \quad (6)$$

where $j_{Zn}^{ins} + j_{Al}^{ins} + j_{Mg}^{ins}$ describe the oxidation currents resulted in formation of oxidized Zn^{2+}, Al^{3+} and Mg^{2+} which stays in the residual surface film and can not be detected by ICP.

Assuming a constant surface oxide film at steady state:

$$j_{Zn}^{chem} = j_{Al}^{chem} = j_{Mg}^{chem} = 0 \quad (7)$$

the difference between the anodic part of the electrochemical current, j_a (Eq.6) and the sum of the elemental currents, j_Σ (Eq. 4) can be used to estimate the rate of oxide formation (insoluble species) [22-23]

$$j_a - j_\Sigma = j_{Zn}^{ins} + j_{Al}^{ins} + j_{Mg}^{ins} \quad (8)$$

Under applied anodic potential, in hypothesis of homogenous oxidation of the alloy with molar fractions of Zn, Mg and Al as X_{Zn}, X_{Mg}, X_{Al}, the fractions of oxidized Zn, Al and Mg, j_{Zn}(%), j_{Al}(%) and j_{Al}(%), can be written as

$$j_{Zn}\,(\%) = (j_{Zn}^{ech} + j_{Zn}^{ins})/j_e = 2X_{Zn}/(2X_{Zn} + 2X_{Mg} + 3X_{Al})\ 100\% \quad (9a)$$

$$j_{Mg}\,(\%) = (j_{Mg}^{ech} + j_{Mg}^{ins})/j_e = 2X_{Mg}/(2X_{Zn} + 2X_{Mg} + 3X_{Al})\ 100\% \quad (9b)$$

$$j_{Al}\,(\%) = (j_{Al}^{ech} + j_{Al}^{ins})/j_e = 3X_{Al}/(2X_{Zn} + 2X_{Mg} + 3X_{Al})\ 100\% \quad (9c)$$

Using Eq. (9a-c) the contributions of each term in Eq. (6) can be calculated (in % of the total current) and the stoichiometry of the residual "steady-state" film can be estimated. Similar calculation could be made if the dissolution is not homogenous but if the stoichiometry of dissolved phases is known.

For rapidly changing transients, because of the difference in the time resolution of current and concentration measurements, it is necessary to transform one into the time resolution of the other by performing a numerical convolution. In the current work, we were focused mainly on the conditions at which the quasi steady state can be obtained, and

the convolution was not performed because its influence in quasi steady state is less important than for rapid transients.

1.2.2. Measuring cathodic reactivity

If the oxide film reduction can be neglected, assuming the cathodic reaction in the form of:

$$2H_2O + O_2 + 4e^- \rightarrow 4OH^- \quad (10a)$$

$$2H_2O + 2e^- \rightarrow H_2 + 2OH^- \quad (10b)$$

the OH^- generation rate v_{OH} and the hydroxide generation current j_{OH} can be calculated:

$$j_{OH} = -j_c = -(j_e - j_a) = -(j_e - j_\Sigma) \quad (11a)$$

$$v_{OH} = j_{OH} / F = (j_\Sigma - j_e) / F \quad (11b)$$

For Al-containing compounds, the electrochemically generated hydroxide destabilizes Al oxides forming soluble aluminates,

$$Al_2O_3 + 3H_2O + 2OH^- \rightarrow 2Al(OH)_4^- \quad (12)$$

Depassivated metallic Al is immediately oxidized by either the electrochemical reaction

$$2Al + 6OH^- \rightarrow Al_2O_3 + 6e^- + 3H_2O \quad (13)$$

or by the chemical reaction with dissolved oxygen

$$2Al + 3/2O_2 \rightarrow Al_2O_3 \quad (14)$$

AESEC measures the rate of the chemical dissolution reaction given by Eq. (12) for which

$$v_{OH}^{chem} = v_{Al}^{chem} \quad (15)$$

Formally, the cathodic dissolution rate of Al from the oxide film, given by Eq. (12), is

$$j_{Al}^{chem} = 3F\, v_{Al}^{chem} \quad (16)$$

and

$$j_{OH} = F\, v_{OH}^{chem} = F\, v_{Al}^{chem} = j_{Al}^{chem} / 3 \quad (17)$$

For the chemical dissolution of Al from the oxide film by reaction of Eq. (12) or from the metal (reaction pass given by Eq. (12)/(14)), in which the oxidation cannot contribute to the electrochemical current, the only electrochemical reaction is given by Eq. (10). This result in

$$j_{Al} = j_{Al}^{chem} \quad (18a)$$

$$j_a = 0 \quad (18b)$$

and

$$j_e = j_c = -j_{OH} = -1/3\, j_{Al} \tag{19}$$

so

$$|j_e / j_{Al}| = 1/3 \tag{20}$$

Ratios $|j_e / j_{Al}| > 1/3$ should indicate the presence of a parallel reaction consuming hydroxide ions. A limited evacuation of soluble Al species to the bulk solution, due to a difficult diffusion through an oxide layer, can also contribute to the increasing of the ratio $|j_e / j_{Al}|$. The values $|j_e / j_{Al}| < 1/3$ may indicate a parallel process producing soluble Al at neutral pH, which may be, for example, the case of soluble salts which were incorporated into insoluble films during a previous anodic reaction.

For the reaction pass given by Eq. (10)/(12)/(13), the electrochemical reactions are Eq. (10) and (13), which are the cathodic and the anodic reactions respectively, resulting in

$$j_{Al} = j_{Al}^{chem} \text{ and } j_a = j_{Al}^{ins} \tag{21}$$

and

$$j_e = j_c + j_a = -j_{OH} + j_{Al}^{ins} \tag{22}$$

which are different from reaction pass of Eq. (12)/(14) described in Eq. (18). For reaction from Eq. (13), one oxidized Al requires 3 hydroxide ions:

$$v_{OH}^{ins} = 3\, v_{Al}^{ins} \tag{23}$$

which results in

$$v_{OH} = v_{OH}^{chem} + v_{OH}^{ins} = v_{Al}^{chem} + 3\, v_{Al}^{ins} \tag{24}$$

Or assuming no diffusion limitation, so $v_{Al}^{chem} = v_{Al}^{ins} = v_{Al}$,

$$v_{OH} = 4\, v_{Al} \tag{25}$$

and

$$j_c = -j_{OH} = -F\, v_{OH} = -4\, F\, v_{Al} = -4/3\, j_{Al} \tag{26}$$

therefore

$$j_e = j_c + j_a = -4/3\, j_{Al} + j_{Al} = -1/3\, j_{Al} \tag{27}$$

This demonstrates the same ratio between the total current and dissolved Al as in case of pure chemical dissolution (Eq. 20). The ratio v_{OH} / v_{Al} close to 4 (Eq. 25) is predicted from the soluble complex stoichiometry and observed for a number of Al alloys in diluted solutions [24-26].

2 Experimental

2.1 Materials

The coated steel samples were supplied by ArcelorMittal. Conventional hot dip galvanized steel (GI), with coating thickness of 20 µm, and composition Zn-Al(0.2 wt. %), and Galfan® (ZA), with coating thickness of 20 µm and composition Zn-Al(5 wt. %) were used as the reference materials. The ZnMgAl coated steel (ZM) was prepared by hot dip process with thickness of 20 µm and composition Zn-Mg(3.0 wt. %)-Al(3.7 wt. %) which corresponds to molar fractions X_{Zn}=0.845, X_{Mg}=0.074, X_{Al}=0.081. The mean coating composition and thickness are summarized in Table 1. Typical microstructure of the three studied coatings was presented in our previous publication [17]: GI coating contains homogenous Zn layer; ZM coating is composed by Zn dendrites and a ternary eutectic containing Zn, Al and intermetallic Zn_2Mg; ZA coating contains Zn dendrites in a binary Zn/Al matrix.

Table 1. Thickness and chemical composition of the coatings.

Label	Coating	Thickness	Zn %wt	Al %wt	Mg %wt
GI	Conventional hot-dip galvanized	20µm	99.8	0.2	-
ZM	ZnMgAl	20µm	93.3	3.7	3.0
ZA	Galfan ®	20µm	95.0	5.0	-

2.2 Experimental parameters

Ultima 2C Horiba Jobin Yvon ICP-OES was used for the concentration measurement and an EGG 273 potentiostat for the total dissolution current measurement. A detailed description of the flow cell can be found in a previous publication [19]. The emission intensity of Zn, Mg and Al in the plasma was monitored at 213.856, 285.213 and 167.081 nm respectively, using a polychromator system (focal distance 50 cm) purged by flowing nitrogen with oxygen concentration lower than 3 ppm for UV region application. A 50 mL cyclonic chamber and MEINHARD† K3 nebulizer were used for NaCl solutions. The MIRAMIST nebulizer was used for the measurement with high bicarbonate concentrations, because of its high viscosity. The flow rate of the electrolyte through the

cell was fixed at 3.00 cm^3 min^{-1} and the surface area of the sample was 0.51 cm^2. Sensitivity of the analytical system was evaluated by considering the $C_{2\sigma}$ parameter (twice standard deviation of the intensity of the electrolyte not contacted with the sample). The typical values of $C_{2\sigma}$ for Al, Mg and Zn in different electrolytes are presented in Table 2. One may observe that the detection of Mg and Al is significantly degraded in presence of bicarbonate.

Table 2. Analytical parameters of sensitivity (C2σ) for ICP experiment, which are twice the standard deviation of the intensity of the electrolyte not contacted with the sample.

Electrolyte	$C_{2\sigma}$ (Al) µA/cm^{-2}	$C_{2\sigma}$ (Zn) µA/cm^{-2}	$C_{2\sigma}$ (Mg) µA/cm^{-2}
0.1 M NaCl	1.9	1.0	0.4
0.1 M NH_4Cl	1.7	1.6	0.6
0.1 M NaCl + 0.01 M $NaHCO_3$	4	1.7	2
0.1 M NH_4Cl + 0.1 M $NaHCO_3$	4	1.6	2

A first series of experiments were performed on GI and ZM coatings with different electrolytes in order to evaluate their reactivity in presence of 0.1 M Cl^- and/or 0.01-0.1 M NH_4^+ and/or 0.01-0.1 M HCO_3^- ions. This first series was performed as follows:

1. Acid wash (0.1 wt. % HCl solution) during 5 s for natural oxides elimination;
2. Measurement of open circuit (OC) reactivity until the signal is stable;
3. Application of anodic potential E = -0.95 V vs. SCE for 15 min;
4. Measurement of OC reactivity.

The second series was executed on ZM and on ZA coatings in 0.1 M NaCl and 0.1 M NH_4Cl + 0.1 M $NaHCO_3$ electrolytes with replacing step 3 above by a cathodic polarization followed by a cyclic application (2 cycles) of anodic and cathodic potentials for 15 minutes each (E_{anodic} = -0.95 V vs. SCE and $E_{cathodic}$ = -1.25 V vs. SCE).

2.3 Corrosion products characterization

The corrosion products were characterized by X-ray diffraction (XRD) using the Cu(Ka1) radiation in a PANalytical X'Pert diffractometer, directly on the corroded surface of the samples. The analyzed area was approximately 20 mm x 20 mm. The XRD were collected with angular resolution of 0.02° over the angular range 5-80° (2θ) with 0.3 s

acquisition time for each. The evaluation of the data was done using the HighScore Plus software package, containing the JCPDS (ICDD) database files (version 2013).

3 Results

3.1 Coatings reactivity measured by AESEC at open circuit and under applied anodic potential

Typical dissolution profiles of Zn, Mg and Al from GI and ZM coatings are shown in Fig. 1 and Fig. 2, respectively, in various electrolytes at open circuit potential and under applied anodic potential. The evolution of elemental dissolution rates of Zn, Al and Mg (j_{Zn}, j_{Al} and j_{Mg}), the total current j_e and the sum of elemental current j_Σ are shown. The open circuit (OC) reactivity in a chosen electrolyte was measured until the open circuit potential E_{OC} and dissolution rates were stable. Than, an anodic potential (E_a = -0.95V vs. SCE) was applied for about 15 minutes. Finally, the potential switched off and the system evolved once more at OC. Initial NaCl and HCO_3^--containing solutions pH was adjusted to 8.5; for NH_4Cl, the pH was 7. The pH of the electrolyte after the reaction cell measured downstream did not change for all solutions, except for 1 M NaCl, which decreased in 1 unit.

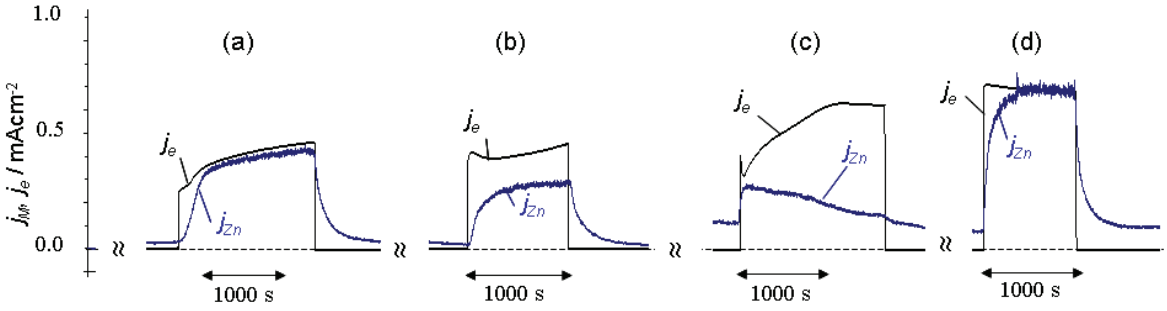


Fig. 1. Evolution of the elemental leaching rate of Zn (j_{Zn}) and of the total current (j_e) for GI coating in various electrolytes during spontaneous dissolution rates before and after applying potential and under applied anodic potential -0.95 V vs. SCE (middle peaks with $j_e > 0$). (a) 0.1 M NaCl at pH 8.5, (b) 0.1 M NaCl + 0.01 M $NaHCO_3$ at pH 8.5, (c) 0.1 M NH_4Cl + 0.1 M $NaHCO_3$ at pH 8.5, (d) 0.1 M NH_4Cl at pH 7.

Table 3 summarizes the values of the currents and the contribution of different species during the last 100 s of anodic polarization of ZM shown in Fig. 2. The fractions of formation of soluble species (j_{Zn} (%), j_{Mg} (%)) were calculated from the ICP data; the fractions of the insoluble currents j^{ins} were calculated from the balance equations as

described in section 1.2 in hypothesis of homogenous oxidation of the bulk composition (j_{Zn} (%) = 81 %, j_{Mg} (%) = 7 %, j_{Al} (%) = 12 %).

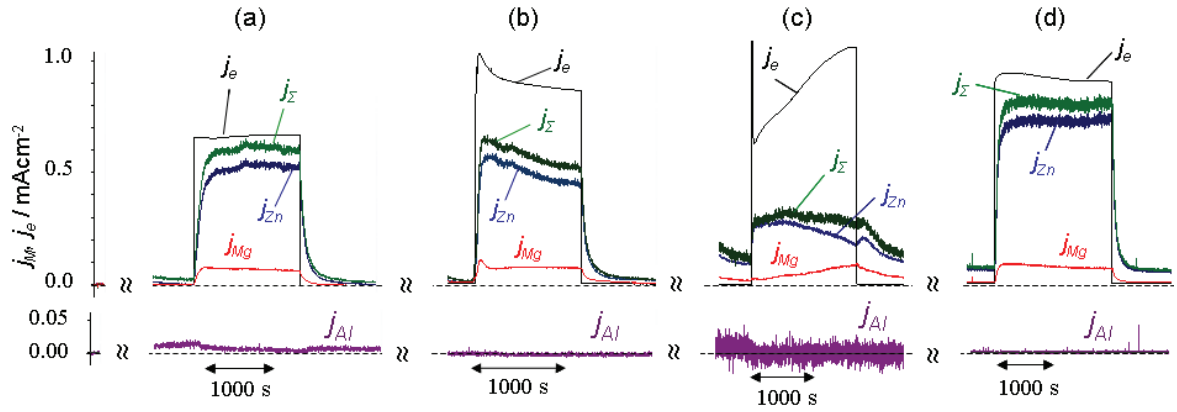


Fig. 2. Evolution of the elemental leaching rates of Zn, Al and Mg (j_{Zn}, j_{Al} and j_{Mg}) and of the total current (j_e) from ZM coating in various electrolytes during spontaneous dissolution rates before and after applying potential and under applied anodic potential -0.95 V vs. SCE (middle peaks with $j_e > 0$). (a) 0.1 M NaCl at pH 8.5, (b) 0.1 M NaCl + 0.01 M $NaHCO_3$ at pH 8.5, (c) 0.1 M NH_4Cl + 0.1 M $NaHCO_3$ at pH 8.5, (d) 0.1 M NH_4Cl at pH 7.

Several observations may be made from Fig. 1 and 2 and Table 3, which will be analyzed in sections 3.1.1 to 3.1.4.

Table 3. Anodic reactivity of ZM coating in different electrolytes at the end of anodic polarization (quasi steady-state). Initial pH was adjusted to 8.5 if not indicated. The fractions of soluble Zn and Mg currents in the total current (%) are calculated from the ICP data. All values which are calculated using the methodology presented in section 1.2. are marked by *. The total insoluble current jins is calculated from the balance equation (3). The fractions of the insoluble currents of elements j_{Zn}^{ins}, j_{Mg}^{ins}, j_{Al}^{ins} are calculated in the hypothesis of homogenous oxidation of the coating (fractions of oxidation currents of Zn, Mg and Al expected as 81%, 7% and 12% respectively). Results from electrolyte number 4) 0.1 M NaCl + 0.1 NaHCO3 are not shown in the Fig.

Electrolyte	j_e	j_Σ^s	j_Σ^{ins*}	*Solution* j_{Zn}	*Solution* j_{Mg}	*Residual film* j_{Zn}^{ins*}	*Residual film* j_{Mg}^{ins*}	*Residual film* j_{Al}^{ins*}	**Stoichiometry of the residual film formation***
	(mA cm^{-2})			(contributions to the total current j_e %)					
1) 0.1 M NaCl	0.64	0.61	0.03	83	11	-	-	6	$Al(0)_1 + Al(III)_1$
2) 0.1 M NH_4Cl (initial pH 7)	0.89	0.79	0.10	81	8	0	0	11	$Al(0)_1+Al(III)_{11}$
3) 0.1 M NaCl + 0.01 M $NaHCO_3$	0.87	0.53	0.34	53	8	28	0	12	$Al(III)_1Zn_{3.5}$
4) 0.1 M NaCl + 0.1 M $NaHCO_3$	1.40	0.27	1.13	13	7	68	0	12	$Al(III)_1Zn_{11.5}$
5) 0.1 M NH_4Cl + 0.1 M $NaHCO_3$	1.03	0.27	0.76	18	8	63	0	12	$Al(III)_1Zn_{7.9}$

3.1.1 Reactivity of ZM compared to GI

The total anodic current and the sum of elemental currents j_Σ of ZM were systematically higher than the ones on GI in all tested electrolytes under applied anodic potential. Higher anodic reactivity of the ZM coating compared to GI together with the fact that ZM is known to be more resistant against corrosion than GI [2,14,16-17,27-37] demonstrated that the corrosion of ZM is governed by cathodic reaction, like it is for GI [38], and other factors than the dissolution rate should be considered for corrosion mechanisms. It also illustrates that the electrochemical results cannot be directly extrapolated to corrosion rates.

3.1.2 Effect of ammonium ions on selective dissolution

From the comparison of Fig. 1a/d for GI and 2a/d for ZM, one may notice that the reactivity of both coatings increases in presence of NH_4^+ ions.

For GI coating (Fig. 1), the difference between j_e and j_Σ (= j_{Zn}) under applied anodic potential can be assigned to the accumulation of zinc corrosion products, j_{Zn}^{ins}. At quasi steady-state, $j_{Zn}^{ins} > 0$ in NaCl but $j_{Zn}^{ins} = 0$ in NH_4Cl electrolyte. The increase of j_e in NH_4Cl compared to NaCl electrolyte can be interpreted as the accumulated zinc corrosion products having an inhibiting effect on the anodic reactivity of zinc in NaCl.

For ZM (Fig. 2), the sum of the elemental currents j_Σ is still lower than the total current j_e suggesting that some corrosion products are still accumulated in both electrolytes. Considering that for ZM, as for GI, $j_{Zn}^{ins} = 0$ in 0.1 M NH_4Cl, insoluble film in this electrolyte can contain only Al and/or Mg at steady state. It seems, however, from the comparison of the elemental currents in Fig. 2d and 2a, that the reactivity of Mg is not affected by the presence of ammonium. Moreover, the calculation, showed in Table 3, of the fraction of Mg current to the total current (about 8%) in NH_4Cl is close to the expected from the bulk composition, which can be interpreted as the insoluble oxide formed in this electrolyte is mainly composed by Al product. In contrast, the value of j_{Mg} (%) = 11% in NaCl electrolyte is significantly higher than the expected from homogenous oxidation model (7%) implying the j_{Al} (%) = 6% which is twice less than the expected value (12%) in 0.1 M NaCl. This result suggests that Mg if selectively dissolved, in particular in NaCl electrolyte, but also slightly in the others solutions, which can be interpreted either that the

initial surface oxides were formed during OC exposure or that some Al stayed in metallic form.

Very small Al dissolution at OCP was detected in NaCl. This can be attributed to the cathodic Al dissolution or to the dissolution of a residual Al compounds formed at OC exposure (see section 3.2.). In NH_4Cl, no soluble Al was detected neither at OC nor under applied anodic potential.

The fact that the solution pH decreased about 1 unit in NaCl after the contact with the sample was coherent with the low contribution of cathodic reaction and hydrolysis of soluble zinc salts formed by strong acid but weak base:

$$Zn^{2+} + H_2O \rightarrow [ZnOH]^+ + H^+ \quad (28)$$

3.1.3 Effect of hydrogen-carbonate ions

In all carbonate containing solutions the pH did not change significantly after the reaction confirming the buffering capacity of bicarbonate ions in large concentration range. With the addition of a relatively small (0.01 M) concentration of HCO_3^- ions in 0.1 M NaCl solution (Fig. 1b, 2b), the total anodic current stabilized at values close to the observed in 0.1 M NaCl electrolyte for GI (Fig. 1b) but is about 25% higher for ZM (Fig. 2b). Dissolution rates at open circuit (OC) are near the same as in NaCl, but zinc dissolution seems to be significantly lower under applied anodic potential. The rate of the accumulation of insoluble products j^{ins} estimated from the difference between the total current j_e and the sum of elemental currents j_Σ, in Figures 1 and 2 is much larger in presence of HCO_3^- for both coatings.

Comparing the results for ZM in presence of 0.01 and 0.1 M HCO_3^- (lines 3 and 4 in Table 3), it is clear that both, the accumulation of the insoluble Zn species and the total oxidation current increase drastically with increasing carbonate concentration. This indicates that the formed product does not inhibit the anodic reactivity of ZM. Curiously, Mg dissolution does not change significantly and the fraction of Mg current to the total current is still very close to the value expected from the bulk composition. Considering that all metals could be oxidized at this potential, one can expect that the oxidized product contains more Zn(II) than expected from the stoichiometry of known layered double hydroxides – last column in table 3 shows the stoichiometry of the residual film very different from the usually expected for Zn-Al layered double hydroxides (Zn:Al close to 3) - implying the formation of zinc corrosion patinas which is coherent with the results on GI.

3.1.4 Synergic effect of hydrogen-carbonate and ammonium ions

In the mixed electrolyte of NH_4Cl and $NaHCO_3$ (Fig. 1c), a surprising kinetic effect is observed when the potential is applied or removed. The system needs about 1000 s to reach the quasi steady state when switched to applied potential or even more when returned to OC potential. In this electrolyte, under applied anodic potential the total current j_e increases and the difference between the total current j_e and the sum of elemental currents j_Σ show much higher accumulation of insoluble corrosion products than in NaCl. Zn dissolution decreases and Mg dissolution reaches near the same level as in NaCl at the end of polarization. From the current balance (Table 3) one may expect the accumulation of all elements, Zn(II), Mg(II) and Al(III) in corrosion product after anodic polarization. At OC condition, the reactivity of the coatings increases compared to NaCl. Al dissolution is inhibited for ZM coating at both, OC and applied anodic potentials. Interestingly, the ratio between Zn and Mg dissolution currents under applied anodic potential is close to 2 which can lead to a conclusion that only Zn_2Mg phase is dissolved anodically.

3.2 Anodic reactivity of ZM under anodic-cathodic polarization cycles

Selective leaching of Zn, Al and/or Mg from ZM and ZA was studied for both anodic and cathodic reactivity in presence of NaCl and of NH_4Cl + $NaHCO_3$ solutions (Fig. 3-6). For this study, the polarization cycle was performed as follows: after the background measurement and the surface activation (first 1000 s not shown in the figures) the OC reactivity was measured for about 15 min, followed by the cathodic polarization under -1.25 V vs. SCE, then an anodic polarization under -0.95 V vs. SCE, and finally a cathodic polarization again, all steps during 15 min approximately. The cycle "anodic-cathodic" was repeated 2 times and then, after the last cathodic polarization, the OC reactivity was re-measured.

Fig. 3 and 4 show the anodic "portion" of the ZM dissolution, with j_{Zn}, j_{Mg} and j_Σ and the total dissolution current j_e (positive during anodic polarization) from ZM in NaCl in the mixed electrolyte (0.1 M NH_4Cl + 0.1 M $NaHCO_3$), respectively.

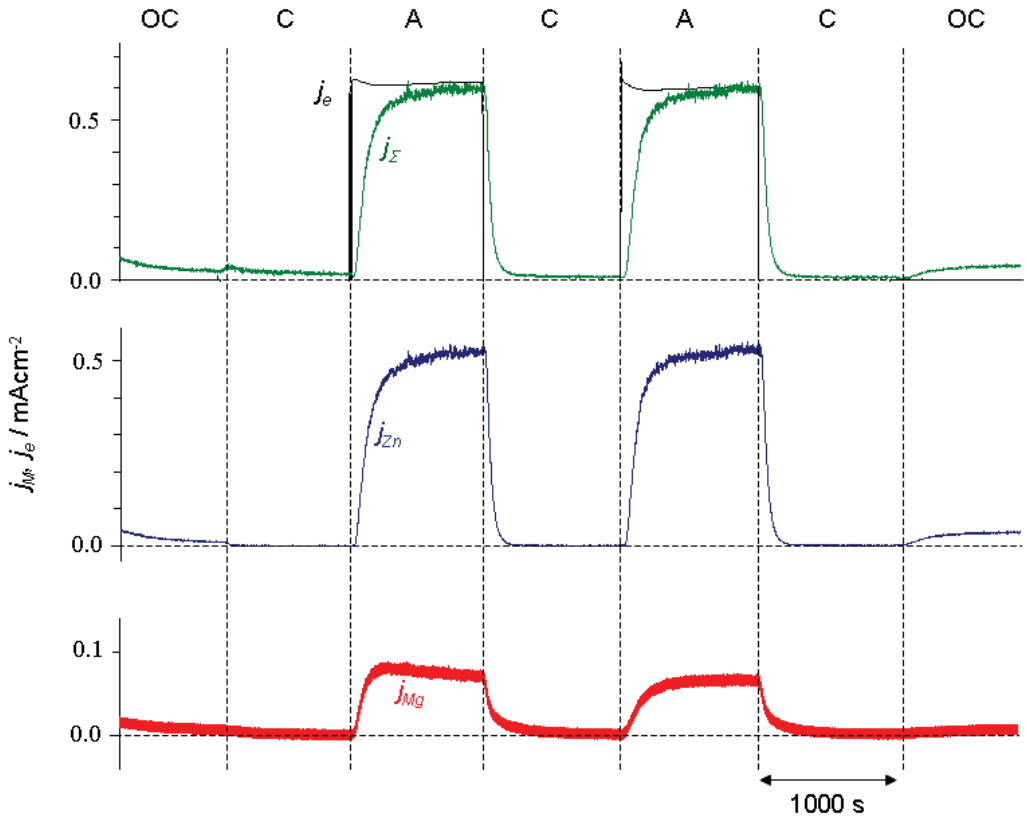


Fig. 3. Evolution of the elemental leaching rates (j_{Zn} and j_{Mg}) and of the total current (j_e) from ZM coating in 0.1 M NaCl under applied cycles of anodic (A) and cathodic (C) potentials. Only anodic current and dissolution of elements detectable in anodic domain are shown. OC domains represent the spontaneous dissolution rates before and after cycling. Applied potential sequence is C: -1.25 V vs. SCE, A: -0.95 V vs. SCE.

As in case of anodic polarization after OC exposure (Fig. 2), after cathodic impulse (Fig. 3), ZM presents a selective dissolution of Mg under anodic polarization – the molar fraction of Zn and Mg in the soluble ions is 87 % and 13 % respectively in NaCl and 86 % and 14 % in NH_4Cl + $NaHCO_3$, compared to 81 % of Zn and 7 % of Mg expected from the bulk composition and 66 % of Zn and 33 % of Mg expected for Zn_2Mg intermetallic. In contrast, in NaCl (Fig. 3) the total current at steady state match with an error less than 2% with the sum of the dissolution currents, in particular in the end of the second cycle. This correlates with the preferential attack of the ternary phase containing Zn_2Mg and demonstrates that in the OC-anodic experiment (Fig. 2) oxides formed by a spontaneous reaction create local barriers for soluble ions to escape. It also shows that the Al is not oxidized in these conditions and no corrosion product is accumulated during the anodic reaction in NaCl.

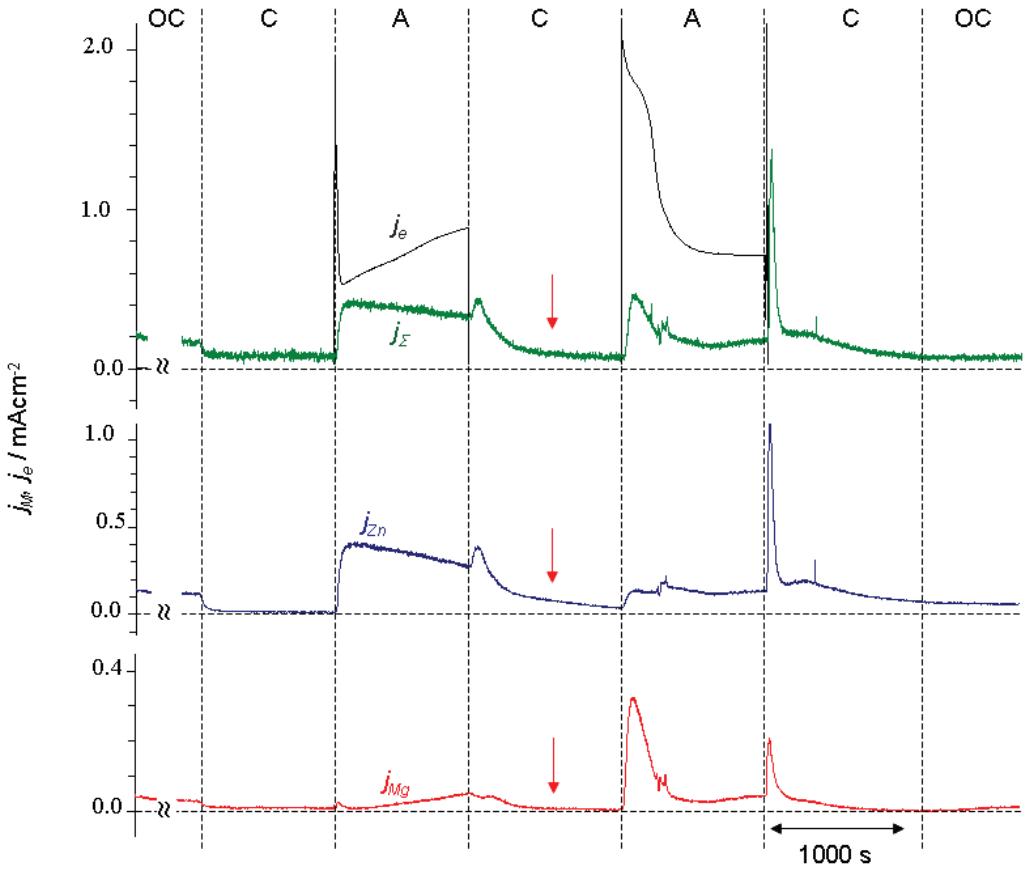


Fig. 4. Evolution of the elemental leaching rates (j_{Zn} and j_{Mg}) and of the total current (j_e) from ZM coating in 0.1 M NH_4Cl + 0.1 M $NaCO_3$ under applied cycles of anodic (A) and cathodic (C) potentials. Only anodic currents and Zn and Mg leaching are shown. OC domains represent the spontaneous dissolution rates before and after cycling. Applied potential sequence: C: -1.25 V vs. SCE, A: -0.95 V vs. SCE.

Similar to the OC-anodic experiment from Fig. 2c, the kinetic effects are observed in the mixed electrolyte and a significant quantity of corrosion products is accumulated during the anodic pulse.

3.3 Cathodic reactivity of ZM under anodic-cathodic polarization cycles

Fig. 5 shows the cathodic part of the polarization experiment (anodic part shown in Fig. 3 and 4): the total dissolution current j_e (negative during cathodic polarization) and j_{Al} from ZM coating in (a) 0.1 M NaCl and in (b) the mixture 0.1 M NH_4Cl + 0.1 M $NaHCO_3$.

Under cathodic polarization in NaCl electrolyte (Fig.5a), Al selective dissolution from ZM is detected, which is in accordance with previous publications [1,2,19,24-25]. The measured total current j_e during the first cathodic polarization is approximately 3-4 times higher than the Al dissolution current j_{Al}. During all three cathodic polarizations, the

total cathodic current stays similar, but the Al dissolution decreases, which increases the ratio between j_e to j_{Al}.

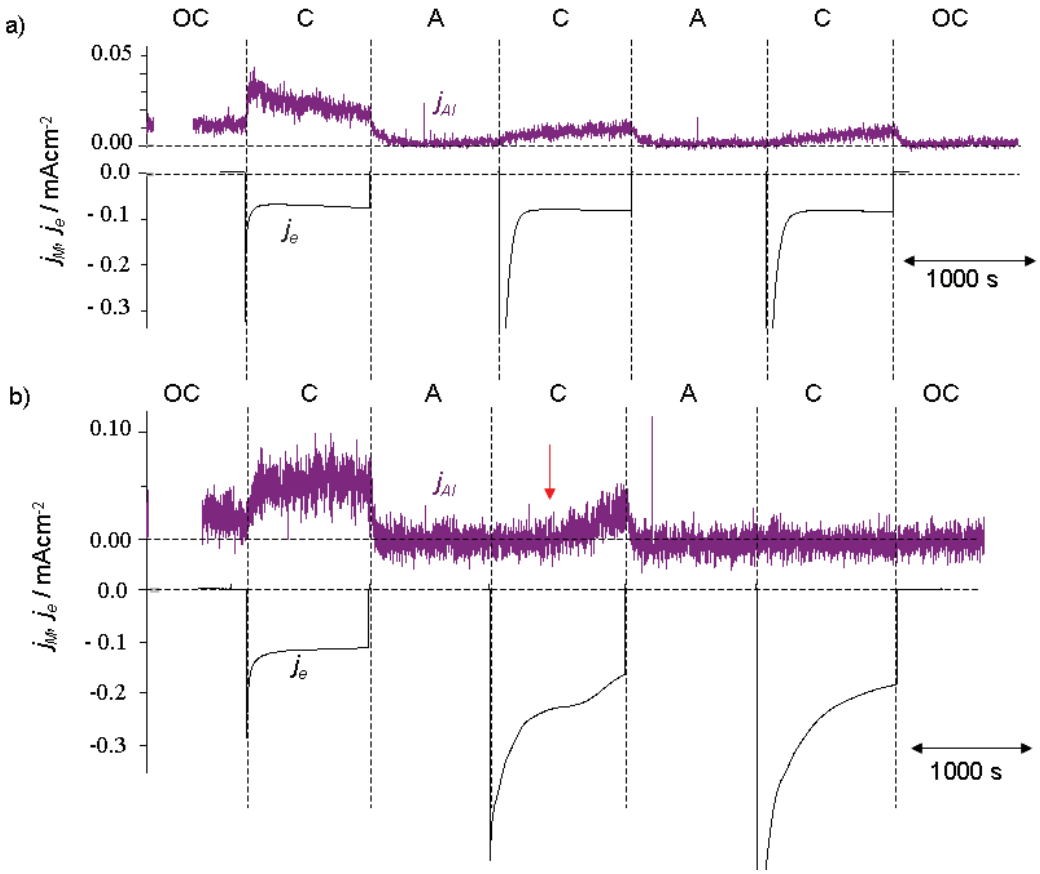


Fig. 5. Evolution of the elemental leaching rates of Al (j_{Al}) and of the total current (j_e) from ZM coating in (a) 0.1 M NaCl and (b) 0.1 M NH_4Cl + 0.1 M $NaHCO_3$ under applied cycles of anodic (A) and cathodic (C) potentials. Only cathodic currents are shown. OC domains represent the spontaneous dissolution rates before and after cycling. Applied potential sequence is C: -1.25 V vs. SCE, A: -0.95 V vs. SCE.

Under cathodic polarization in 0.1 M NH_4Cl + 0.1 M $NaHCO_3$ electrolyte (Fig. 5b), j_e from ZM during the first cathodic polarization is about 2 times higher than j_{Al}; at the same time, from Fig. 4, some soluble Mg signal is detected.

The decrease of the absolute value of j_e follows the decrease j_{Mg}. One may notice that on the second cathodic polarization, once the Mg signal is no more detected and Al starts to dissolve (indicated by an arrow on Fig. 4b and 5b) with a ratio of j_e to j_{Al} higher than 7, indicating that another reaction consumes the electrochemically generated hydroxide. In the 3rd cathodic polarization, Al dissolution was not detected at all.

3.4 Reactivity of ZA compared to ZM under anodic-cathodic polarization cycles

In order to verify that the presence of Mg would be responsible for the delayed Al cathodic dissolution in mixed electrolyte, similar "anodic-cathodic" cycling was made for ZA alloy which contains higher Al (5 wt. %) but no Mg. The results are presented in Fig. 6. In the cathodic domain, the total current on ZA in NaCl (Fig. 6a) is about 50 % higher than on ZM (Fig. 5a), but Al dissolution is about 3 times smaller. At the same time, for ZA, the reactivity is the same for all 3 cathodic polarizations. In mixed NH_4Cl + $NaHCO_3$ electrolyte (Fig. 6b) the total current j_e increases under anodic applied potential which is similar to ZM. However, the Al activation in the second cathodic polarization, just after the anodic polarization, starts much quicker. Moreover, the cathodic Al dissolution in mixed electrolyte is about 3 times higher than in NaCl. This means that lower cathodic dissolution of Al from ZM in NH_4Cl + $NaHCO_3$ electrolyte compared to NaCl can not be explained only by the properties of the electrolyte.

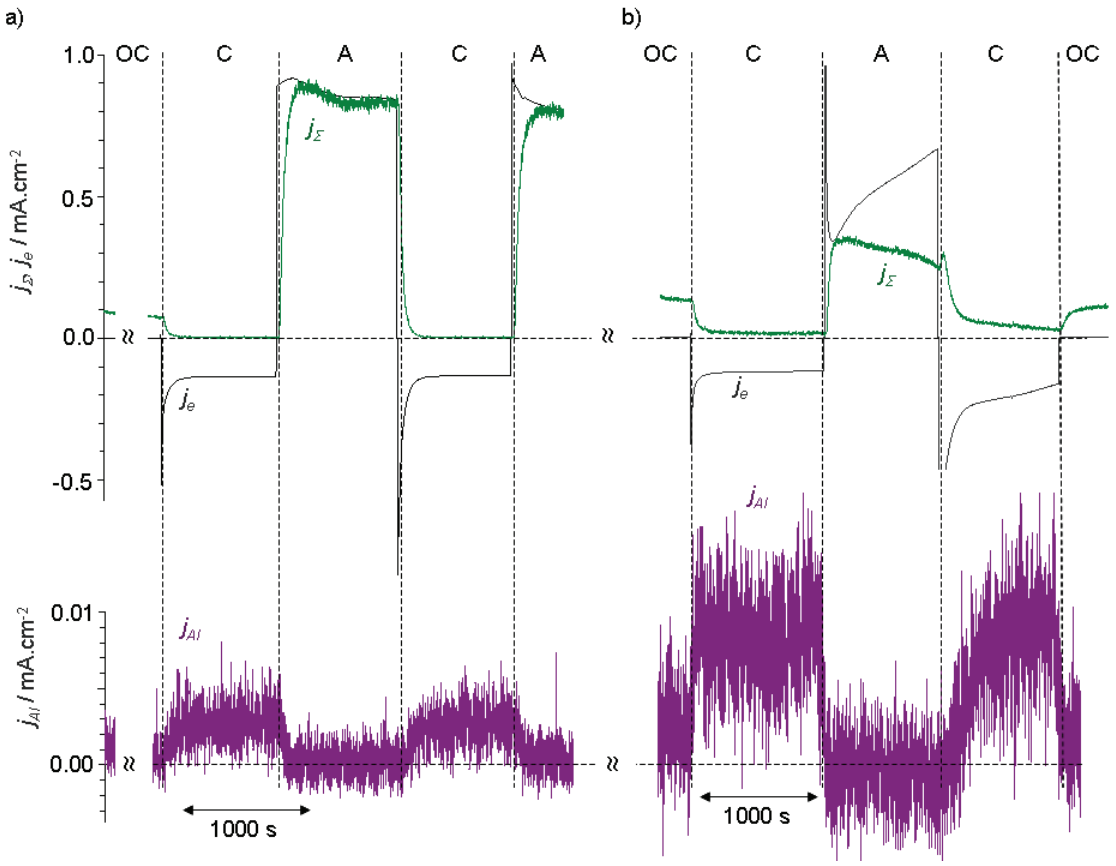


Fig. 6. Evolution of the sum of elemental leaching rates ($j_\Sigma = j_{Zn} + j_{Al}$), the Al leaching rate (j_{Al}) and the total current (j_e) for ZA coating in (a) 0.1 M NaCl and (b) 0.1 M NH_4Cl + 0.1 M $NaHCO_3$. Applied potential sequence is C: -1.25 V vs. SCE, A: -0.95 V vs. SCE.

Because of significant difference between j_e and j_Σ indicating precipitation of insoluble products on the surface of the samples and different cathodic reactivity between ZM and ZA, the samples were analyzed by XRD at the end of both cyclic experiments in order to identify the corrosion products. The results are summarized in Table 4.

Table 4. Water insoluble crystalline products detected by XRD on ZM and on ZA after the cyclic polarization tests shown in Fig. 3 - 6.

Coating	Detected corrosion products after cyclic polarization experiment	
	in NaCl	in NH_4Cl + $NaHCO_3$
ZM	LDH	$ZnCO_3$, $Mg(OH)_2$
ZA	LDH	$ZnCO_3$

The ZM from the NaCl test contained only LDH product, which correlates well with Al cathodic dissolution furnishing necessary Al ions. In contrast, after the test in NH_4Cl + $NaHCO_3$ electrolyte, no LDH was detected on ZM but $ZnCO_3$ and $Mg(OH)_2$.

ZA coating also formed LDH after the polarization test in NaCl and only $ZnCO_3$ after the test in NH_4Cl + $NaHCO_3$ electrolyte.

4 Discussion: role of the electrolyte composition for intrinsic reactivity of ZnMgAl coatings

4.1 Cathodic and anodic reactivity and the formation of corrosion products

Higher intrinsic anodic reactivity of ZM compared to GI in different electrolytes observed in AESEC experiments indicates the importance of cathodic reactions and of the barrier effect of formed corrosion products on the corrosion mechanisms of this coating.

The intrinsic reactivity of ZM in NaCl, observed by AESEC for reactions of short times, is different from the reactivity in NH_4Cl + $NaHCO_3$ electrolyte. In NaCl electrolyte, the selective anodic dissolution of Mg-rich phase, binary and ternary eutectic (reactions from Eq. 29a,b), is observed for ZM, which is coherent with previous observations [2,12,14].

$$Zn \rightarrow Zn^{2+} + 2e^- \quad (29a)$$

$$Zn_2Mg \rightarrow 2Zn^{2+} + Mg^{2+} + 6e^- \quad (29b)$$

Under anodic polarization, no evidence of the significant accumulation of corrosion products due to anodic reaction in 0.1 M NaCl (at least at short times and with renewed electrolyte) was observed, which is coherent with the idea that corrosion product precipitation (reactions given by Eq. 30) requires a pH increase usually associated with the cathodic reaction.

$$Zn^{2+} + 2OH^- \rightarrow Zn(OH)_2 \qquad (\text{or } ZnO + H_2O) \tag{30a}$$

$$5Zn^{2+} + 8OH^- + 2Cl^- \rightarrow Zn_5(OH)_8Cl_2 \tag{30b}$$

$$5Zn^{2+} + 6OH^- + 2CO_3^{2-} \rightarrow Zn_5(OH)_6(CO_3)_2 \tag{30c}$$

$$Zn_5(OH)_8Cl_2 + 2HCO_3^- \rightarrow Zn_5(OH)_6(CO_3)_2 + 2H_2O + 2Cl^- \tag{30d}$$

In contrast, in mixed electrolyte the formation of Zn and Mg carbonates is possible even at neutral pH (Fig. 7) due to low solubility of carbonates compared to chlorides.

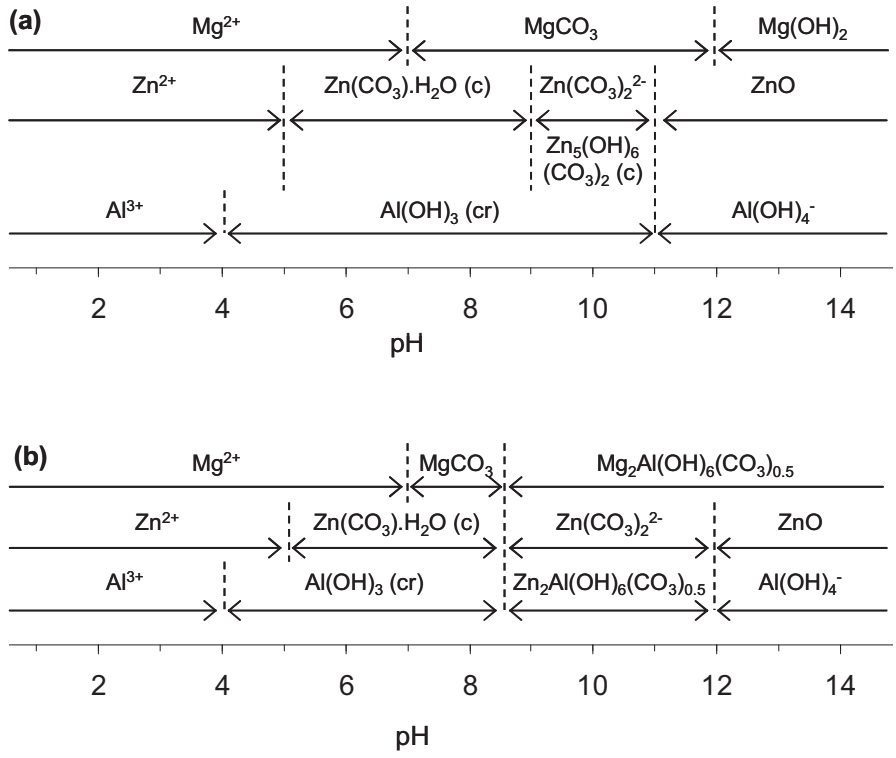


Fig. 7. Predominant equilibrium species predicted for 2mM Zn^{2+} + 1mM Mg^{2+} + 1mM Al^{3+} + CO_3^{2-} using the Hydra-Medusa software [41] and associated database of equilibrium constants at 25C°. The complexes used in the simulation include (a) for Mg species alone: $Mg_4(OH)_4^{4+}$, $MgOH^+$, $Mg(OH)_2$ (c), with CO_3^{2-}: $MgCO_3$, $MgCO_3$ (c), $MgHCO_3^+$, $MgCO_3.3H_2O$ (c), $Mg_5(CO_3)_4(OH)_2.4H_2O$ (c), $MgCO_3$:$Mg(OH)_2.3H_2O$ (c), MgO (cr); Zn species alone: $Zn(OH)_2$, $Zn(OH)_3^-$, $Zn(OH)_4^{2-}$, $Zn_2(OH)_6^{2-}$, Zn_2OH^{3+}, $Zn_4(OH)_4^{4+}$, $ZnOH^+$, ZnO (cr), with CO_3^{2-}: $Zn(CO_3)_2^{2-}$, $ZnCO_3$, $ZnCO_3$ (c), $ZnCO_3.H_2O$ (c), $ZnHCO_3^+$, $Zn_5(OH)_6(CO_3)_2$ (c); Al species alone: $Al(OH)_2^+$, $Al(OH)_3$, $Al(OH)_4^-$, $Al_2(OH)_2^{4+}$, $Al_3(OH)_4^{5+}$, $AlOH^{2+}$, $Al(OH)_3$ (am), $Al(OH)_3$ (cr), AlOOH (cr); mixed species: $MgAl_2O_4$ (c); (b) including layered double hydroxides (LDH): $Mg_2Al(OH)_6(CO_3)_{0.5}$, $Zn_2Al(OH)_6(CO_3)_{0.5}$ [40].

From Fig. 3 and 5a, the cathodic current in NaCl is not affected by the presence of an intermediate anodic polarization, indicating that if a barrier effect is related to the formed corrosion product, this product is stable during both cathodic and anodic polarization in NaCl.

Regarding the cyclic polarization experiment for ZM, the ratio j_e / j_{Al} is higher in NaCl than in mixed electrolyte during the first cathodic polarization but increases much quicker in mixed electrolyte after anodic pulse indicating that some Al stays on the surface in an insoluble form. The cathodic dissolution of Al from ZM after an anodic pulse was strongly delayed compared to ZA coating and started only once soluble Mg is no longer detected implying the effect of Mg on the cathodic reactivity.

Some explanations of the decrease of Al dissolution are possible.

1. The accumulation of corrosion products under cathodic pulse can be due to the combination with the ions previously formed during anodic pulse (Zn^{2+}, Mg^{2+}) forming LDH:

$$2Al(OH)_4^- + 6Zn^{2+} + 8OH^- + CO_2^{2-} \rightarrow Zn_6Al_2(OH)_{16}CO_3 \quad (31a)$$

$$2Al(OH)_4^- + 6Zn^{2+} + 8OH^- + 2Cl^- \rightarrow Zn_6Al_2(OH)_{16}Cl_2 \quad (31b)$$

$$2Al(OH)_4^- + 6Mg^{2+} + 8OH^- + CO_3^{2-} \rightarrow Mg_6Al_2(OH)_{16}CO_3 \quad (31c)$$

Etc.

This scenario seems to be probable in NaCl electrolyte in which LDH compounds were observed after the experiment. The small decrease of the Al dissolution correlates with the fact that the quantity of Zn and Mg, which are available after the anodic reaction, is not very high because insoluble products do not accumulate at the surface.

2. Another possibility is that the increase of pH, which is necessary to dissolve already oxidized Al, is delayed by a direct recombination of ions released during anodic pulse (Mg^{2+}, Zn^{2+}) or corrosion products ($MgCO_3$, $ZnCO_3$) with the electrochemically generated hydroxide, as in reactions

$$Mg^{2+} + 2OH^- \rightarrow Mg(OH)_2 \quad (32a)$$

$$MgCO_3 + H_2O + OH^- \rightarrow Mg(OH)_2 + HCO_3^- \quad (32b)$$

$$ZnCO_3 + H_2O + OH^- \rightarrow Zn(OH)_2 + HCO_3^- \quad (32c)$$

The idea of pH buffering by precipitation of $Mg(OH)_2$ [16,39], which could work in NaCl electrolyte, seems, however, to be insufficient to explain the stronger difference between ZM and ZA in the NH_4Cl + $NaHCO_3$ electrolyte with high buffer capacity than in unbuffered NaCl.

3. Corrosion products formed during the anodic pulse or in the beginning of the cathodic pulse by reactions from Eq. (32) can physically block the oxidized Al which couldn't escape into the electrolyte flow.

4. In case of cathodic reduction of residual oxides, formed during the anodic step, the Eq. (11) is no more valid. Hence the stoichiometry can not be calculated without quantification of this parallel cathodic process.

For the mixed electrolyte, it seems that either scenarios 2 or 3 are more probable than 1 because LDH was not detected on the surface after the experiment. In the contrary, $Mg(OH)_2$ was detected by XRD after the test on ZM in this electrolyte. Hence, the importance of the kinetic effects is also coherent with two facts: (i) Al was dissolved at the end of the second cathodic polarization on the cyclic experiment, (ii) $Mg(OH)_2$ was detected, which is less thermodynamically stable than MgAl-LDH (pK_{sp}(LDH) = 25,43, for $Mg_2Al(OH)_6(CO_3)$ [40]; $pK_{sp}(Mg(OH)_2)$ = 16,85 [40-41]).

The differences between ZA and ZM observed in cathodic domain imply the fundamental role of Mg ions on the cathodic Al dissolution. This was previously discussed for pure Al and Al-Mg alloys [24-26].

Zinc carbonates probably initiates the kinetic effects similar to Mg carbonates, however due to destabilization of zinc carbonates in presence of NH_4^+, the kinetic effects on the cathodic reactivity are less pronounced than in presence of Mg.

The processes which occur during cathodic and anodic cycles are schematically presented in Fig. 8.

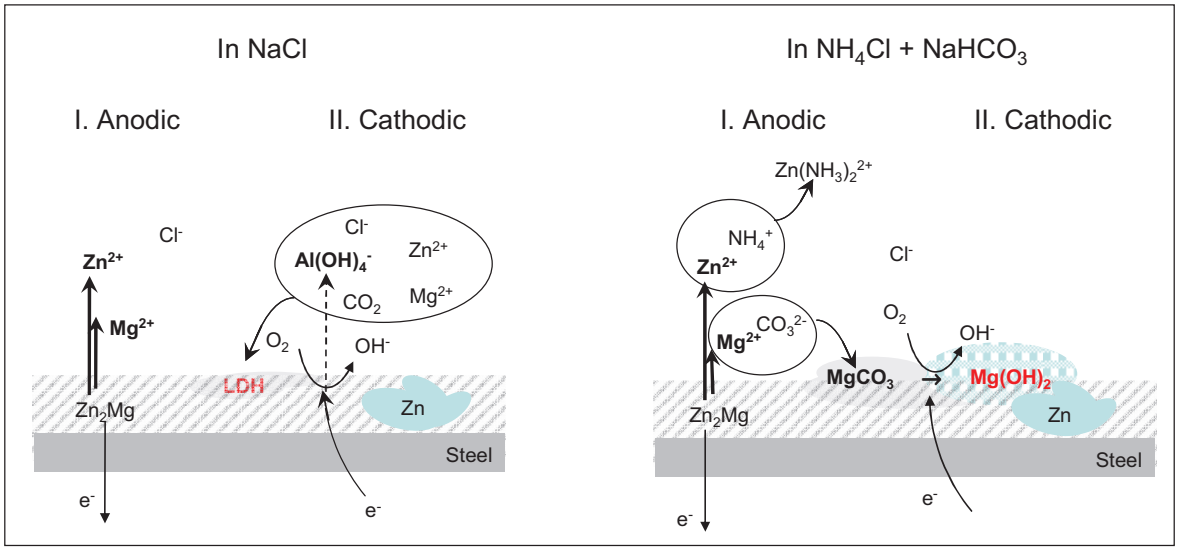


Fig. 8. Intrinsic reactivity of ZnMgAl coating in NaCl and NH_4Cl + $NaHCO_3$ electrolytes for cyclic polarization experiment.

On the basis of these observations we conclude that the cathodic reaction is mandatory for the formation of LDH. The AESEC results confirm the hypothesis that the Al-containing product accumulation in NaCl electrolyte is due to cathodic reactivity. It is also evident that the accumulation of some insoluble products during the anodic reaction can have consequences on the cathodic reactions.

4.2 Role of hydrogen-carbonate and ammonium ions on the formation of a barrier layer

In 0.1 M NH_4Cl + 0.1 M $NaHCO_3$ electrolyte, the kinetic effects are very strong for ZM coating. The stabilization of the current or dissolution rates takes more than 1000 s in both anodic and cathodic domains. The total current is higher than in NaCl electrolyte and the cathodic current increases with cycling. These results can be interpreted as the compound responsible for the barrier effect in this solution is destabilized during anodic polarization or does not form immediately once the cathodic potential is applied.

The LDH was not detected on ZM after the cyclic polarization in NH_4Cl + $NaHCO_3$ electrolyte. This can not be explained just by a buffering effect of the electrolyte, which results in the impossibility to dissolve Al, because $Mg(OH)_2$ was detected after the test and the equilibrium calculation using Hydra Medusa© software [41] using the 0.1 M carbonate concentration and Mg and Al ions concentrations equal to 1 mM (which corresponds in order of magnitude to the maximal concentrations detected by ICP during experiment) demonstrates that the pH necessary to form soluble Al species, pH = 11, can be reached if $Mg(OH)_2$, pH = 12) is formed (Fig. 7a). Moreover, as shown in Fig. 7b, LDH and not $Mg(OH)_2$ is expected at the equilibrium taking into account the solubility constants for LDH (constants taken from [40]) underlining the role of kinetic factors for corrosion product formation.

The total current on the fresh ZA surface under cathodic polarization is similar in both electrolytes, demonstrating the electrochemical neutrality of the electrolyte under applied potential -1.25 V vs SCE. For ZM, during the second and the third cathodic pulses the total current in NH_4Cl + $NaHCO_3$ electrolyte is higher than in NaCl, indicating that the barrier effect of the product formed on ZM in the first solution is lower than that of the product formed in the second solution.

Comparing cathodic currents in the experiments resulting in formation of LDH (in NaCl electrolyte) and in formation of $Mg(OH)_2$ (in NH_4Cl + $NaHCO_3$ electrolyte), one

may suppose that the LDH should play an important role for cathodic reactivity of ZM coating and the effect of Mg in ZM coatings can not be simply reduced to pH buffering.

5 Conclusion

1. In all tested electrolytes the intrinsic anodic reactivity of ZM is higher compared to GI. This result combined with previously communicated corrosion tests results [17], in which ZM is more efficient against corrosion than GI, indicates that for ZM coating the corrosion is governed by cathodic reactions.

2. AESEC measurement confirmed the selective anodic dissolution of Mg-rich phase from ZM. In NaCl, the stoichiometry correlates with anodic dissolution of Zn and Zn_2Mg; the situation is more complex in other electrolytes. No anodic dissolution of Al was observed during short experiments (up to 2 hours). The enrichment of the surface in metallic Al can be also expected in NaCl electrolyte. At open circuit, the dissolution of Al is detected only in NaCl electrolyte, not in presence of NH_4^+ and HCO_3^-.

3. For both, GI and ZM coatings, NH_4^+ increases the anodic reactivity of Zn and suppresses the accumulation of zinc corrosion products on the surfaces by forming soluble zinc complexes. In electrolytes containing this ion, the stoichiometry of Zn and Mg dissolution and the total anodic current indicates that the whole surface can be anodically oxidized but Al stays in an insoluble form.

4. The bicarbonate ions increase the accumulation of insoluble zinc corrosion products but do not decrease the total anodic current. The rapidly formed Zn-rich corrosion product does not decrease the anodic reactivity.

5. The cathodic dissolution of Al from both, ZA and ZM, is higher in the mixture of NH_4Cl and $NaHCO_3$ than in NaCl electrolyte in a cathodic polarization just after a open circuit exposure (without preliminary anodic polarization). However, after anodic pulse, it is delayed or even suppressed on ZM in the mixed electrolyte. The last effect is not observed in ZA coating. We suppose that this delay is due to the kinetics effects related to the presence of Mg ions, expected in form of carbonates, formed during anodic polarization.

6. No LDH (but $Mg(OH)_2$) on ZM was detected after short experiments in presence of bicarbonate on ZM and ZA coatings indicating the importance of kinetics factors for the formation of corrosion products during first stages of corrosion.

Acknowledgements

The results of this work were presented during European Conference EUROCORR 2013 in Estoril (Portugal). Authors are grateful for all colleagues participating in discussions of this work during these conferences.

Reference

[1] L. Jiang, P. Volovitch, M. Wolpers, K. Ogle "Activation and inhibition of Zn-Al and Zn-Al-Mg coatings on steel by nitrate in phosphoric acid solution" Corros. Sci. 60 (2012) 256–264

[2] P. Volovitch, T.N. Vu, C. Allély, A. Abdel Aal, K. Ogle "Understanding corrosion via corrosion products characterization: II. Role of alloying elements in improving the corrosion resistance of Zn-Al-Mg coatings on steel" Corros. Sci. 53 (2011) 2437–2445

[3] P. Volovitch, C. Allély, K. Ogle "Understanding corrosion via corrosion products characterisation: I. Case study of the role of Mg alloying in Zn-Mg coating on steel" Corros. Sci. 51 (2009) 1251-1262

[4] Z.Y. Chen, D. Persson, C. Leygraf "Initial NaCl-particle induced atmospheric corrosion of zinc – Effect of CO_2 and SO_2" Corros. Sci. 20 (2008) 11-123

[5] T. Prosek, D. Thierry, C. Taxén, J. Maixner "Effect of cations on corrosion of zinc and carbon steel covered with chloride deposits under atmospheric conditions" Corros. Sci. 49 (2007) 2676–2693

[6] S. Oesch, M. Faller "Environmental effects on materials: the effect of the air pollutants SO_2, NO_2, NO and O_3 on the corrosion of copper, zinc and aluminium. A short literature survey and results of laboratory exposures" Corros. Sci. PII: S0010-938X(97)00047-4

[7] D. B. Blüncher, J.-E. Svensson, L.-G. Johansson "The influence of CO_2, $AlCl_3.6H_2O$, $MgCl_2.6H_2O$, Na_2SO_4 and NaCl on the atmospheric corrosion f aluminium" Corros. Sci. 48 (2006) 1848-1866

[8] T.N. Vu, M. Mokaddem, P. Volovitch, K. Ogle "The Anodic Dissolution of Zinc and Zinc Alloys in Alkaline Solution II. Al and Zn partial dissolution from 5% Al-Zn coatings" Electrochim. Acta 4 (2012) 130-138

[9] C. Commenda, J. Pühringer "Microstructural characterization and quantification of Zn-Al-Mg surface coatings" Materials Charact. 61 (2010) 943-951

[10] Tanaka, K. Honda, A. Takahashi, Proc. 5th Int. Conf. on Zinc and Zinc Alloy Coated Steel Sheet, Verlag Stahleisen GmbH, Düsseldorf, (2001) p. 153

[11] T. Tsujimura, A. Komatsu And A. Andoh, Proc. 5th Int. Conf. on Zinc and Zinc Alloy Coated Steel Sheet, Verlag Stahleisen GmbH, Düsseldorf, (2001), p. 145

[12] M. Dutta, A. K. Halder, S. B. Singh "Morphology and properties of hot dip Zn-Mg and Zn-Mg-Al alloy coatings on steel sheet" Surface & Coatings Technology 205 (2010) 2578-2584

[13] J. Sullivan, S. Mehraban, J. Elvins, "In situ monitoring of the microstructural corrosion mechanisms of zinc–magnesium–aluminium alloys using time lapse microscopy" Corros. Sci. 53 (2011) 2208-2215

[14] S. Schuerz, M. Fleischanderl, G.H. Luckeneder, K. Preis, T. Haunschmied, G. Mori, A.C. Kneissl "Corrosion behaviour of Zn-Al-Mg coated steel sheet in sodium chloride-containing environement" Corros. Sci. 51 (2009) 2355-2365

[15] N. LeBozec, D. Thierry, M. Rohwerder, D. Persson, G. Luckeneder, L. Luxem "Effect of carbon dioxide on the atmospheric corrosion of Zn-Mg-Al coated steel" Corros. Sci. 74 (2013) 379-386

[16] D. Persson, D. Thierry, N. LeBozec, T. Prosek "*In situ* infrared reflection spectroscopy studies of the initial atmospheric corrosion of Zn-Al-Mg coated steel" Corros. Sci. 72 (2013) 54-63

[17] M. S. Azevedo, C. Allély, K. Ogle, P. Volovitch "Corrosion mechanisms of Zn(Mg,Al) coated steel in accelerated tests and natural exposure: 1. The role of electrolyte composition on the nature of corrosion products and relative corrosion rates" Corros. Sci. (2014) – submitted

[18] K. Ogle, S. Morel, D. Jacquet "Observation of self-healing functions on the cut edge of galvanized steel using SVET and pH microscopy" J.Electrochem. Soc. B 153 (2006) B1-B5

[19] K. Ogle, J. Baeyens, J. Swiatowska, P. Volovitch "Atomic emission spectroelectrochemistry applied to dealloying phenomena: I. The formation and dissolution of residual copper films on stainless steel" Electrochim. Acta 54 (2009) 5163-5170

[20] M. Mokaddem, P. Volovitch, F. Rechou, R. Oltra, K. Ogle "The anodic and cathodic dissolution of Al and Al-Cu-Mg alloy", Electrochim. Acta 55 (2010) 3779-3786

[21] J. Swiatowska, P. Volovitch, K. Ogle "The anodic dissolution of Mg in NaCl and Na_2SO_4 electrolytes by atomic emission spectroelectrochemistry" Corros. Sci. 52 (2010) 2372-2378

[22] K. Ogle, M. Mokaddem, P. Volovitch, "Atomic emission spectroelectrochemistry applied to dealloying phenomena II. Selective dissolution of iron and chromium during active - passive cycles of an austenitic stainless steel" Electrochimica Acta 55 (2010) 913-921

[23] M. Mokaddem, P. Volovitch, K. Ogle "The anodic dissolution of zinc and zinc alloys in alkaline solution. I. Oxide formation on electrogalvanized steel" Electrochim. Acta 55 (2010) 7867-7875

[24] K. Ogle, M. Serdechnova, M. Mokaddem, P. Volovitch "The cathodic dissolution of Al, Al_2Cu, and Al alloys" Electrochim. Acta 56 (2011) 1711-1718

[25] P. Volovitch, M. Serdechnova, K. Ogle "Aqueous Corrosion of Mg-Al binary alloys: roles of Al and Mg" Corrosion 68 (2012) 557-570

[26] M. Sederchnova, P. Volovitch, Fr. Brisset, K. Ogle "On the cathodic dissolution of Al and Al alloys" Electrochim. Acta http://dx.doi.org/10.1016/j.electacta.2013.09.145 - Article in Press

[27] S. Schürz, G.H. Luckeneder, M. Fleischanderl, P. Mack, H. Gsaller, A.C. Kneissl, G. Mori "Chemistry of corrosion products on Zn–Al–Mg alloy coated steel" Corros. Sci. 52 (2010) 3271–3279

[28] P. Schouller-Guinet, C. Allely, P. Volovitch "ZnAlMg: an innovative metallic coating that offers protection in the harshest environments" in: Proceedings of Galvatech '11, Genova, Italy, 2011

[29] T. Prosek, D. Thierry, D. Persson, J. Stoulil "Corrosion products formed on ZnMg and ZnAlMg coatings in model atmospheric conditions" in: Proceedings of Galvatech '11, Genova, Italy, 2011

[30] T. A. Keppert, G. Luckeneder, K-H Stellnberger, G. Mori "Influence of the pH value on the corrosion of Zn-Al-Mg hot-dip galvanized steel sheets in chloride containing

environments" in: Proceedings of NACE International – Corrosion Conference & Expo 2012, C2012-0001493

[31] G. Luckeneder, M. Fleichanderl, T. Steck, K-H Stellnberger, J. Faderrl, S. Schuerz, G. Mori "Corrosion mechanisms and cosmetic corrosion aspects of zinc-aluminium-magnesium and zinc-chromium alloy coated steel strip" in: Proceedings of Galvatech '11, Genova, Italy, 2011

[32] K. Ueda, A. Takahashi, Y. Kubo, "Investigation of corrosion resistance of pre-painted Zn-11%Al-3%Mg-0.2%Si alloy coated steel sheet through outdoor exposure test in Okinawa" La Metallurgia Italiana – Corrosione (2012) pp. 13-19

[33] T. Prosek, N. Larché, M. Vlot, F. Goodwin, D. Thierry "Corrosion stability of Zn-Al-Mg coatings in open and confined zones in conditions simulating automotive applications" in: Proceedings of Galvatech '11, Genova, Italy, 2011

[34] D. Thierry, T. Prosek, N. Le Bozec, E. Diller "Corrosion protection and corrosion mechanisms of continuous galvanised steel sheet with focus on new coatings alloys" in: Proceedings of Galvatech '11, Genova, Italy, 2011

[35] M. Uranaka, T. Shimizu "Corrosion resistance of hot dip Zn-6%Al-3%Mg alloy coated steel sheet used in automotive parts" in: Proceedings of Galvatech '11, Genova, Italy, 2011

[36] N. LeBozec, D. Thierry, A. Peltola, L. Luxem, G. Luckeneder,G. Marchiaro, M. Rohwerder "Corrosion performance of Zn–Mg–Al coated steel in accelerated corrosion tests used in the automotive industry and field exposures" Mater. Corros. 64 (2013) No. 9999 pp. 1-10

[37] N. Shimoda, M. Nakazawa, H. Nomura, Y. Marimoto "Atmospheric corrosion resistance of Zn-11%Al-3%Mg-0.2%Si coated steel" in: Proceedings of Galvatech '11, Genova, Italy, 2011

[38] A. Nazarov, D. Thierry "Rate-determining reactions of atmospheric corrosion" Electrochim. Acta 49 (2004) 2717-272

[39] N. C. Hosking, M. A. Ström, P. H. Shipway, C. D. Rudd "Corrosion resistance of zinc-magnesium coated steel" Corros. Sci. 49 (2007) 3669-3695

[40] C. A. Jonhson, F. P. Glasser "Hydrotalcite-like minerals $M_2Al(OH)_6(CO_3)_{0.5}.XH_2O$, where M = Mg, Zn, Co, Ni) in the environment: synthesis, characterization and thermodynamic stability" Clays Clay Miner. 51 (2003) N. 1 pp. 1-8

[41] I. Puigdomenech, Hydra/Medusa Chemical Equilibrium Database and Plotting Software KTH Royal Institute of Technology, 2004

Chapter V

The effect of Mg and Al on the formation and properties of corrosion products

M. Salgueiro Azevedo, C. Allély, K. Ogle, P. Volovitch

Corrosion Science (submitted in April 2014)

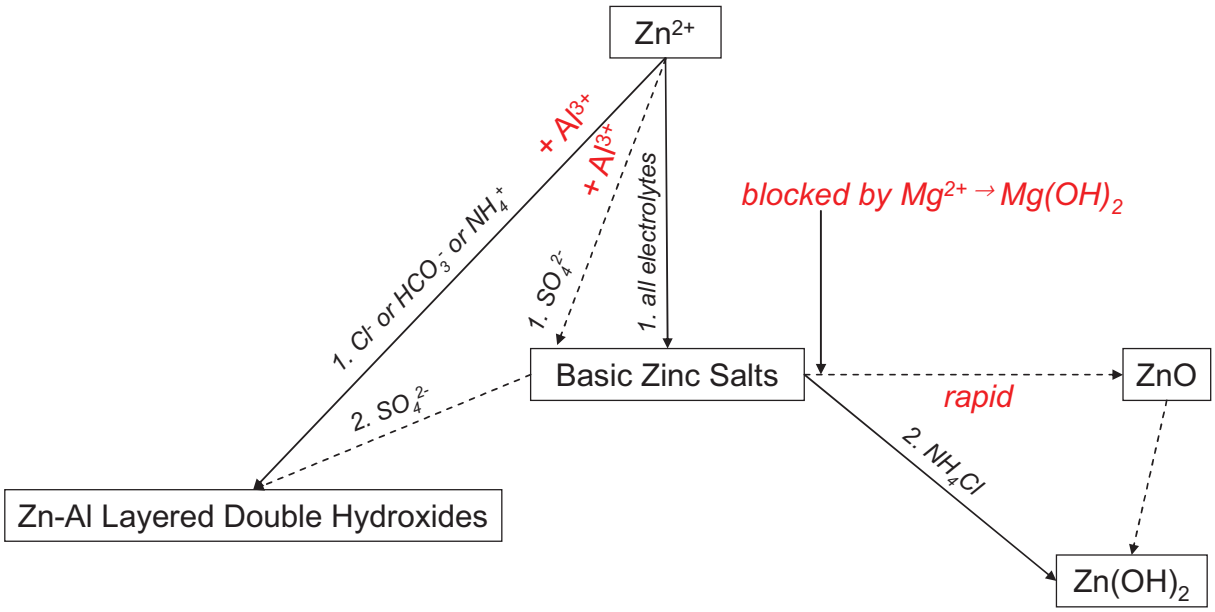
Corrosion mechanisms of Zn(Mg,Al) coated steel: The effect of Mg and Al on the formation and properties of corrosion products

Abstract

Basic zinc salts (BZS) on GI and BZS and layered double hydroxides (LDH) on ZnMgAl were showed efficient to reduce the oxygen reduction rate. On GI, their transformation, under cathodic polarization, into ZnO loses the inhibiting effect. On ZnMgAl, in contradiction to GI, they stay stable. Acid-base titrations of Zn^{2+}-containing solutions with and without Mg^{2+} and Al^{3+} explained that Mg^{2+} ions are able to delay the transformation of BZS into ZnO and Al^{3+} forms LDH that is stable even in very alkaline pH. A residual Al "skeleton" during corrosion could be able to increase the compactness of the corrosion products formed on ZnMgAl.

Keywords: Electrogalvanized steel (A); ZnAlMg (A); Polarization (B); Corrosion product (C), Corrosion mechanisms (C)

Graphical abstract



1 Introduction

ZnMgAl coatings for steel are known to be more resistant against corrosion than conventional hot-dip galvanized steel in many different environments – accelerated and atmospheric corrosion tests [1-17]. Their better anti-corrosion behavior is considered to be due to the combined addition of Mg and Al in the Zn-based coating that changes the microstructure and the nature of precipitated corrosion products.

The atmospheric corrosion rate of galvanized steel is governed by oxygen reduction which is often limited by diffusion through a layer of corrosion products. Therefore, the nature and the stability of corrosion products may be fundamental for the corrosion mechanisms of zinc-based coatings. [7,18]

Mg alloying results in the formation of an intermetallic phase with Zn, usually Zn_2Mg. Zn-Mg intermetallics are more active on the galvanic series than pure Zn, causing preferential corrosion. Binary and ternary eutectics are also detected in ZnMgAl coatings (Fig. 1) which are known to corrode preferentially compared to Zn dendrites [1-3]. The dissolution of the intermetallic phase could lead to the formation of Mg^{2+}-containing corrosion products as discussed by many authors [6-8]. Some authors observed Mg^{2+}-rich zinc compounds (oxides [6-7] and basic salts [8]). One hypothesis proposed is that Mg^{2+} doping enhances the insulating character of zinc compounds [9]. A second hypothesis is that the charge transfer at grain boundaries can also be limited in presence of Mg [10]. In other works [1,3,6], an important effect was assigned to pH buffering during precipitation of $Mg(OH)_2$. It should however be noted that insoluble corrosion products rich in Mg^{2+} were frequently not detected [1,3,6]. Therefore a third hypothesis has been proposed: Mg^{2+} stabilizes protective corrosion products of zinc such as simonkolleite ($Zn_5(OH)_8Cl_2.H_2O$) and zinc hydroxysulfate ($Zn_4(OH)_6SO_4.xH_2O$) against their transformation into soluble hydroxide complexes [1,3,6]. This stabilization effect may be attributed to pH buffering or to consumption of the excess anions. The importance of Mg content in the alloy for the corrosion resistance has also been noted [7].

From the microstructure of ZM samples [1], it seems that Al remains at early stages on the coating in an insoluble form, and at later stages, it participates as a layered double hydroxide (LDH). The LDH species are considered to possess good barrier properties [1,8,11,13,19]. However, in a recent work [14], it was demonstrated that, in humid atmosphere, the corrosion rate of ZnMgAl, for which LDH was detected, was higher than the corrosion rate of the same coating for which LDH was not detected. The absence of

LDH was also noted on ZnMgAl coatings in various NaCl-corrosion tests with neutral to slightly alkaline bulk pH (pH from 7 to 10) [12] or under wet exposure to NaCl in ambient air [14]. A heterogeneous distribution of Al on heavily corroded cross sections of the coatings was also observed by the authors. In contrast, other authors tested some conditions in which the formation of LDH is observed or claimed from the initial stages of corrosion [2,8,11,13].

The presence of Al also modifies the stability of different Zn patinas. Al promotes simonkolleite precipitation in place of ZnO at pH 9 and modifies the morphology of the Zn-product, increasing its compactness [20].

This work is focused on the role of Mg and Al on the formation and stability of different corrosion products. The effect of "natural" corrosion products formed on GI and on ZnMgAl on the oxygen reduction rate is evaluated by means of electrochemistry. Titration is used to study the precipitation of "synthetic" corrosion products in function of presence/absence of Mg^{2+} and Al^{3+} together with Zn^{2+} and different anions. The data are completed with the spatial distribution of corrosion products after corrosion tests using various electrolytes.

2 Experimental

2.1 Materials

The coated steel samples were supplied by ArcelorMittal. The reference sample used was the conventional hot dip galvanized steel (GI), with coating thickness of 20 μm, and composition Zn-Al(0.2 wt. %). The ZnMgAl coated steel (ZM) was also prepared by hot dip process with thickness of 20 μm and composition Zn-Mg (3.0 wt. %)-Al (3.7 wt. %). The mean coating composition and thickness are summarized in Table 1. GI coating is formed by a Zn layer (Fig. 1a) and ZM coating consists of Zn dendrites surrounded by a ternary phase of Zn, Al and intermetallic Zn_2Mg. Prior to experiments the samples were degreased with ethanol, but no surface activation was done (surface's oxides were still present).

Table 1. Thickness and chemical composition of the coatings.

Label	Coating	Thickness	Zn %wt	Al %wt	Mg %wt
GI	Conventional hot-dip galvanized	20µm	99.8	0.2	-
ZM	ZnMgAl	20µm	93.3	3.7	3.0

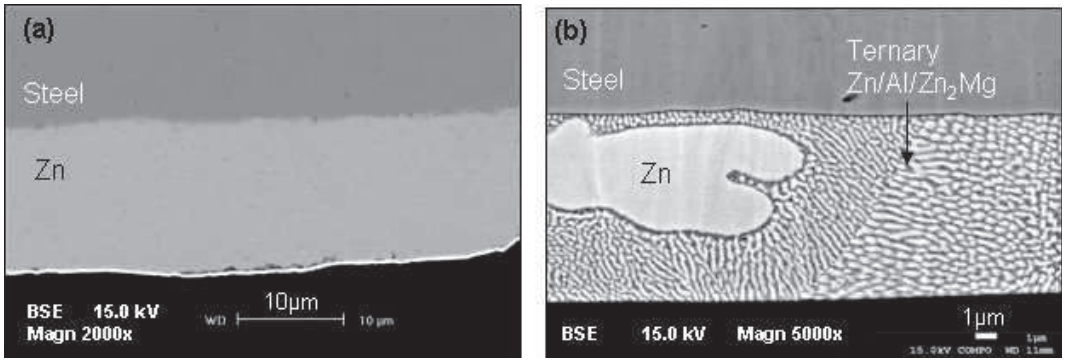


Fig. 1. SEM backscattered electron (BSE) images of uncorroded coatings in cross section with their respective phases.

2.2 Electrochemical experiments

All tests used a BioLogic VMP3 potentiostat for the potential/current control and measurement. A three electrode cell was used with a saturated calomel electrode as the reference electrode, a platinum wire as the counter electrode and the sample as the working electrode. For the oxygen reduction rate measurement, GI and ZM samples were immersed vertically in two different electrolytes, 10 g l^{-1} NaCl and 10 g l^{-1} "rain water" (RW) electrolyte (composition shown in Table 2). Initial pH was adjusted to 9 by NaOH.

Additional dissolution experiments were performed in 10 g l^{-1} Na_2SO_4 and 10 g l^{-1} NaCl (initial pH 7) using either (a) immersion of the surface of the ZM coating under applied potential (E = -0.95 V vs. SCE). The corrosion products at the cut-edge were removed using an ultrasonic bath of glycine 200 g l^{-1} of de-ionized water during 15 minutes.

2.3 Titration experiments

Titration experiments were performed with a Mettler Toledo One Click® Titration G20 titrometer using a 1.0 M NaOH solution. The pH was continuously monitored with a combined 3 M KCl glass electrode (Mettler Toledo), calibrated with disposable standard

buffer solutions (Merck). The pH evolution was recorded using Mettler Toledo LabX® light titration software.

Table 2. Composition and concentration of the Rain Water (RW) electrolyte.

Salts	Average content (mg/l)
$CaCl_2$	3.91
$(NH_4)_2SO_4$	1.82
Na_2SO_4	1.77
$NaNO_3$	1.81
$NaHCO_3$	0.69
Total:	10.00

All solutions were prepared with analytical reagent grade (> 99.5 %) reagents produced by MERCK and Millipore water (resistance $18\Omega^{-1}$). The composition of tested solutions is presented in Table 3. The initial volume of the solutions was 50 ml and the added volume of 1.0 M NaOH was 50 µl every 60 s. The temperature of the solutions was stable (25 ± 2 °C).

Table 3. Experimental conditions of the titration experiments, with label used on the figures and number of the figures where they are shown.

Label	Solution	Solvent	Fig.
1	0.04 M Zn^{2+}	0.171 M NaCl	2a
2	0.04 M Zn^{2+} + 0.02 M Mg^{2+}		
3	0.04 M Zn^{2+} + 0.02 M Al^{3+}		
4	0.04 M Zn^{2+} + 0.02 M Mg^{2+} + 0.02 M Al^{3+}		
1	0.04 M Zn^{2+}	0.171 M Na_2SO_4	2b
2	0.04 M Zn^{2+} + 0.02 M Mg^{2+}		
3	0.04 M Zn^{2+} + 0.02 M Al^{3+}		
4	0.04 M Zn^{2+} + 0.02 M Mg^{2+} + 0.02 M Al^{3+}		
1	0.04 M Zn^{2+}	0.008 M $NaHCO_3$	2c
2	0.04 M Zn^{2+} + 0.02 M Mg^{2+}		
3	0.04 M Zn^{2+} + 0.02 M Al^{3+}		
4	0.04 M Zn^{2+} + 0.02 M Mg^{2+} + 0.02 M Al^{3+}		
1	0.04 M Zn^{2+}	0.171 M NH_4Cl	2d
2	0.04 M Zn^{2+} + 0.02 M Mg^{2+}		
3	0.04 M Zn^{2+} + 0.02 M Al^{3+}		
4	0.04 M Zn^{2+} + 0.02 M Mg^{2+} + 0.02 M Al^{3+}		

2.4 Corrosion products and corrosion profile characterization

Corrosion products were characterized by X-ray diffraction (XRD) using the Cu(Ka1) radiation in a PANalytical X'Pert on powder. The XRD were collected with angular resolution of 0.02°. The data were scanned over the angular range 5–80° (2θ) and a counting time of 0.3 s/step. The evaluation of the data was done using the HighScore Plus software package, containing the JCPDS (ICDD) database files.

Raman spectrometry was performed using a LabRAM Aramis spectrometer, from Horiba Jobin Yvon, with green laser 532 nm. The results were compared with reference spectra taken from the literature [13,21-23] and from the RRUFF™ spectral database for minerals [24].

Table 4 shows the detected corrosion products in this work, with their respective formula and chosen abbreviation.

Table 4. Equivalence between the name of corrosion products, its composition and the chosen abbreviation.

Label	Name	Abbreviation	Chemical formula
1	Layered double hydroxide	LDH	$M(II)_xM(III)_y(A^-)_m(OH^-)_n\ zH_2O$ $M(II) = Zn^{2+}, Mg^{2+}$, $M(III) = Al^{3+}$ $A^- = CO_3^{2-}, Cl^-, SO_4^{2-}$
2	Simonkolleite	ZHC	$Zn_5(OH)_8Cl_2\ H_2O$
3	Zinc hydroxysulphate	ZHS	$Zn_4(OH)_6SO_4\ nH_2O$, n=3-5
4	Hydrozincite	HZ	$Zn_5(OH)_6(CO_3)_2\ H_2O$
5	Zincite	ZnO	ZnO
6	Zinc hydroxide	$Zn(OH)_2$	$Zn(OH)_2$
7	Magnesium hydroxide	$Mg(OH)_2$	$Mg(OH)_2$
8	Aluminium hydroxide	$Al(OH)_3$	$Al(OH)_3$

The samples were observed by scanning electron microscopy (SEM), using a Gemini 1530 microscope with FEG-source (Scottky-type) and energy dispersive spectroscopy (EDS) for elemental analysis with Si(Li) detector and QUANTAX evaluation software (Bruker AXS). The cross section observations were done on samples mounted in resin cut in cross section and polished mechanically. Before observation, a layer of 10 nm

of C was sputtered on the cross section in order to ensure charge evacuation from the surface that could contain non-conducting corrosion products.

Additional SEM observations together with EDS analysis were performed on corroded ZM coating from accelerated corrosion Salt Spray Test (SST) [25], with modified electrolyte called "rain water" (RW) in a concentration of 1.0 wt. % after 100 h of test, as described in [15].

Confocal Raman spectrometry was performed on the cross section of corroded ZM coating from accelerated cyclic corrosion test, VDA 233-102 [26], with 1 wt. % NaCl as electrolyte, after five cycles (correspondent to five weeks) of humid and dry phases.

3 Results

3.1 Effect of precipitated corrosion products on oxygen reduction rate

Fig. 2 shows the measured cathodic current under an applied cathodic potential of E_a = -1.15 V vs. SCE on GI and ZM coatings in (a) standard electrolyte for corrosion tests 10 g l^{-1} NaCl [25] and in (b) "rain water" (RW) electrolyte (composition in Table 2). The initial pH of the NaCl electrolyte was chosen to be about 9 in order to approach the "natural" pH of RW electrolytes and facilitate corrosion products precipitation. The RW electrolyte was chosen as it is expected to enhance the corrosion mechanisms in accelerated tests which are closer to mechanisms in the atmospheric corrosion than in NaCl tests [15]. The applied potential value was chosen in order to put the samples in the oxygen reduction domain [30].

One can observe in Fig. 2 that, in a NaCl electrolyte, the initial cathodic current measured for ZM was smaller than that for GI, which means a lower oxygen reduction rate on ZM than on GI (with natural oxides on the top layer). The current did not stabilize in RW electrolyte on either coating.

After the first step of applied cathodic potential, the system was returned to the open circuit potential (OC exposure) for 12 hours and the samples allowed to corrode spontaneously. Then the cathodic potential was again applied during 30 hours (Fig. 2). At the beginning of the second cathodic polarization, the cathodic current decreased significantly in both electrolytes and for both coatings as compared to the first cycle. However, it is clear from the figure that the cathodic reactivity of GI increases with time

under cathodic polarization while it remains stable for ZM. This is true for both electrolytes.

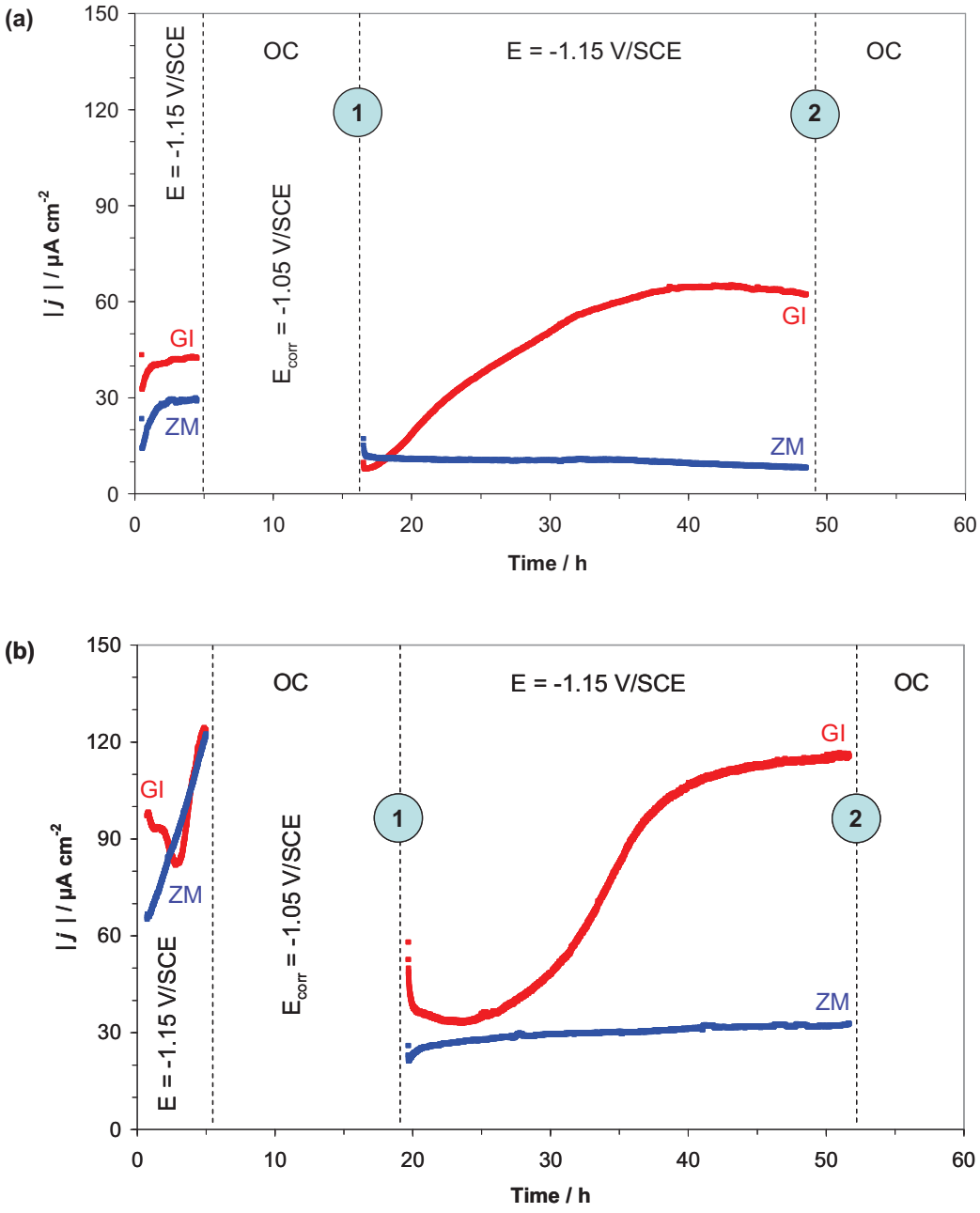


Fig. 2. Polarization experiment performed in (a) NaCl and (b) Rain water (RW) [15] electrolyte. Cathodic currents before and after open circuit (OC) exposure on GI and ZM coatings. Numbers 1 and 2 show points at which the experiment was stopped for corrosion product characterization.

Table 5 shows the corrosion products detected by X-ray diffraction at the beginning and at the end of cathodic pulses applied to GI and ZM coatings in both electrolytes (circled points 1 and 2 in Fig. 2). Directly after OC immersion in NaCl solution, ZHC and HZ, which can be both described as basic zinc salts (BZS), were formed on GI and LDH

on ZM. After immersion in RW electrolyte, BZS were formed on both coatings. At the end of the polarization, ZnO was detected on GI in both electrolytes, while the corrosion products of ZM did not change in NaCl electrolyte and, in RW, LDH was detected after cathodic polarization. Comparing the behavior of GI in RW and NaCl electrolytes, a longer period of the initial inhibitive effect is observed in RW, which can be associated with the buffer capacity of this electrolyte. Cathodic reactivity in RW was higher than in NaCl for both coatings and for fresh surfaces and after OCP exposure.

Table 5. Corrosion products identified on GI and ZM from the polarization experiment. The circled numbers 1 and 2 represent the sampling time (Fig. 2).

Electrolyte	Coating	Corrosion products characterization	
		①	②
		After OCP exposure	After cathodic polarization
NaCl	GI	ZHC, HZ	ZHC, ZnO
	ZM	LDH	LDH
RW	GI	ZHS, ZHC, HZ	HZ, ZnO
	ZM	ZHS, HZ	LDH, HZ

3.2 Morphology of corroded samples after different exposures

In order to determine common features in the spatial distribution of the corrosion products, SEM observations and Raman spectroscopy analysis on the cross section of ZM after 100 h of SST in 1 wt % NaCl and 1 wt % RW electrolytes were made. An example in Fig. 3 shows the cut edge of a ZM sample after 100 h of salt spray test (SST) in “rain water” electrolyte (RW) as described in [15]. The preferential corrosion of the ternary phase is observed and is in agreement with previous studies [1-3]. Al and Zn keep their relative positions inside the lamellas (a ternary phase of a non-corroded ZM shows lamellas of Zn together with lamellas of Zn_2Mg and Al is mostly found with the Zn_2Mg lamellas).

Raman spectroscopic analysis on a cut edge of ZM after SST with NaCl electrolyte is shown in Fig. 4. LDH was only found in the internal layer of corroded coating, not in the external layer of precipitated products. This figure illustrates the general tendency which

was observed in different exposure conditions: LDH is formed only inside the corroded coating in place of the former ternary phase.

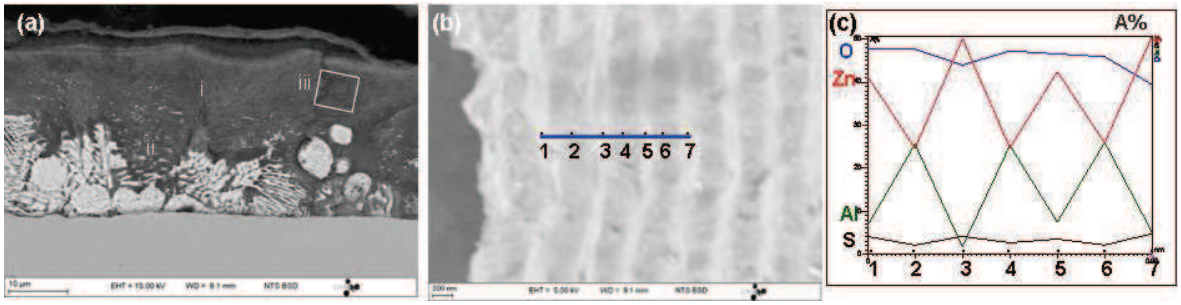


Fig. 3. SEM images and EDS analysis of ZM after 100h of SST performed in Rain water (RW) electrolyte. (a) ZM partially corroded: i. corroded ternary phase; ii. preferentially corroded ternary phase (Zn lamellas still metallic); iii. zoomed zone for Fig. (b) . (b) lamellas of the corroded ternary phase of ZM in which the numbered points shows the position of EDS punctual analysis of Fig. (c). (c) EDS punctual analysis: Al is mainly present at the dark lamellas (labelled by even numbers).

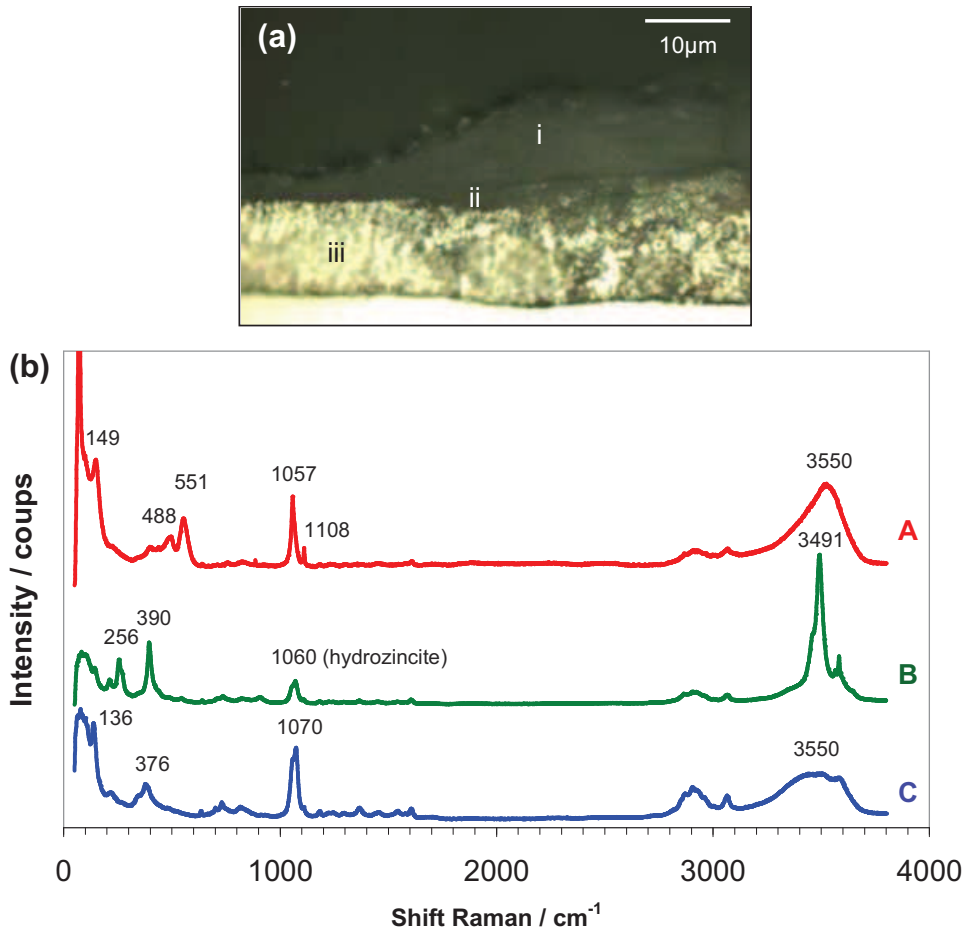
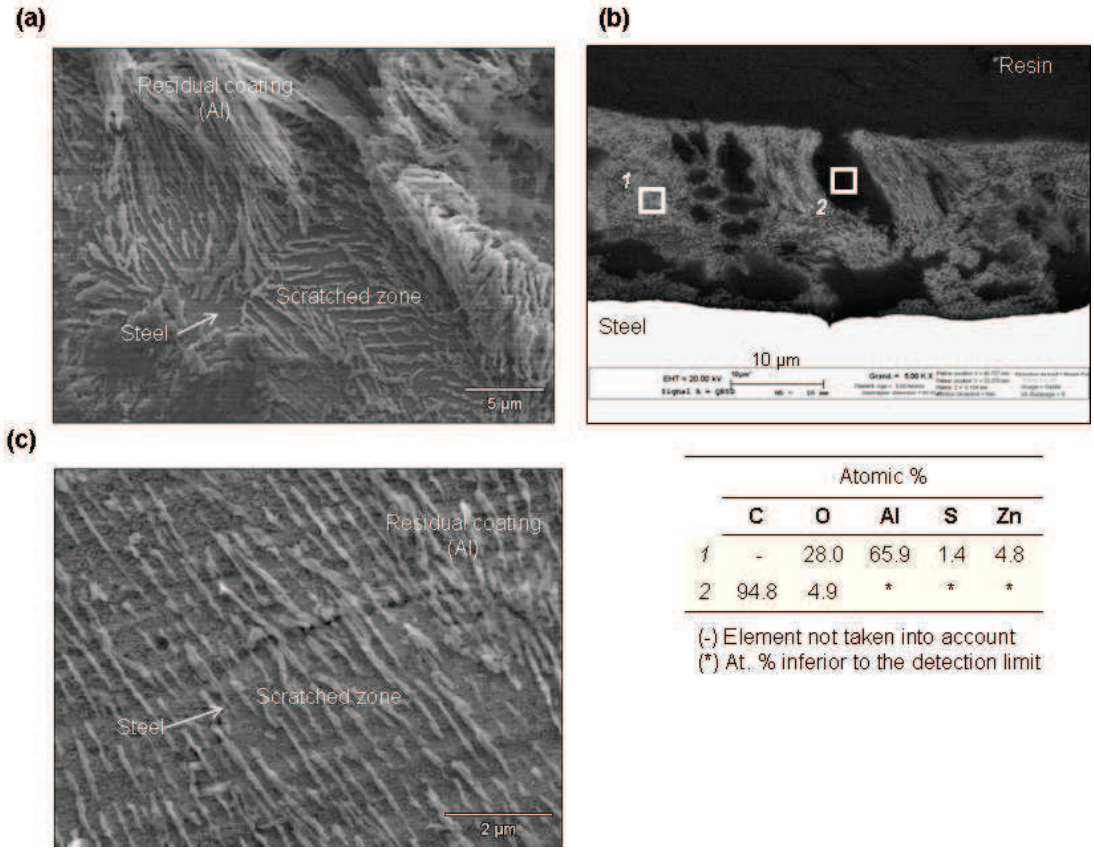


Fig. 4. (a) Optical micrograph of ZM after five weeks of cyclic VDA corrosion test [26] with NaCl 10 g l^{-1} electrolyte: (i) external layer of precipitated corrosion products; (ii) corroded coating; (iii) metallic coating. **(b)** Raman spectra 'A' obtained at (i) and spectra 'B' and 'C' obtained at (ii). 'A' is identified as LDH; 'B' shows presence of ZHC and HZ; 'C' is identified as HZ.

Fig. 5 shows SEM images of ZM coating after anodic dissolution (E_a = -0.95 V vs. SCE) in different electrolytes: Fig. 5(a) shows the top view of the remaining coating, in which it is possible to identify the steel substrate in a scratched zone and Al fiber forming a mesh; Fig. 5(b) shows the cut edge of the same sample, in which some cavities are seen, due to the Zn dendrites dissolution. EDS analysis confirmed that the remaining coating consists mostly of Al (less than 5 % of Zn) and that the cavities are filled with resin (mostly carbon is detected). Some oxidation of the Al mesh is detected, but as the atomic % of Al is more than twice bigger than that of oxygen, it is impossible that all Al is oxidized, so Al is found in a metallic form.

Considering the possibility of formation of LDH, as some zinc and sulfur were detected, one can verify the ratio Zn:Al:O:S for e.g. $Zn_2Al(OH)_6(SO_4)_{0.5}.H_2O$ compound is 4:2:18:1. This ratio is very close to the one found at the EDS analysis for Zn, O and S (Al is in excess). We propose, hence, that LDH is probably formed locally around the Al skeleton, inside the ternary phase.



	Atomic %				
	C	O	Al	S	Zn
1	-	28.0	65.9	1.4	4.8
2	94.8	4.9	*	*	*

(-) Element not taken into account
(*) At. % inferior to the detection limit

Fig. 5. Typical residual microstructure of ZM coating showing residual metallic Al after anodic dissolution at applied potential -0.95 V vs SCE in different electrolytes and following removal of zinc patinas in glycine solution. **(a)** Top view of the remaining coating (Al fiber) after dissolution in 0.171 M Na_2SO_4 . **(b)** Cut edge view of the same sample with EDS analysis showing at (1) the Al fiber forming a mesh or "skeleton" due to the dissolution of Zn and Zn_2Mg lamellas and (2) the filled with resin cavity from Zn dendrites dissolution. **(c)** Top view of the remaining coating (Al fiber) after dissolution in 0.171 M NaCl.

The residual structure of the Al-rich phase observed in all tested conditions suggests the importance of the initial phase distribution for the barrier effect of the corrosion products.

3.3 Formation and stability of the precipitated artificial corrosion products

Fig. 6 shows the titration curves obtained for the different solutions (Table 3), organized by matrix. Note that the x-axis is presented as the ratio of the hydroxide added to the metal Zn^{2+} ion initially present.

In all solutions containing Al^{3+} (curves.3 and 4 in Fig. 6a-d) the first plateau from pH 4 to 4.5 is due to the formation of $Al(OH)_2^-$ [27]. In absence of Al^{3+} (curves 1 and 2) the first plateau around pH 6.5 to 7 corresponds to the formation of basic zinc salts (BZS) – simonkolleite (Fig. 6a and Fig. 6d), zinc hydroxysulphate (Fig. 6b), hydrozincite (Fig. 6c). With addition of Mg^{2+} (curves 2 and 4) an additional plateau at pH around 10 is observed due to precipitation of $Mg(OH)_2$ [27]. The buffer effect is visible in the NH_4Cl solution (Fig. 6d) at pH 8 to 10.

Table 6 summarizes the composition of precipitates which were sampled, filtered and dried at different points in the titrations as indicated on the titration curve (i, ii and iii). The identification was made using XRD and Raman spectroscopy, the supplementary EDS analysis was made to verify that the expected anion is not replaced by carbonate due to drying. This was necessary because the XRD peaks were large and the peak positions of basic salts and layered double hydroxides with different anions are very close. The XRD and Raman spectra of the products are presented in the Appendix, section 4 “Synthesis of artificial corrosion products”.

Fig. 7 shows SEM images and EDS analysis of the precipitated corrosion products identified as layered double hydroxides (LDH) for verification of the anion present in the compound’s structure. This was necessary because LDH products have a very similar crystalline structure, independently of the specific anion present [28-29]. It was verified that Cl^- and SO_4^{2-} are present in the precipitated compound, confirming the formation of LDH with these anions.

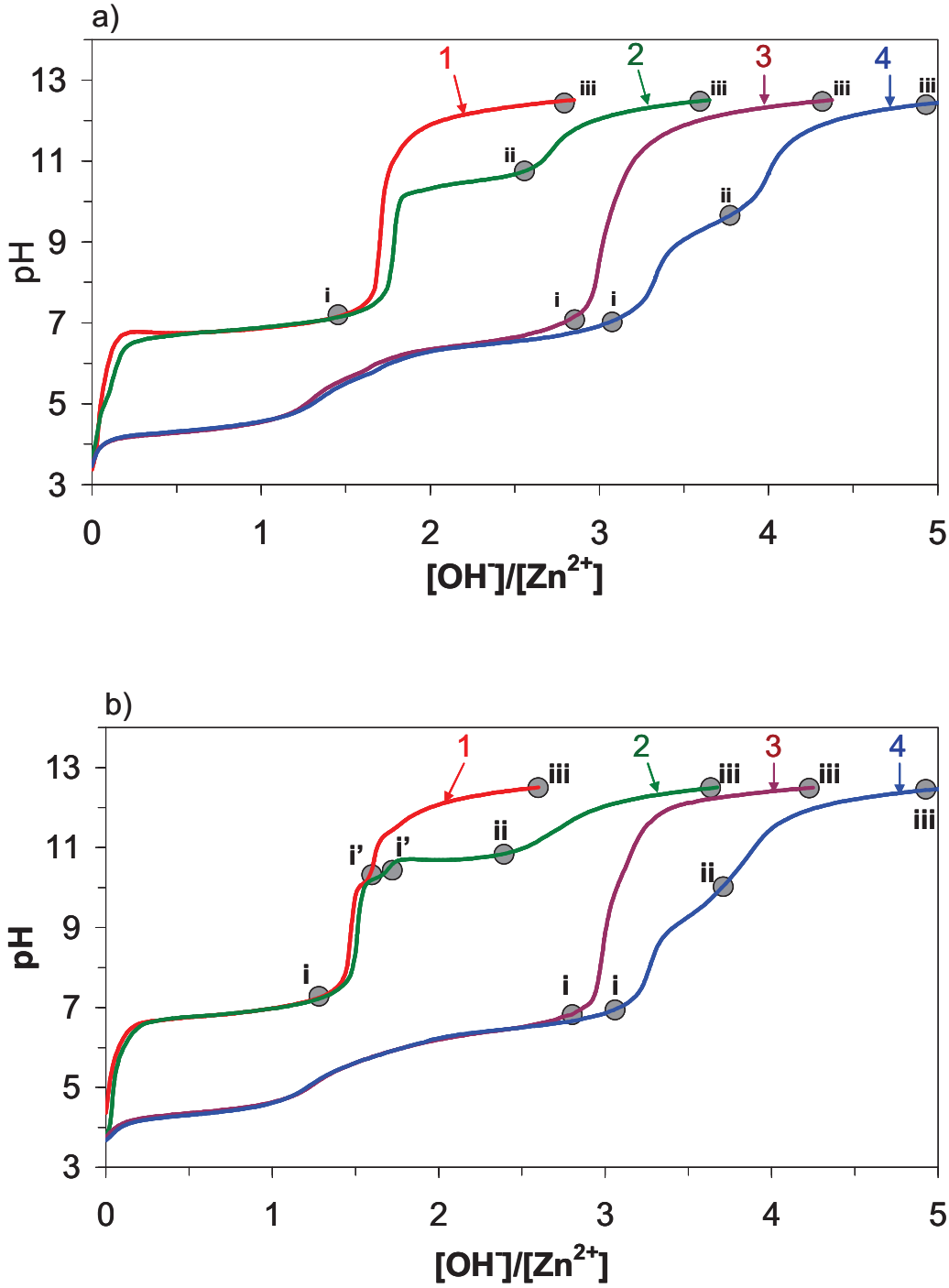


Fig. 6. Titration curves of different electrolytes with 1.0 M NaOH at 50 µl/min. The numbers (i), (ii) and (iii) show the sampling for characterization of the precipitate. **(a)** 0.171 M NaCl and **(b)** 0.171M Na_2SO_4 solvent in presence of (1) 0.04M Zn^{2+}, (2) 0.04 M Zn^{2+} + 0.02 M Mg^{2+}, (3) 0.04 M Zn^{2+} + 0.02 M Al^{3+}, (4) 0.04 M Zn^{2+} + 0.02 M Mg^{2+} + 0.02 M Al^{3+}.

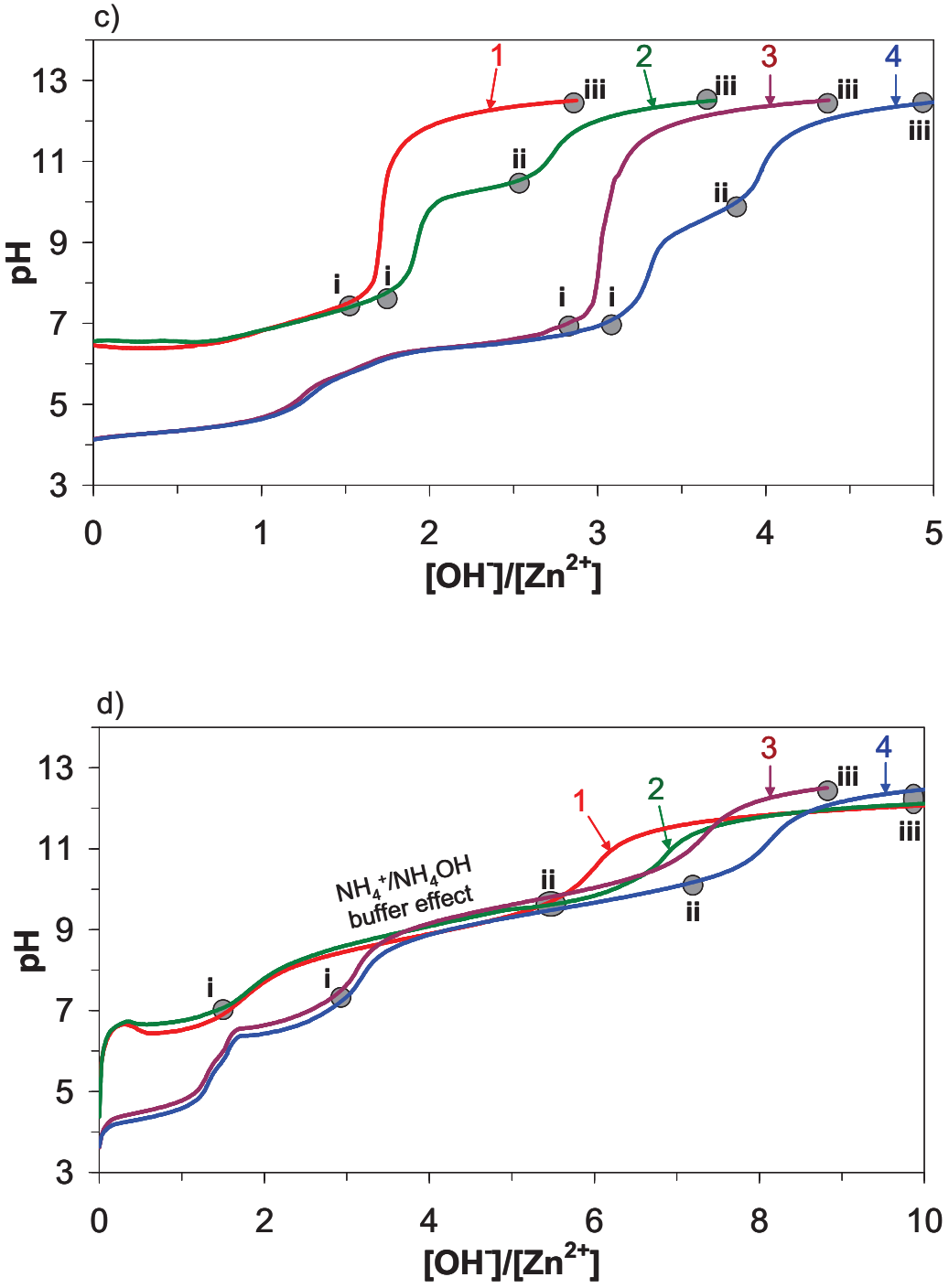


Fig. 6. Titration curves of different electrolytes with 1.0 M NaOH at 50 µl/min. The numbers (i), (ii) and (iii) show the sampling for characterization of the precipitate. **(c)** 0.008 M $NaHCO_3$, **(d)** 0.171 M NH_4Cl solvent in presence of (1) 0.04M Zn^{2+}, (2) 0.04 M Zn^{2+} + 0.02 M Mg^{2+}, (3) 0.04 M Zn^{2+} + 0.02 M Al^{3+}, (4) 0.04 M Zn^{2+} + 0.02 M Mg^{2+} + 0.02 M Al^{3+}.

Table 6. Summary of synthesized corrosion products in each titration condition described at Table 3.

Electrolyte:		a - NaCl				b - Na_2SO4			
Cation:		1 Zn	2 Zn+Mg	3 Zn+Al	4 Zn+Mg+Al	1 Zn	2 Zn+Mg	3 Zn+Al	4 Zn+Mg+Al
i / i'	pH ~ 7 / 9	ZHC ZnO	ZHC	LDH	LDH	ZHS	ZHS	ZHS	ZHS
ii	pH ~ 10	-	ZHC $Mg(OH)_2$	-	LDH $Mg(OH)_2$	-	ZHS $Mg(OH)_2$	-	ZHS $Mg(OH)_2$
iii	pH ~ 12	ZnO	ZHC $Mg(OH)_2$	LDH	LDH $Mg(OH)_2$	ZnO	ZHS $Mg(OH)_2$	LDH	LDH $Mg(OH)_2$

Electrolyte:		c - $NaHCO_3$				d - NH_4Cl			
Cation:		1 Zn	2 Zn+Mg	3 Zn+Al	4 Zn+Mg+Al	1 Zn	2 Zn+Mg	3 Zn+Al	4 Zn+Mg+Al
i	pH ~ 7	HZ ZnO	HZ ZnO	LDH	LDH	ZHC	ZHC	LDH	LDH
ii	pH ~ 10	-	HZ $Mg(OH)_2$	-	LDH $Mg(OH)_2$	ZHC	ZHC $Mg(OH)_2$	LDH	LDH $Mg(OH)_2$
iii	pH ~ 12	ZnO	HZ $Mg(OH)_2$ ZnO	LDH	LDH $Mg(OH)_2$ ZnO	$Zn(OH)_2$	ZHC $Mg(OH)_2$ $Zn(OH)_2$	LDH $Al(OH)_3$	LDH $Mg(OH)_2$ $Zn(OH)_2$

The NaCl solution with only Zn^{2+} ions showed the formation of ZnO together with simonkolleite at neutral pH and consequent complete transformation into ZnO at alkaline pH. In presence of Mg^{2+} and/or Al^{3+} ions, only simonkolleite (for mixtures of Zn^{2+} and Mg^{2+}) or LDH (when Al^{3+} was present) were detected even at pH 12.

In Na_2SO_4 electrolyte with only Zn^{2+} ions, zinc hydroxysulfates (ZHS) were formed at neutral pH, and were completely transformed into ZnO at alkaline pH. As for NaCl, in presence of Mg^{2+} and Al^{3+}, only ZHS or LDH were formed.

In $NaHCO_3$ solutions containing only Zn^{2+}, hydrozincite (zinc hydroxycarbonates, HZ) and ZnO were detected at neutral pH and only ZnO was detected at alkaline pH. As in NaCl and Na_2SO_4 electrolytes, in presence of Mg^{2+}, the transformation of HZ into ZnO was also avoided. In presence of Al^{3+} only LDH was formed in both, neutral and alkaline conditions. In the solution containing all three cations LDH was detected at neutral pH and at pH 10, but at pH 12.5 (after the third plateau due to the precipitation of $Mg(OH)_{2)}$, ZnO was also formed.

Chemical analysis of the precipitates formed in NH_4Cl electrolyte before and after the plateau related to buffer capacity of ammonium (pH 8-10) revealed only ZHC at pH 8 and 10 and only $Zn(OH)_2$ at pH 12. In the presence of Mg^{2+} ions the behavior was similar. With the addition of Al^{3+}, LDH alone was detected at neutral pH but small quantities of $Al(OH)_3$ were detected at the end of the experiment in the absence of Mg^{2+} at pH 12.5. In

trication mixtures at very alkaline pH (pH > 12) aluminum hydroxides were not detected but a partial transformation of the LDH into $Zn(OH)_2$ was detected.

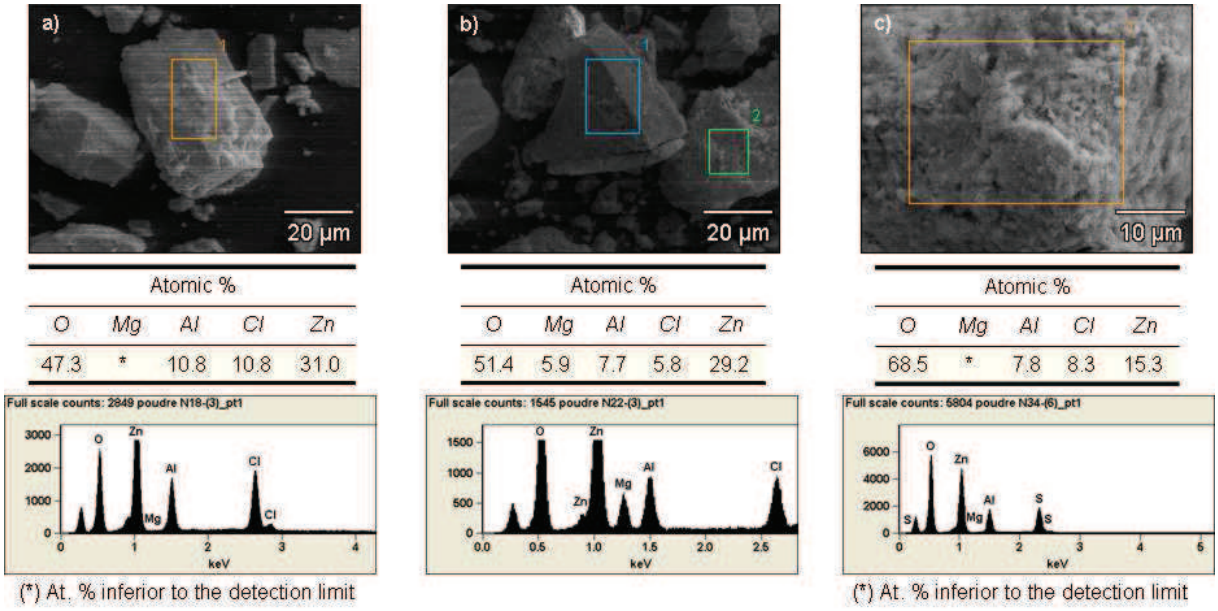


Fig. 7. SEM images and EDS analysis of recovered precipitated at some steps of the titration experiment: (a) Zn^{2+} + Al^{3+} in 0.171 M NaCl solvent after the second plateau (Fig. 6a, curve 3 i); (b) Zn^{2+}+ Mg^{2+} + Al^{3+} in 0.171 M NaCl solvent after the third plateau (Fig. 6a, curve 4 ii); and (c) Zn^{2+} + Al^{3+} in 0.171 M Na_2SO_4 solvent after the second plateau (Fig. 6b, curve 3 i).

3.3.1 Kinetic effect of Mg^{2+}

The titration of the mixtures containing both Zn^{2+} and Mg^{2+} suggested the absence (in NaCl and Na_2SO_4) or the delay (in $NaHCO_3$ and NH_4Cl) of the transformation of BZS into ZnO or $Zn(OH)_2$. In order to verify this result, additional experiments were made. After the titration was finished, the solution was not filtered immediately but was stirred for 48h. Than the precipitates were filtered, dried and analyzed in the same manner as the others titration experiments.

Fig. 8 shows the X-ray diffractograms of the precipitates formed in the solution containing Zn^{2+} + Mg^{2+} in 0.171 M NaCl immediately after the end of titration at pH 12.5 without (Fig. 8a) and with stirring for 48 h (Fig. 8b). Immediately after titration only ZHC and $Mg(OH)_2$ were detected, while after 48 h of stirring the transformation ZHC→$Zn(OH)_2$ occurred.

Similar experiments were made for the solutions when the titration was stopped at pH 10 (Fig. 6a, point ii at curve 2). It was observed that ZHC was stable after 48 h of stirring in the presence of $Mg(OH)_2$.

The results demonstrated strong stabilization of BZS against the transformation BZS→ZnO/$Zn(OH)_2$ at alkaline pH. The effect is clearly kinetic.

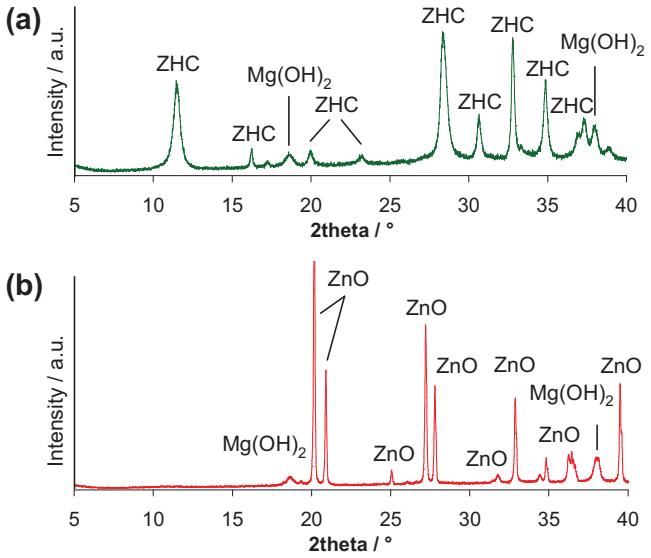


Fig. 8. XRD analysis of the precipitated products of Zn^{2+} + Mg^{2+} in 0.171 M NaCl (a.2 iii) at (a) the end of titration experiment and (b) after 48h of stirring. The corrosion products abbreviations are identified in Table 4.

4 Discussion

4.1 Influence of Mg and Al on the stability of Zn-containing corrosion products

According to the titration results, Mg^{2+} ions are able to avoid/delay the transformation of basic zinc salts (BZS) at alkaline pH. This effect can be caused by different factors.

First, the precipitation of $Mg(OH)_2$ can buffer the pH at values which are below the necessary to transform BZS (like ZHC, ZHS, HZ) into ZnO or $Zn(OH)_2$, as suggested in [1,3,6]. This means, in case of ZM corrosion, that as much as there is Mg^{2+} in solution, the pH is buffered and the transformation of the BZS is avoided. This mechanism however contradicts the equilibrium calculations presented in our previous work [31], demonstrating that, the pH at which $Mg(OH)_2$ precipitates, ZnO is more stable than BZS.

The effect is therefore expected to be kinetic in nature. A possible reason is that the rapidly formed $Mg(OH)_2$ physically blocks the access of hydroxide ions to initially formed BZS, delaying the transformation at alkaline pH (pH > 12). The delay of the transformation BZS → ZnO and $Zn(OH)_2$ can be an important factor for corrosion resistance because (i) every transformation can disturb the structure and increase porosity, and (ii) zinc oxides are known to be more porous than the other Zn-patinas [1,3,6,19-20].

Al^{3+} in solution enables the precipitation of LDH, which is considered by many authors as good barrier for oxygen diffusion [1,2,8,11-13,19]. We observed that this compound was stable at least up to pH = 12. The peak positions in the XRD spectra were very large and a complete characterization of the LDH was not achieved in this work. However, according to the bibliography [28-29], the stability constant of ZnAl-LDH is higher than that for MgAl-LDH. The participation of Mg^{2+} in the LDH formation cannot be completely excluded because even if the $Mg(OH)_2$ precipitation plateau at pH ~ 10 is still present in presence of Al^{3+}, it is shorter than in the absence of Al^{3+}, which can be interpreted as some Mg^{2+} has been already precipitated at lower pH (during the precipitation of LDH at pH ~ 6).

The effect of Mg^{2+} and Al^{3+} on the formation and transformation of zinc patinas in different electrolytes is schematically summarized in Fig. 9.

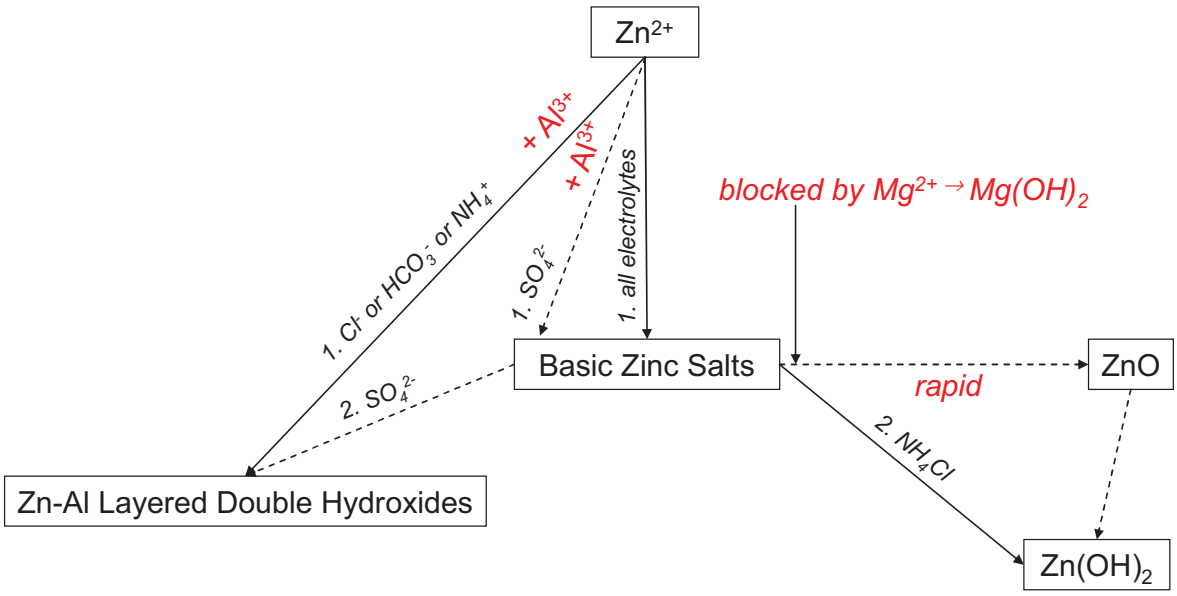


Fig. 9. Schematic illustration of the formation and transformation of different corrosion products.

4.2 Effect of precipitated corrosion products on the oxygen reduction rate

The polarization experiment (section 3.2) demonstrates that a layer of corrosion products is able to decrease the cathodic reaction on the surface of both GI and ZM coatings. However, during cathodic polarization on corroded GI, the barrier effect disappears, as the current magnitude increases with time (Fig. 2). We interpret this current increase in terms of the transformation BZS → ZnO (detected by XRD) due to the pH increase by cathodically generated hydroxide (reaction given by Eq. 1).

$$O_2 + 2H_2O + 4e^- \rightarrow 4OH^- \quad (1)$$

The cathodic current on ZM is constant due to stabilization of corrosion products discussed in previous section.

We suggest that the barrier effect on both coatings is due to BZS, as the cathodic current after OCP exposure is (i) initially present on GI in both electrolytes and (ii) is present and stable on ZM in RW electrolyte even if LDH is not formed.

The fact that ZHS and ZHC disappear from GI and only HZ is detected at the end of cathodic polarization in RW electrolyte is consistent with the instability of ZHS [32-33] and with the fact that, among BZS, the carbonates species are the most stable [21]. The instability of BZS and the absence of the stabilizing Mg effect result in the lost of barrier protection on GI. On ZM, the stabilizing effect of Mg^{2+} and Al^{3+} ions protect the system against the loss of barrier protection.

Slower increase of cathodic current on GI covered by patina in RW electrolyte than in NaCl can be assigned to the buffer capacity of this electrolyte due to the presence of NH_3^+ and HCO_3^- [15]. The delayed formation of LDH in RW electrolyte in cyclic experiment correlates with the results of accelerated corrosion tests from our previous work [15], where the effect of the RW electrolyte was featured as being responsible for the retardation of Al dissolution.

The formation of a residual Al skeleton observed in section 3.3 can reinforce the barrier effect by retaining the patinas in a compact structure. Our results suggest that the Al distribution inside the corroded coating reflects the distribution in the initial alloy. This result is coherent with Keppert et al. [12], who observed a heterogeneous distribution of Al inside the corroded coating and the low mobility of Al^{3+} is consistent with the absence of Al in soluble corrosion products after accelerated corrosion tests [15].

5 Conclusion

1. During OC exposure, corrosion products were formed on both GI and ZnMgAl coatings. Cathodic polarization before and after this OC exposure in NaCl and in synthetic rain water (RW) electrolytes demonstrated good initial barrier effect of BZS and BZS/LDH on the oxygen reduction in both environments.

2. On GI, but not on ZnMgAl, under cathodic polarization, BZS transforms into ZnO with loss of barrier properties. This loss is delayed in RW.

3. The stabilization of BZS on ZnMgAl is explained by a kinetic effect of Mg^{2+} confirmed by acid-base titrations of $Zn^{2+}/Mg^{2+}/Al^{3+}$ mixtures, because, from thermodynamic calculations, this stabilization occurs at a pH in which ZnO is expected to be formed.

4. The effect of Mg^{2+} varies in function of the electrolyte composition. Mg^{2+} suppress the direct ZnO precipitation and retards the transformation of BZS into $ZnO/Zn(OH)_2$ at pH7-13 in NaCl and Na_2SO_4 and at pH 10 in $NaHCO_3$. The effect is not present at neutral or strongly alkaline pH in $NaHCO_3$ and in NaH_4Cl electrolytes.

5. In presence of $Zn^{2+}/Mg^{2+}/Al^{3+}$, ZHS is preferentially formed in Na_2SO_4 solution and its transformation into LDH occurs at alkaline pH (~ 12).

6. An additional effect is achieved through a skeleton of non-oxidized Al which keeps the corrosion product compact.

References

[1] P. Volovitch, T.N. Vu, C. Allély, A. Abdel Aal, K. Ogle "Understanding corrosion via corrosion products characterization: II. Role of alloying elements in improving the corrosion resistance of Zn-Al-Mg coatings on steel" Corros. Sci. 53 (2011) 2437–2445

[2] S. Schuerz, M. Fleischanderl, G.H. Luckeneder, K. Preis, T. Haunschmied, G. Mori, A.C. Kneissl "Corrosion behaviour of Zn-Al-Mg coated steel sheet in sodium chloride-containing environement" Corros. Sci. 51 (2009) 2355-2365

[3] M. Dutta, A. K. Halder, S. B. Singh "Morphology and properties of hot dip Zn-Mg and Zn-Mg-Al alloy coatings on steel sheet" Surface & Coatings Technology 205 (2010) 2578-2584

[4] J. Elvins, J. a. Spittle, J. H. Sullivan, D. A. Worsley "The effect of magnesium additions on the microstructure and cut edge resistance of zinc aluminium alloy galvanized steel" Corros. Sci. 50 (2008) 1650-1658

[5] P. Volovitch, C. Allély, K. Ogle "Understanding corrosion via corrosion products characterisation: I. Case study of the role of Mg alloying in Zn-Mg coating on steel" Corros. Sci. 51 (2009) 1251-1262

[6] N.C. Hosking, M.A. Strom, P.H. Shipway, C.D. Rudd "Corrosion resistance of zinc–magnesium coated steel" Corros. Sci. 49 (2007) 3669–3695

[7] T. Prosek, A. Nazarov, U. Bexell, D. Thierry, J. Serak, "Corrosion mechanism of model zinc–magnesium alloys in atmospheric conditions" Corros. Sci. 50 (2008) 2216–2231

[8] T. Tsujimura, A. Komatsu, A. Andoh "Influence of Mg content in coating layer and coating structure on corrosion resistance of hot-dip Zn–Al–Mg alloy coated steel sheet" in: Proceedings of the Galvatech '01, International Conference on Zinc and Zinc Alloy Coated Steel, June 26–28, Brussels, Belgium, 2001, pp. 145–152

[9] E. Diler, S. Rioual, B. Lescop, D. Thierry, B. Rouvellou "Chemistry of corrosion products of Zn and MgZn pure phases under atmospheric conditions" Corros. Sci. 65 (2012) 178-186

[10] B. Li, A. Dong, G. Zhu, S. Chu, H. Qian, C. Hu, B. Sun, J. Wang "Investigation of the corrosion behaviors of continuously hot-dip gavanizing ZN-Mg coating" Surfaces & Coatings Technology 206 (2012) 3989-3999

[11] D. Persson, D. Thierry, N. LeBozec, T. Prosek "In situ reflection spectroscopy studies of the initial atmospheric corrosion of Zn-Al-Mg coated steel" Corros. Sci. 72 (2013) 54-63

[12] T. A. Keppert, G. H. Luckeneder, K-H. Stellnberger, G. Mori "Influence of the pH value on the corrosion of Zn-Al-Mg hot-dip galvanized steel sheets in chloride containing environments" NACE International Corrosion Conference 2012, C2012-0001493

[13] S. Schürz, G.H. Luckeneder, M. Fleischanderl, P. Mack, H. Gsaller, A.C. Kneissl, G. Mori "Chemistry of corrosion products on Zn-Al-Mg alloy coated steel" Corros. Sci. 52 (2010) 3271-3279

[14] N. LeBozec, D. Thierry, M. Rohwerder, D. Persson, G. Luckeneder, L. Luxem "Effect of carbon dioxide on the atmospheric corrosion of Zn–Mg–Al coated steel" Corros. Sci. 74 (2013) 379-386

[15] M. Salgueiro, C. Allély, K. Ogle, P. Volovitch "Corrosion mechanisms of Zn(Mg,Al) coated steel in accelerated tests and natural exposure: 1. The role of electrolyte composition on the nature of corrosion products and relative corrosion rates" Corros. Sci. (2014) – submitted

[16] K. Ueda, A. Takahashi, Y. Kubo, "Investigation of corrosion resistance of pre-painted Zn-11%Al-3%Mg-0.2%Si alloy coated steel sheet through outdoor exposure test in Okinawa" La Metallurgia Italiana – Corrosione, n. 2/2012, 13-19

[17] N. LeBozec, D. Thierry, A. Peltola, L. Luxem, G. Luckeneder,G. Marchiaro, M. Rohwerder "Corrosion performance of Zn–Mg–Al coated steel in accelerated corrosion tests used in the automotive industry and field exposures" Materials and Corrosion, 2013, 64, No. 9999

[18] D. Landolt "Corrosion and Surface Chemistry of Metals" EPFL Press, 2007, first English edition. Originally published in French as *Corrosion et Chimie de Surfaces des Métaux*, Copyright 1993, 1997, 2003 Presses Polytechinques et Universitaires Romandes. Translated and updated from the revised second French version

[19] T. Ishikawa, M. Ueda, K. Kandori, T. Nakayama "Air permeability of the artificially synthesized Zn-Al-Mg alloy rusts" Corros. Sci. 49 (2007) 2547-2556

[20] T. Ishikawa, K. Matsumoto, A. Yasukawa, K. Kandori, T. Nakayama, T. Tsubota "Influence of metal ions on the formation of artificial zinc rusts" Corros. Sci. 46 (2004) 329-342

[21] C. Merlin "Approches analytique et électrochimique de la dégradation des tôles d'acier revêtues cataphorésées en atmosphères corrosive contenant des ions sulfates" Thèse de doctorat de l'université Henri Poincaré, Nancy I, 1999

[22] M.C. Bernard, A. Hugot-Le Goff, D. Massinon, N. Phillips "Underpaint corrosion of zinc-coated steel sheet studied by in situ Raman spectroscopy" Corros. Sci. 35 (1993) 1339–1349

[23] R. Autengruber, G. Luckeneder, A. W. Hassel "Corrosion of press-hardened galvized steel" Corros. Sci. 63 (2012) 12-19

[24] RRUFF database, available at http://rruff.info

[25] ISO 9227:2006 "Corrosion tests in artificial atmospheres"

[26] F. Beier, K-H. Dtellnberger, S. Geisler "A new accelerated cyclic corrosion test for automotive substrates" EUROCORR Congress September 2009, Nice France

[27] P. Volovitch, M. Serdechnova, K. Ogle "Aqueous Corrosion of Mg-Al binary alloys: roles of Al and Mg" Corrosion – Vol. 68, No. 6, (2012) 557-570

[28] C. Forano, T. Hibino, F. Leroux, C. Taviot-Guého, Chapter 13.1 "Layred Double Hydroxides" in Handbook of Clay Science, published by Elsevier Ltd. (2006) 1021-1095

[29] C. A. Johnson, F. P. Glasser "Hydrotacilte-like minerals ($M_2Al(OH)_6(CO_3)_{0.5}.xH_2O$, where M = Mg, Zn, Co, Ni) in the environment: synthesis, characterization and thermodynamic stability" Clays Clay Miner., Vol. 51, No. 1, 1-8, 2003

[30] P. Schouller-Guinet, C. Allély, P. Volovitch “ZnAlMg: an innovative metallic coating that offers protection in the harshest environments” in: Proceedings of Galvatech ‘11, Genova, Italy, 2011

[31] M. Salgueiro Azevedo, C. Allély, K. Ogle, P. Volovitch “Corrosion mechanisms of Zn(Mg,Al) coated steel: The effect of HCO_3^- and NH_4^+ ions on the intrinsic reactivity of the coating” Electrochim. Acta (2014) – submitted

[32] J.D. Yoo, K. Ogle, P. Volovitch “The effect of synthetic zinc corrosion products on corrosion of electrogalvanized steel: I. Cathodic reactivity under zinc corrosion products” Corros. Sci. 81 (2014) 11-20

[33] J.D. Yoo, K. Ogle, P. Volovitch “The effect of synthetic zinc corrosion products on corrosion of electrogalvanized steel. II. Zinc reactivity and galvanic coupling zinc/steel in presence of zinc corrosion products” Corros. Sci. (2014) – article in press

Chapter VI

Comparative study of coatings with different compositions

Confidential

Corrosion mechanisms of ZnMgAl coated steel in accelerated tests: Comparative study of coatings with different compositions

Abstract

Accelerated corrosion tests with varied electrolytes with corrosion product characterization were performed comparing three different compositions of ZnMgAl coated steel among them and with conventional galvanized steel. The phase distribution between the ternary and the pure zinc phase seems to be the most important for corrosion resistance. ZnMgAl coatings with continuous ternary phase demonstrated similar corrosion behavior and better corrosion resistance than ZnMgAl with continuous Zn matrix. The corrosion products formed on different ZnMgAl coatings are similar; therefore the importance of a homogenous microstructure and consequently a homogenous distribution of corrosion products is discussed.

Keywords: Electrogalvanized steel (A); ZnAlMg (A); X-ray diffraction (B); Polarization (B); Corrosion product (C); Corrosion mechanisms (C)

1 Introduction

ZnMgAl coatings with different compositions have recently been commercialized by the steel industry, varying from 0.1 to 3.0 wt. % Mg and 0.2 to 11.0 wt. % Al [1]. All of them are known to present better performance in corrosion tests than conventional hot dip galvanized steel [1-8], but there are very few comparative studies of the corrosion mechanisms of ZnMgAl alloys with different compositions. A slight decrease of the corrosion rate in open condition with higher alloying content was observed for different ZnMgAl coatings from 1 to 4 wt. % Mg and 1 to 4 wt. % Al in an accelerated NaCl corrosion test [2] but there was no major difference in field exposure between three low-alloyed coatings (from 1 to 2 wt. % of each, Mg and Al). Slight decrease of corrosion rates was also observed in [3] when changing from low alloyed ZnMgAl coating (1.5 wt. % Mg and 1.5 wt. % Al) to a high alloyed one (3 wt. % Mg and 11 wt. % Al) in a NaCl-corrosion test with salt concentration similar to natural coastal atmospheres.

Comparing different alloying fractions, coatings with less than 1 wt. % of alloying elements [4] did not show any remarkable improvement of corrosion resistance compared to conventional galvanized coating, a strong improvement with alloying content was observed for coatings with 2 to 5 wt. % of alloying elements, but no significant difference is observed between alloys with more than 9 wt. % of Al and Mg together. The authors attributed the better corrosion resistance of high alloyed coatings to the formation of passive layer of natural oxides blocking the rate of oxygen reduction or anodic dissolution.

In field exposure [5], two ZnMgAl coatings, with 4 and 6.5 wt. % of alloying elements, demonstrated lower weight loss than Zn coating, but no significant difference was observed between the ZnMgAl coatings.

Despite some phenomenological evidence about the microstructure evolution related to the fraction of alloying elements [2,5], the role of this microstructure on corrosion resistance is still unclear. Our previous work [9] showed that the residual Al structure can be important for corrosion mechanisms and which probably depend on the phase distribution in alloys.

In our previous works [11] we demonstrated some specific features of corrosion mechanisms of Zn-Mg(3 wt. %)-Al(3.7 wt. %) coating in different electrolytes. The specific action of Mg and Al ions on the formation, stability and barrier properties of corrosion products [9] and the intrinsic reactivity of coating in function of the electrolyte composition [10] were discussed. The corrosion rates and corrosion products formed in

accelerated tests using different electrolytes and after field exposure were compared and a complex electrolyte, named as “Rain water” (RW) was proposed for which the ratios between corrosion rates of different Zn-based coatings and the formation of corrosion products were the closest to field exposure [11]. In the present work, we continue the logic of this work comparing the behavior of three different ZnMgAl coating in accelerated corrosion tests and electrochemical tests with conventional NaCl and RW electrolyte in order to distinguish the common features and differences in corrosion mechanisms of different coating’s compositions. The relative corrosion rates, the nature of formed corrosion products and their effect on the oxygen diffusion currents on different coatings will be analyzed.

2 Experimental

2.1 Materials

The coated steel samples were supplied by ArcelorMittal. The reference sample used was the industrial conventional hot dip galvanized steel (GI), with coating thickness of 20 µm, and composition Zn-Al(0.2 wt. %). Three ZnMgAl coated steel (called in this work ZM1, ZM2, ZM3) with different compositions were used: Zn-Mg(1.5 wt. %)-Al(1.5 wt. %), ZM1, and Zn-Mg(3.0 wt. %)-Al(11.0 wt. %), ZM3, with thickness of 10 µm and prepared by a pilot line of hot dip process and Zn-Mg(3.0 wt. %)-Al(3.7 wt. %), ZM2, prepared by industrial hot dip process with thickness of 20 µm. The mean coating composition and thickness are summarized in Table 1. Typical microstructures of the coatings are shown in Fig. 1: GI coating (Fig. 1a) contains homogenous Zn layer, ZM coatings (Fig. 1b-d) are composed by Zn or Al dendrites, a binary eutectic of Zn and intermetallic Zn_2Mg and a ternary eutectic of Zn/Al/Zn_2Mg.

Table 1. Thickness and chemical composition of the coatings.

Label	Coating	Thickness	Zn %wt	Al %wt	Mg %wt
GI	Conventional hot-dip galvanized	20 µm	99.8	0.2	-
ZM1	ZnMgAl	10 µm	97.0	1.5	1.5
ZM2	ZnMgAl	20 µm	93.3	3.7	3.0
ZM3	ZnMgAl	10 µm	86.0	11.0	3.0

For corrosion testing, the exposed surface was 100 mm x 100 mm; prior to exposure, the samples were degreased in an ether solution at room temperature during 20 min and the cut edges were protected with adhesive tape.

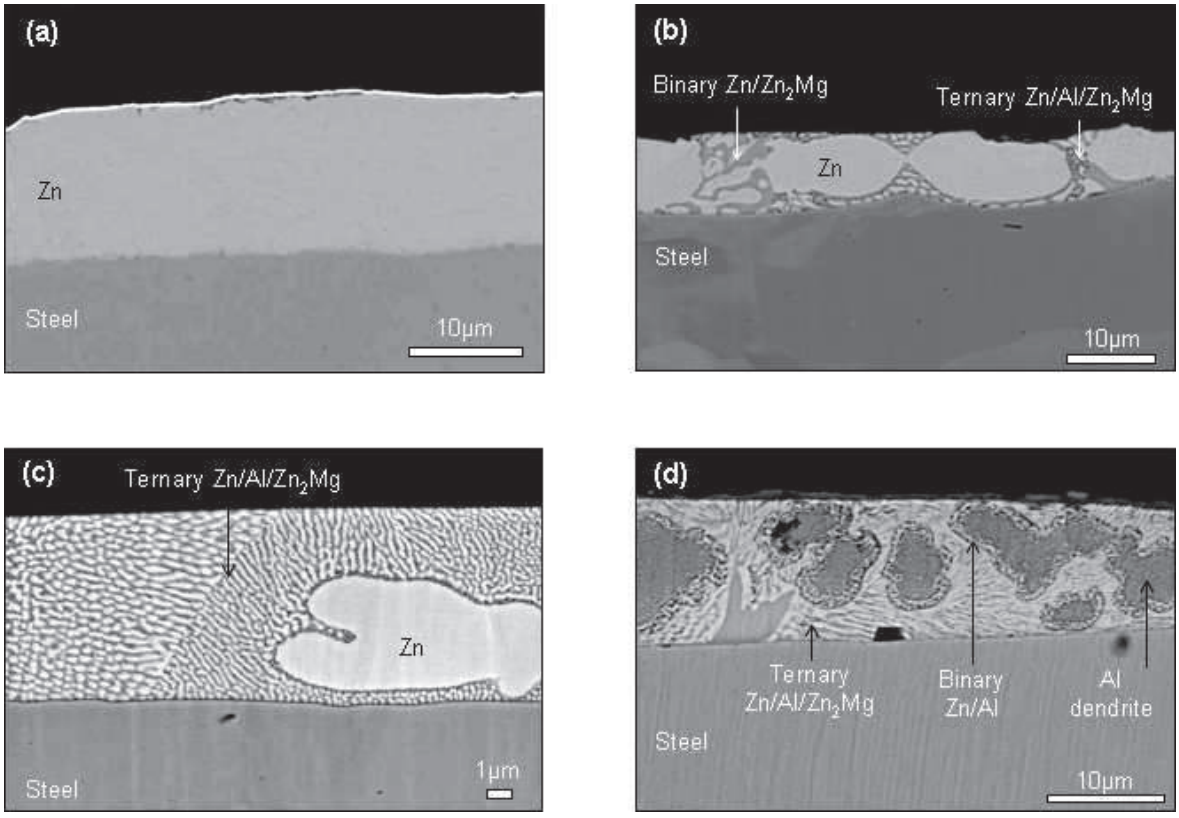


Fig. 1. Backscattered electron (BSE) images of uncorroded (a) GI, (b) ZM1, (c) ZM2 and (d) ZM3 coatings in cross section with their respective phases.

2.2 Corrosion tests

Continuous salt spray tests (SST) [12] were performed with samples at an angle of 20° to the vertical by changing the original procedure in terms of electrolyte but keeping the same temperature, relative humidity, pH and flow rate. The SSTs were performed in a SUGA chamber during variable periods of time. The accelerated tests conditions are summarized in Table 2 and correspond to the corrosion tests used in our previous publication [11].

Different electrolytes were used in the accelerated tests: NaCl, “rain water” (RW) – a new electrolyte proposed by our group [11] – and a modified-RW electrolyte that is a variation of RW also described before [11]. Both RW and modified-RW compositions are described in Table 3.

Table 2. Description of the performed corrosion tests.

	Corrosion test	Electrolyte	Concentration	Duration
1	SST-NaCl	NaCl	0.4 wt. %	400h
2	SST-RW	RW*	1 wt. %	200h
3	SST modified-RW	modified-RW *	1 wt. %	200h

(*) See Table 3 for electrolyte's composition.

Each material was represented by four samples in every test – three for weight loss measurement and one for corrosion products characterization. Different samples were needed because both analyses are destructive.

Table 3. Composition and concentration of (a) Rain Water (RW) electrolyte and (b) modified-RW electrolyte used on the corrosion test described in Table 2.

(a) Salts	Average content (mg/l)
$CaCl_2$	3.91
$(NH_4)_2SO_4$	1.82
Na_2SO_4	1.77
$NaNO_3$	1.81
$NaHCO_3$	0.69
Total:	10.00

(b) Salts	Average content (mg/l)
$CaCl_2$	3.91
Na_2SO_4	3.71
$NaNO_3$	1.81
Total:	9.45

2.3 Corrosion damage characterization

The samples were compared on the basis of their average consumed thickness, calculated from the weight loss, measured as a difference between the initial weight of the uncorroded sample and the final weight of the corroded sample after removing the corrosion products. The stripping of corrosion products was done by dipping the sample in an ultrasonic bath with glycine according to standard ISO 8407 procedure [13].

2.4 Corrosion product characterization

The corrosion products were characterized by X-ray diffraction (XRD) using the Cu(Ka1) radiation in a PANalytical X'Pert diffractometer, directly on the corroded surface of the samples. The analyzed area was approximately 20 mm x 20 mm. The XRD were collected with angular resolution of 0.02° over the angular range 5–80° (2θ) with 0.3 s

acquisition time. The evaluation of the data was done using the HighScore Plus software package, containing the JCPDS (ICDD) database files (version 2013).

Raman spectroscopy was performed directly on the corroded samples using a LabRAM Aramis spectrometer, from Horiba Jobin Yvon, with green laser 532 nm. The results were compared with reference spectra taken from the literature [7,14-16] and from the RRUFF™ spectral database for minerals [17].

The samples were observed by scanning electron microscopy (SEM), using a Gemini 1530 microscope with FEG-source (Scottky-type). The cross section observations were done on samples mounted in resin, cut and mechanically polished or ion polished with Jeol Cross-section Polisher. Before observation, a layer of 10 nm of carbon was sputtered on the cross section in order to ensure the charge evacuation from the surface that could contain non-conducting corrosion products.

2.5 Electrochemical experiments

Electrochemical measurements were performed in 1.0 wt. % NaCl and 1.0 wt. % RW electrolytes with initial pH 9 (see Table 3a for composition) using a BioLogic VMP3 potentiostat. The electrolytes were aerated during 15 min before experiment starts. A three electrode cell was used with saturated calomel as reference electrode, a platinum wire as counter electrode and the coating sample as working electrode. The working electrode was placed vertically in the cell. The temperature was controlled at 35°C. Prior to experiments the samples were degreased with ethanol.

3 Results

3.1 Corrosion rates from different accelerated corrosion tests

Table 4 summarizes the thickness consumed after the accelerated corrosion tests calculated from the weight loss result, assuming uniform corrosion. The ratio of corrosion rates between GI and ZM coatings is given at the last column in Table 4.

From Table 4, the corrosion rates of coatings ZM2 and ZM3 are very close in all corrosion tests while ZM1 has a corrosion behavior intermediary between GI and ZM2/3.

As in our previous publication for ZM2 [11], the presence of NH_4^+ and HCO_3^- ions in the RW electrolyte is determinant. In an accelerated test with RW electrolyte exempt of

these two ions, so-called SST modified-RW, the behavior of all ZM compositions was close to their behavior in NaCl electrolyte (Table 4, in which the ratio of corrosion rates of GI and ZM after SST-NaCl is almost the same after SST modified-RW). It is important to notice that, for both tests, the concentration of electrolyte and duration are not the same, which renders the comparison of the consumed thickness meaningless. In these two corrosion tests, NaCl and modified-RW, the ratio between ZM2 or ZM3 and GI is higher than 6. On the contrary, for ZM1, this ratio is less than 3.

Regarding the RW corrosion test, ZM2 and ZM3 show slow corrosion rate than ZM1, as in SST-NaCl and SST modified-RW, but in SST-RW this difference is less important.

Table 4. Consumed thickness of GI, ZM1, ZM2 and ZM3 coatings after corrosion tests.

	Corrosion test	GI	ZM1	ZM2	ZM3	Ratio of consumed thickness		
		consumed thickness (µm)	consumed thickness (µm)	consumed thickness (µm)	consumed thickness (µm)	GI/ZM1	GI/ZM2	GI/ZM3
1	SST-NaCl	14.0± 1.0	5.5 ± 0.3	2.3 ± 0.1	2.1 ± 0.1	2.5	6.1	6.7
2	SST-RW	8.5± 0.6	6.1 ± 0.7	3.1 ± 0.2	3.3 ± 0.2	1.4	2.7	2.6
3	SST modified-RW	4.7± 1.2	1.6 ± 0.2	0.7 ± 0.2	0.7 ± 0.1	2.9	6.7	6.7

3.2 Corrosion products

Table 5 shows the equivalence between the corrosion product, its abbreviation and label used on the figures. The detailed XRD spectra of the surfaces after corrosion tests are presented in Fig. 2.

Table 5. Equivalence between the name of corrosion products, its composition and the chosen abbreviation.

Label	Name	Abbreviation	Chemical formula
1	Layered double hydroxide	LDH	$M(II)_xM(III)_y(A^-)_m(OH)_n.zH_2O$ $M(II) = Zn^{2+}, Mg^{2+}, M(III) = Al^{3+}$ $A^- = CO_3^{2-}, Cl^-, SO_4^{2-}$
2	Simonkolleite	ZHC	$Zn_5(OH)_8Cl_2.H_2O$
3	Zinc hydroxysulphate	ZHS	$Zn_4(OH)_6SO_4.nH_2O$, n=3-5
4	Hydrozincite	HZ	$Zn_5(OH)_6(CO_3)_2.H_2O$
5	Gordaite	ZSC	$NaZn_4(SO_4)Cl(OH)_6.6H_2O$
6	Zincite	ZnO	ZnO
7	Metallic zinc		Zn
8	Intermetallic zinc-magnesium		Zn_2Mg
9	Metallic alumimium		Al
10	Metallic iron		Fe

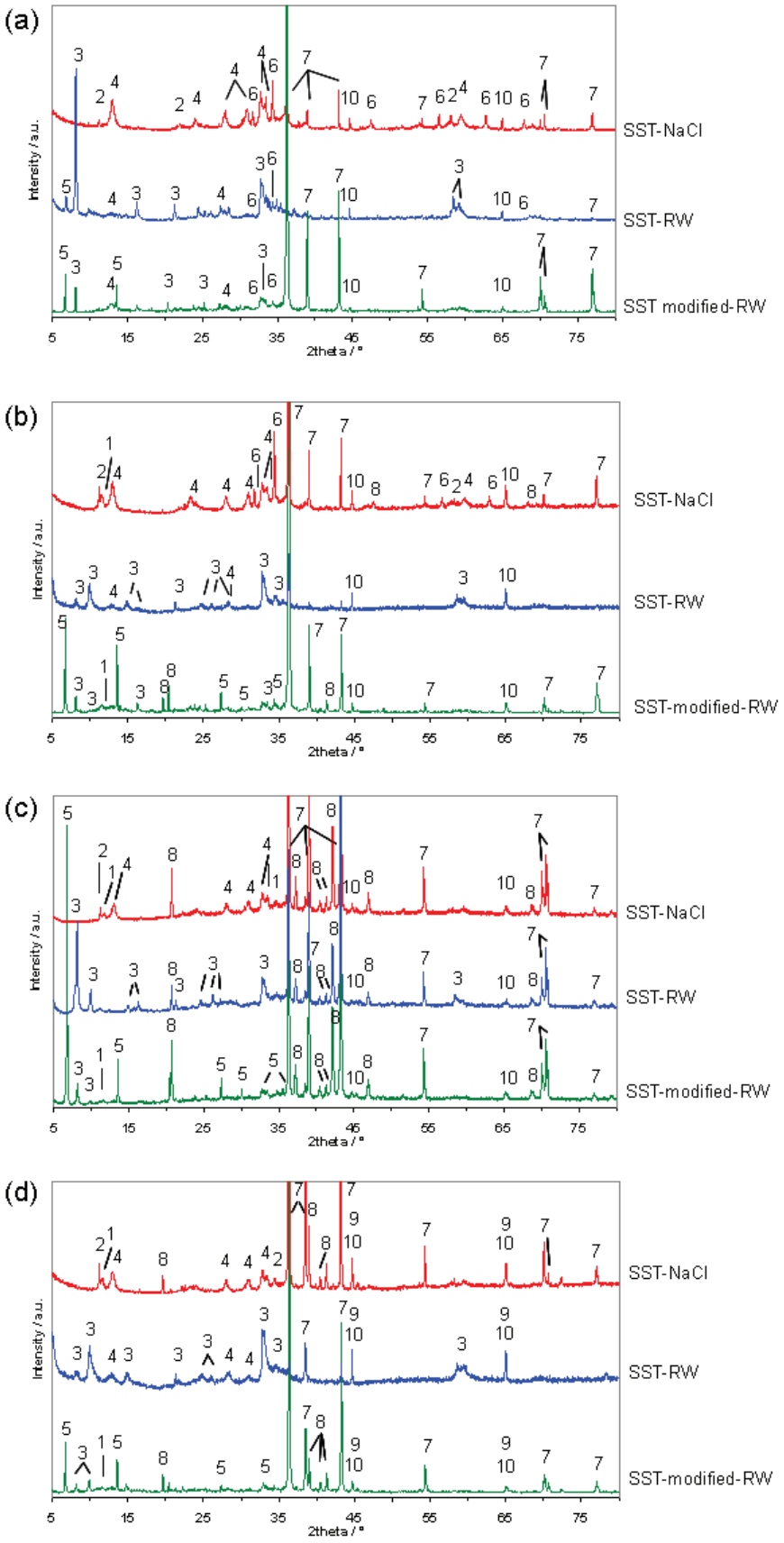


Fig. 2. X-ray diffraction patterns of (a) GI, (b) ZM1, (c) ZM2 and (d) ZM3 coatings after accelerated corrosion tests described in Table 2. The numbers in the figures correspond to the detected products (see Table 5 for identification).

Table 6 summarizes the corrosion products identified after the accelerated tests using XRD and Raman spectroscopy. Corrosion products formed on different ZM coatings are similar for different compositions; only two differences can be noted: after SST-NaCl, ZnO is found on ZM1 and not on other compositions; after SST-RW, HZ is found on ZM1 and ZM3.

Table 6. Summary of corrosion products observed by XRD and/or Raman spectroscopy on different samples.

	Corrosion test	Detected corrosion products on the coatings after corrosion tests			
		GI	ZM1	ZM2	ZM3
1	SST-NaCl	ZHC, HZ, ZnO	LDH, ZHC, HZ, ZnO	LDH, ZHC, HZ	LDH, ZHC, HZ
2	SST-RW	ZHS, HZ, ZSC, ZnO	ZHS, HZ	ZHS	ZHS, HZ
3	SST modified-WR	ZHC, HZ, ZSC, ZnO	LDH, ZHS, ZSC	LDH, ZHS, ZSC	LDH, ZHS, ZSC

3.3 Corrosion product distribution

Fig. 3-6 show the typical BSE images of corroded surfaces of GI, ZM1, ZM2 and ZM3 respectively, after the three accelerated corrosion tests, (a) SST-NaCl, (b) SST-RW and (c) SST modified-RW.

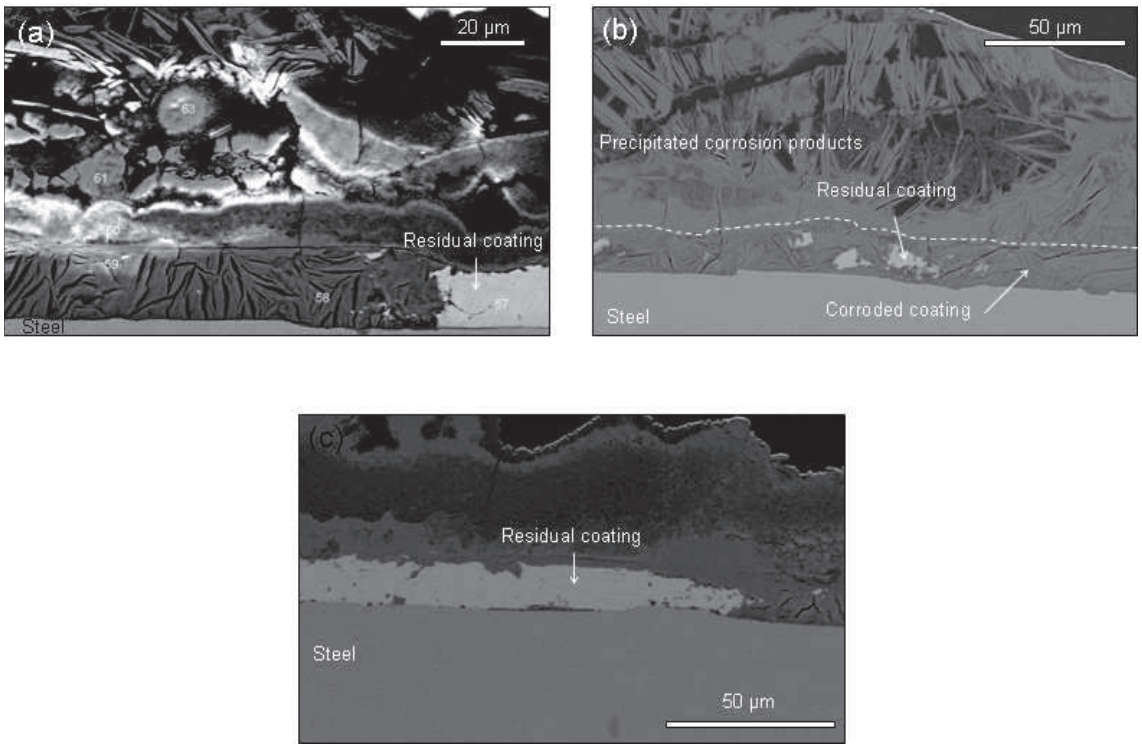


Fig. 3. SEM BSE images of GI coating after (a) SST-NaCl, (b) SST-RW and (c) SST modified-RW.

All coatings were corroded heterogeneously and the images do not represent the entire corroded surface but demonstrate typical features like preferential corrosion of ternary phase and the compactness of the corrosion product inside the corroded coating. Several images were analyzed in order to verify the reproducibility of the phenomena.

GI coating, shown in Fig. 3, is characterized by voluminous precipitated corrosion products and a very cracked corroded coating.

The selective corrosion of Zn_2Mg is verified on ZM1 coating (more evidenced in Fig. 4c). Also the preferential corrosion of the ternary phase compared to the Zn dendrites is clearly observed in Fig. 4b, in which all the ternary phase is consumed and the Zn dendrites begin to be corroded. In Fig. 4a and (c), the layer of precipitated corrosion products is thin and the corroded coating looks dense. However, Fig. 4b shows a more advanced stage of corrosion for ZM1, characterized by voluminous precipitated corrosion products and a cracked corroded coating, like for GI coating (Fig. 3).

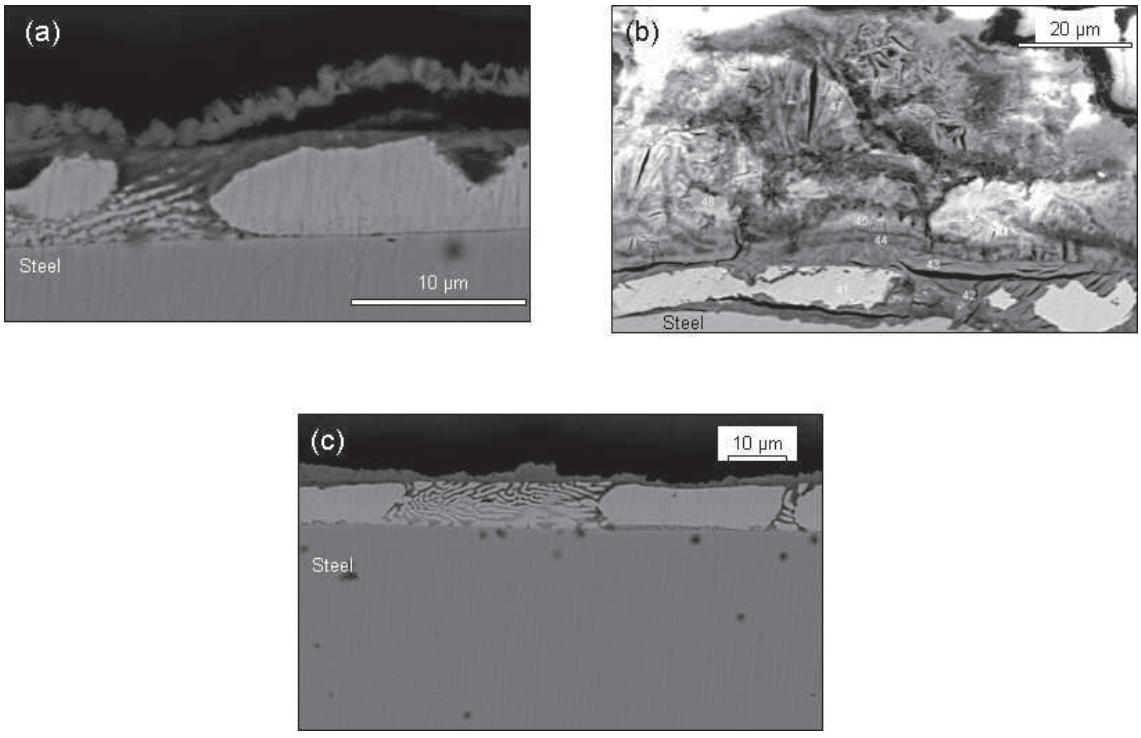


Fig. 4. SEM BSE images of ZM1 coating after (a) SST-NaCl, (b) SST-RW and (c) SST modified-RW

Fig. 5 shows the corrosion profile of ZM2 coated steel, in which the selective corrosion of Zn_2Mg and a consequently preferential corrosion of the ternary phase are also observed. On the contrary to ZM1, even at the more advanced stage of corrosion (Fig. 5b), ZM2 coating looks dense and only few cracks were found.

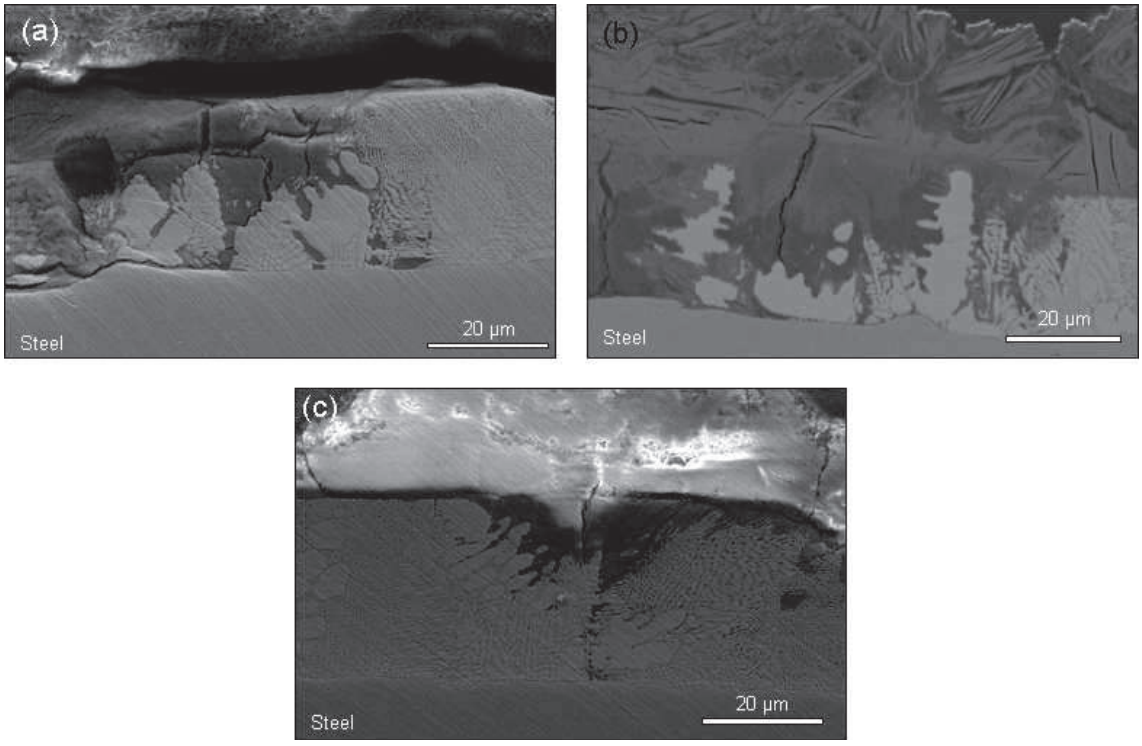


Fig. 5. SEM BSE images of ZM2 coating after (a) SST-NaCl, (b) SST-RW and (c) SST modified-RW.

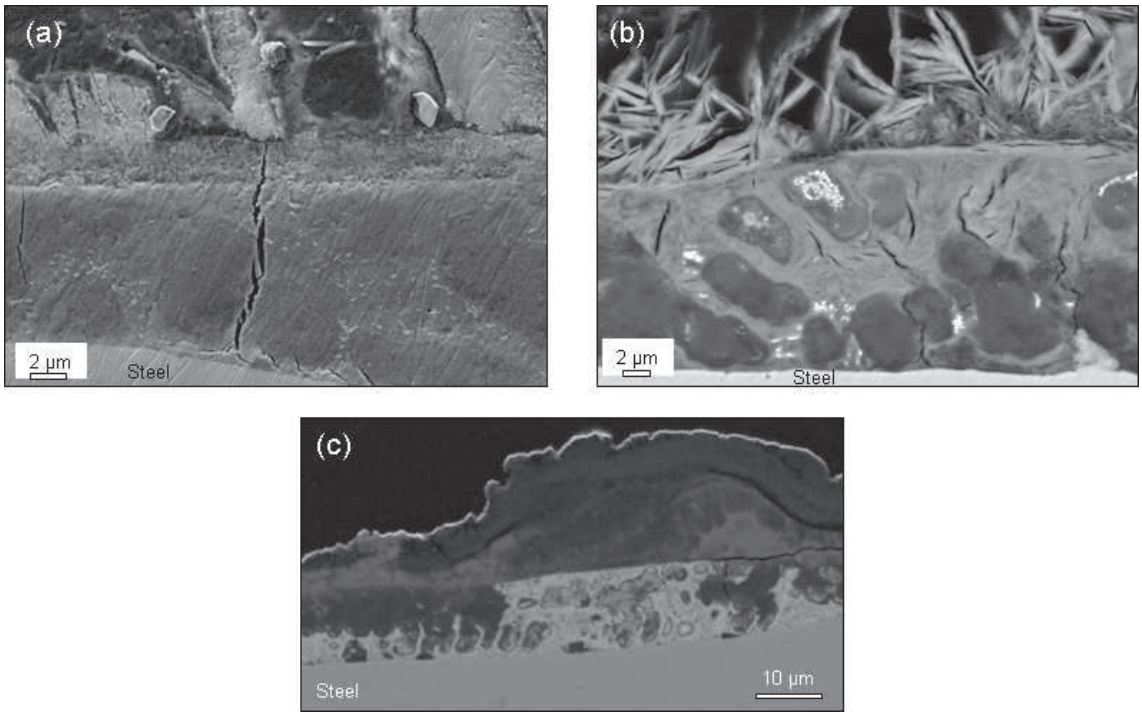


Fig. 6. SEM BSE images of ZM2 coating after (a) SST-NaCl, (b) SST-RW and (c) SST modified-RW.

A very dense layer of corrosion product on ZM3 coating is visible in Fig.6a – in this image, the entire coating is corroded and very few disruptions could be notice. From

the analysis of several images of the corroded coating, it could be observed that it is not at the same level of the GI or ZM1 coating.

3.4 Electrochemical behavior – effect of corrosion products on oxygen reduction rate

Oxygen reduction is considered to be the main cathodic process and the rate determining step for atmospheric corrosion of galvanized steel [18-19]. It was therefore of interest to investigate the barrier effect of corrosion products on oxygen reduction. This was accomplished by a novel amperometric experiment in which the coaching material was cycled between the open circuit potential and an applied cathodic potential of -1.15 V. During the open circuit period, corrosion products form spontaneously on the surface of the material. During the applied cathodic potential, the rate of oxygen reduction (proportional to the cathodic current) is monitored as a function of time. By comparing the amplitude of the cathodic current before and after the open circuit exposure, the effect of the corrosion product film on oxygen reduction may be deduced. Typical results are shown in Fig.7.

The surface is initially polarized at -1.15 V vs SCE for 6 hours (period 1), than the potential is switched off and the system evolves for 12 h at open circuit (period 2). Then (period 3), cathodic potential -1.15 V vs. SCE is applied once more and the cathodic current is measured for 30 hours. After that, the cycle is repeated. Fig. 7a shows the results in 1 wt. % NaCl and Fig. 7b in 1% wt. RW electrolytes with initial pH 9. These experiments are complementary to the previous published work for GI and ZM2 [11].

Considering the experiment in NaCl (Fig. 7a), before the first free corrosion (OC) the values of j_c are markedly different for the four samples, with GI a factor of 2 larger than ZM3. The value of j is affected, in this case, by the natural oxides present on the coating surfaces. In RW electrolyte (Fig. 7b), the currents densities are not stable, but the magnitude of the cathodic current in the first period vary from 60 to 110 μA cm^{-2}.

After 12 hours of free corrosion, resulting in an accumulation of corrosion products, the current magnitudes were decreased for all coatings. However, as the cathodic polarization continued, the current density of GI and ZM1 increased in both electrolytes. The current density was stable for the 2 other compositions.

A second OC exposure resulted in another $|j|$ decrease for all coatings and in both electrolytes. However, it increased again on GI in both electrolytes and on ZM1 in RW electrolyte – and was approximately stable in NaCl.

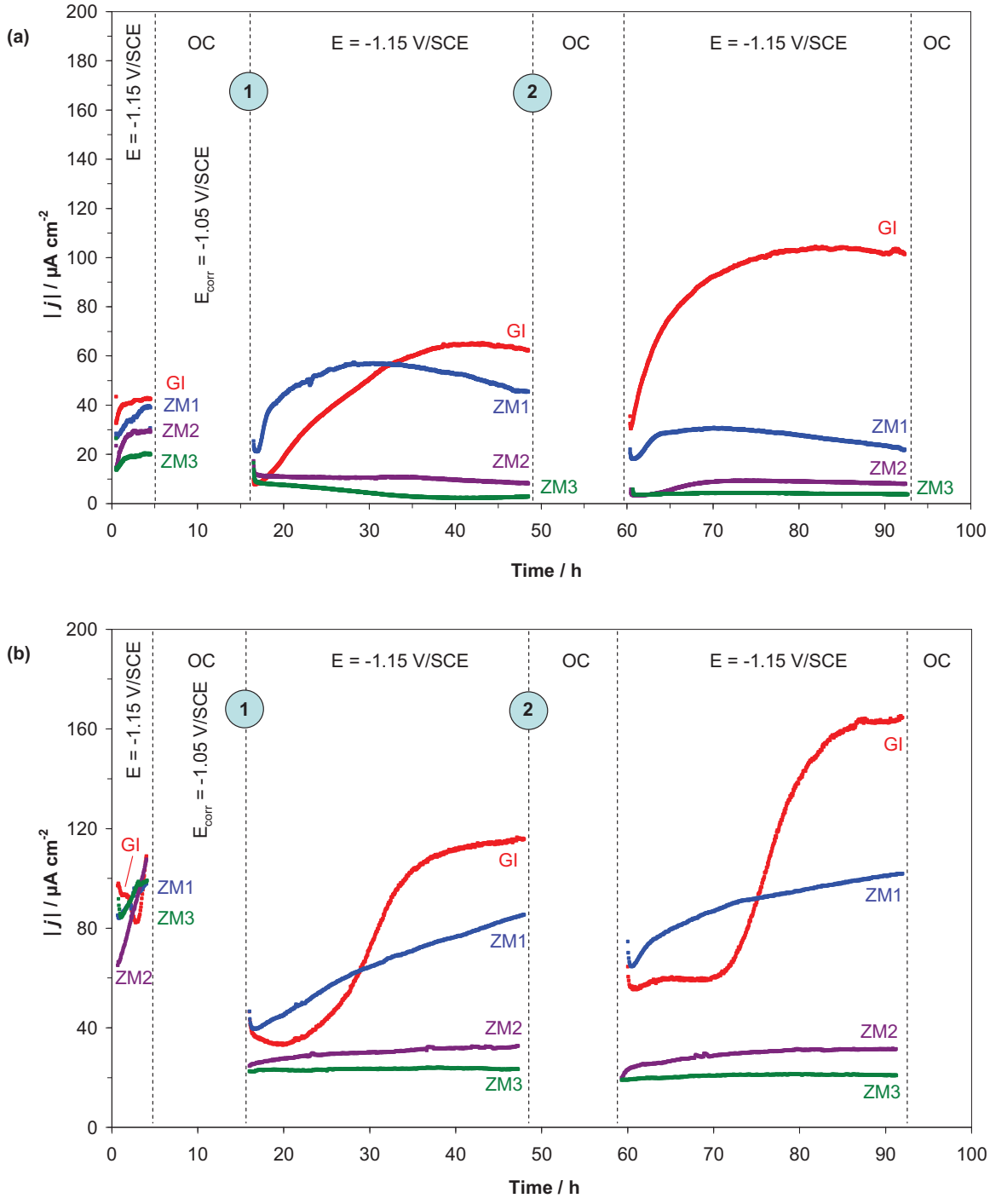


Fig. 7. Evolution of cathodic current |j] during polarization cycles of different coatings as indicated in (a) NaCl and (b) Rain water (RW) [11] electrolyte. The applied cathodic potential (Ec = -1.15 V vs SCE) is alternated with free corrosion at open circuit (OC) potential in order to accumulate corrosion products. Numbers 1 and 2 show the sampling for corrosion products analysis.

In separate experiments, the polarization was stopped at the point labeled (1) and (2). The sample was removed from the electrolyte, rinsed with deionized water, dried and

transferred to the XRD instrument. XRD analysis demonstrated the initial formation of basic zinc salts (BZS) like simonkolleite, hydrozincite and zinc hydroxysulphate etc. on all coatings in RW; in NaCl, the formation of LDH on ZM coatings and BZS on GI (Table 7). After cathodic polarization, BZS are transformed into ZnO only on GI (in both electrolytes) and on ZM1 (in RW electrolyte). Another important observation is the formation of LDH just after OC exposure for ZM coatings in NaCl, but only after the second cathodic polarization in RW electrolyte.

Table 7. Corrosion products identified on GI and ZM from the polarization experiment. The circled numbers 1 and 2 represent the sampling time (Fig. 7).

Electrolyte	Coating	Corrosion products characterization	
		①	②
		After OC exposure	After cathodic polarization
NaCl	GI	ZHC, HZ	ZHC, ZnO
	ZM1	LDH, HZ	LDH
	ZM2	LDH	LDH
	ZM3	LDH	LDH
RW	GI	ZHS, ZHC, HZ	HZ, ZnO
	ZM1	ZHS, ZHC, HZ	ZHS, LDH, HZ, ZnO
	ZM2	ZHS, HZ	LDH, HZ
	ZM3	ZHS, ZHC, HZ	LDH, HZ

4 Discussion

4.1 Corrosion rate and corrosion products of ZM coatings in accelerated corrosion tests

ZM1 corroded more than ZM2 and ZM3, and ZM2 is very similar to ZM3 in all studied tests. Considering the composition of these three coatings (Table 1) and their microstructure (Fig. 1), it seems that the distribution of the ternary phase containing Al is the main factor controlling the difference between compositions rather than the fraction of Al. ZM3 which contains 11 wt. % Al behaved in the same manner as ZM2 containing less than the half amount of Al.

On the basis of our previous observations [9], we suppose that due to selective dissolution of Mg-rich phase, Al is able to stay in the metallic form, retaining the corrosion products of zinc in compact structure and enhancing the barrier effect on oxygen reduction. It is also responsible for the formation of LDH [1-3,6-11], however, the improved barrier effect on ZM2 and ZM3 coatings in RW was observed even before the LDH was detected. That means that BZS can be efficient barriers for oxygen reduction if they are homogenously distributed on the surface and remain compact and stable. In this context, we propose that Al is more efficient when it stays dissolved in the ternary phase, covering all the coating volume.

The barrier properties of the corrosion products were previously considered as one of the main factors responsible for the corrosion resistance improvement of ZM coatings in comparison with GI [1,6,11,20-24]. However, in this work we observe that not only the nature, but also the distribution of corrosion products is important. The corrosion products formed on different coatings during OC exposure were almost the same after the three corrosion tests, but the corrosion rate varied between ZM1 and ZM2/3.

The formation of ZnO under cathodic polarization and after SST-NaCl, which was not previously detected on ZM2 composition, was detected in this work not only on GI but also on ZM1. The is in agreement with the hypothesis that Mg ions, leached during the anodic reaction, hinder the transformation of the BZS into ZnO [9,20]. GI, that does not contains Mg, undergoes this transformation and ZM1 is less concentrated in Mg than ZM2 and ZM3, which could suggest that consuming all Mg from the coating, the transformation is no longer avoided. This is illustrated by the accelerated corrosion test SST-NaCl, which was twice longer than SST-RW and modified SST RW (Table 2). In this test, ZM1 shows a large consumed thickness (Table 4) suggesting that Mg was leached, which results in the destabilization of BZS and their subsequent transformation into ZnO (Table 6).

Cross section observations (Fig. 3-6) demonstrated that ZM1 was the most cracked and the less dense of the ZM coatings in an advanced stage of corrosion. This can be related to the absence of continuous eutectic phase containing Al which results in the impossibility to preserve the compact structure of patinas at advanced stages of corrosion, when zinc dendrites are corroded.

In our previous work [11], we studied one composition of ZM coatings, the ZM2, and we proposed that RW electrolyte reproduces the corrosion mechanisms which are close to rate determining stages of atmospheric corrosion. The results obtained in the present work on 3 different compositions seem to confirm it for ZnMgAl coatings in

general. The slight difference in terms of corrosion rate between the ZM's is in accordance with field exposure corrosion tests [5].

4.2 Effect of corrosion products on the corrosion rate of ZM coating

From the results of the electrochemical experiment in NaCl on the fresh surface (first applied potential in Fig. 7a), it is seen that the cathodic current is inversely proportional to the Al content. This is probably linked to the presence of Al oxides responsible for the passivation of the coating before corrosion. In addition, the order between the ZM coatings stays the same during cycling.

We proposed in our previous work [9] that the stabilization of the oxygen reduction rate is due to the stabilization of the corrosion products and/or the formation of stable corrosion products during polarization. On ZM2 and ZM3, after the initial formation of corrosion products, the cathodic currents remained stable during both following polarizations. This can be linked to the stability of LDH [6-8] in NaCl and to the transformations BZS→LDH in RW (Table 7).

ZM1 also formed LDH just after the first OC exposure in NaCl. However, the cathodic current was not stable (as it was for ZM2/3) and increased during the second polarization and once more decreased in the third polarization, but at this point it starts to be stable. In RW electrolyte, $|j|$ also increased during the second polarization but did not decrease after the second OC exposure. The slope of the curve is smaller in the third polarization than it is in the second one indicating the possible beginning of stabilization. From the microstructure observations, the smaller content of Al and heterogeneous distribution of the ternary phase containing Al in this coating avoids a homogeneous formation of LDH. In the other hand, the smaller content of Mg is not enough to avoid the transformation of BZS into ZnO. Consequently, ZM1 shows a slower stabilization of the cathodic current than either ZM2 or ZM3.

The initial barrier effect of corrosion products formed on GI coating after OC exposure in both electrolytes (Fig. 7) was previously assigned to BZS. This barrier effect disappears with the transformation of the BZS into porous ZnO [25]. The delayed degradation of the barrier effect of corrosion product on GI in RW electrolyte can be related to the benefit of the buffer capacity of RW electrolyte [11].

5 Conclusion

This work demonstrates the importance of the phase distribution for the formation of corrosion products and for the corrosion rate of ZnMgAl coatings. The nature of corrosion products may be the most important difference between GI and ZnMgAl coatings; however between ZnMgAl coatings with different compositions, the distribution of the corrosion products determines the relative corrosion rates and is related to the homogeneity of the coating microstructure.

A homogenous mesh of Al well distributed along the coating's volume would explain the better corrosion performance of more Al alloyed ZnMgAl coatings.

Regarding Mg, it is important for corrosion product stability, hence the more Mg is available in the coating, the longer the coating is protected.

References

[1] S. Schuerz, M. Fleischanderl, G.H. Luckeneder, K. Preis, T. Haunschmied, G. Mori, A.C. Kneissl "Corrosion behaviour of Zn-Al-Mg coated steel sheet in sodium chloride-containing environment" Corros. Sci. 51 (2009) 2355–2363

[2] N. LeBozec, D. Thierry, A. Peltola, L. Luxem, G. Luckeneder,G. Marchiaro, M. Rohwerder "Corrosion performance of Zn–Mg–Al coated steel in accelerated corrosion tests used in the automotive industry and field exposures" Materials and Corrosion, 2013, 64, No. 9999

[3] T. Prosek, D. Thierry, D. Persson, J. Stoulil "Corrosion products formed on ZnMg and ZnAlMg coatings in model atmospheric conditions" in: Proceedings of Galvatech '11, Genova, Italy, 2011

[4] N. Larché, T. Prosek, A. Nazarov, D. Thierry, "Zn-Mg Automotive Steel Coatings – Final Report", Institut de la Corrosion (French Corrosion Institute), IC Report 2008:3, Project Number: 79046, April 2008, available at *www.zinc.org/general/zco-45_april_2008.pdf*

[5] D. Thierry, G. Rannou, A. Trabelsi, "Worldwide exposure of metallic coated steel panels – Results from one year exposure", Institut de la Corrosion (French Corrosion Institute), Technical report, Project number: 79096:2, May 2013

[6] P. Volovitch, T.N. Vu, C. Allély, A. Abdel Aal, K. Ogle "Understanding corrosion via corrosion products characterization: II. Role of alloying elements in improving the corrosion resistance of Zn-Al-Mg coatings on steel" Corros. Sci. 53 (2011) 2437–2445

[7] S. Schürz, G.H. Luckeneder, M. Fleischanderl, P. Mack, H. Gsaller, A.C. Kneissl, G. Mori "Chemistry of corrosion products on Zn–Al–Mg alloy coated steel" Corros. Sci. 52 (2010) 3271–3279

[8] D. Persson, D. Thierry, N. LeBozec, T. Prosek "In situ infrared reflection spectroscopy studies of the initial atmospheric corrosion of Zn-Al-Mg coated steel" Corros. Sci. 72 (2013) 54-63

[9] M. Salgueiro Azevedo, C. Allély, K. Ogle, P. Volovitch "Corrosion mechanisms of Zn(Mg,Al) coated steel: II. The effect of Mg and Al on the formation and properties of corrosion products" Corr. Sci., (2014) – submitted

[10] M. Salgueiro Azevedo, C. Allély, K. Ogle, P. Volovitch "Corrosion mechanisms of Zn(Mg,Al) coated steel: The effect of HCO_3^- and NH_4^+ ions on the intrinsic reactivity of the coating" Electrochim. Acta (2014) – submitted

[11] M. Salgueiro Azevedo, C. Allély, K. Ogle, P. Volovitch, Corrosion mechanisms of Zn(Mg,Al) coated steel in accelerated tests and natural exposure: I. The role of electrolyte composition on the nature of corrosion products and relative corrosion rates, Corr. Sci., (2014) – submitted

[12] ISO 9227:2006 "Corrosion tests in artificial atmospheres"

[13] ISO 8407:2009 "Corrosion of metals and alloys – Removal of corrosion products from corrosion test specimens"

[14] C. Merlin "Approches analytique et électrochimique de la dégradation des tôles d'acier revêtues cataphorésées en atmosphères corrosive contenant des ions sulfates" Thèse de doctorat de l'université Henri Poincaré, Nancy I, 1999

[15] M.C. Bernard, A. Hugot-Le Goff, D. Massinon, N. Phillips "Underpaint corrosion of zinc-coated steel sheet studied by in situ Raman spectroscopy" Corros. Sci. 35 (1993) 1339–1349

[16] R. Autengruber, G. Luckeneder, A. W. Hassel "Corrosion of press-hardened galvized steel" Corros. Sci. 63 (2012) 12-19

[17] RRUFF database, available at http://rruff.info

[18] D. Landolt "Corrosion and Surface Chemistry of Metals" EPFL Press, 2007, first English edition. Originally published in French as *Corrosion et Chimie de Surfaces des Métaux*, Copyright 1993, 1997, 2003 Presses Polytechinques et Universitaires Romandes. Translated and updated from the revised second French version

[19] T. Prosek, A. Nazarov, U. Bexell, D. Thierry, J. Serak, "Corrosion mechanism of model zinc–magnesium alloys in atmospheric conditions" Corros. Sci. 50 (2008) 2216–2231

[20] P. Volovitch, C. Allély, K. Ogle "Understanding corrosion via corrosion products characterisation: I. Case study of the role of Mg alloying in Zn-Mg coating on steel" Corros. Sci. 51 (2009) 1251-1262

[21] N.C. Hosking, M.A. Strom, P.H. Shipway, C.D. Rudd "Corrosion resistance of zinc–magnesium coated steel" Corros. Sci. 49 (2007) 3669–3695

[22] E. Diler, S. Rioual, B. Lescop, D. Thierry, B. Rouvellou "Chemistry of corrosion products of Zn and MgZn pure phases under atmospheric conditions" Corros. Sci. 65 (2012) 178-186

[23] B. Li, A. Dong, G. Zhu, S. Chu, H. Qian, C. Hu, B. Sun, J. Wang "Investigation of the corrosion behaviors of continuously hot-dip gavanizing ZN-Mg coating" Surfaces & Coatings Technology 206 (2012) 3989-3999

[24] D. Persson, D. Thierry, N. LeBozec, T. Prosek "In situ reflection spectroscopy studies of the initial atmospheric corrosion of Zn-Al-Mg coated steel" Corros. Sci. 72 (2013) 54-63

[25] T. Ishikawa, M. Ueda, K. Kandori, T. Nakayama "Air permeability of the artificially synthesized Zn-Al-Mg alloy rusts" Corros. Sci. 49 (2007) 2547-2556

Chapter VII

Conclusion and perspectives

Chapter VII – Conclusions and perspectives

This work confirmed that the behavior of ZnMgAl coated steel in accelerated tests differs significantly in function of the electrolyte composition. A new synthetic electrolyte, based on the mean rain water composition, called "rain water" (RW), was suggested for corrosion tests. The relative corrosion rates of different zinc-based coatings and the nature of the corrosion products in accelerated corrosion tests using this new electrolyte more closely resembled those obtained during natural exposure than was the case for tests using conventional NaCl electrolyte. These results suggest that the rate determining steps of the corrosion mechanisms in the new RW electrolyte were closer to the rate determining steps during atmospheric exposure.

We propose that the action of RW electrolyte is determined by HCO_3^- and NH_4^+ ions, due to their buffering effect at slightly alkaline pH (between 8 and 10). This buffer capacity prevents the initial dissolution of Al and delays the formation of layered double hydroxides (LDH) on ZnMgAl. The buffer capacity of RW electrolyte also improved the corrosion resistance of GI stabilizing basic zinc salts (BZS) and therefore decreasing the apparent benefit of ZnMgAl compared to GI. Fig. 1 shows a schematic diagram of the proposed mechanism by which NH_4^+ and HCO_3^- ions influence the corrosion mechanism of Zn(Mg,Al) coatings during accelerated corrosion tests (see Chapter III). Steps shown by numbers in Fig. 1 are: I. Electrochemical reactions at neutral pH; II. Precipitation at medium pH; III. Dissolution at high pH (cathodic Al dissolution; dissolution of BZS); IV. Formation of ZnO and LDH.

Considering a dissolution-precipitation mechanism of corrosion, specific actions of the ions present in RW electrolyte on (i) the electrochemical dissolution, (ii) the corrosion products precipitation and (iii) the barrier effect on oxygen reduction were separately studied.

(i) Electrochemical dissolution

The intrinsic anodic reactivity of ZnMgAl coating was showed to be higher than that of GI in different electrolytes (containing Cl^- and/or NH_{4+} and/or HCO_3^-). Considering that from corrosion tests the weight loss of ZnMgAl was significantly smaller than the weight loss of GI, this indicated clearly that the ZnMgAl's corrosion mechanisms are governed by cathodic reactions.

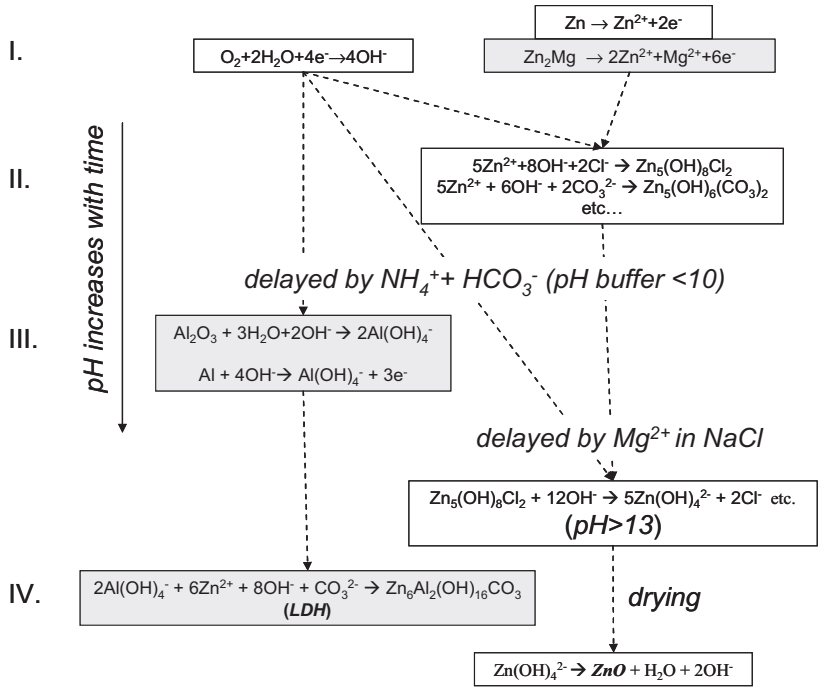


Fig. 1. Schematic illustration of the mechanism of formation of ZnO and LDH in NaCl and RW electrolytes on GI and ZM coatings. The reactions which are possible only on ZnMgAl are shown with grey background. Steps of corrosion mechanisms shown by numbers: I. Electrochemical reactions at neutral pH; II. Precipitation at medium pH; III. Dissolution at high pH (cathodic Al dissolution, dissolution of basic zinc salts); IV. Formation of ZnO and LDH. In RW electrolyte, the buffering effect of NH_4^+ and HCO_3^- ions can delay step III which can be considered as positive for GI (stabilization of zinc corrosion products) but controversial for ZM (stabilization of zinc corrosion products but delayed formation of LDH).

Cathodic Al dissolution and selective anodic Mg dissolution were demonstrated to be typical for ZnMgAl in NaCl electrolyte. In RW electrolyte, the cathodic dissolution of Al was initially stronger than in NaCl electrolyte but it was delayed or even suppressed if preliminary anodic polarization was applied before cathodic polarization. This effect was less significant for ZnAl alloys. We propose that the inhibition of cathodic Al dissolution in RW electrolyte is due to the kinetic effect related to the presence of Mg^{2+} ions. Low soluble magnesium carbonates formed during anodic polarization formed a physical barrier between Al-rich phases and the solution. This could have two possible consequences: 1) consumption of some electrochemically formed hydroxide for the transformation $MgCO_3 \rightarrow Mg(OH)_2$ or 2) the hindering of the diffusion of oxidized Al into the solution.

Fig. 2 shows a schematic illustration of the proposed LDH formation mechanisms and the effect of Mg^{2+} ions after anodic and cathodic polarization in different electrolytes (see Chapter IV).

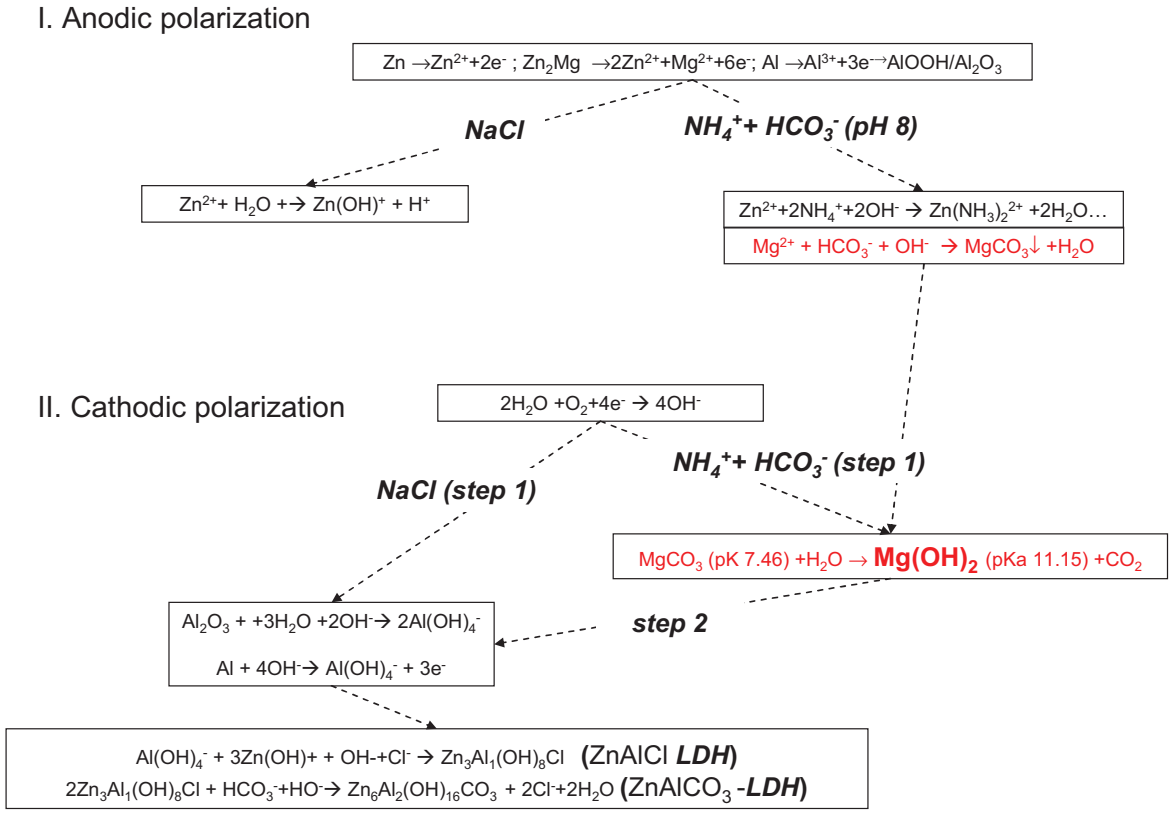


Fig. 2. Schematic illustration of the effect of Mg^{2+} and of the mechanism of formation of LDH in different electrolytes (containing Cl^- and/or NH_4^+ and HCO_3^-).

(ii) Corrosion products precipitation

The ions leached during selective cathodic or anodic reactivity could participate in the formation of a barrier layer of corrosion products. The titration experiments demonstrated that the presence of Mg^{2+} and Al^{3+} in the solution has several effects:

- Mg^{2+} ions delay the transformation of BZS formed at neutral pH into more porous ZnO or $Zn(OH)_2$ or soluble zinc complexes when the pH increases. This kinetic effect is due not only to the buffering of pH by $Mg(OH)_2$ precipitation, but also to the formation of a physical barrier [$Mg(OH)_2$] around initially formed BZS.
- Al^{3+} ions enable the formation of LDH in place of BZS. LDH are more stable than BZS against their transformation into ZnO or $Zn(OH)_2$ at high pH.

Fig. 3 shows the different steps of precipitation of corrosion products in function of electrolyte composition (see Chapter V).

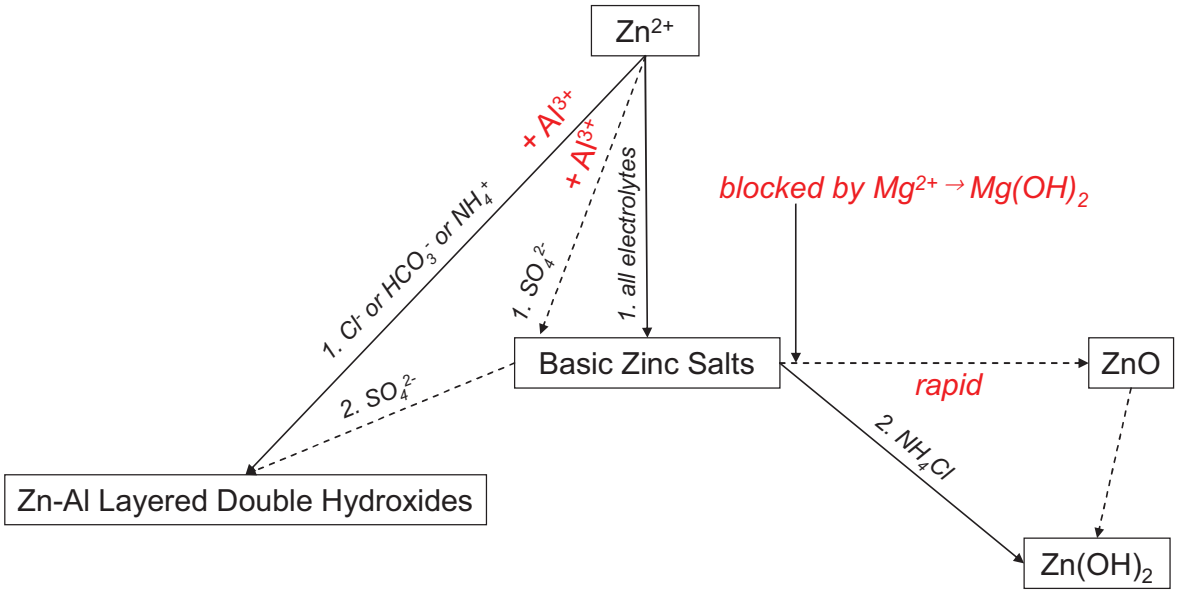


Fig. 3. Schematic illustration of the different steps of corrosion products precipitation.

(iii) Barrier effect on the oxygen reduction

The barrier effect of corrosion products, formed during open circuit (OC) exposure on GI and on ZnMgAl coating was demonstrated by electrochemical experiments. Cathodic polarization before and after this OC exposure in NaCl and RW electrolytes demonstrated good initial barrier effect of BZS and BZS/LDH on the oxygen reduction in both environments. Under cathodic polarization, which results in the surface pH increasing, as expected from Fig. 3, BZS transformed into ZnO with loss of barrier properties on GI. The loss of barrier properties of corrosion products on GI was delayed in RW due to its buffer capacity. The transformation into zinc oxides did not occur on ZnMgAl during the time scale of the experiment, which was in accordance with the effect of Mg^{2+} and Al^{3+} ions. At the same time the barrier properties did not degrade on this coating.

The microstructure observations of the corroded coatings after different tests have shown that even at complete dissolution of Mg-rich phase, Al partly stays in metallic form and Al-rich skeleton progressively corrodes to form a highly compact product (LDH) at the same place. We suppose that the Al skeleton decreases the diffusion of zinc ions from the corroded surface favoring precipitation in a compact structure close to the intact coating. This probably reinforces the barrier effect. The distribution of the corrosion products can be hence related to the homogeneity of the coatings' microstructure which varies with fractions of alloying elements.

Perspectives

Although this work has clarified some elementary steps of the corrosion mechanisms of ZnMgAl and explains the role of Mg and Al alloying and the role of some ions in the electrolyte on the intrinsic reactivity of the coating and on the formation of corrosion product, there are still several points open for discussion.

First of all, all the studies of this work were made under aerated conditions. Some recent works demonstrated that a CO_2 free atmosphere can result in a very different behavior of ZnMgAl coatings. This subject will require a separate study. This can result in different behavior in confined zone or under paint. The present work also did not take into account the surface modification which can be introduced for instance by pre-treatment procedure before painting etc. Therefore, the role of different parameters such as surface pre-treatment, presence of the paint layer, confinement, galvanic coupling, temperature and the role of the dry period during corrosion requires further investigation. This work did not treat the galvanic effect of the ZnAlMg coating on exposed steel such as would occur at a coating defect penetrating to the steel or on the cut edge of the galvanized steel. Also of considerable interest for further study would be the "self-healing" effect, when cations produced at the ZnMgAl surface precipitate on the exposed steel and thereby block the cathodic reaction. It is clear that mechanisms analogous to what are proposed here concerning the ionic composition of the electrolyte should also play an important role in determining the nature and efficiency of the "self-healing" precipitate layers.

Appendix

APPENDIX

1 Accelerated corrosion tests



Fig. A.1. Climatic chamber used for accelerated corrosion tests. [Courtesy of ArcelorMittal R&D]

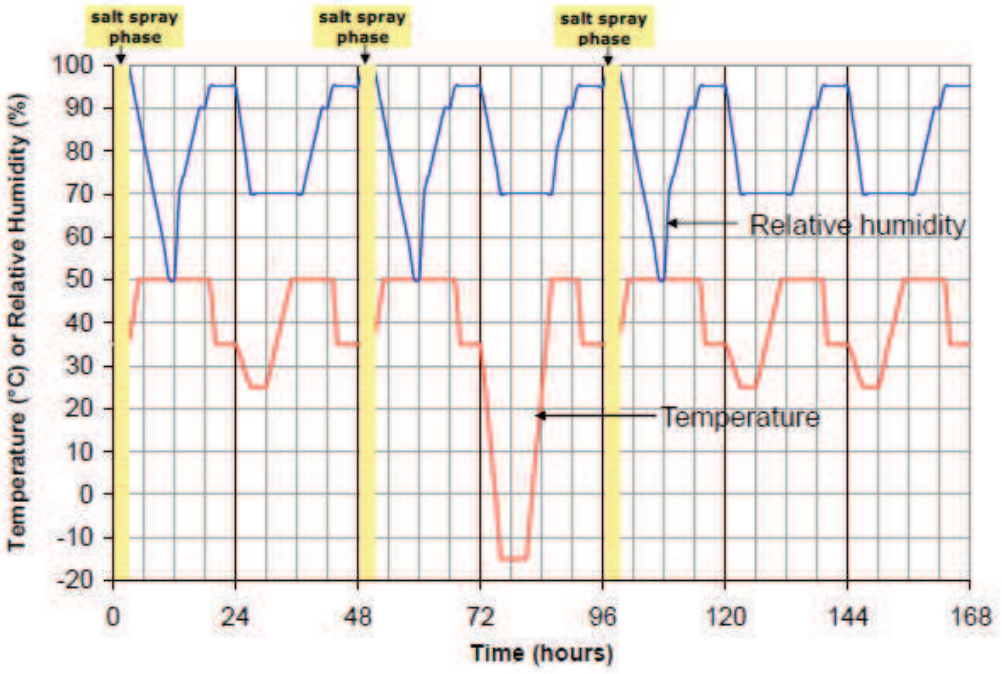


Fig. A.2. Temperature and humidity variation during a one week single cycle of the accelerated corrosion test VDA 233-102 [1].

2 Natural environment corrosion test



Fig. A.3. Sample desk in natural exposure site in Maizières, France. [Courtesy of ArcelorMittal R&D]

3 Atomic emission spectroelectrochemistry (AESEC)

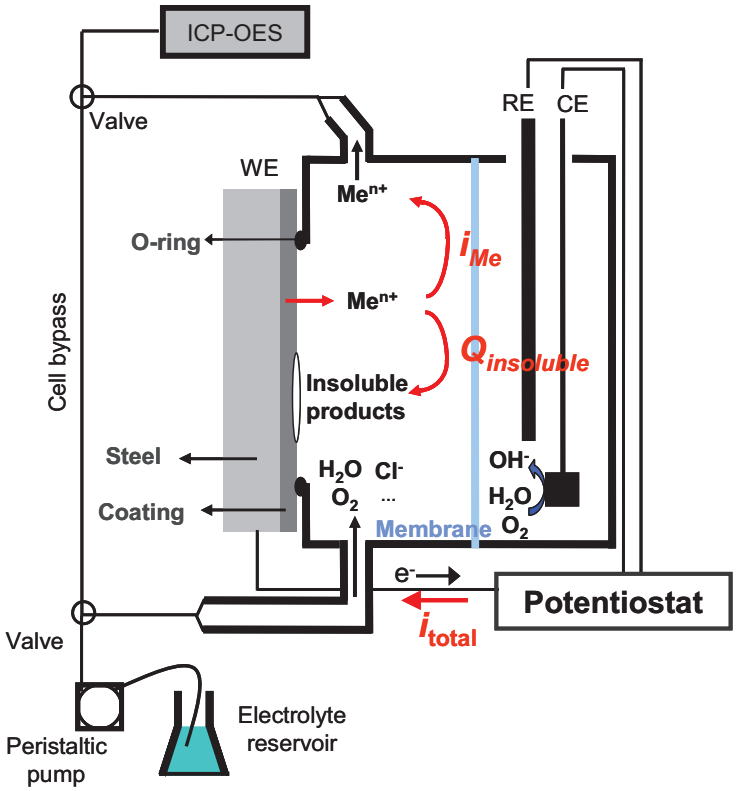


Fig. A.4. Schematic illustration of the flow cell used for the measurement with the AESEC technique. The represented schema shows an anodic polarization, in which i_{total} is the total current measured by the potentiostat; i_{Me} is the elemental dissolution rate of a metal *Me*, expressed as current and calculated from downstream electrolyte concentration measured with the ICP-OES; and $Q_{insoluble}$ is the quantity of insoluble products (precipitated oxides).

4 Precipitation of artificial corrosion products

Table A.1. Equivalence between the name of corrosion products, its composition, the chosen abbreviation and label used on the XRD figures.

Label	Name	Abbreviation	Chemical formula
1	Layered double hydroxide	LDH	$M(II)_xM(III)_y(A^-)_m(OH)_n.zH_2O$ $M(II) = Zn^{2+}, Mg^{2+}$, $M(III) = Al^{3+}$ $A^- = CO_3^{2-}, Cl^-, SO_4^{2-}$
2	Simonkolleite	ZHC	$Zn_5(OH)_8Cl_2.H_2O$
3	Zinc hydroxysulphate	ZHS	$Zn_4(OH)_6SO_4.nH_2O$, n=3-5
4	Hydrozincite	HZ	$Zn_5(OH)_6(CO_3)_2.H_2O$
5	Zincite	ZnO	ZnO
6	Zinc hydroxide	$Zn(OH)_2$	$Zn(OH)_2$
7	Magnesium hydroxide	$Mg(OH)_2$	$Mg(OH)_2$
8	Aluminium hydroxide	$Al(OH)_3$	$Al(OH)_3$

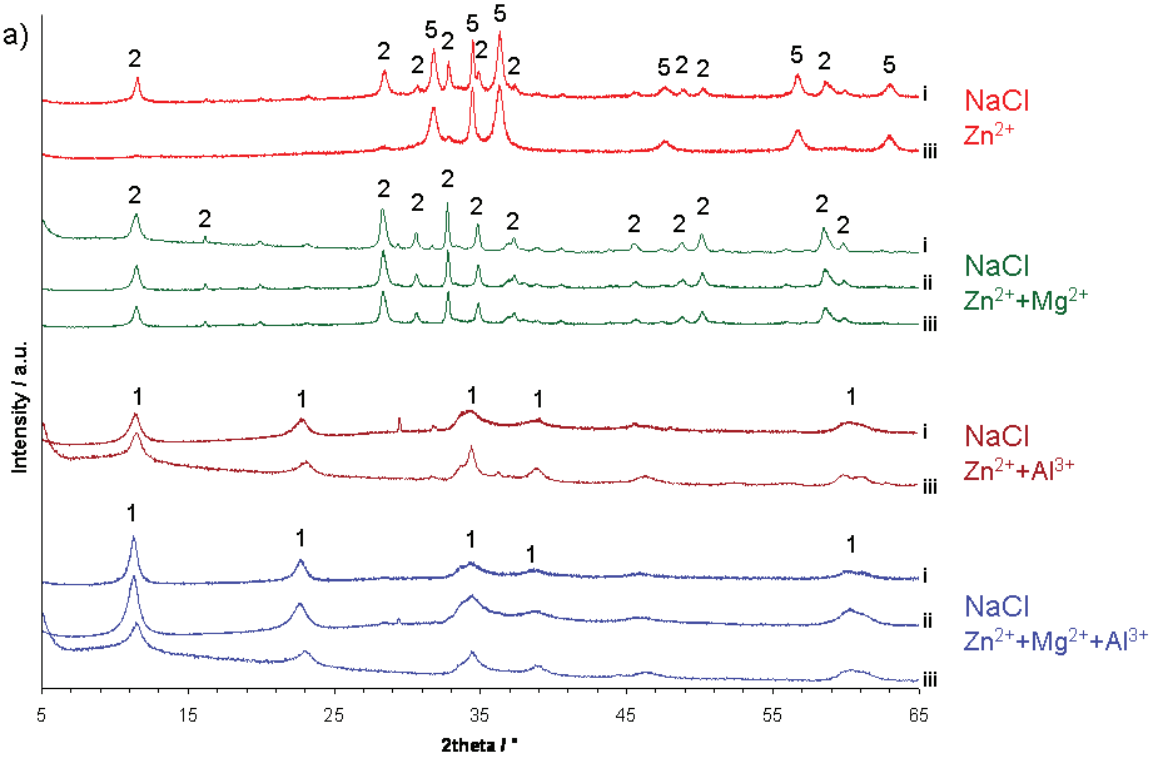


Fig. A.5. XRD patterns of the precipitated artificial corrosion products (Chapter V – section 3.1) by means of titration with 1.0 M NaOH at 50 µl / s in 0.171 M NaCl in presence of Zn^{2+} and/or Mg^{2+} and/or Al^{3+}. The numbers correspond to the corrosion products identified in Table A.1. The numbers (i, ii, iii, iv) represent the sampling time from the titration curves showed in Fig.2 of section 3.1 (Chapter V).

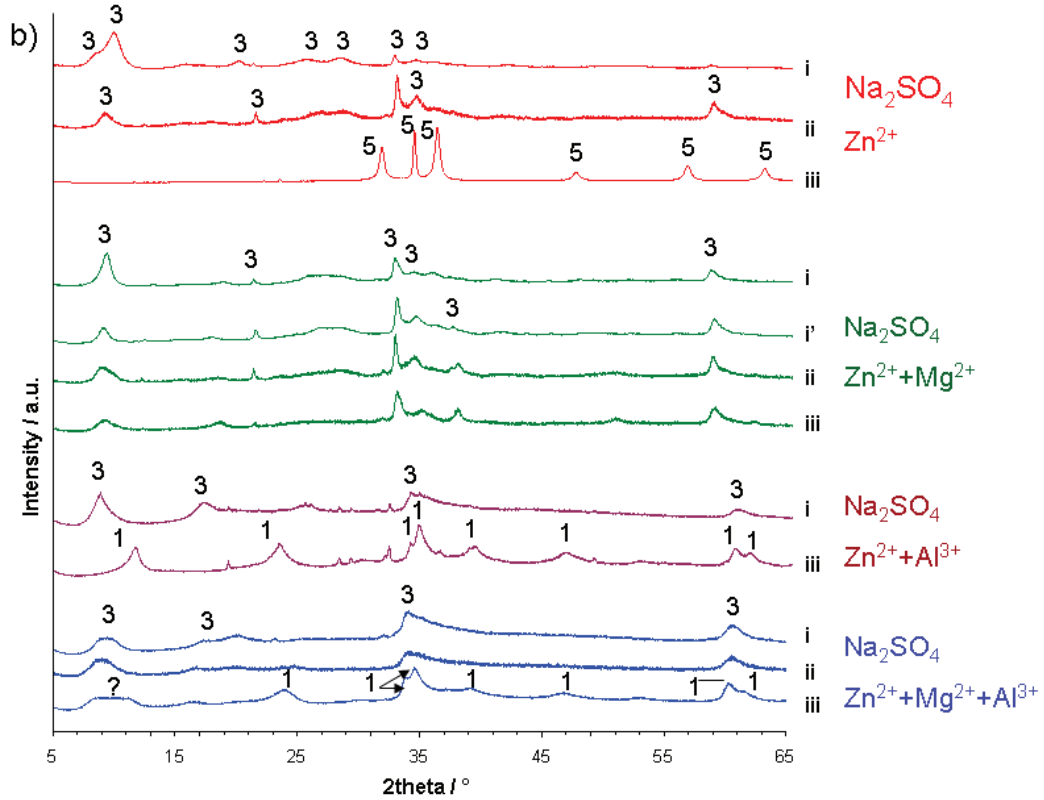


Fig. A. 6. XRD patterns of the precipitated artificial corrosion products (Chapter V – section 3.1) by means of titration with 1.0 M NaOH at 50 µl / s in 0.171 M Na_2SO_4 in presence of Zn^{2+} and/or Mg^{2+} and/or Al^{3+}. The numbers correspond to the corrosion products identified in Table A.1. The numbers (i, ii, iii, iv) represent the sampling time from the titration curves showed in Fig.2 of section 3.1 (Chapter V).

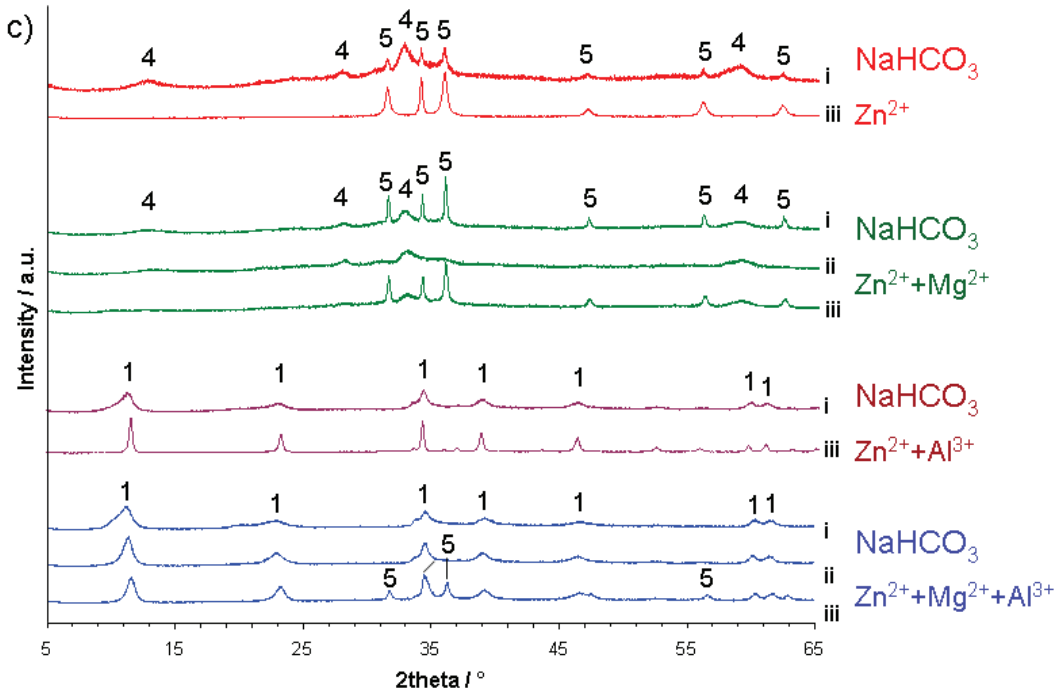


Fig. A. 7. XRD patterns of the precipitated artificial corrosion products (Chapter V – section 3.1) by means of titration with 1.0 M NaOH at 50 µl / s in 0.008 M $NaHCO_3$ in presence of Zn^{2+} and/or Mg^{2+} and/or Al^{3+}. The numbers correspond to the corrosion products identified in Table A.1. The numbers (i, ii, iii, iv) represent the sampling time from the titration curves showed in Fig.2 of section 3.1 (Chapter V).

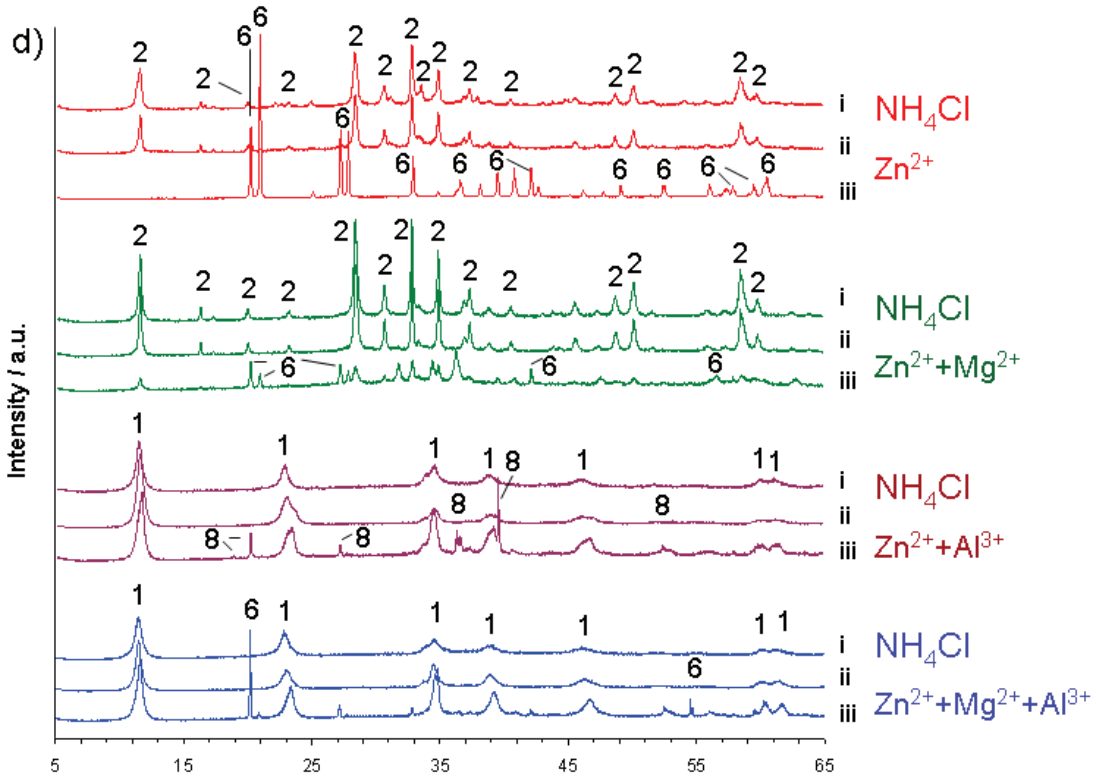


Fig. A. 8. XRD patterns of the precipitated artificial corrosion products (Chapter V – section 3.1) by means of titration with 1.0 M NaOH at 50 µl / s in 0.171 M NH_4Cl in presence of Zn^{2+} and/or Mg^{2+} and/or Al^{3+}. The numbers correspond to the corrosion products identified in Table A.1. The numbers (I, ii, iii, iv) represent the sampling time from the titration curves showed in Fig.2 of section 3.1 (Chapter V).

References

[1] VDA 233-102 “Cyclic corrosion testing of materials and components in automotive construction” June 2013

Résumé

« Mécanismes de corrosion de l'acier revêtu d'alliage à base de ZnMgAl en tests accélérés et environnements naturels »

Par Marcele SALGUEIRO AZEVEDO

Thèse de doctorat en Chimie Physique et Chimie Analytique

RESUME

1 Introduction

Le revêtement métallique à base de zinc est utilisé depuis plus d'une centaine d'années pour protéger l'acier de la corrosion. Les deux raisons majeures sont :

- ses bonnes propriétés barrières, du fait de sa faible vitesse de corrosion en environnement naturel ;

- la protection cathodique qu'il apporte à l'acier, grâce à son potentiel électrochimique environ 400 mV plus négatif que celui du fer.

Pour les marchés de l'automobile, de la construction ou de l'industrie, en vue principalement, d'améliorer la résistance à la corrosion de ce revêtement à base de zinc, généralement produit par trempé à chaud (ligne de galvanisation), l'aluminium et le magnésium ont été intégrés au bain de zinc comme éléments d'alliage.

Plusieurs compositions de revêtement ZnMgAl ont été développées par différents sidérurgistes. Les compositions varient entre 1.0 et 11.0 %m en Al et 0.1 et 3.0 %m en Mg. La microstructure de ces revêtements est dépendante des taux respectifs d'Al et de Mg. Toutefois, ils sont tous constitués des mêmes phases, mais dont les proportions sont étroitement liées à la composition (Fig. 1): dendrites de Zn (qui peuvent aussi être riches en Al, en fonction de la teneur en Al du revêtement), eutectique binaire Zn-Zn_2Mg (intermétallique), eutectique binaire Al-Zn, et eutectique ternaire Zn-Zn_2Mg-Al.

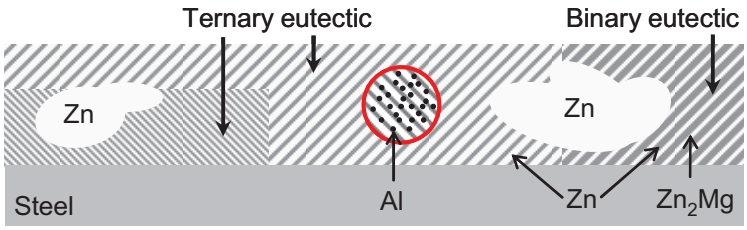


Fig. 1. Schéma d'un revêtement type ZnMgAl avec les différentes phases qui peuvent être présentes.

Au cours de ces 30 dernières années, de nombreux travaux ont été réalisés pour évaluer la résistance à la corrosion de ces revêtements ZnMgAl. Différents tests de corrosion sont pratiqués : des tests accélérés en laboratoire type brouillard salin continu ou cyclique, également des tests en exposition naturelle et « sur véhicule ».

Les tests de corrosion accélérés ont pour vocation de pouvoir comparer les différents revêtements de façon rapide, en essayant de se rapprocher le plus possibles des conditions réelles de corrosion que subiront ces matières au cours de leur vie. Les tests conventionnels pratiqués par les constructeurs automobiles sont réalisés dans des chambres climatiques où les échantillons d'acier revêtu sont mis en contact avec une solution saline, généralement à base de NaCl, en contrôlant le pH, l'humidité relative, et la température..

Ce sont ces tests accélérés qui ont permis de montrer l'excellente résistance à la corrosion du ZnMgAl. En comparaison avec l'acier galvanisé (revêtu à base de Zn, appelé GI), le ZnMgAl se montre en moyenne 6 à 10 fois plus résistant. Il a effectivement été observé que le rapport de corrosivité entre ZnMgAl et GI est étroitement lié aux conditions d'essai, notamment à la concentration des solutions salines.

Récemment, des données issues de tests en environnement naturel, qui servent à tester la corrosion atmosphérique, ont aussi confirmé la meilleure résistance à la corrosion du ZnMgAl par rapport au GI. Néanmoins, l'amélioration observée n'est pas au même niveau que celui démontré par les tests accélérés. Ce constat a amené des questionnements sur le comportement en corrosion des revêtements ZnMgAl en conditions réelles d'utilisation, et justifie en partie les études visant à mieux comprendre les mécanismes de corrosion de ces produits.

L'analyse de la littérature à ce sujet fait toutefois apparaître des divergences sur l'explication des mécanismes, et force est de constater que l'influence de l'environnement corrosif sur le comportement des revêtements ZnMgAl reste insuffisamment explorée. Un point commun ressort toutefois de la majorité de ces études, c'est le rôle important que jouent les produits de corrosion formés à la surface du ZnMgAl sur les mécanismes de protection.

Les produits de corrosion, en fonction de leurs caractéristiques physico-chimiques, peuvent en effet avoir un effet barrière vis-à-vis de la diffusion de l'oxygène vers la surface métallique, et ainsi contribuer à réduire la vitesse de corrosion. En condition de corrosion atmosphérique, c'est effectivement la réaction de réduction de l'oxygène (Eq. 1) à la surface d'un métal qui contrôle sa vitesse de dissolution (Eq. 2), et les revêtements

possédant de bonnes propriétés barrière sont ceux dont les propriétés de surface impactent fortement l'accès de l'oxygène dissous.

$$O_2 + 2H_2O + 4e^- \rightarrow 4OH^- \quad (1)$$

$$M \rightarrow M^{n+} + ne^- \text{ , où } M \text{ est le métal} \quad (2)$$

La composition et microstructure des produits de corrosion sont dépendantes du revêtement (Zn, ZnAl, ZnMgAl) et de l'environnement (nature et concentration des espèces ioniques, pH, température, alternance des phases humides/sèches…). Des produits plus ou moins protecteurs peuvent être formés en fonction de ces conditions. Les propriétés physico-chimiques des produits de corrosion, comme porosité, solubilité, adhérence, etc. vont en partie conditionner leur effet barrière vis-à-vis de la diffusion de l'oxygène.

En ce qui concerne le revêtement GI, souvent la présence de simonkolleite (ZHC), hydrozincite (HZ), zinc hydroxysulfate (ZHS) et zincite (ZnO) est rapportée. Les trois premiers produits sont des sels basiques (« Basic Zinc Salts » BZS), considérés comme protecteurs. Néanmoins, le ZnO, en raison de sa porosité, de sa grande solubilité dans l'eau et de sa faible adhérence sur les surfaces métalliques, n'a pas la même efficacité que les autres produits cités.

Contrairement au GI, le ZnO est rarement détecté sur ZnMgAl. Les produits qu'on identifie sont les BZS (ZHC, HZ et ZHS), mais également des composés type « layered double hydroxydes » (LDH), reconnus comme étant très efficaces en termes de barrière à l'accès de l'oxygène. Les LDH sont des composés à base Al^{3+} en liaison avec du Zn^{2+} et/ou du Mg^{2+}. Parfois, des produits à base Mg sont aussi rapportés et considérés comme protecteurs.

L'amélioration de la résistance à la corrosion du ZnMgAl apparaît donc majoritairement liée à la précipitation de produits de corrosion protecteurs et à l'absence de produits peu ou non-protecteurs, tandis que le GI forme un mélange de produits protecteurs et non-protecteurs.

Différents mécanismes sont proposés pour expliquer comment l'aluminium et le magnésium impactent la précipitation des produits de corrosion. En ce qui concerne le Mg, certains auteurs proposent la formation d'une couche protectrice qui contient du Mg ; d'autres suggèrent que la précipitation de l'hydroxyde de Mg tamponne le pH, ce qui empêche la transformation de produits de corrosion protecteurs comme ZHC, HZ et ZHS,

qui ne sont pas stables en pH très alcalin, en produits peu protecteurs comme le ZnO, qui se forment à des pH plus alcalins.

Bien que sur les vingt dernières années, les sidérurgistes européens aient développé des revêtements ZnMgAl de compositions différentes, la littérature relate peu d'études sur l'influence de la teneur en Mg et en Al du revêtement sur ses mécanismes de corrosion. En outre, l'aspect microstructure n'est pas discuté. Les rares articles sur le sujet sont restés très empiriques, avec des résultats corrosion se limitant au constat que les compositions les plus chargées en Mg et Al sont les plus performantes. Néanmoins, il n'y a pas de justifications disponibles.

De toute évidence, il existe un manque de connaissances sur les mécanismes de corrosion des revêtements ZnMgAl dans les milieux naturels. En outre, la non-représentativité des tests de corrosion accélérés pour simuler la corrosion atmosphérique a été soulignée par divers auteurs, mais là encore, aucun mécanisme n'est suggéré.

2 Objectifs

Pour répondre aux différentes questions sans réponses identifiées à travers l'analyse de la littérature, le présent travail de thèse cible trois principaux objectifs :

• Construire une base de données des produits de corrosion de revêtements ZnMgAl dans des environnements corrosifs différents et l'utiliser pour mettre en évidence les mécanismes de corrosion en milieu naturel, en expliquant la différence avec les tests de corrosion accélérés.

• Investiguer le rôle de l'Al et du Mg, non seulement dans la formation de produits de corrosion, mais plus généralement sur les mécanismes de corrosion.

• Comprendre comment les teneurs en Al et en Mg des revêtements ZnMgAl impactent leur résistance à la corrosion dans divers environnements corrosifs.

3 Structure de la thèse et principaux résultats

Cette thèse est organisée en sept chapitres : le premier fait l'état de l'art sur les mécanismes de corrosion de revêtements GI et ZnMgAl pour l'acier ; le deuxième décrit de façon succincte et générale la méthodologie utilisée dans ce travail (la description plus fine des paramètres des essais sont données au début de chaque chapitre technique) ; les troisième, quatrième, cinquième et sixième chapitres sont purement techniques, et visent à

répondre aux différentes questions mentionnées ci-dessus ; le septième et dernier chapitre donne les conclusions générales apportés par cette thèse. Les quatre chapitres techniques sont écrits sous forme d'article et sont structurés de façon identique en cinq parties : (i) introduction, (ii) méthodologie, (iii) résultats, (iv) discussion et (v) conclusion. L'objectif est de publier ces articles dans des revues scientifiques de renommée mondiale, de manière à apporter de nouveaux éléments sur les mécanismes de corrosion des revêtements ZnMgAl.

Le premier chapitre « Etat de l'art » détaille l'état de l'art décrit brièvement dans l'introduction de ce résumé. Les travaux majeurs sont répertoriés et les mécanismes de corrosion déjà proposés sont analysés en détail.

La méthodologie utilisée est décrite dans **le deuxième chapitre**. On y définit les principales caractéristiques des tests et techniques utilisées :

- Les tests de corrosion accélérés (brouillard salin continu, SST, et tests cycliques, VDA), et tests d'exposition naturelle réalisés, qui sont utilisés pour comparer les différents revêtements pour l'acier en fonction de ses vitesses de corrosion.

- La procédure utilisée pour mesurer la vitesse de corrosion des revêtements : cette vitesse est donnée en épaisseur consommée du revêtement pendant une durée de test de corrosion, calculée par la perte de masse lors de ce test, en prenant en compte la densité et la surface exposée de l'échantillon.

- La méthodologie mise en place pour analyser les produits de corrosion, avec un rappel des aspects majeurs des techniques employées : diffraction de rayons-X (XRD), spectroscopie Raman ; microscopie électronique à balayage (SEM) avec analyse chimique par analyse dispersive en énergie (EDS). La XRD permet d'analyser de façon globale les produits de corrosion cristallins formés à la surface du revêtement ; le Raman est complémentaire à la XRD, en permettant l'analyse de produits amorphes ; le SEM permet l'observation des profils de corrosion, et avec les analyses EDS il est possible d'identifier la localisation de différents éléments dans la section transversale du revêtement corrodé.

- La technique de spectroélectrochimie d'émission atomique (AESEC) utilisée pour étudier la dissolution sélective des phases du revêtement Zn(Mg,Al) et sa réactivité intrinsèque en différents électrolytes. L'AESEC est composé par une cellule électrochimique, où l'échantillon est placé pour être en contact avec l'électrolyte. Cette cellule est couplée à un spectromètre à torche à plasma (ICP) qui analyse la dissolution du revêtement « on line ». L'échantillon est également couplé à un potentiostat, permettant la mesure ou imposition de potentiel ou de courant.

- La technique de titration pour les études sur les aspects (i) tampon pH des électrolytes utilisés lors de tests de corrosion accélérés et (ii) synthèse des produits de corrosion dans différentes conditions.

- Les techniques électrochimiques pour évaluer l'effet barrière des produits de corrosion. Les essais électrochimiques ont été effectués avec une cellule classique à trois électrodes.

Le troisième chapitre, « Le rôle de la composition de l'électrolyte sur la nature des produits de corrosion et sur la vitesse de corrosion relative », est essentiellement axé sur les tests de corrosion. Ce chapitre synthétise les résultats sur la vitesse de corrosion des revêtements et la nature des produits de corrosion en différents sites d'exposition naturelle et en tests accélérés avec des électrolytes variés (Tableau 1). On y explique la logique qui nous a conduit à proposer un nouvel électrolyte pour les tests accélérés, appelé « eau de pluie » (RW, d'après l'anglais « rain water ») et contenant de l'ammonium (NH_4^+) et du bicarbonate (HCO_3^-). L'idée était de mieux simuler l'environnement naturel lors de tests accélérés (respect au rapport de vitesse de corrosion entre ZnMgAl et GI et aux produits de corrosion formés sur ces deux revêtements).

Le Tableau 1 montre les rapports de l'épaisseur consommée entre GI et ZM : après les tests avec des électrolytes « standard » NaCl et Na_2SO_4 (lignes 1 à 6), ce rapport est toujours plus grand que 6. Avec le nouvel électrolyte RW (lignes 7 à 9), ce rapport est d'environ 3, donc très proche de celui mesuré après l'exposition naturelle. L'absence (pour les SST-RW), ou au moins la formation retardée (pour le VDA-RW) des produits type LDH sur ZnMgAl, est aussi en accord avec ce qui est observé en exposition naturelle.

Le rôle de l'effet tampon pH de l'électrolyte « eau de pluie » est ensuite discuté. On montre qu'il résulte de la présence des ions HCO_3^- et NH_4^+, qui modifient les conditions de précipitation des produits de corrosion par rapport à un test standard avec NaCl.

Les résultats montrent en particulier que l'effet tampon de l'électrolyte retarde la dissolution de l'Al (Eq. 3), et par conséquent la formation du produit de corrosion LDH (Eq. 4).

$$Al + 4OH^- \rightarrow Al(OH)_4^- + 3e^- \quad (3)$$

$$2Al(OH)_4^- + 6Zn^{2+}/Mg^{2+} + 8OH^- + CO_3^{2-} \rightarrow (Zn/Mg)_6Al_2(OH)_{16}CO_3 \quad (4)$$

En raison de l'importance des ions présents dans l'électrolyte sur les mécanismes de corrosion des revêtements, le **quatrième chapitre**, « L'effet des ions HCO_3^- and NH_4^+ sur la réactivité intrinsèque du revêtement », étudie le rôle des ces ions sur la dissolution

sélective des différentes éléments constitutifs du revêtement Zn(Mg,Al). Les mesures par AESEC ont été réalisées en alternant la polarisation de l'échantillon : potentiel libre, polarisation cathodique et polarisation anodique.

Tableau 1. Rapport de l'épaisseur consommées entre GI et ZM après différent testes de corrosion et produits de corrosion détestés sur ZM. SST – test accéléré de brouillard salin continu. VDA – test de corrosion accéléré cyclique. RW (« eau de pluie ») – nouveau électrolyte. Modified-RW – le même électrolyte RW sans les ions NH_4^+ et HCO_3^-. Les valeurs en pourcentage représentent la concentration massique de l'électrolyte.

	Test de corrosion	Rapport de l'épaisseur consommée	Produits de corrosion détectés après test de corrosion
		GI / ZM	ZM
	Exposition naturelle - Brest	2.4	LDH, ZHC, ZHS, HZ
	Exposition naturelle - Chicago	2.8	ZHS
	Exposition naturelle - Maizières	3.3	ZHS
1	SST-NaCl 0.1%	10	LDH, ZHC, HZ
2	SST-NaCl 1%	20	LDH, ZHC, HZ
3	SST-NaCl 5%	13	LDH, ZHC, HZ
4	SST-NaCl 0.4%	6.1	LDH, ZHC, HZ
5	VDA-NaCl 1%	9.1	LDH, ZHC, HZ
6	SST-Na_2SO_4	11	LDH, ZHS, HZ
7	SST-RW 0.1%	3.0	ZHS
8	SST-RW 1%	2.7	ZHS
9	VDA-RW 0.1%	3.8	LDH, ZHC, ZHS
10	SST modified-WR	6.7	LDH, ZHS, ZSC

Les résultats attestent de la dissolution cathodique sélective de l'Al (Fig. 2 – j_{Al} (C) > j_{Al} (A)) et la dissolution anodique sélective de l'intermétallique Zn_2Mg en présence des différents ions testés (Fig. 3 – j_{Zn}, j_{Mg} (A) > j_{Zn}, j_{Mg} (C)). La dissolution de l'Al est néanmoins supprimée après la polarisation anodique en présence de NH_4^+ et HCO_3^- (Fig. 2b), en contraste avec NaCl seul (Fig. 2a). Il est supposé que ce retard est associé à des effets cinétiques liés à la présence d'ions Mg^{2+} formés au cours de la polarisation anodique. La Fig. 3 montre la dissolution du Mg pendant la deuxième polarisation cathodique jusqu'au temps indiqué par la flèche, qui correspond au moment où l'Al commence à se dissoudre (Fig. 2b).

En effet, des produits de types LDH, qui contiennent de l'Al, n'ont pas été détectés à la fin de ces essais en présence de NH_4^+ et HCO_3^-, mais $Mg(OH)_2$ a été détecté sur le ZnMgAl, ce qui indique l'importance des facteurs cinétiques pour la formation des produits de corrosion pendant les premières étapes de corrosion.

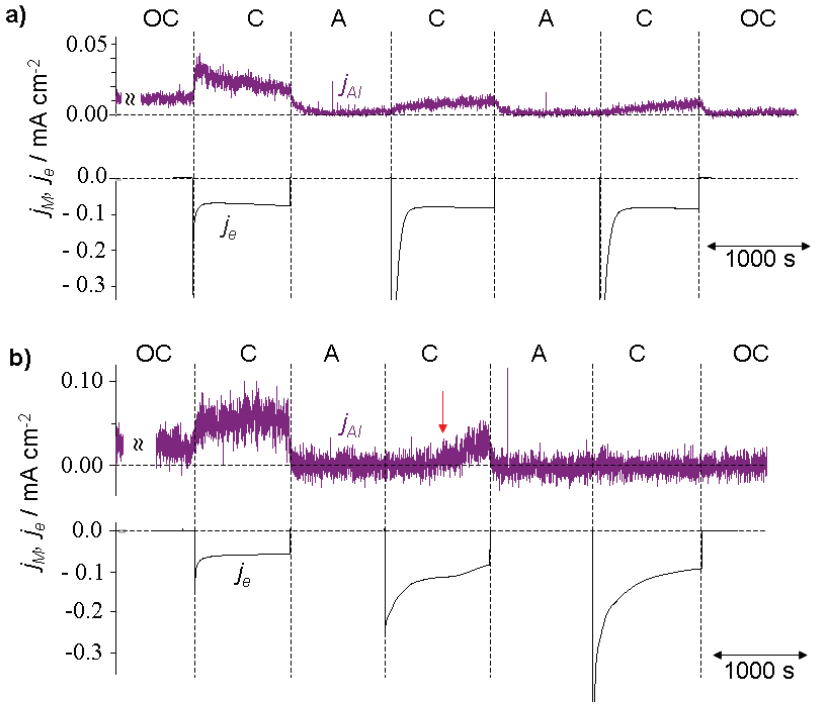


Fig. 2. Evolution de la vitesse de dissolution élémentaire de l'Al (j_{Al}) et du courant total (j_e) du revêtement ZM en (a) 0.1 M NaCl et (b) 0.1 M NH_4Cl + 0.1 M $NaHCO_3$ à potentiel cyclique anodique (A) et cathodique (C). Uniquement les courants cathodiques sont montrés. OC représente la vitesse de dissolution spontanée. Le cycle de potentiel imposé est : C = -1.25 V vs. SCE, A = -0.95 V vs. SCE.

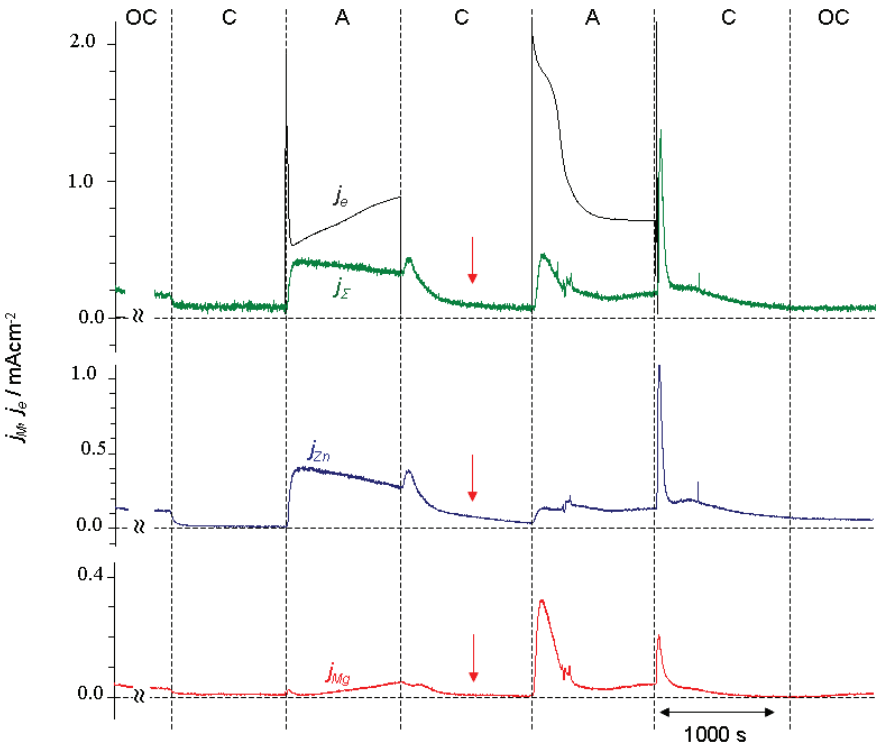


Fig. 3. Evolution des vitesses de dissolution élémentaires (j_{Zn} and j_{Mg}) et du courant total (j_e) du ZM dans 0.1 M NH_4Cl + 0.1 M $NaCO_3$ à potentiel imposé cyclique anodique (A) et cathodique (C). Uniquement le courant anodique est montré (le cathodique est sur la Fig. 2b). OC représente le domaine de dissolution spontanée. Les potentiels imposés sont : $E_{(C)}$ = -1.25 V vs. SCE, $E_{(A)}$ = -0.95 V vs. SCE.

Le **cinquième chapitre**, « L'effet du Mg et de l'Al sur la formation et propriétés des produits de corrosion », concerne l'investigation du rôle du Mg et de l'Al sur les mécanismes de corrosion du revêtement ZnMgAl, et plus spécifiquement sur l'étape de précipitation de produits de corrosion.

Pour cela, des essais électrochimiques ont été mis en œuvre pour évaluer l'impact des produits de corrosion sur la cinétique de réduction de l'oxygène. Les résultats montrent qu'en milieux NaCl et RW, les produits de corrosion BZS, c'est-à-dire ZHC, HZ et ZHS, sont efficaces pour réduire la vitesse de réduction de l'oxygène à la surface des deux revêtements, GI et ZnMgAl. La méthodologie utilisée a consisté tout d'abord à mesurer le courant cathodique à la surface nue de ces revêtements, puis à les laisser au potentiel libre (potentiel de corrosion) pendant 12h, période pendant laquelle les produits de corrosion se sont formés. Ensuite, une nouvelle polarisation cathodique est réalisée. Le courant cathodique diminue à la surface des deux revêtements. D'après l'analyse des produits de corrosion, des BZS ont été formés (aussi des LDH sur ZnMgAl en NaCl). Néanmoins, alors que la polarisation continue, ces produits se transforment en ZnO sur GI – dû à l'augmentation du pH (Eq. 1). Cette transformation entraine la perte de l'effet barrière de la couche de produits de corrosion. Au contraire du GI, les produits sur ZnMgAl restent stables en milieu NaCl et se transforment en partie en LDH en milieu RW. Le Tableau 2 identifie les différents produits de corrosion formés sur GI et ZM avant et après la polarisation cathodique.

Tableau 2. Produits de corrosion identifies sur GI et ZM après le test de polarisation. Les chiffres circulés déterminent le moment d'échantillonnage: 1- juste après exposition de 12 h à l'abandon (formation de produits de corrosion), avant polarisation; 2- après la suivante polarisation cathodique de 30 h.

		Corrosion products characterization	
Electrolyte	Coating	①	②
		After OCP exposure	After cathodic polarization
NaCl	GI	ZHC, HZ	ZHC, ZnO
	ZM	LDH	LDH
RW	GI	ZHS, ZHC, HZ	HZ, ZnO
	ZM	ZHS, HZ	LDH, HZ

Dans une deuxième étape, des essais de titration par la soude de solutions contenant des ions Zn^{2+}, Mg^{2+} et Al^{3+} ont été effectués afin d'observer la précipitation des différents

oxydes métalliques en fonction du pH et ensuite les identifier par DRX. Les résultats obtenus montrent que les ions Mg^{2+} retardent la transformation des BZS en ZnO, non seulement par la précipitation de $Mg(OH)_2$ qui tamponne le pH à une valeur où la transformation ne peut se faite (conformément à la thermodynamique),mais aussi cinétiquement. Il est en effet observé que même à pH très alcalin, cette transformation n'a pas lieu instantanément, probablement via une barrière physique formée par le $Mg(OH)_2$ autour des BZS. Le tableau 3 montre les produits de corrosion formés dans les différentes conditions testées. On y constate également la formation rapide des LDH en présence de l'Al et une bonne stabilité de ces produits même à pH très alcalins. En bains chlorure et carbonate, la précipitation des LDH correspondants débute à pH neutre ; en milieu sulfate, ce sont tout d'abord les ZHS qui se forment à pH neutre et les LDH précipitent ensuite à des pH plus alcalins.

Tableau 3. Produits de corrosion synthétisés dans NaCl et dans Na_2SO_4 en présence de Zn^{2+} et/ Mg^{2+} et/ou Al^{3+}.

Electrolyte:	a - NaCl				b - Na_2SO4			
Cation:	1 Zn	2 Zn+Mg	3 Zn+Al	4 Zn+Mg+Al	1 Zn	2 Zn+Mg	3 Zn+Al	4 Zn+Mg+Al
pH ~ 7 / 9	ZHC ZnO	ZHC	LDH	LDH	ZHS	ZHS	ZHS	ZHS
pH ~ 10	-	ZHC $Mg(OH)_2$	-	LDH $Mg(OH)_2$	-	ZHS	-	ZHS $Mg(OH)_2$
pH ~ 12	ZnO	ZHC $Mg(OH)_2$	LDH	LDH $Mg(OH)_2$	ZnO	ZHS $Mg(OH)_2$	LDH	LDH $Mg(OH)_2$

Pour mieux observer le profil de corrosion du revêtement ZnMgAl résultant de la dissolution sélective des phases discutée dans le chapitre IV, des essais de dissolution par polarisation anodique du revêtement ont été effectués, suivis d'observations MEB. Les vues en coupe après polarisation anodique et dissolution des produits de corrosion révèlent la présence d'un «squelette» d'Al (Fig. 4) qui reste à la surface de l'acier. Ce squelette contribue très probablement à amplifier le rôle barrière des produits de corrosion en les confinant dans cette structure compacte.

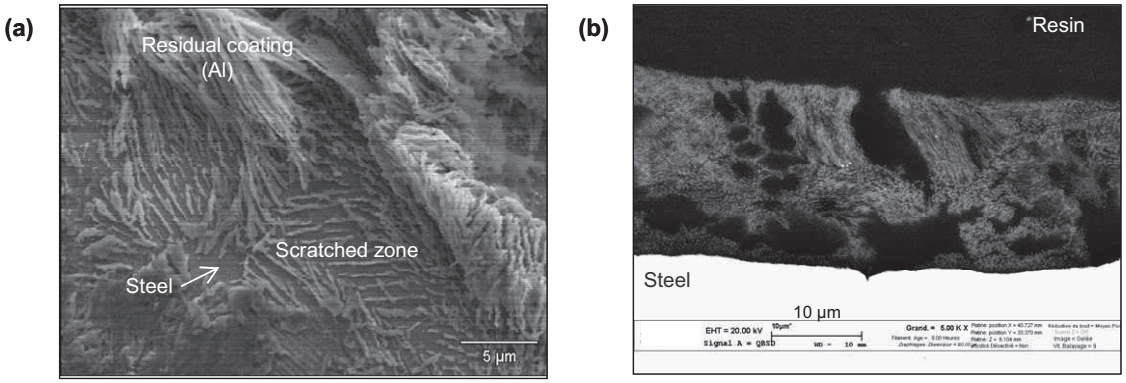


Fig. 4. Images MEB du ZM après dissolution anodique en Na_2SO_4. (a) Vue supérieure du revêtement restant (fibres d'Al) et (b) bord découpé du même échantillon – les fibres d'Al forment un "squelette" due à la dissolution des lamelles de Zn-Zn_2Mg et des dendrites de Zn (cavités).

Le **sixième chapitre,** « Etude comparative des revêtements ZnMgAl avec différentes compositions », étudie avec la même méthodologie l'influence de la composition du revêtement ZnMgAl sur le comportement en corrosion et les mécanismes associés. Dans cette optique, trois compositions de ZnMgAl ont été sélectionnées, dont les caractéristiques sont résumées dans le Tableau 4. Les trois ZM sont composés par des dendrites de Zn (ou Zn/Al) et des phases binaires Zn/Zn_2Mg et/ou ternaires Zn/Zn_2Mg/Al. Le ZM1 contient plus de dendrites de Zn que de phases binaire et ternaire en comparaison avec les ZM2 et ZM3, qui ont une matrice de phase ternaire avec des dendrites de Zn et de Zn/Al, respectivement – Fig. 5.

Tableau 4. Epaisseur et composition chimique des revêtements.

Label	Coating	Thickness	Zn %wt	Al %wt	Mg %wt
GI	Conventional hot-dip galvanized	20 µm	99.8	0.2	-
ZM1	ZnMgAl	10 µm	97.0	1.5	1.5
ZM2	ZnMgAl	20 µm	93.3	3.7	3.0
ZM3	ZnMgAl	10 µm	86.0	11.0	3.0

Des tests de corrosion accélérés avec différents électrolytes ont été réalisés, suivis de caractérisation des produits de corrosion formés. Les résultats des tests de corrosion permettent de classer les revêtements en termes de vitesse de corrosion : GI > ZM1 > ZM2 = ZM3. Néanmoins les produits de corrosion sur les différent ZM sont les mêmes : LDH et BZS. De cette manière, l'analyse qualitative des produits de corrosion n'est pas suffisante pour faire une distinction entre les revêtements ZnMgAl.

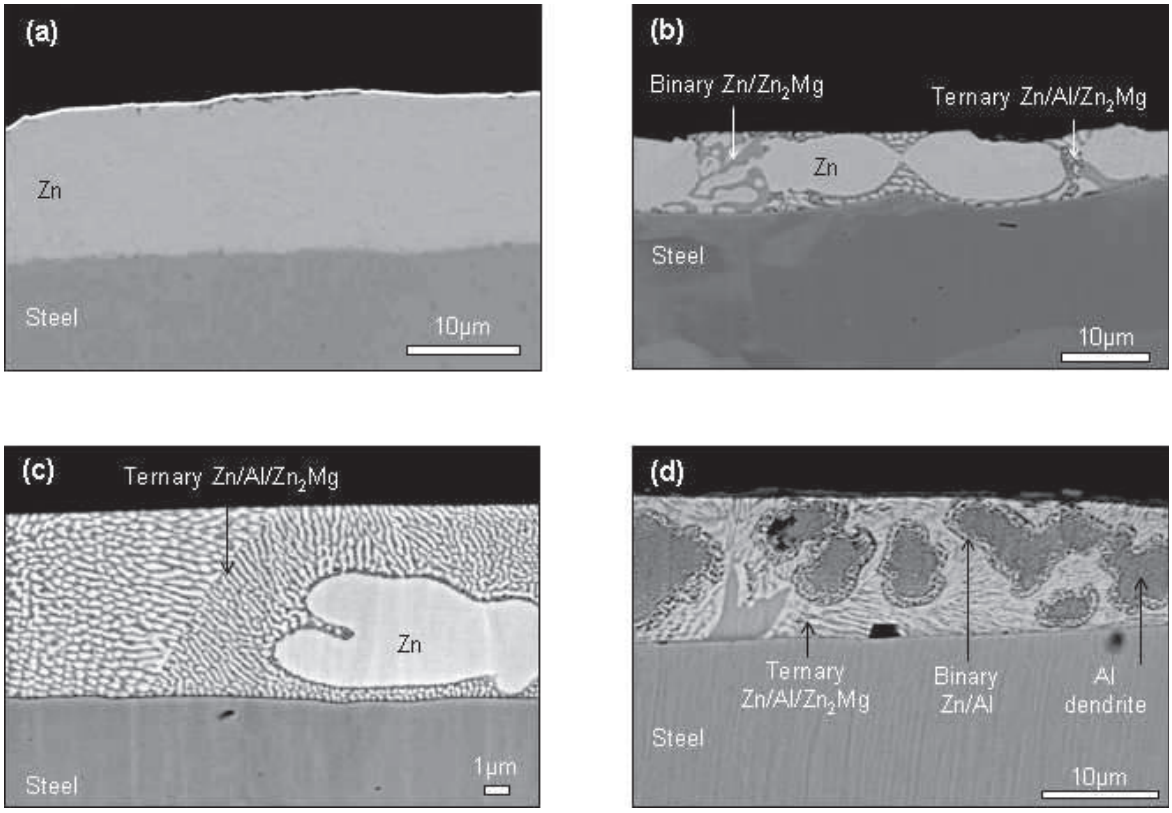


Fig. 5. Images SEM de vues en coupe des échantillons non-corrodés (a) GI, (b) ZM1, (c) ZM2 and (d) ZM3 avec ces phases respectives.

Pour évaluer l'efficacité des produits de corrosion formés sur les différents revêtements, une nouvelle série d'essais électrochimiques utilisant la méthodologie décrite dans le chapitre V ont été réalisés. Néanmoins, une deuxième exposition à l'abandon suivi de la mesure du courant cathodique a été faite – Fig. 6, qui montre la mesure du courant cathodique à chaque étape délimitée dans la figure : E_c est la polarisation cathodique, OC est l'exposition à l'abandon. Après la première exposition à l'abandon (OC), les mêmes produits de corrosion LDH (en NaCl) et BZS (en RW) sont formés sur les trois compositions de revêtements ZM. Néanmoins, on peut remarquer que le ZM1 perd l'effet barrière lors de la polarisation cathodique (E_c). Une nouvelle exposition OC se produit et c'est à ce moment-là que le courant commence à se stabiliser sur ZM1 dans NaCl (Fig. 6a) – dans RW cette stabilisation n'est pas encore obtenue. Au contraire du ZM1, les ZM2 et ZM3 présentent de faibles courants, stabilisés dés la première polarisation dans les deux électrolytes.

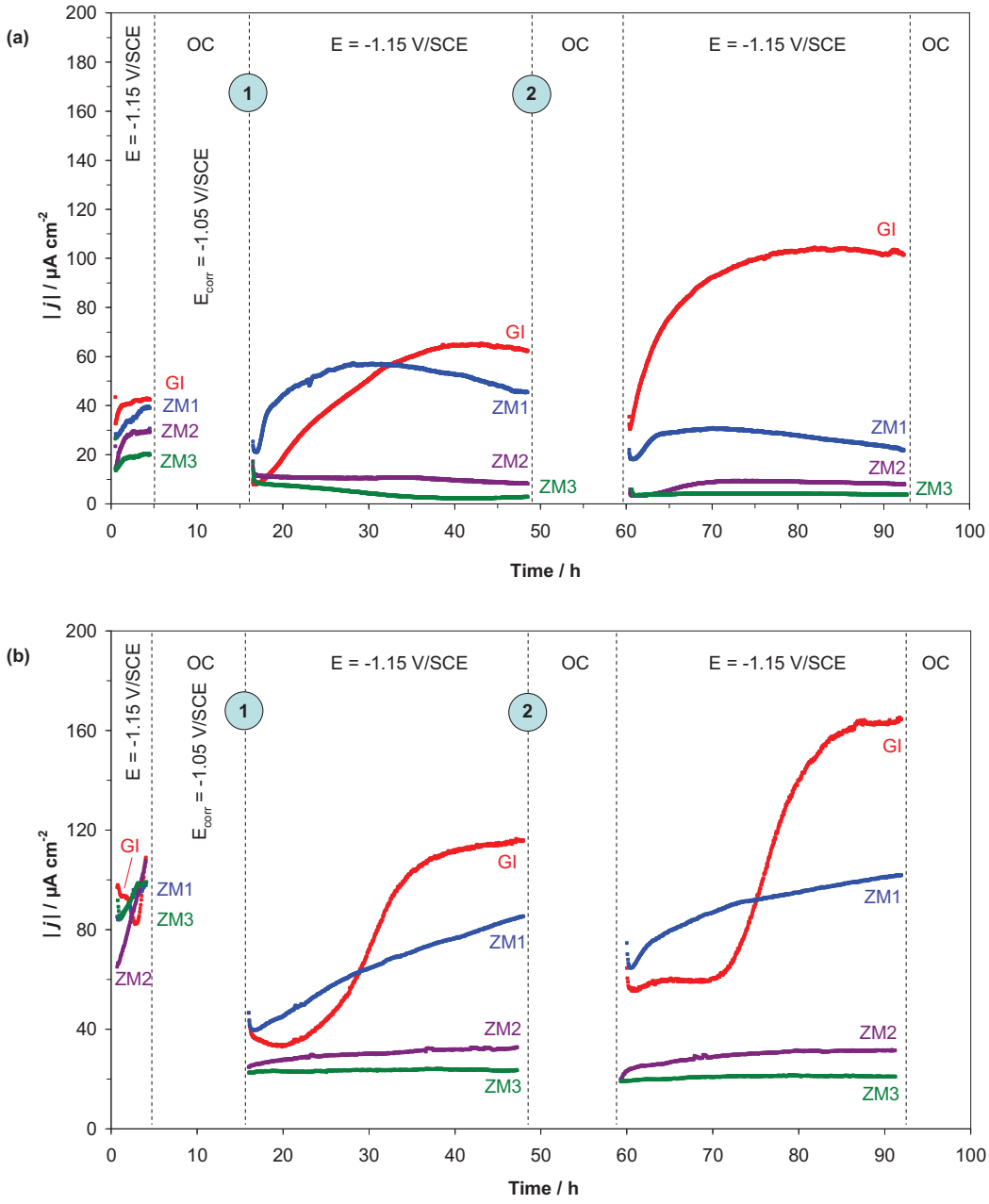


Fig. 6. Test de polarisation dans (a) NaCl et (b) électrolyte RW développé dans ce travail, qui contient NH_4^+ et HCO_3^-. Les graphiques montrent les courants cathodiques avant et après l'exposition à circuit ouvert (OC) du GI et des ZM. Les chiffres 1 et 2 montrent le moment d'échantillonnage pour la caractérisation de produits de corrosion.

L'effet barrière des produits de corrosion apparaît donc similaire sur ZM2 et ZM3, et inférieur sur ZM1, même si les produits de corrosion sont les mêmes sur les 3 modalités. Ce constat nous a amené à émettre l'idée que l'effet de la microstructure pourrait être plus important que l'effet composition sur le plan de la résistance à la corrosion. En se fondant sur l'analyse des résultats du chapitre V, on comprend l'intérêt d'avoir le Mg et l'Al distribués de façon homogène dans le volume du revêtement. Pour cette raison, les

revêtements ZnMgAl avec microstructure similaire - phase ternaire comme matrice (ZM2 et ZM3) - est démontrée plus résistante à la corrosion que ZnMgAl avec plus grande quantité de dendrites de Zn (ZM1).

Le **septième chapitre** donne la conclusion globale de cette thèse. La présence des ions bicarbonate, ammonium et sulfate est capable d'influencer de manière significative la cinétique des différentes étapes élémentaires des mécanismes de corrosion de revêtements ZnMgAl.

La Fig. 7 illustre le schéma du mécanisme proposé pour la dissolution des revêtements Zn(Mg,Al) et la formation des produits de corrosion en présence des ions Cl^-, NH_4^+ et HCO_3^-. Dans l'électrolyte « eau de pluie » (RW), l'effet tampon de NH_4^+ et HCO_3^- peut retarder l'étape III (dissolution chimique), et donc avoir un effet positif pour le GI (les produits de corrosion sont stabilisés) mais plutôt négatif pour ZnMgAl (produits de corrosion stabilisés mais formation de LDH retardée).

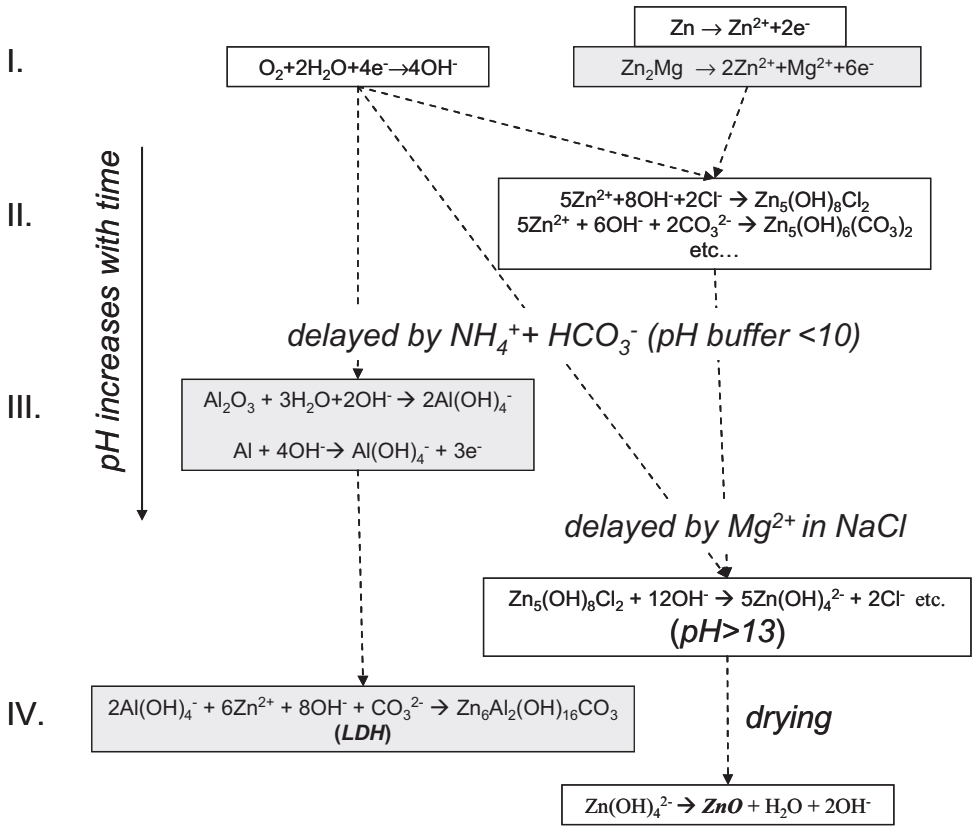


Fig. 7. Illustration schématique du mécanisme de formation des produits de corrosion ZnO et LDH à la surface des revêtement Zn(Mg,Al) dans NaCl et dans l'électrolyte RW (« eau de pluie », qui contient les ions NH_4^+ et HCO_3^-). Les différentes étapes sont listées par les chiffres : I. Réactions électrochimiques à pH neutre ; II. Précipitation de produits de corrosion à pH intermédiaire ; III. Dissolution chimique à pH élevé (dissolution cathodic de l'Al, dissolution des « Basic Zinc Salts » ; IV. Formation de ZnO et LDH.

En considérant les premières étapes de la corrosion, juste après un pulse anodique, la dissolution cathodique de l'Al est retardée ou même supprimée en présence des ions bicarbonate et ammonium. L'hypothèse que nous formulons est que cet effet est la conséquence d'une forte réduction de la cinétique de diffusion de l'Al par les produits de corrosion contenant du Mg qui sont formés pendant la polarisation anodique. La Fig. 8 illustre sous forme schématique les mécanismes de formation des LDH après polarization anodique et cathodique.

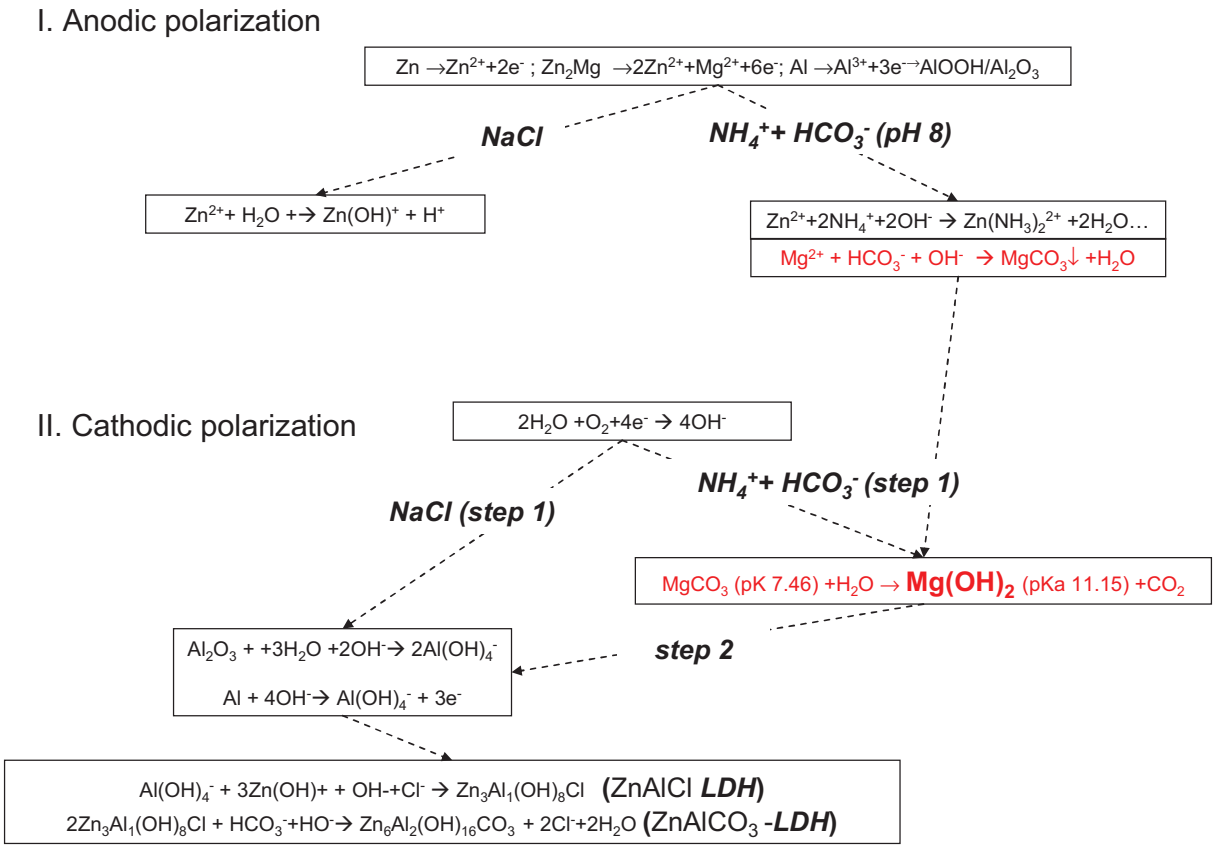


Fig. 8. Illustration schématique de l'effet du Mg^{2+} et du mécanisme de formation des LDH en différent électrolytes (contenant des Cl^- et/ou NH_4^+ et HCO_3^-).

En ce qui concerne la formation de produits de corrosion en présence des différents ions (Fig. 9), il a été montré que la présence des ions Mg^{2+} est capable de retarder la transformation des BZS en ZnO ; les LDH sont toujours précipités en présence de l'Al^{3+} – déjà à pH neutre dans des solutions avec des chlorures et carbonates, mais à pH plus alcalin en milieu sulfate (des ZHS sont précipités préférentiellement). L'Al est aussi capable de former un squelette en début de corrosion, qui est suggéré maintenir les produits de corrosion (type BZC) sous forme compacte à la surface du revêtement.

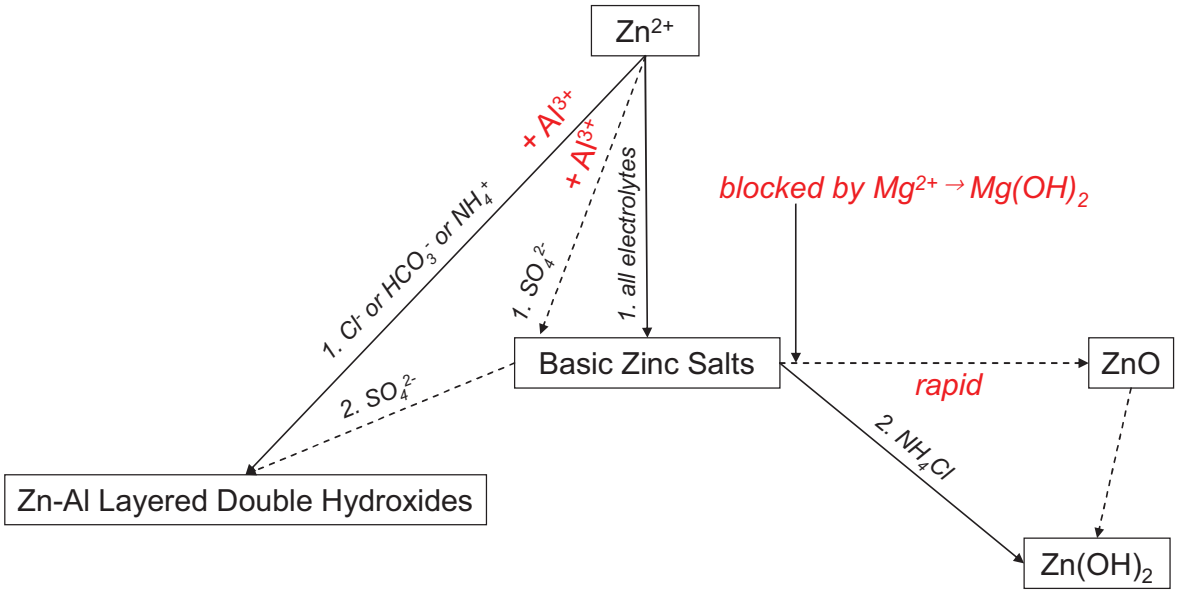


Fig. 9. Schéma illustratif de la précipitation de produits de corrosion en fonction des ions. L'Al forme toujours des LDH et le Mg retarde la transformation des BZS en ZnO.

L'importance de la microstructure du revêtement pour sa résistance à la corrosion a été mise en évidence. En effet, si la nature des produits de corrosion permet d'expliquer les différences de comportement entre GI et ZnMgAl, elle s'avère insuffisante pour interpréter les comportements en corrosion de revêtements ZM de compositions différentes. En corrélant observations MEB et résultats électrochimiques, on démontre alors que le facteur de premier ordre est la microstructure du revêtement, qui conditionne la dissolution sélective des phases, et donc la distribution des produits de corrosion. Une distribution homogène des produits de corrosion est bénéfique pour la résistance à la corrosion, et on l'observe ici pour les revêtements dont le ternaire Zn/Al/Zn_2Mg constitue la fraction volumique majoritaire.

Corrosion mechanisms of ZnMgAl coated steel in accelerated tests and natural environment

Factors differing corrosion mechanisms of ZnMgAl coatings on steel in natural environments and in accelerated tests with NaCl solution were identified. A new electrolyte (RW) containing NH_4^+, HCO_3^-, Cl^- and SO_4^{2-} was developed, for which the accelerated tests respected the relative corrosion rates of different Zn-based coatings and the delayed formation of layered double hydroxides (LDH) known for field exposure. Considering dissolution-precipitation mechanism of corrosion, the role of ions present in RW electrolyte on the leaching kinetics and on the accumulation of insoluble products was studied. NH_4^+ and HCO_3^- were demonstrated to increase the anodic reactivity and cathodic Al dissolution. LDH formation was delayed by NH_4^+, HCO_3^- and SO_4^{2-}. Higher anodic reactivity of ZnMgAl than zinc coating combined with better resistance in corrosion tests indicated the importance of cathodic reaction (oxygen reduction). Comparing oxygen reduction currents on fresh coatings and on the surface under patinas, clear barrier effect of basic zinc salts (BZS) and LDH was demonstrated. The barrier effect was lost under cathodic polarization on Zn coating due to the transformation BZS→ZnO/$Zn(OH)_2$ but was stable on ZnMgAl in the same conditions – the inhibiting effect of Mg^{2+} on the kinetics of this transformation was evidenced. A residual "skeleton" of unreacted Al contributed to the increased compactness of the corrosion products.

Keywords: Electrogalvanized steel; ZnMgAl; Corrosion product; Atmospheric corrosion; Corrosion mechanisms; Selective dissolution.

Mécanismes de corrosion de l'acier revêtu d'alliage à base de ZnMgAl en tests accélérés et en environnement naturel

Les facteurs qui différencient les mécanismes de corrosion du revêtement ZnMgAl pour l'acier en environnement naturel de tests accélérés avec du NaCl ont été identifié. Un nouvel électrolyte (RW) qui contient NH_4^+, HCO_3^-, Cl^- and SO_4^{2-} a été développé pour des tests accélérés en respectant la vitesse de corrosion relative entre les revêtements à base de Zn et la formation tardive des hydroxydes à double couche (LDH), qui sont connus pour l'exposition naturelle. En considérant le mécanisme de corrosion type dissolution-précipitation, le rôle des ions présents dans l'électrolyte RW sur la cinétique de dissolution et sur l'accumulation de produits insolubles a été étudié. NH_4^+ et HCO_3^- ont été démontrés capables d'augmenter la réactivité anodique et la dissolution cathodique de l'Al. La formation des LDH a été retardée par NH_4^+, HCO_3^- et SO_4^{2-}. La réactivité anodique plus élevée du ZnMgAl en comparaison avec le revêtement de zinc pur combinée avec sa meilleure résistance à la corrosion montrent l'importance de la réaction cathodique (réduction de l'oxygène). En comparant les courants dues à la réduction de l'oxygène sur les revêtements frais et sur la surface sous une couche de produits de corrosion, l'effet barrière des sels basiques de zinc (BZS) et LDH a été clairement démontré. Cet effet barrière est disparu sur le revêtement de zinc pur sous polarisation cathodique en raison de la transformation BZS→ZnO/$Zn(OH)_2$ mais est resté stable sur ZnMgAl dans les mêmes conditions – l'effet d'inhibition du Mg^{2+} sur le cinétique de cette transformation a été mis en évidence. Un « squelette » résiduel d'Al non-réagi a contribué à la compacité de produits de corrosion.

Mots clés: acier galvanisé ; ZnMgAl ; Produits de corrosion ; Corrosion atmosphérique ; Mécanismes de corrosion ; Dissolution sélective.